



MARCH 11-14, 2013 | DARMSTADT | GERMANY
6th INTERNATIONAL SYMPOSIUM ON
ADAPTIVE MOTION OF ANIMALS AND MACHINES

AMAM 2013 Proceedings

Understanding adaptive motion in humans and animals can help us to improve the adaptive behavior of machines. On the other hand, experiments with technical devices that adapt to a changing environment can shed more light on the basic principles of biological systems. We believe that such a bidirectional approach is essential to incorporate biological "intelligence" in machines. The AMAM 2013 encourages researchers from different fields to interact and exchange ideas in this interdisciplinary field. These fields are covering neuromechanics, neurophysiology, biomechanics, robotics, brain science, and other fields related to adaptive behavior of animals and machines. Previous symposia were held in Montreal, Canada (2000); Kyoto, Japan (2003); Ilmenau, Germany (2005); Cleveland, USA (2008) and Hyogo, Japan (2011).

Scientific Committee

Prof. Peter Aerts (University of Antwerp)

Prof. Koh Hosoda (Osaka University)

Prof. Auke Ijspeert (École Polytechnique Fédérale de Lausanne- EPFL)

Prof. Roy Ritzmann (Case Western Reserve University)

Prof. Josef Schmitz (University of Bielefeld)

Prof. André Seyfarth (Technical University of Darmstadt)

Prof. Hartmut Witte (Technical University of Ilmenau)

Prof. Hiroshi Kimura (Kyoto Institute of Technology)

Oganizing Comittiee

André Seyfarth (Lauflabor Locomotion Lab, Technical University of Darmstadt)

Martin Groß (Lauflabor Locomotion Lab, Technical University of Darmstadt)

Maziar A. Sharbafi (Lauflabor Locomotion Lab, Technical University of Darmstadt)

Christian Rode (Lauflabor Locomotion Lab, Technical University of Darmstadt)

Frank Peuker (Lauflabor Locomotion Lab, Technical University of Darmstadt)

Christian Ludwig (Lauflabor Locomotion Lab, Technical University of Darmstadt)

Marc Deisenroth (IAS Group, Technical University of Darmstadt)

Inna Mikhailova (SIM Group, Technical University of Darmstadt)

Opening Talk

No.	authors	Title
1	Carlo J. DeLuca	Neural Control of Force: A New Perspective

Keynote Talks

No.	authors	Title
1	Barry Trimmer	Moving Softly: Locomotion Strategies for Deformable Animals and Robots
2	Sangbae Kim	Toward highly dynamic locomotion: design challenges in MIT cheetah robot
3	Hitoshi Aonuma	Emergence of social adaptability in insects

Tandem Talks

No.	authors	Title
1	Noah Cowan and Volker Dür	Unraveling unrestrained locomotion: (1) natural statistics of steps and patterns and (2) system identification of feedback control
2	Manny Azizi and Dai Owaki	Role of Passive Properties in Producing Adaptive Motion in Robotic and Biological Systems
3	Koh Hosoda and Monica Daley	Leg design and control for stable locomotion

Public Lecture

No.	authors	Title
1	Roy Ritzmann	Orchestrating Movement through Complex Terrain: Interactions between Brains and Local Neural Circuits

Tutorials

No.	authors	Title
1	Jørgen Christian Larsen	LocoKit - robotic construction kit for legged locomotion
2	Ioannis Poulakakis	Hybrid Zero Dynamics Control of Legged Robots

Oral Presentations

No.	authors	Title
1	Maziar Ahmad Sharbafi and Andre Seyfarth	Human leg adjustment in perturbed hopping
2	Sabine Böker, Philipp Beckerle, Janis Wojtusich and Stephan Rinderknecht	A Novel Design Approach and Operational Strategy for an Active Ankle-Foot Prosthesis
3	Ivo Boblan, Andreas Schulz, Ivan Perfilov and Björn Bertrand	A Compliant Lightweight Universal Joint Cascadable to a Multi-joint Kinematics
4	Qu Cao and Ioannis Poulakakis	Self-stable Bounding with a Flexible Torso
5	Tetsuro Funato, Shinya Aoi, Nozomi Tomita and Kazuo Tsuchiya	The contribution of kinematic synergy on feedback control of human walking
6	Hugo Gravato Marques, Christophe Maufroy, Alexander Lenz and Konstantinos Dalamagkidis	MYROBOTICS: a modular toolkit for legged locomotion research using musculoskeletal designs
7	Stefan Hochstein and Reinhard Blickhan	Human underwater undulatory swimming: flow characteristics around a human swimmer, technical swimmer model, and numerical simulations
8	Marco Hutter, Christian Gehring, Mark Hoepflinger, Michael Bloesch and Roland Siegwart	Dynamic Locomotion with StarLETH
9	Karl Kalveram, Madelein Georg, Jasmin Kensche, Philipp König, Tim Lauer, Tobias Schröder, Saskia Schwering and Edith Eichhorn	Humans adapt to a changed arm dynamics - with or without visual feedback in the same manner
10	Matthieu Lapeyre, Pierre Rouanet and Pierre-Yves Oudeyer	Poppy: a new bio-inspired humanoid robot platform
11	Manu Madhav, Mert Ankarali, Shahin Sefati, Jusuk Lee, Julia Choi, Amy Bastian and Noah Cowan	Stride-to-Stride vs. Step-to-Step Return Maps for Human Running
12	Roy Müller, Michael Ernst and Reinhard Blickhan	Running across visible and non visible changes in ground level
13	Xiaoxiang Yu and Fumiya Iida	Maximizing the Energy Efficiency of the Robot Hopping

Poster Presentations

No.	authors	Title
1	Mostafa Ajallooeian, Alexander Sproewitz, Alexandre Tuleu and Auke Ijspeert	Data-driven Extraction of Drive Functions for Legged Locomotion: A Study on Cheetah-cub Robot
2	Emanuel Andrada, John Nyakatura and Reinhard Blickhan	Terrestrial locomotion of the common quail: one leg function for all gaits?
3	Philipp Beckerle, Florian Stuhlenmiller, Jochen Schuy, Janis Wojtusch, Stephan Rinderknecht and Oskar von Stryk	Friction Compensation and Stiffness Evaluation on a Variable Torsion Stiffness
4	Philipp Beckerle, Janis Wojtusch, Stephan Rinderknecht and Oskar von Stryk	Mechanical Influences on the Design of Actuators with Variable Stiffness
5	Jorgen Christian Larsen and Kasper Stoy	Active shifting of center-of-mass in quadruped bounding robot
6	Michael Ernst, Martin Götze, Roy Müller and Reinhard Blickhan	Different strategies for different situations? Adaptations of the CoM-trajectories to visible and camouflaged ground level changes in human running
7	Ikumi Fujiwara, Naomichi Ogihara, Koh Hosoda, Takeo Nagura and Toshiyasu Nakamura	Measurement of 3D human foot deformation during walking by digital image correlation method
8	Toshihiko Fukushima, Satoshi Nishikawa and Yasuo Kuniyoshi	Transitional Buckling Model for Active Bending Effect in Pole Vault
9	Vincent Godivier	Simulation study of human slope walking gait based on a musculoskeletal model
10	Nalin Harischandra and Volker Dürr	Prediction of Self-induced Mechanoreceptive Sensor Readings in An Insect-inspired Active Tactile Sensing System
11	Khai-Long Ho Hoang, Katja Mombaur and Sebastian I. Wolf	Quantifying dynamic stability in healthy and pathological human locomotion
12	Shuhei Ikemoto, Yosuke Inoue, Masahiro Shimizu and Koh Hosoda	Minimalistic Decentralized Modeling for a Skeletal Muscle based on Stochastic Resonance
13	Akio Ishiguro, Takeshi Kano and Dai Owaki	Toward unified understanding of inter-limb coordination mechanism underlying multi-legged locomotion
14	Kohta Ito, Naomichi Ogihara, Koh Hosoda, Takeo Nagura, Toshiyasu Nakamura, Nobuaki Imanishi and Masahiro Jinzaki	Three dimensional reconstruction of foot skeletal movement using biplanar fluoroscopic system
15	Takeshi Kano, Dai Owaki and Akio Ishiguro	FromWalk to Trot to Bound: Quadruped Gait Transition Induced by Simple Local Force Feedback Mechanism
16	Takeshi Kano, Shota Suzuki, Eiki Sato, Hitoshi Aonuma and Akio Ishiguro	Toward realization of resilient locomotion: Lessons from the locomotion of arm-amputated ophiuroids
17	Takeshi Kano, Yuki Watanabe, Fuyuhiko Satake and Akio Ishiguro	Development of sheet-like robot for multi-terrestrial locomotion
18	Hamza Khan, Claudio Semini and Darwin G. Caldwell	Scaling of Versatile Quadruped Robots for Running Trot.
19	Mahdi Khoramshahi, Auke Ijspeert and Majid Nili Ahmadabadi	Exploiting Natural Dynamics of Nonlinear Compliance Using Adaptive Oscillators
20	Taiki Kobayashi, Masahiro Shimizu, Koh Hosoda and Naomichi Ogihara	Anatomically Detailed Three Dimensional Dynamical Finite Element Analysis of the Human Foot
21	Xin Liu and Ioannis Poulakakis	A Simple Controller for Quadrupedal Bounding
22	Inna Mikhailova	Energy-based State-Feedback Hopping Control
23	Alberto Minetti	Internal combustion based transport: humans vs. vehicles
24	Satoshi Nishikawa, Kazuya Shida, Ryuma Niiyama and Yasuo Kuniyoshi	Angle-Dependent Moment Arm with Biased Pivot for Jumping from Various Squatting Positions
25	Takaaki Oku and Naomichi Ogihara	Human Locomotor Adjustment to a Perturbation Induced by a Split-Belt Treadmill

Poster Presentations

No.	authors	Title
26	Sebastian Reitelshöfer, Maximilian Landgraf, Jörg Franke and Sigrid Leyendecker	Qualification of dielectric elastomer actuators as artificial muscles for highly dynamical N-DOF robot kinematics
27	Andre Rosendo, Shogo Nakatsu, Kenichi Narioka and Koh Hosoda	Toward a stable biomimetic walking: Exploring muscle roles on a feline robot
28	Tsuyoshi Saito, Naomichi Ogihara, Tomohiko Takei and Kazuhiko Seki	Inverse dynamic analysis of precision grip in the Japanese macaque based on an anatomical musculoskeletal model
29	Brian Satzinger and Katie Byl	Control of Planar Bounding Quadruped with Passive Flexible Spine
30	Kazuya Shida, Satoshi Nishikawa and Yasuo Kuniyoshi	Design and Test of Torque-Angle Relationship Control System
31	Alexander Sproewitz, Alexandre Tuleu, Mostafa Ajallooeian, Michiel D'Haene, Rico Moeckel, Jonas Degrave, Sebastien Gay, Benjamin Schrauwen and Auke Jan Ijspeert	Towards Dynamically Running Quadruped Robots: Performance, Scaling, and Comparison
32	Yasuhiro Sugimoto, Hidetaka Yoshioka and Koichi Osuka	Gait Analysis of Multi-legged Passive Dynamic Walking focused on Diagonality of the Gait
33	Takuya Umedachi, Ryo Idei, Kentaro Ito and Akio Ishiguro	True-Slime-Mold-Inspired Hydrostatic-Skeletal Amoeboid Robot Driven by Fully Decentralized Control
34	S. Danyal Yazdi Mirmokhalesouni, Maziar Ahmad Sharbafi, M. Javad Yazdanpanah and Majid Nili Ahmadabadi	Foot design for bipedal walking using HZD-based control approach

Hardware Demonstrations

No.	authors	Title
1	P. Beckerle, F. Stuhlenmiller, J. Schuy, J. Wojtusich, S. Rinderknecht and O. v. Stryk	Friction compensation and stiffness evaluation on a variable torsion stiffness
2	Ivo Boblan, Andreas Schulz, Alexej Tuchscherer, Ivan Perfilov and Björn Bertrand	A compliant universal joint cascaded to a multi-joint kinematics - Tripedale Alternanzkaskade, TAK -
3	Hugo Gravato Marques, Christophe Maufroy, Alexander Lenz, Konstantinos Dalamagkidis, Utku Culha, Maik Siee and Paul Bremner	MYOROBOTICS: a modular toolkit for legged locomotion research using musculoskeletal designs
4	Marco Hutter, Christian Gehring, Michael Bloesch, Mark Hoepflinger and Roland Siegwart	Walking and running with StarIETH
5	Karl T. Kalveram, Inna Mikkailova, Daniel Häufle and Andre Seyfarth	The MARCO robot hopper
6	Matthieu Lapeyre, Pierre Rouanet and Pierre Yves Oudeyer	Poppy: A new bio-inspired humanoid robot platform
7	Jørgen Christian Larsen and Kasper Støy	LocoKit - A robotic construction kit for developing and validating models of locomotion
8	Steven Lindley and Nick Kundu	Control of a Flying Drone via Wireless EMG and Inertial Sensors
9	Andre Rosendo, Shogo Nakatsu, Kenichi Narioka and Koh Hosoda	Toward a stable biomimetic walking: exploring muscle roles on a feline robot
10	Alexander Sproewitz, Alexandre Tuleu, Michiel D'Haene, Rico Möckel, Jonas Degrave, Massimo Vespignani, Sebastien Gay, Mostafa Ajalloeian, Benjamin Schrauwen and Auke Jan Ijspeert	Towards dynamically running quadruped robots: performance, scaling, and comparison
11	Xiaoxiang Yu, Fumiya Iida	Maximizing Energy Efficiency of the Robot Hopping based on Free Vibration

Opening Talk

Time: Monday, 11th , 09:00 - 10:00

Titel: ***Neural Control of Force: A New Perspective***

Referee: ***Carlo J. DeLuca***

Abstract: We have developed a technology that can decompose the surface EMG signal and identify the shape and firing instances of individual motor unit action potentials that contribute to the surface EMG signal with an average accuracy of 95%. Using this technology we have document a hierarchal construct of the motor-unit firing rate, whereby the firing rate of any motor unit is inversely proportional to the force at which it is recruitment. Thus, at any time and force, the firing rate of subsequently recruited greater force-twitch faster-fatiguing motor units is less than the previously recruited. This construct opposes the previously belief held for over 50 years.

Our findings have the following implications: 1) the control of motor units within a muscle is not designed to maximize the force output of a muscle, but instead it seems to have optimized some combination of force magnitude and time duration. (The control scheme is well suited for the flight-and-fight response by providing the capacity to generate force and the capacity to sustain it.) 2) As the force level increase, the variability increases. 3) It provides a greater economy of force generation during ordinary functional daily activities, such as normal walking, that require bursts of low force levels generated over short periods of time. Such activities rely on the activation of lower threshold motor units that fire faster and tetanize relatively quickly to produce force at lower levels.

When we investigated the co-activation of synergist and antagonistic muscles around a joint, we found a substantial amount of cross-correlation between the firing rates of the two muscles. This finding indicates that muscles are activated as a functional group even at the motor unit level.

The implications of these findings for designing control systems for robots that intend to mimic human based movement will be pointed out.

Keynote Talks

Time: Monday 11th, 13:30 - 14:30

Titel: ***Moving Softly: Locomotion Strategies for Deformable Animals and Robots.***

Referee: Barry Trimmer

Abstract: One approach to the design of new devices and materials is to study how problems have been solved in nature and to adapt these solutions for our own uses. This “biomimetic” approach is currently being used at Tufts to develop a new class of robots fabricated from soft materials. These soft robots will perform tasks outside the capability of current robots including climbing textured surfaces, crawling along ropes and wires and burrowing into winding, confined spaces.

Making these machines move accurately will require the application of new concepts based on neuromechanics and embodiment (morphological computation). These conceptual breakthroughs also allow for the future production of machines that are entirely biosynthetic and biodegradable and that can be grown rather than assembled.

This talk will focus on recent discoveries in the locomotion of soft animals and the application of these findings to the development of moving machines that are highly deformable. These are the early prototypes of a new type of engineering based on controlling structures built entirely of soft materials.

Time: Tuesday 12th, 09:00 - 10:00

Titel: ***Toward highly dynamic locomotion: design challenges in MIT cheetah robot.***

Referee: Sangbae Kim

Abstract: Robot designers are increasingly searching for ideas from biology. The talk will introduce such bio-inspired robots that embody the hypothesized principles from the insights obtained by animal studies. Through these examples, the intricate processes of design principle extraction will be discussed. Current research in the MIT biomimetics lab is centered on the development of a cheetah-inspired running robot. Three major associated research thrusts are optimum actuator design, biotensegrity structure design, and the impulse-based control architecture for stable galloping control. Each research component is guided by biomechanics of runners such as dogs and cheetahs capable of the fast traverse on rough and unstructured terrains.

Time: Thursday 14th, 09:00 - 10:00

Titel: ***Emergence of social adaptability in insects.***

Referee: Hitoshi Aonuma

Abstract: The emergence of social adaptability must be common interest between biologists and robotics engineers. In animals, social interaction is important factor for the decision making of behaviors. In order to understand how animals alter their behaviors on the demand of changing social environment, I have focus on aggressive behavior in insects. It is widely observed in animals that dominant hierarchy is established by agonistic behavior, through the complex interaction among physiological, motivational, and behavioral systems. Crickets exhibit intensive aggressive behavior when one encounters another male. The battle starts out slowly and escalates into a fierce struggle to establish dominant-subordinate relationship. We have investigated the neuronal mechanism underlying cricket aggressive behavior. Pharmacological experiments suggest that nitric oxide signaling mediates octopaminergic system in the brain, which in turn mediates aggressive motivation. Based on the results of experiments, we established dynamic behavior models and neurophysiological models to understand the mechanisms of social adaptability. We hypothesize that important mechanism underlying behavior adaptability is a multiple feedback structure that is composed of feedback loop in the nervous systems and through the social environment.

Tandem Talks

Time: Monday 11th, 15:30 - 17:00

Titel: ***Unraveling unrestrained locomotion: (1) natural statistics of steps and patterns and (2) system identification of feedback control.***

Referees: Noah Cowan and Volker Dürr

Time: Wednesday 13th, 09:00 - 10:30

Titel: ***Role of Passive Properties in Producing Adaptive Motion in Robotic and Biological Systems***

Referees: Manny Azizi and Dai Owaki

Abstract: Locomotor control is not limited to the commands of the central nervous system. The physical interactions between the body and the external environment play a crucial role in generating adaptive motion in biological and robotic systems. These interactions are often mediated by the passive mechanical properties of a moving body and define a set of intrinsic control mechanisms.

In the field of Biology, passive mechanical properties have been shown to be the first line of defense against destabilizing perturbations allowing biological systems to self-correct without nervous input. In addition, variation in the mechanical properties of muscles and tendons can determine the boundaries of locomotor performance in human and animal systems. Based on these biological findings, Pfeifer et al. have coined the term “morphological computation” to describe how the physical properties of the body provide a passive control mechanism in moving robots. Many researchers have demonstrated the potential of morphological computation for the generation of stable and versatile behavior in robotic systems.

In this tandem talk, we will discuss how passive properties in biological and robotic systems determine posture, gait and stability during locomotion.

Time: Thursday 14th, 16:30 - 18:00

Titel: ***Leg design and control for stable locomotion.***

Referees: Koh Hosoda and Monica Daley

Abstract: There are roughly two approaches for understanding bipedal locomotion: starting from observation of bipedal animals and from constructing and controlling of bipedal robots. In this tandem talk, Dr. Daley will discuss inferences about control of bipedal locomotion from observations of birds' behavior. She will introduce a simple bio-inspired leg control policy that has emerged from these observations. Prof. Hosoda will then talk about constructive approach toward understanding bipedal locomotion. He will introduce several muscular-skeletal biped robots imitating biological systems. Finally, they will conclude the talk discussing on simplification of the controller based on appropriate morphological design, and on understanding of the adaptability of the bipedal locomotion.

Public Lecture

Time: Wednesday 13th March, 18:30 - 20:00

Titel: ***Orchestrating Movement through Complex Terrain: Interactions between Brains and Local Neural Circuits***

Referee: Roy Ritzmann

Abstract: Animals provide remarkable models for elegant movement through extremely complex terrains. Robotics seminars often begin with envious video of mountain goats jumping around hill sides and insects moving seamlessly around numerous barriers to a goal. AMAM is unique in its serious attempt to bring together biologists who study these behaviors and roboticists who are trying to capture this kind of movement in their devices. The benefits of robots that could move with animal-like behavior are readily apparent. However, much of the work that is done in the field breaks the problem into smaller units. We see fabulous work on legged movement generating algorithms for stability and efficient propulsion but ignoring the role of higher centers. At the other extreme wheeled vehicles are connected to sensors that allow navigation around barriers but without the benefits of legs. Biologists likewise focuses upon small subsets of the problem. Neurobiologists have made great progress examining local control in spinal cords or thoracic ganglia by eliminating or ignoring descending brain control and restricting movement to a small subset of actions on a treadmill or a narrow track or studying rapidly moving behaviors that may occur with limited sensory intervention. Such research is clearly important and has been very successful in making progress in both fields. But at some point, we must consider the interactions between higher centers and local control that is necessary for the elegant movements that roboticists seek to capture. The issue is similar to progress made by an orchestra working on complex musical pieces. Individual sections must work on their own to reach proficiency on their passages. But the symphony only reaches its full potential when all the parts are brought together with all the complex interactions that make it wonderful.

In this talk, I will discuss the differences in behavior that occur in insect locomotion when brain circuits are present or absent and then describe the research that our laboratory is conducting to understand how these brain circuits function and interact with local control systems that include the reflexes and pattern generators of the thoracic ganglia to produce the kinds of behavior seen in those initial videos. The ultimate goal is both to understand the neural properties that underlie complex behavior and to generate the kinds of robotic control that would capture those behaviors with minimal external control from a driver.

Tutorials

Time: Monday 11th March, 17:30

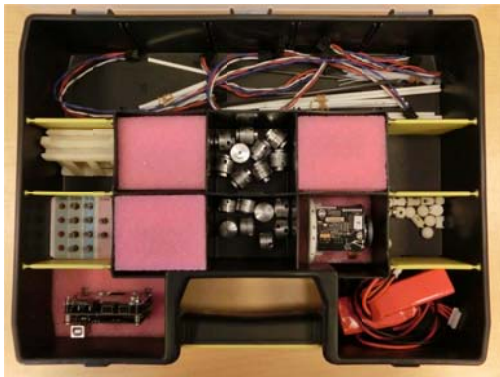
Titel: LocoKit - robotic construction kit for legged locomotion

Referee: Jørgen Christian Larsen

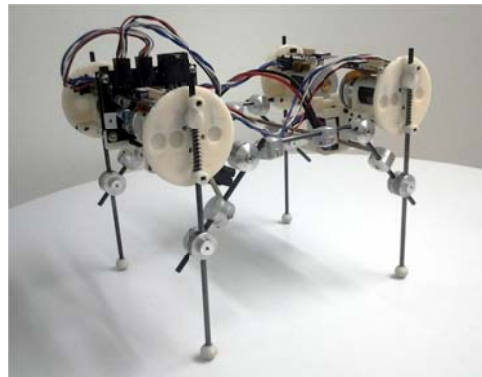
Abstract: It is common to observe locomotion in animals and based on these observations develop hypotheses and models of locomotion. However, it is difficult and time consuming to obtain observation data due to practical and ethical issues. In addition, verification of the developed models is difficult in particular when it comes to verifying the completeness of a model. LocoKit is an alternative tool researchers can use to understand locomotion. LocoKit allows researchers with no background in mechanics, electronics, or programming to build robotic models of locomotion. A robotic model complements the other approaches by being complete since there is no cheating in the real world.

At this tutorial you will first be introduced to the LocoKit construction kit, to see what it is capable of doing. In the second half you will have the possibility to get to work with the system on your own. You will be getting a pre-configured quadruped robot build from LocoKit, on which you will have to optimize various parameters to get it to walk/run as fast as possible. In the end of the tutorial we will have a competition where the fastest robot wins.

To be part of the tutorial you will only need to bring your laptop and you will connect to the robot through a standard wifi connection. If anything else is needed we will provide it at the tutorial.



The LocoKit toolbox



Robot build from LocoKit

Time: Wednesday 13th March, 11:00

Titel: Hybrid Zero Dynamics Control of Legged Robots

Referee: Ioannis Poulakakis

Abstract: The combined difficulties of hybrid dynamics and underactuation inherent in legged robots render the direct application of nonlinear controller synthesis tools to these systems a challenging task. To resolve complexity, the idea of task encoding through the enforcement of a lower-dimensional target dynamics (rather than through the prescription of a set of reference trajectories) has been employed in the relevant literature. Along these lines, the Hybrid Zero Dynamics (HZD) method was proposed as a systematic way to design control laws for legged robots with provable stability properties. In essence, this method "embeds" walking and running gaits in the dynamics of a legged robot by defining a set of (holonomic) output functions with the control objective being to drive these outputs to zero. The goal of this tutorial is to introduce the audience to the concepts that underlie Hybrid Zero Dynamics and its application to the control of walking and running robots. A broad range of models will be considered, and theoretical aspects as well as implementation details will be discussed.

Oral Presentations

Human leg adjustment in perturbed hopping

Maziar A. Sharbafi* and Andre Seyfarth*

* Locomotion Laboratory, TU Darmstadt, Darmstadt, Germany

{seyfarth, sharbafi}@sport.tu-darmstadt.de

1 Motivation

Robots can help to demonstrate and prove concepts on human locomotion such as concepts based on springlike leg behavior. Hopping is a fundamental requirement for running in two basic functions: bouncing and balancing. In addition, for robust hopping against perturbations, swinging the leg in flight/swing phase is observed. These three elements need to be integrated for stable/robust locomotion in bipeds. Unlike running [1] and walking [2], stable hopping cannot be achieved with a fixed angle of attack with respect to the ground. So, finding an appropriate leg direction during the flight phase is needed for stable hopping in place. In this study, different methods of leg adjustment during swing phase are compared both in simulation with SLIP (Spring Loaded Inverted Pendulum) model and in human experiment. Because of the lack of space and since we reported the simulation results previously [3], in this paper, it is just reported with a few sentences. Our presented method called VBLA (Velocity Based Leg Adjustment) shows better performance in modeling and is also closer to what humans do.

2 Methods

Most leg adjustment strategies rely on sensory information about the CoM velocity, following the Raibert approach [4] in which the foot landing position is adjusted based on the horizontal velocity (for example [5])

$$x_f = \frac{v_x T_s}{2} + k(v_x - v_x^d) \quad (1)$$

in which x , v_x and v_x^d are the horizontal position, speed and desired horizontal speed of the Center of Mass (CoM), re-

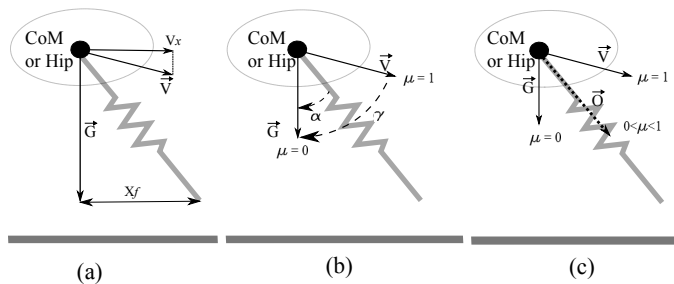


Figure 1: Different leg Adjustment approaches. a) Raibert method, b) Peuker approach c) VBLA.

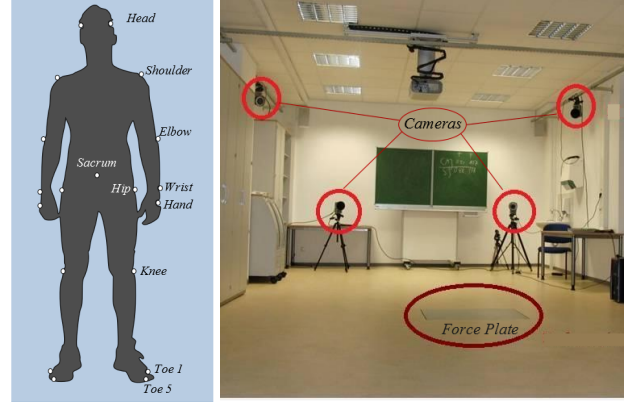


Figure 2: Experimental setting. Left: marker positions, right: lab setup

spectively. Also, k is a control constant and T_s is the stance time. The output of this controller is the horizontal distance between the desired foot point at Touch Down (TD) and hip point named x_f (see Fig. 1(a)). For hopping, where $v_x^d = 0$, Eq. (2) converts to $x_h = \mu v_x$ (for hopping the stance time is fixed and we can have a constant μ).

Recently, various strategies were investigated by Peuker et al. [6] who concluded that leg placement with respect to both the CoM velocity and the gravity vectors yielded the most robust and stable hopping and running motions with the SLIP model. Defining the angles of the gravity vector with the velocity vector and leg orientation by γ and α as shown in Fig. 1, this method gives the leg orientation by $\alpha = \mu \gamma$, where μ is a constant between 0 and 1. A modified version of this strategy, called VBLA, is presented [3]: the leg direction is given by vector \vec{O} , a weighted average of the CoM velocity vector \vec{V} and the gravity vector \vec{G} . The weight of each vector is determined by coefficient $0 < \mu < 1$ (see Fig. 1(c)). Unlike Peuker's approach which just consider the angle of velocity vector, in VBLA, both direction and angle of the velocity vector affects the desired leg direction

$$\begin{aligned} \vec{V} &= [v_x, v_y]^T; \vec{G} = [0, -g]^T \\ \vec{O} &= \mu \vec{V} + (1 - \mu) \vec{G} \end{aligned} \quad (2)$$

In all methods, when $\mu = 0$, the leg is exactly vertical and in the two recent ones, the leg is parallel to the CoM velocity vector for $\mu = 1$.

3 Results

It is analytically proved for SLIP model that with proper selection of μ in VBLA the dead beat response is achievable. Thus, with this approach it is possible to remove all perturbations at most in two steps. The perfect results of applying this method beside VPPC (Virtual Pendulum Posture Controller) to SLIP model with upper-body (called TSLIP for Trunk+SLIP) are reported in our previous work [3].

We did an experiment to investigate which method approximates to human leg adjustment best. In this experiment, the subject hops in place with arms akimbo and suddenly a perturbation occurs at apex by pushing him/her from behind. The pushing point is near sacrum which is an approximation of CoM. The kinematic behavior of the body is derived using markers shown in Fig. 2. We use a force-plate to measure GRF during stance phase. CoM motion was obtained by integrating the GRFs twice. Initial values for velocity and position of CoM were obtained from the sacrum position [7]. The markers positions, cameras and the force-plate are shown in Fig. 2.

To evaluate the aforementioned methods, the velocity at touch down and the leg orientation (the vector from the CoM to the foot contact point with the ground) are detected. In order to approximate μ in different approaches, two parameters (assume a and b) are computed and then a least square approximation is used to find μ such that $a = \mu b$. In Raibert approach, $a = x_f$ and b is the horizontal velocity. For the second approach, $a = \alpha$ and $b = \gamma$. Finally, from (3) for VBLA $a = n$ and $b = m$ are obtained by

$$\begin{aligned} \frac{O_y}{O_x} &= \frac{\mu V_y - (1-\mu)g}{\mu V_x} \Rightarrow \\ \underbrace{gO_x}_n &= \underbrace{\mu(O_x V_y + gO_x - O_y V_x)}_m \end{aligned} \quad (3)$$

All these parameters and their linear estimations are plotted in Fig. 3. VBLA has the best fitting to the data which describes the human leg adjustment by a fixed value of μ . In addition, Table. 1 shows the statistical information about these data. The maximum R^2 index (for correlation) and the minimum variance correspond to VBLA. The closer R^2 correlation index to one, the better fitting of data points to a line. This value is about 0.95 for VBLA, showing an appropriate matching of the data to this method. At each TD moment, related μ is also obtained by a/b and then the variance of these values are computed.

4 Discussion

The VBLA shows the best performance of leg adjustment for perturbed hopping in simulation of SLIP model. The ability of this method to converge from any point in the

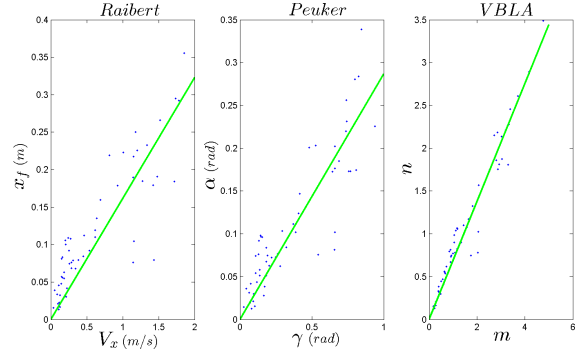


Figure 3: Fitting data to a line. From left to right Raibert, Peuker and VBLA approaches.

region of attraction to the limit cycle of the periodic vertical hopping is provable. In this paper, its validity for human hopping is investigated. The proposed method fits perfectly to the human experiment data which is shown by correlation and variance computation. This method can also be evaluated for running. Application of this approach in addition to a stance phase control schemes can be evaluated for more complex models.

5 Format

We prefer to present this paper as an oral presentation.

References

- [1] A. Seyfarth, H. Geyer, M. Guenther, and R. Blickhan, "A movement criterion for running," *Journal of Biomechanics*, vol. 35, no. 5, pp. 649–655, 2002.
- [2] H. Geyer, A. Seyfarth, and R. Blickhan, "Compliant leg behaviour explains basic dynamics of walking and running," *Proc. Roy. Soc. B*, vol. 273, no. 1603, pp. 2861–2867, 2006.
- [3] M. A. Sharbafi, C. Maufroy, A. Seyfarth, M. J. Yazdanpanah, and M. N. Ahmadabadi, "Controllers for robust hopping with upright trunk based on the virtual pendulum concept," in *IEEE/RSJ International Conference on Intelligent Robots and Systems (Iros 2012)*, 2012.
- [4] M. H. Raibert, *Legged Robots that Balance*. MIT Press, Cambridge MA, 1986.
- [5] A. Sato, "A planar hopping robot with one actuator: Design, simulation, and experimental results," 2004.
- [6] F. Peuker, C. Maufroy, and A. Seyfarth, "Leg adjustment strategies for stable running in three dimensions," *Bioinspiration and Biomimetics*, vol. 7, no. 3, 2012.
- [7] S. A. Gard, S. C. Miff, and A. D. Kuo, "Comparison of kinematic and kinetic methods for computing the vertical motion of the body center of mass during walking," *Human Movement Science*, vol. 22, pp. 597 – 610, 2004.

Table 1: Different approaches statistical characteristics

Method	μ	R^2 index	Variance
Raibert	0.1614	0.6753	0.0182
Peuker	0.2865	0.763	0.0248
VBLA	0.6881	0.9486	0.0162

A Novel Design Approach and Operational Strategy for an Active Ankle-Foot Prosthesis

S. Böker^{1,2}, P. Beckerle^{2,3}, J. Wojtuszczyk^{2,4}, and S. Rinderknecht^{2,3}

¹ *sabine.boeker@stud.tu-darmstadt.de* | ² Technische Universität Darmstadt, Germany

³ Institute for Mechatronic Systems in Mechanical Engineering, *lastname@ims.tu-darmstadt.de*

⁴ Simulation, Systems Optimization and Robotics Group, *lastname@sim.tu-darmstadt.de*

1 Introduction

In order to enable lower limb amputees to regain natural and versatile walking patterns, the development of active ankle-foot prostheses is required. During locomotion, above-knee amputees show a lower walking speed for keeping the energy effort in the range of non-amputee walking [2]. To avoid this, prostheses with adaptable characteristics and the possibility to store and reuse energy can provide advantages like more dynamic locomotion and secure operation on uneven terrains without increasing the user's energy effort. Using an actuated prosthesis, a supporting torque can be applied to the ankle joint and thus enable users to walk with less energy effort. By this, such components might also protect amputees against medical consequences due to compensation movements [1].

2 State of Art

The large majority of commercially available foot prostheses are passive prostheses with a fixed angle between shank and foot [3]. The applied elastic elements like carbon springs are designed for a basic adjustment to uneven terrain and a partial recuperation of energy during a gait cycle. Further, the mechanical characteristics can be customized by design, e.g. by splitting those springs to support eversion or inversion motions. Semi active foot prostheses do not support users with direct actuation, but are able to adjust position or characteristics of the foot and thus can reduce energy effort and provide more natural gait patterns. Currently, there are two active ankle foot prostheses coming into the market: The iWalk BiOM [4] and the Springactive Odyssey [5]. Further, active prosthetic ankle joints are developed in academic research projects such as the AMP Foot 2.0 [6]. Those prostheses support locomotion with a motor spring complex. While most active approaches use a serial elastic actuator (SEA) composed of a motor, gears to transform rotational into translational motion, and springs, parallel setups of spring and actuator can also be applied.

3 Concept

In [1] it is shown that the creation of a natural walking pattern requires variable ankle stiffness, energy storage as well as active support synchronized with individual gait.

The authors' concept to achieve these goals is given in Figure 1.

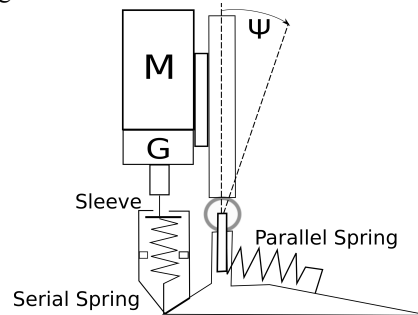


Figure 1 Mechanical setup of the ankle-foot prosthesis

The drive train consists of two DC motors with a power of 90W and a continuous torque of 0.2Nm. Two ball screws with gear ratios of 6283 are attached to the motors to transform the rotational motion of the motor's shaft into a translational motion of the screws. The lower ends of the screws are connected to two parallel extension springs placed in a sleeve. Each spring can be loaded with 739N and has a maximal extension of 18mm. In the sleeve two mechanical stops limit the maximal extension of the springs. With the lower mechanical stop, the actuator and gears are able to bring a force on the heel without compressing the extension springs, which might result in a damage of those. The upper mechanical stop protects the springs from increased tensile loads. Parallel to the SEA the so-called parallel spring is installed. For implementation, the parallel spring can be realized by two parallel springs with equal dimensions and stiffness. The springs are connected to the foot and to the drives that are fixed on the shank. During dorsiflexion, energy is stored by elastic deformation of the spring due to the angle deviation between shank and foot. Beyond the angle range from -5° to $+10^\circ$, the spring is inactive due to the kinematics design of the foot. For this, a conventional low-profile carbon device with a split toe is proposed. The split toe enables the device to fulfill an inversion or eversion motion and to adapt on uneven surfaces. For visualization a conceptual CAD-Model is shown in Figure 2. The serial springs are invisibly located in the blue dyed sleeve.

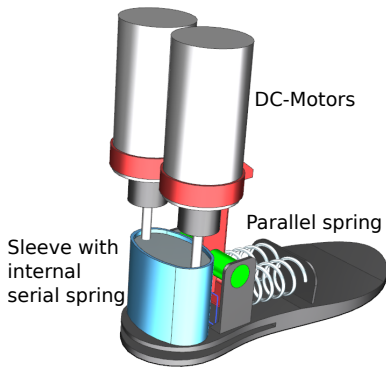


Figure 2 CAD-Model of the ankle-foot prosthesis

4 Operational Strategy

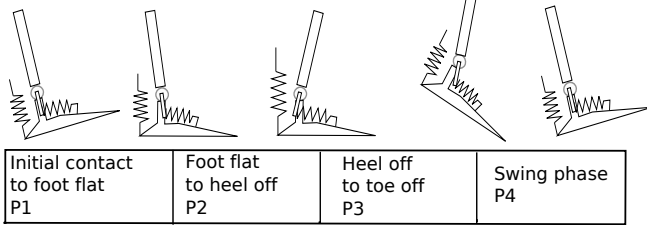


Figure 3 The operational strategy

Figure 3 shows the prosthetic foot in different moments of the gait cycle. In P1 a negative torque is created around the ankle joint axis by the ground reaction forces. The torque will rotate the foot from initial contact to foot flat. During P2 the sign of the external torque switches from negative to positive because the body is moving in walking direction over the on the standing foot. In P2, the parallel spring extends due to the angle deviation between foot and shank and hereby creates a negative torque around the joint axis. The serial spring is extended through the motors and creates a negative torque. At the end of P2, the torques created by the springs are equal to the external torque and the bodyweight is held due to the extensions of both springs. Hence, parallel and serial spring store energy in form of elastic deformation energy. P3 follows with a positive external torque around the ankle joint. In order to support locomotion, the torque created by the parallel and serial spring must be greater than the external torque. This is accomplished by a further tensile load of the serial spring introduced by the motor. The sum of all torques -the external torque and the torques created by the springs- is negative so that the heel starts to rise from the floor. In this phase the parallel spring is deactivated by a sliding mechanism as soon as a compression load acts on it. In the swing phase no external torque appears due to the missing contact to the ground. In this phase, the mechanical stops in the sleeve are used to provide forces on the heel and bypass the serial spring. Hereby, a positive torque around the joint axis rotates the foot to a right angle relative to the shank.

5 Results and Discussion

To survey the design concept and operational strategy, simulations of the system dynamics are conducted based on measured data from human walking [7]. In the simulation environment the shank is fixed and the foot acts like a pendulum around the lower end of the shank. To ensure a realistic simulation, joint angles are used as desired trajectories, while an external torque is introduced to model the floor reaction forces. The system is modeled by two equations of motion: One representing the drive sided dynamics and one depicting the foot mechanics. The angle ψ between foot and shank is the controlled variable of the system and is compared to the reference angle. The output of the controller represents the motor torque. In the left part of Figure 4 the angle of the ankle-foot prosthesis and of the human data is presented. Here, the trajectory provided by the proposed prosthesis deviates only slightly from human data. The variation at the end of P2 and beginning of P3 implies that the angle between shank and foot is greater than the human data. The required mechanical power, given in the right part of Figure 4 shows the ankle power of the prosthesis and of the human data. The peak appears at the time of push off, in which the prosthesis mimics the catapult effect and thus the propulsion in walking direction. In comparison to the human data the variations occur because the prosthesis mimics the human walk but has a different assembling i.e. the mechanical stops. The simulation is a first and good approach to verify that the design connected with the operational strategy is able to mimic human gait.

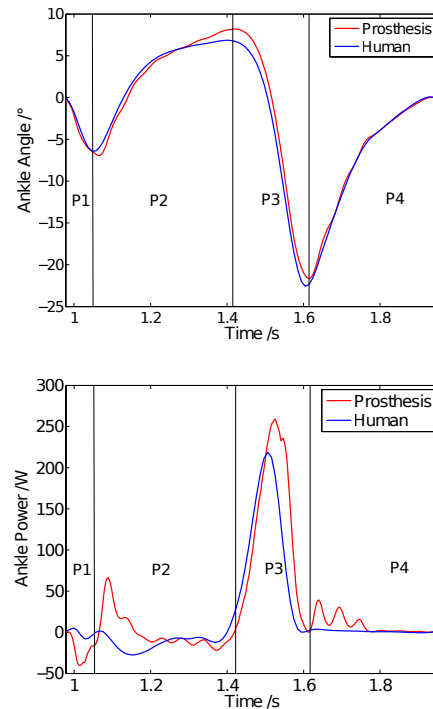


Figure 4 (a) the ankle angle; (b) the ankle power

6 Conclusion

The main innovation of the proposed concept is the interaction of the SEA with a partially active parallel spring, which is used for energy storing and for creating a counter torque to the external torque. In contrast to existing concepts using a parallel spring as the one in [1], this spring is designed to exploit stored energy specifically. The energy is stored during P2 and used to support the actuators during P3. The force applied by motors to the heel during P2 is decreased because the parallel spring creates up to 25% of the required ankle torque. The peak motor torque in simulation exceeds the nominal motor torque for a negligible period of time. This might be provided by overloading the drives. The simulations reveal that it is possible to nearly imitate the biomechanical model with a realistic power requirement using a PID controller. In reality, the control strategy should be extended to a hybrid control system with a position and force controller for realization and better usability.

7 Open Questions

Further simulations should consider the interaction of human and prosthesis by applying more enhanced human model. Regarding the motor torque, the overloading capabilities of the drives have to be considered for implementation.

References

- [1] S. K. Au, et. al.: An Ankle-Foot Emulation System for the Study of Human Walking Biomechanics, in IEEE ICRA 2006.
- [2] R. L. Waters, et. al.: Energy cost of walking of amputees: the influence of level of amputation ,1967
- [3] R. Versluys, et al.: From conventional prosthetic feet to bionic feet: A review study, in IEEE BioRob, 2008
- [4] <http://www.iwalkpro.com/Prosthetists.html>
- [5] <http://www.springactive.com/odyssey.php>
- [6] P. Chelle, et al.: The AMP-Foot 2.0: Mimicking intact ankle behavior with a powered transtibial prosthesis, in IEEE BioRob, 2012
- [7] S. Lipfert: Kinematic and dynamic similarities between walking and running, 2010

A Compliant Lightweight Universal Joint Cascadable to a Multi-joint Kinematics - Tripedale Alternanzkaskade, TAK -

Ivo Boblan*, Andreas Schulz*, Alexej Tuchscherer*,
Ivan Perfilov* and Björn Bertrand**

*Control System Group, TU Berlin, Berlin, Germany
{boblan, schulz, tuchscherer, perfilov}@control.tu-berlin.de

**Weißensee Kunsthochschule Berlin, Berlin, Germany
bjoernbertrand@gmx.net

1 Motivation

In the development of robotic assistance systems with safe human-robot interaction for flexible personal and industrial applications size, weight, redundancy and compliance play an important role. For a redundant multi-joint kinematics with long range, high payload and variable resilience the elephant's trunk is the ideal biological role model. The elephant's trunk is a continuous kinematics which has no traditional joints of bones. It is a muscular hydrostat which can multiple bend in different directions over the entire length by longitudinally disposed muscle packets.

2 State of the Art

Present industrial articulated robots are manipulators, which are rigid multi-body systems with revolute joints driven by inherent stiff electric motors. The simple dynamics is bought with heavy weight and large construction space [1-2].

Under the heading trunk, worm, snake or more generally continuous or hyper-redundant kinematics many solutions are known. Some developments from the past named continuum robots [3-6] begin to make use of the operating principle of the elephant's trunk [7-11] and some show first technical applications up to commercial products [12-13]. The field of application is limited generally to the conduct of a tool or a camera in an inaccessible object.

The continuum manipulator OctArm replaces the serial chain of rigid links in conventional manipulators with smooth, continuous, and flexible links. OctArm generally based on the principle of a trunk driven by antagonistic pneumatic muscles, but is more of a hook than a manipulator [14-16]. The Rice and Clemson Universities have developed a trunk like kinematics based on a centrally located rubber backbone which acts as counterforce to a cable actuation system driven by electric motors [17-19]. The also tendon driven Air-Octor furthermore regulates its stiffness by pneumatic pressure [20].

The British company OCRobotics has developed snake-arm robots based on a skeleton with cable as a commercial product.

The nearly simultaneously developed trunk kinematics "Serielle Modularkinematik" SMK from the German Fraunhofer Gesellschaft IFF is equipped with local electric motors and thus not inherently compliant, can only bend to about 60 degrees, move only a few 100 grams payload and the motion speed is limited by screw jacks [21-22]. The snake like robot from the Carnegie Mellon University [23] and the redundant chain robot HRCR from the Bernstein Center for Computational Neuroscience [24] are also more suitable for inspection tasks than for manipulation of payload.

By closer look all approaches have an articulated basic structure. This is clearly visible in approaches with servo motors such as the great manipulator EMMA from GreyPilgrim [25] used in nuclear power plants. By the rigid elements with servo motors except the high number of degrees of freedom is retained none of the above advantages of the trunk kinematics.

The outstanding trunk kinematics "Bionic Handling Assistant" from the German company Festo is a demonstrator for lightweight by additive manufacturing and compliance but is not designed for precision and payload [26].

A continuum manipulator inspired by real properties of an elephant's trunk like radius of action, payload, compliance and speed of motion does not exist.

3 Contribution

The idea presented here is to combine a 3 fluidic muscle driven universal joint with lightweight construction by new materials. By the special design this joint can be connected not only in series but also alternate cascaded into each other to save manipulator length at the same amount of flexion. It can be stated that the more lightweight the single joint is built and the stronger the further up joints are designed, the more can be cascaded to a continuous manipulator.

Our modular joint named segment consist of two parts named bones which are connected via a universal joint

with each other and are tilted by three fluidic muscle actuators against each other. The lower bone of a segment is the upper bone of next distal segment and so on. This cascading leads to a smaller manipulator length with the same number of degrees of freedom.

The lever arms of the bones for the connecting muscle actuators are made of polyamide 12 (PA12) [27] in the laser sintering process (SLS) [28] and strengthen with spring steel reinforcements similar to ferroconcrete [29]. The upper side of the arms is additionally reinforced by a tension belt made from carbon and the shape of the lower side is optimized for notch stress free [30] (Figure 1).

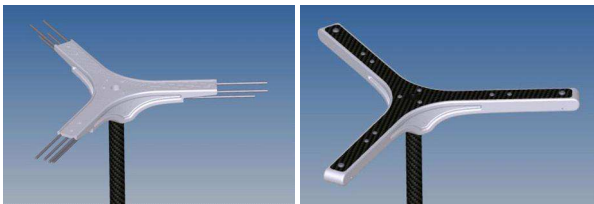


Figure1 Build-up of a bone with spring steel reinforcements (left) and with an upper carbon tension belt and lower optimized shape (right).

Not only is the lower side of the lever arms (Figure 1) optimized for notch stresses, but also the complete lever arm is analyzed for von Mises stress (Figure 2).

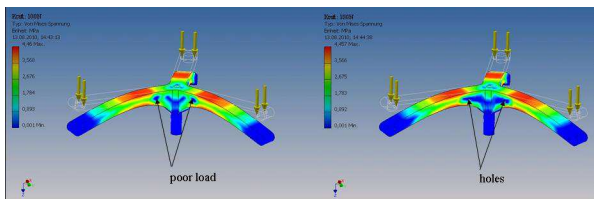


Figure2 Stress analysis where blue regions have poor load (left) and can be used to e.g. mounting holes (right).

The areas with stress peaks are marked in red and have to be reinforced. The blue marked regions are minor stress areas which do not contribute to the rigidity. In principle, these areas can be removed to save weight or to use for mounting holes to hold cables, circuit boards or sensors.

Each configuration with and without inner reinforcements, with or without tension belt and combinations is tested for break. By a fluidic muscle, the tension force on the outer lever arm is continuously increased up to 1000 N, and is measured by a force sensor (Table 1 and Figure 3).

Table 1: Specification of the pulling actuator and the force sensor used in the breaking test stand

	Name	Company	Force	Length
Actuator	DMSP-20	Festo AG	1600 N	400 mm
Sensor	KD 9363s	ME-Meßsys.	500 kg	61 mm

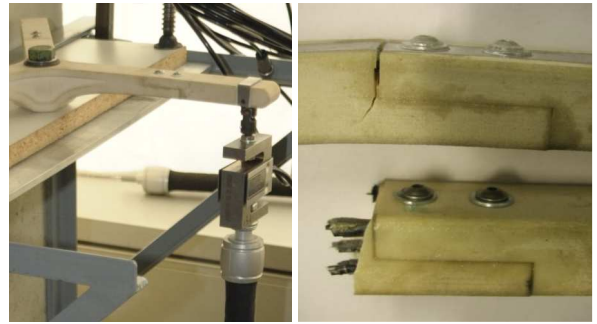


Figure3 Breaking test stand with pulling actuator, force sensor and to test lever arm (left) and breaking test example (right).

The breaking test results presented here show that the lever arm of the big star equipped with a 2 mm carbon tension belt without any reinforcements breaks at about 600 N pulling force. This is the force that can be hold solely by the polyamide 12. When equipped with 4 times 1.5 mm carbon reinforcements the breaking force increased up to about 850 N. If the arm equipped with 4 times 2.5 mm carbon reinforcements the material does not break up to a pulling force of 1000 N (Figure 4). This is the estimated maximum force that can be occurring in the segment. In our configuration we use 4 times 2.5 mm spring steel reinforcements, so we also have fail-safe feature. In case of fault the kinematics bends first before it breaks and collapses.

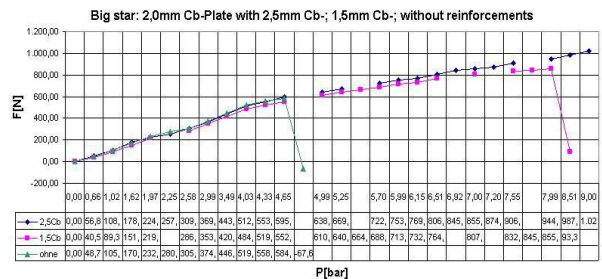


Figure4 Breaking test results of a lever arm of the big star without reinforcements (green), with 4 times 1.5 mm (magenta) and 4 times 2.5 mm carbon reinforcements (blue).

Each segment has a modular design and can be fitted with different types of muscles. In the trunk kinematics “Tripedale Alternanzkaskade” TAK version 3, both the fluidic muscles DMSP-10 from the company Festo with the maximum force of 630 N as well as DMSP-20 with the maximum force of 1500N are fitted. The next state (start not ground position) of a segment with antagonistic connected muscles all muscles are contracted about 50 % of the maximum contraction of the resting length. Only the joint can be moved, when muscles shorten and in return other muscles extend. The case that more than one muscle pulls on the lever arm with its maximum force never occurs by design.

All electronic components of each modular joint are located around the central carbon compression strut of the dorsal bone of the segment. The complete electronics are located on three printed circuit boards, which are arranged in a triangle around the strut. Two redundant designed boards containing the ARM microcontroller STM32F107R, which are supplied from the third board with voltage. The microcontrollers enable transparent segment addressing, communication with other segments via CAN bus and a logging or emergency communication via Ethernet bus. The proprietary operating system on the controllers is implemented in C/C++ and includes a dynamic and segmented memory management, semaphores for process synchronization, shared memory of the processes on a microcontroller, interrupt-driven collision detection in real-time and sensor fusion between redundant sensors. Each segment gets its target angles, joint stiffness, controller structure and control parameters from an external path planning via CAN bus. The segments operate independently from each other, but the control parameters take into account the respective position in the chain.

The current version 3 is equipped with both muscle types DMDP-20 and DMSP-10. The bulky muscles DMSP-20 of the upper 4 segments are driven by proportional valves in order to realize a good positioning accuracy and low noise. The smaller muscles DMSP-10 of the lower 4 segments are driven by light switching valves in order to realize a wide range of motion and sufficient payload. The following Table 2 shows the main differences of the two valve types.

Table 2: Characteristics of the two used valve types

	proportional	switching
Name	PVQ	MH1
Manufacturer	SMC	Festo
Muscle type	DMSP-20	DMSP-10
Noise emission	low	high
Valve function	2/2	3/2
Nominal flow rate	100 l/min	10 l/min
Weight	80 g	10 g
Hysteresis	10 %	-
Cut-off frequency	no information	20 Hz
Control	0-180 mA	PWM
Dead zone	± 54 mA ($\approx 30\%$)	± 1.2 V ($\approx 5\%$)

Each segment requires only 5 V for electronics, 24 V for the pneumatic valves and compressed air from the outside to be able to work autonomously and independently.

All construction details together lead to a very lightweight, but stable and sufficiently rigid kinematics that can withstand the high tensile force of the fluidic muscle actuators of approximately 1000 N (Figure 5).



Figure 5 Part of the biomimetic trunk kinematics "Tripedale Alternanzkaskade" TAK as CAD drawing of two segments (left) and photograph of a segment in the chain (right).

The main performance parameters of the current version 3 of the TAK consist of 8 segments and 16 degrees of freedom can be found in Table 3.

Table 3: Performance parameters of the TAK v3

Target speed normal/max.	250 mm/sec	1000 mm/sec
Position-/repeat accuracy	± 15 mm	± 5 mm
Handling/max. payload	500 g	2000 g
Power stand-by/operation	10 W	50W+air

4 Discussion

Robotic systems are rated according to their capabilities such as motion speed, payload, positioning accuracy as well as energy consumption and costs. These properties are primarily determined by the used **materials and structures** as well as actuators. Light in the fast laser sintering process produced solids (e.g. polyamide) combined with selected materials with special mechanical properties (e.g. spring steel) positioned in the right places in the solid (e.g. in the distribution of forces) can not only reduce production costs but also open up new fields of application. The better the requirements can be quantified, the better the kinematics can be aligned and optimized in that effect.

The changing of the **joint stiffness** can be achieved in certain areas independent of the joint position by the simultaneous actuation of all muscles (co-contraction). Thus, the impedance can be adjusted over the entire length of the trunk to the surrounding environment.

When multiple segments are connected to a redundant kinematics, the supernumerary **degrees of freedom** for the path planning objectives as an energy-optimal position in space can be used. The maximum achievable angle over the entire length of the trunk can be optimized over the degree of cascading of the segments, the position of the universal joint along the central compression strut and the length of the lever arms. With currently 8 segments, the

TAK bend to about 135 degrees. The present combination of materials and the thus achieved weight per segment allows a maximum cascading into each other of up to about 12 segments.

By design, the **positioning accuracy** depends only on the stiffness of the central pressurized components and not of the lever arms of the muscles. A potential in lightweight unavoidable bending of the lever arms of the muscles only leads to a reduction in the effectiveness of muscle contraction. By function, the positioning accuracy depends mainly on the minimum adjustment of the used valves and the resolution of the sensors.

A redundant trunk kinematics is a **multivariable control system** with couplings. These couplings have to be modeled, so that the controllers of each segment can take into account e.g. the appropriate weight per lever arm.

The trunk kinematics TAK is designed for use both in the automated assembly as well as in households.

References

- [1] Spong, M.W. and M. Vidyasagar: Robot Dynamics and Control. John Wiley & Sons, 1989.
- [2] Sciavicco, L.; Siciliano, B.: Modelling and Control of Robot Manipulators, 2nd Edition, Springer-Verlag Advanced Textbooks in Control and Signal Processing, p. 378, 2005.
- [3] Anderson, V.C. and R.C. Horn: Tensor Arm Manipulator Design. In ASME Paper 67-DE-57, 1965.
- [4] Chirikjian, G.S.: Theory and Applications of Hyperredundant Robotic Mechanisms. Ph.D. thesis, Department of Applied Mechanics, CaTech, 1992.
- [5] Robinson, G. and J.B.C. Davies: Continuum Robots - A State of the Art. In Proc. 1999 IEEE Conf. on Robotics and Automation, pp. 2849-2854, 1998.
- [6] Wilson, J.F. et al.: Flexible Robot Manipulators and Grippers: Relatives of Elephant Trunks and Squid Tentacles. In Robots and Biological Systems: Towards a New Bionics?, pp. 474-494, 1993.
- [7] Hirose, S.: Biologically Inspired Robots. Oxford University Press, 1993.
- [8] Cieslak, R. and A. Morecki: Elephant Trunk Type Elastic Manipulator - A Tool for Bulk and Liquid Type Materials Transportation. In Robotica, Vol. 17, 1999, pp. 11-16.
- [9] Hannan, M.A. and I.D. Walker: Kinematics and the Implementation of an Elephant's Trunk Manipulator and Other Continuum Style Robots. In Journal of Robotic Systems, Vol. 20, No. 2, 2003, pp. 45-63.
- [10] McMahan, W.; Jones, B.A. and I.D. Walker: Design and Implementation of a Multi-Section Continuum Robot: Air-Octor. In Proc. IEEE/RSJ Int. Conf. on Intelligent Robots and Systems (IROS), Edmonton, Canada, 2005, pp. 3345-3352.
- [11] Tsukagoshi, H.; Kitagawa, A. and M. Segawa: Active Hose: an Artificial Elephant's Nose with Maneuverability for Rescue Operation," In Proc. IEEE Int. Conf. on Robotics and Automation, Seoul, Korea, 2001, pp. 2454-2459.
- [12] Buckingham, R. and A. Graham: Reaching the Unreachable - Snake Arm Robots. In Proc. Int. Symposium of Robotics, Chicago, 2003.
- [13] Immega, G. and K. Antonelli: The KSI Tentacle Manipulator. In Proc. IEEE Int. Conf. on Robotics and Automation, 1995, pp. 3149—3154.
- [14] Pritts, M.B. and C.D. Rahn: Design of an Artificial Muscle Continuum Robot. In Proc. IEEE Int. Conf. on Rob. and Autom., New Orleans, 2004, pp. 4742-4746.
- [15] Walker et al.: Continuum Robot Arms Inspired by Cephalopods. In Proc. SPIE Conf. on Unmanned Ground Vehicle Techn.VII, Florida, 2005, pp 303-314.
- [16] McMahan, W. et al.: Field Trials and Testing of the OctArm Continuum Manipulator. In Proc. IEEE Int. Conf. on Robotics and Automation, Florida, 2006
- [17] Walker, I.D. and M.W. Hannan: A Novel Elephant's Trunk Robot. In IEEE/ASME Conf. on Advanced Intelligent Mechatronics, 1999, pp. 410-415.
- [18] Hannan, M.W. and I.D. Walker: Analysis and Initial Experiments for a Novel Elephant's Trunk Robot. In IEEE Conf. on Intelligent Robots and Systems, 2000, pp. 330-337.
- [19] Hannan, M.W. and I.D. Walker: Novel Kinematics for Continuum Robots. In 7th Int. Symp. on Advances in Robot Kinematics, 2000, pp. 227-238.
- [20] McMahan, W.; Jones, B.A. and I.D. Walker: Design and Implementation of a Multi-Section Continuum Robot: Air-Octor. In IEEE/RSJ Int. Conf. on Intelligent Robots and Systems, 2005, pp. 3345-3352.
- [21] Behrens, R. et al.: Kinematics Analysis of a 3-DOF Joint for a Novel Hyper-Redundant Robot Arm. In IEEE Int. Conf. on Robotics and Automation, Shanghai, China, 2011
- [22] Behrens, R. et al.: An Elephant's Trunk-Inspired Robotic Arm – Trajectory Determination and Control. In VDE 7th German Conf. on Robotics, Germany, Munich, 2012
- [23] Shamma, E.; Wolf, A. and Choset, H.: Three degrees-of-freedom joint for spatial hyper-redundant robots. In Mech. Mach. Theory, vol.41, pp. 170–190, Feb.2006.
- [24] Ning, K. and Wörgötter, F.: A Novel Concept for Building a Hyper-Redundant Chain Robot. In IEEE Trans.on Robotics, vol.25(6), pp.1237-1248, Dec.2009
- [25] www.designnotes.com/companion/ron/GreyPilgrimHTI.html
- [26] www.festo.com/cms/en_corp/9655.htm
- [27] Bottenbruch, L. and R. Binsack (Hrsg.): Polyamide, Kunststoff-Handbuch Band 3/4: Technische Thermoplaste. In Hanser, 1998, ISBN 3-446-16486-3.
- [28] Deckard, C.: Method and apparatus for producing parts by selective sintering. U.S. Patent 4,863,538, filed October 17, 1986, published September 5, 1989.
- [29] Nilson, A. et al.: Design of Concrete Structures. In the MacGraw-Hill Education, 2003, p. 80-90.
- [30] Baumgartner, L.; Harzheim, C. and Mattheck, C.: SKO (Soft Kill Option): The Biological Way to Find an Optimum Structure Topology. In Int. Journal of Fatigue Vol. 14 No 6, 1992, pp. 387-393.

Self-stable Bounding with a Flexible Torso

Qu Cao and Ioannis Poulakakis

Department of Mechanical Engineering, University of Delaware, USA
 {caoqu, poulakakis}@udel.edu

1 Motivation

Various robotic quadrupeds have been introduced to investigate the realization of dynamically-stable running behaviors. The majority of these platforms involve rigid, non-deformable torsos, a feature that distinguishes them from their counterparts in the animal world, which owe much of their remarkable locomotion abilities to their flexible bodies. Only a few quadrupedal robots employ torso flexibility. An early example is the planar quadruped with articulated torso introduced in the MIT's Leg Lab, [1]. Contemporary robots with flexible torso include Canid [2] and the MIT Cheetah quadruped [3]. However, only limited information on how torso bending movements affect locomotion is available in the context of these platforms.

2 State of the art

To provide insight into the leg-torso coordination mechanisms that produce quadrupedal running in the presence of a segmented torso, models of varying complexity and different actuation schemes have been proposed. In particular, bounding motions have been investigated in [4, 5] using a sagittal-plane model composed of compliant legs and a two-segment torso. In [4], the torso spinal joint was actuated, and bounding was generated via PID control loops enforcing desired values on the relative angle between the two segments of the torso. On the other hand, in [5] the torso was unactuated and compliant, and bounding was achieved by keeping the torso joint angle constant when it reaches maximum flexion and extension. Our recent work in [6] provides a systematic analysis of the conditions under which cyclic bounding motions can be generated passively. In this work, rather than focusing on motion generation in the presence of torso flexibility, we turn our attention to the local stability properties of passively generated bounding motions.

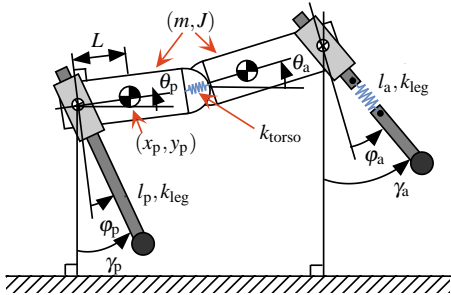


Figure 1: A sagittal-plane model with a segmented torso.

3 Our approach

The lower-dimensional, sagittal-plane model of Fig. 1 is the subject of our study. The torso comprises two identical rigid bodies connected via a torsional spring, intended to introduce flexibility. The posterior and anterior virtual legs are assumed to be massless prismatic springs.

3.1 Non-dimensional dynamics

In the non-dimensional setting, the six physical parameters $\{m, J, L, l_0, k_{\text{torso}}, k_{\text{leg}}\}$, which describe the morphology of the system, can be reduced to four dimensionless parameter groups, namely,

$$I := \frac{J}{mL^2}, \quad d := \frac{L}{l_0}, \quad \kappa_{\text{leg}} := \frac{k_{\text{leg}}l_0}{mg}, \quad \kappa_{\text{torso}} := \frac{k_{\text{torso}}}{mgl_0}. \quad (1)$$

Note that l_0 corresponds to the uncompressed length of the leg spring. The non-dimensional form of the dynamics allows us to explore systematically a much larger fraction of the solution space for various combinations of the dimensionless parameters. We concentrate on the bounding gait described in Fig. 2, which includes extended and gathered flight phases, and apply Poincaré's method. The Poincaré section is selected as the apex height in the extended flight phase, and the resulting map is

$$z_f^*[k+1] = \mathcal{P}^*(z_f^*[k], \alpha_f^*[k]), \quad (2)$$

where $z_f^* := (y_p^*, \theta_p^*, \theta_a^*, x_p^*, \dot{\theta}_p^*, \dot{\theta}_a^*)'$ and α_f^* contains the absolute touchdown angles, i.e., $\alpha_f^* := (\gamma_a^{\text{td}*}, \gamma_p^{\text{td}*})'$; see Fig. 1.

3.2 Self-stable bounding motions

A large number of fixed points has been computed for suitable initial conditions and touchdown angles. To analyze local stability, we linearize (2) at a fixed point $(\bar{z}_f^*, \bar{\alpha}_f^*)$ and compute the eigenvalues of the Jacobian $A := \partial \mathcal{P}^* / \partial z_f^*$. One of the eigenvalues of A is located at 1 reflecting the conservative nature of the system. The location of the rest of the eigenvalues depends on the values of the dimensionless parameters. Of particular interest here are the combinations of the relative torso stiffness κ_{torso} and relative leg stiffness κ_{leg} that generate bounding motions.

Fig. 3 shows how the spectral radius $\rho(A) := \max_i |\lambda_i|$ of A changes as a function of $(\kappa_{\text{leg}}, \kappa_{\text{torso}})$ keeping the rest of the dimensionless parameters constant. Note that the grey area in Fig. 3 represents the irrelevant fixed points that correspond to periodic motions with multiple torso oscillations

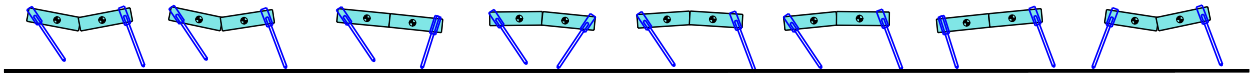


Figure 2: Snapshots of the model during one bounding cycle.

during one stride. Fig. 4(a) shows how the relative pitch $\theta_a^* - \theta_p^*$ evolves for such motions, which appear for small values of leg stiffness; clearly, a softer leg requires a relatively longer time period to go through a complete compression and decompression process during stance, allowing the torso to oscillate multiple times. We neglect such fixed points and focus on bounding motions with a single torso oscillation during one stride, as shown in Fig. 4(b). Such motions are represented by the colored-coded points of Fig. 3, in which we can see that for certain fixed points the spectral radius is equal to 1 implying that all but one of the eigenvalues are within the unit disc. This result shows that *self-stable* bounding can be generated for particular combinations of leg and torso stiffness values.

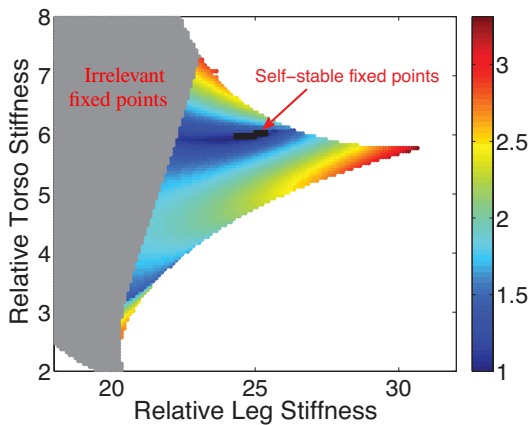


Figure 3: Fixed points computed for the same total energy, average speed and hopping height and for different values of dimensionless leg and torso stiffness. The color code corresponds to the values of the spectral radius of A .

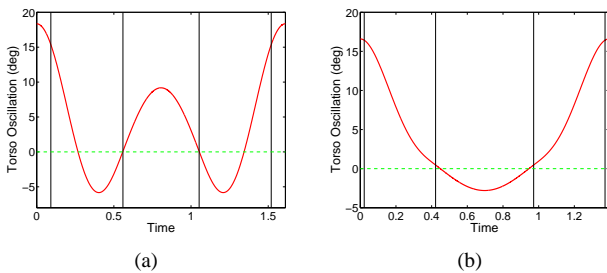


Figure 4: Torso oscillation in one stride. (a) An irrelevant fixed point. (b) A physically meaningful fixed point.

It should be emphasized that the emergence of self-stability in the presence of a flexible segmented torso is not an immediate consequence in view of the self-stable bounding orbits in quadrupeds with rigid torso as in [7]. The reason is that torso bending movements may cause divergent behavior when they are not properly coordinated with the hybrid oscillations of the legs. Also, it should be pointed out

that the domain of attraction of the self-stable fixed points is small, and the system cannot tolerate large perturbations.

4 Discussion outline

In this work, the existence and stability of bounding running gaits were studied in the context of a reductive sagittal-plane model with a flexible segmented torso and compliant legs. The relationship between the leg and torso spring stiffness was discussed, showing that a range of possible leg-torso stiffness combinations can produce stable (within a constant energy level) bounding motions. However, the ability of the system to reject sufficiently large perturbations in an open-loop fashion is limited. Currently, we work on control laws that can enhance the stability of these self-stable motions. In addition, a more complete parametric study that includes I and d is conducted to further understand how physical parameters affect the resulting motions.

5 Acknowledgment

Work supported by the ARO contract W911NF-12-1-0117.

References

- [1] K. F. Leeser, “Locomotion experiments on a planar quadruped robot with articulated spine,” Master’s thesis, Massachusetts Institute of Technology, February 1996.
- [2] G. C. Haynes, J. Pusey, R. Knopf, A. M. Johnson, and D. E. Koditschek, “Laboratory on legs: an architecture for adjustable morphology with legged robots,” in *Proc. SPIE 8387, Unmanned Systems Technology XIV, 83870W*, 2012.
- [3] S. Kim. Cheetah-inspired quadruped: High-speed locomotion platform. Sep. 17, 2012. [Online]. Available: <http://biomimetics.mit.edu:8100/wordpress/>
- [4] U. Culha and U. Saranlı, “Quadrupedal bounding with an actuated spinal joint,” in *Proceeding of IEEE International Conference on Robotics and Automation*, May 2011, pp. 1392–1397.
- [5] Q. Deng, S. Wang, W. Xu, J. Mo, and Q. Liang, “Quasi passive bounding of a quadruped model with articulated spine,” *Mechanism and Machine Theory*, vol. 52, pp. 232–242, 2012.
- [6] Q. Cao and I. Poulakakis, “Passive quadrupedal bounding with a segmented flexible torso,” in *Proceeding of IEEE/RSJ International Conference on Intelligent Robot and Systems*, Oct. 2012, pp. 2484–2489.
- [7] I. Poulakakis, E. Papadopoulos, and M. Buehler, “On the stability of the passive dynamics of quadrupedal running with a bounding gait,” *The International Journal of Robotics Research*, vol. 25, no. 7, pp. 669–687, 2006.

The contribution of kinematic synergy on feedback control of human walking

Tetsuro Funato^{***}, Shinya Aoi^{**** **}, Nozomi Tomita and Kazuo Tsuchiya^{**** **}

* Graduate school of informatics and engineering, The university of electro-communications, Tokyo, Japan
tfunato@ieee.org

** JST, CREST, Tokyo, Japan

*** Department of aeronautics and astronautics, Kyoto university, Kyoto, Japan

**** Department of energy and mechanical engineering, Doshisha university, Kyoto, Japan

1 Motivation

PROBLEM: human mechanism for managing redundancy in whole body motion

Human body is composed of a number of muscles and joints, and whole body motion, represented by walking, is produced as a result of dynamical interaction between this redundant system and environment. Human effectively uses this complex system, composed of body and environment, for conquering the diversity in the environment, but the human mechanism for managing the redundancy to produce such adaptability has not been revealed.

KEY FEATURE: kinematic correlation during motion "kinematic synergy"

Physiological studies on locomotion have shown that the actuation of joints and muscles keeps certain correlation, and statistical analyses have been extracted the correlation embedded in experimentally measured motion. Such as 7 segmental motion of whole body are constrained into 3 coordination group called "kinematic synergy".

Constraint of the motion by kinematic synergy converts the redundant body into easily controllable low dimensional system, so this mechanism is considered to reflect the characteristic of human redundant control. Therefore, it is important to reveal the contribution of kinematic synergy on walking control for understanding the adaptability of human control.

2 State of the Art

Physiological evidence of neural coordination in MOTOR and SENSORY system

Bizzi et al. showed frogs, stimulated several area in spinal cord, actuated their legs in area specific manner, and indicated that a control signal activates modules (called motor primitive) composed of plural actuators [1]. Poppele et al. [2] reported that proprioceptive information transferred through dorsal spinocerebellar tract (DSCT) coded the information corresponding to the pattern of leg orientation and length. The kinematic synergies during locomotion also correspond to the pattern of leg orientation and length [3],

thus low-dimensional sensory information contracted by the kinematic synergy is probably transferred to cerebellum.

Control structure using coordination proposed in past researches

Ting et al. [4] showed fewer individual difference of muscle synergy than individual difference of muscle activation during standing motion of cat, and indicated possible use of time series related to synergy as reference of motion control. They further proposed a control model in which neural mechanism corresponding to synergy integrated plural sensory information and control command was designed for integrated low-dimensional state variables.

3 Our approach to this question

By focusing on the knowledge that low-dimensional information corresponds to kinematic synergy [2], [3], we propose a control model in which sensory information is contracted by kinematic synergy and control command is planned on the low-dimensional space (Fig. 1). In our research, walking experiment is performed on flat and slope floor (Fig. 2). Kinematic synergy is extracted from the measured segmental motion (Fig. 3), and dynamical simulation using human kinematic synergy obtained through experiment are performed (Fig. 4). The effect of different environment on walking posture and the contribution of each

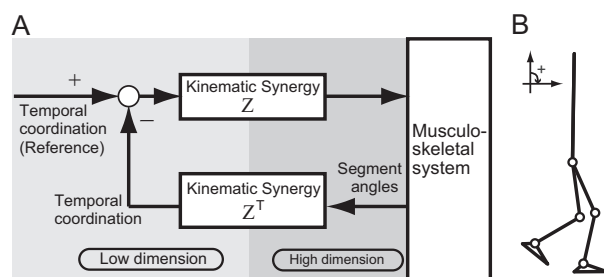


Figure 1: A: Control model using kinematic synergy. Sensory information is compressed by kinematic synergy and control is designed for the low dimensional state variables. B: The skeletal model used for simulation.

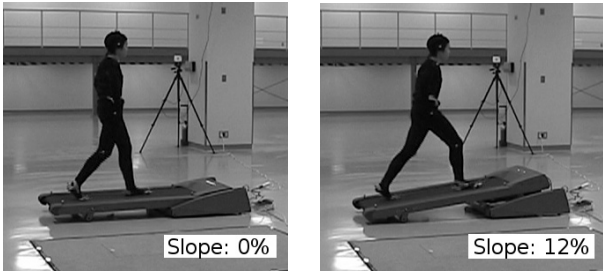


Figure 2: Measurement of kinematic data in human walking by motion capture system. Left and right figures show walking on 0% and 12% slope respectively.

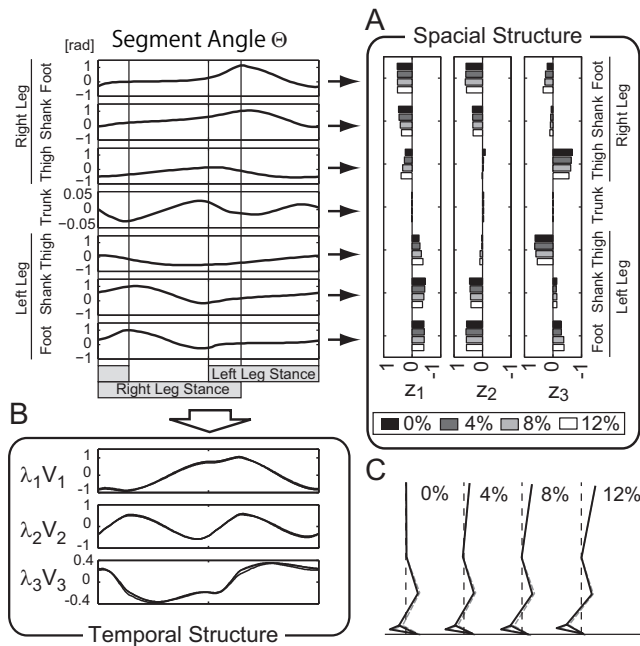


Figure 3: A: Kinematic synergies. B: Temporal coordinations. C: Mean posture of one stride duration.

kinematic synergy are discussed.

4 Discussion outline

Q1: Whether the control of low-dimensional kinematic information enables to realize stable locomotion both flat and slope condition, or not? **Q2:** Whether all the kinematic synergy needs to be controlled, or some kinematic synergy generate as a reaction of the control of other synergy?

A1: Dynamical simulation of the 7-link skeletal system showed stable locomotion both on flat and slope floor. Thus the control of low-dimensional kinematic information enables stable locomotion (Fig. 4). **A2:** Locomotion became unstable by reducing the gain of each synergy control during stable locomotion (Fig.5). Thus three synergies are not generated as reaction but considered to be actively controlled.

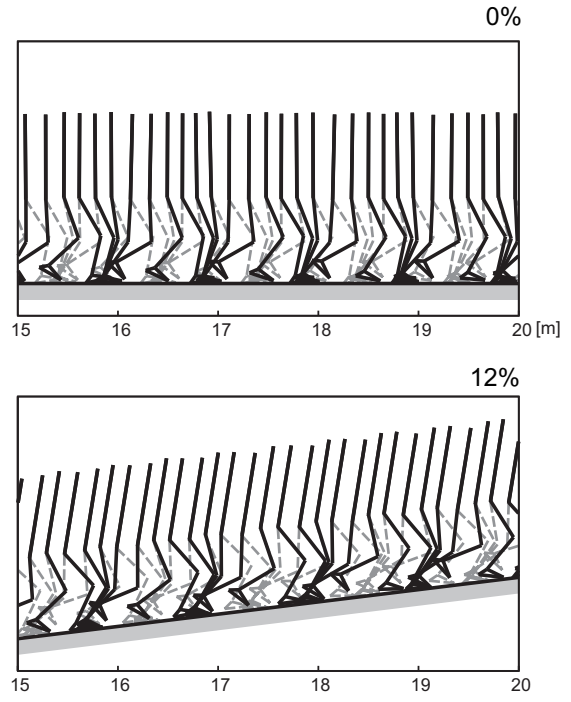


Figure 4: The result of dynamical simulation.

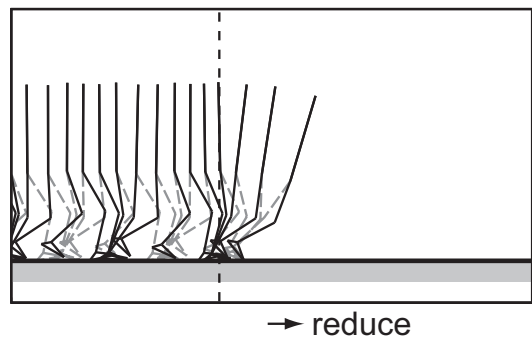


Figure 5: Simulation result reducing synergy 1 control.

Acknowledgments This research was partially supported by a Grant-in-Aid for Young Scientists (B) (No. 23760228) and Scientific Research (B) (No. 23360111) funded by the Ministry of Education, Culture, Sports, Science and Technology, Japan.

References

- [1] E.Bizzi et al.: New perspectives on spinal motor systems, *Nat Rev Neurosci* 1(2): 101/108, 2000.
- [2] RE.Popple et al.: Independent representations of limb axis length and orientation in spinocerebellar response components, *J Neurophysiol*, 87, 409/422, 2002.
- [3] YP.Ivanenko et al.: Modular control of limb movements during human locomotion, *J Neurosci*, 27(41), 111490/11161, 2007.
- [4] LH.Ting: Dimensional reduction in sensorimotor systems: a framework for understanding muscle coordination of posture, *Progress in Brain Res*, 165, 299/321, 2007.

MYOROBOTICS: a modular toolkit for legged locomotion research using musculoskeletal designs

Hugo Gravato Marques*, Christophe Maufroy**, Alexander Lenz***,
Konstantinos Dalamagkidis****, Utku Culha*, Maik Siew**, Paul Bremner***
and the MYOROBOTICS Project Team

*Eidgenössische Technische Hochschule Zrich (ETH), Switzerland
hgmarques@gmail.com, utku.culha@mavt.ethz.ch

**Fraunhofer-Institut für Produktionstechnik und Automatisierung, Germany
Christophe.Maufroy@ipa.fraunhofer.de, maik.siew@ipa.fraunhofer.de

***University of Bristol and University of West of England, UK
Alex.Lenz@brl.ac.uk, paul.bremner@brl.ac.uk

****Technische Universität München (TUM), Germany
dalamagkidis@tum.de

1 Motivation

Musculoskeletal robots try to exploit principles of biological systems in an attempt to replicate their behavioural properties. The intrinsic compliance and lightweight structure of these systems reduce the peak forces resulting from external collisions, and protect the robot's actuators. In addition, the compliance of the muscle-tendon complex can greatly increase the energy efficiency during periodic motions [2], as well as allow for safe interaction with humans [1]. In general these properties are desirable in any robot, but they are especially useful in legged locomotion.

2 State of the art

Currently there are a number of robots built according to musculoskeletal designs; among the most extreme examples are Kojiro [6], Kotaro [7], and ECCEROBOT [1, 8]. In the context of legged locomotion, examples of musculoskeletal robots include the JenaWalker [3], the pneumatic walking and jumping robots [4], and the BioBiped [5]. A common feature shared by all these robots is that they utilize custom-made (and often complex) hardware and software because off-the-shelf components are usually not available. As a result, the total cost of the robotic platform is usually prohibitive and the final system is seldom used by people other than those who built it.

3 Contribution

This abstract introduces the MYOROBOTICS project which aims to spread the use of musculoskeletal robots and to allow innovative research as well as the discovery of application based on this unique design, including in the field of legged locomotion research. The project envisions to provide a modular, configurable, easy-to-use and cost-effective robot construction and development toolkit. The main goal

of the kit is to facilitate the construction and development of new control paradigms for musculoskeletal systems.

The construction toolkit is composed of hardware modules, named Design Primitives (DPs), which embody relevant functionalities of musculoskeletal designs: bones, joints, muscle-tendon complexes, proprioceptive sensors, and sensorimotor loops. The modularity of the DPs allows for quick and simple (re)configuration of the physical properties of the system, such as limb morphology, mass distribution, muscle power, spring characteristics, among others. Details about the DPs will be given in the contribution for the hardware demonstration session, to which will submit a parallel contribution.

The focus of the present abstract lies on the controller library as well as on the software tools for optimization of robot designs and controllers. The controller library aims to provide a set of useful controllers for tendon-driven systems as well as to facilitate the development of user-defined controllers. In the context of locomotion, we are investigating the advantages of semi-intrinsic controllers. These controllers try to exploit (in an unsupervised way) sensorimotor correlations to acquire reflex circuits (such as the stretch reflex). These circuits are endowed with inherent muscle coordination and facilitate the control of the system by reducing its dimensionality [9, 10].

The software optimization tools offer the possibility to optimize the robot design and controller. These tools are coupled with a powerful simulation environment in which parameters of the robot (e.g. tendon-stiffness, or mass distribution) and the controller (e.g. reflex gains) can be tuned according to some fitness criterion, such as efficiency, velocity, or stability.

4 Discussion outline

We are mainly interested in discussing the MY-OROBOTICS legged demonstrator. The demonstrator consists of a bi-articular legged robot which is capable of hopping using the entire infrastructure of the project: (1) the DPs are used to build the robot, (2) reflex-like controllers are learned from the sensorimotor interactions observed induced by the robot's morphology, (3) the robot's morphology and reflex gains are tuned to allow the robot to hop, potentially in an energy efficient way.

5 Preferred format

Talk.

References

- [1] O. Holland and R. Knight, The anthropomorphic principle. "Proc AISB06", 2006.
- [2] R. McN. Alexander, Three Uses for Springs in Legged Locomotion, "IJRR," 1990
- [3] A. Seyfarth et al. Towards Bipedal Running as a Natural Result of Optimizing Walking Speed for Passively Compliant Three-Segmented Legs, "IJRR," 28(2): 257-265, 2009.
- [4] K. Hosoda et al. Pneumatic-driven jumping robot with anthropomorphic muscular skeleton structure. "Auton Robot" 28: 307-316. 2010
- [5] K. Radkhah et al. Concept and design of the Bio-Biped1 robot for human-like walking and running, "IJHR," 8(3), pp. 439-458, 2011
- [6] I. Mizuuchi et al. An advanced musculoskeletal humanoid kojiro, "Proc of International Conference on Humanoid Robots," 2007.
- [7] I. Mizuuchi et al. Development of musculoskeletal humanoid kotaro, "Proc of the 2006 IEEE International Conference on Robotics and Automation," 2006
- [8] H. Marques et al. Ecce1: the first of a series of anthropomorphic musculoskeletal upper torsos, "Humanoids2010", 2010.
- [9] H. Marques et al. Self-organisation of reflexive behaviour from spontaneous motor activity. "Biol Cybern," 2012.
- [10] H. Marques et al. Self-organization of spinal reflexes involving homonymous, antagonist and synergistic interactions. "Proc SAB2012", 2012.
- [11] L. Lamport, "L^AT_EX, a Document Preparation System," Addison Wesley, 1994.
- [12] M. Goossens, F. Mittelbach, and A. Samarin, "The L^AT_EX Companion," Addison Wesley, 1994.

Human underwater undulatory swimming: flow characteristics around a human swimmer, technical swimmer model, and numerical simulations

Stefan Hochstein, Reinhard Blickhan

Department of Motion Science, Friedrich-Schiller-University Jena, Germany

{*stefan.hochstein, reinhard.blickhan*}@uni-jena.de

1 Motivation

From fish locomotion [1] we learned that low drag values from gliding can be achieved during active propulsion [2,3]. Thereby a carefully adjusted traveling body wave pumps the fluid caudally. As a result the probability of flow separation is reduced. To maximize their swimming speed competitive swimmers try to copy successful strategies like undulatory swimming from fish locomotion [4,5] during the gliding period after start and every turn. However, in humans mainly the non-smooth and segmented body with limited flexibility allows no symmetric motion like in fish locomotion. But exactly this asymmetries are interesting because they show us a modified type of undulatory swimming. To reach an optimum motion swimmers check the pros and cons of different variations of the motion. Thereby the human swimmer can be considered as natural paradigm for technical models [6] that must compensate its disadvantages due to evolution through sophisticated kinetics. The dependence of these flow characteristics of frequency, amplitude and coordination will help to deduce strategies to improve economy or thrust.

2 Own approach

To study the flow around the swimmer and in its wake three approaches were combined:

a) Time resolved Particle Image Velocimetry (TR-PIV) at the human swimmer

The path of the levitating particles (illuminated by a green laser light sheet) is monitored at 250 Hz with a high speed video camera (PHANTOM V12). Local flow velocities (Fig. 1b) are calculated using a cross correlation algorithm to get a flow field as well as a qualitative and quantitative characterization of vortex generation and separation [7].

b) PIV experiments at the reduced technical model

The reduced technical five-segment model ("Jena-Swimmer") is based on human swimmer's silhouette in two dimensions (length and width) in the scale 1 to 5 (Fig. 1a). Each segment can be actuated by its own servo

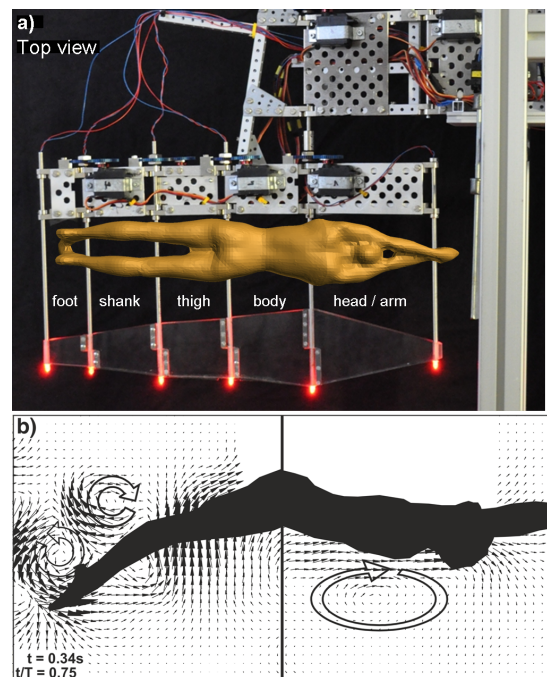


Figure 1: a) Top view on the the scaled technical swimmer model consisting of five segments with comparison to the real swimmer. b) Flow field (thin black arrows) generated during dolphin kicks of a human swimmer in a still water pool at the end of the down stroke. The large bold arrows show vortices mainly in the feet region.

drive (Graupner DS8811) and the motion is captured by active LED-markers. This model should drive with the motion observed in human swimming and compare the flow of the model with the flow of the human swimmer and the numerical simulation.

c) Numerical simulations (in cooperation with TU-Freiberg)

Computational Fluid Dynamics (CFD) of the 3D flow around the moving swimmer using OpenFOAM and deforming meshes should show the vortex generation and the general flow pattern. In experimental measurements it is not possible to measure directly the pressure distribution or the forces of the moving swimmer. Results of CFD provide

information about the active and passive drag as well as the propulsion during a kick cycle.

3 Discussion and open questions

Although the human body is not like a fish swimmers partly use strategies from fish locomotion. The human swimmer shows a highly complex, not simple, flow pattern [6,7]. Due to the edges and the asymmetric movement vortices at head and knee are generated already cranial but are reused pedal for propulsion (Fig. 1b).

The movement patterns of the technical swimmer model prescribed to the servos are modified due to inertia of the segments, bending of the rods, and fluid forces. Tests to check the scope of possible corrections are necessary. Whether the results signal a deficient technique, a tribute to the anatomic limits of our muscle-skeletal system or the advantage to use flow preformation needs further investigation. Is the asymmetric motion always a disadvantage for aquatic locomotion or it is possible to reach a performance comparable to symmetrical and smoothed body swimmers by an appropriate combination of segmental silhouette and correspondent motion. Does the asymmetric motion have advantages?

References

- [1] J. Liao (2007) "A review of fish swimming mechanics and behaviour in altered flows" *Philos Trans R Soc Lond B Biol Sci.*, 362, 1973–1993.
- [2] R. Blickhan (1992) "Biomechanik der axialen aquatischen und pedalen terrestrischen Lokomotion" *Habilitationsschrift*, Universität des Saarlandes.
- [3] R. Blickhan (1993) "Axial aquatic and pedal terrestrial locomotion.-Form, structure, and movement" *Verh Dtsch Zool Ges.*, 68.2, 5-11.
- [4] G. Lauder & E. Tytell (2005) "Hydrodynamics of undulatory propulsion" in *Fish Biomechanics*, Elsevier, 23, 425–468.
- [5] M. Triantafyllou, G. Triantafyllou & D. Yue (2000) "Hydrodynamics of fishlike swimming. *Annu. Rev. Fluid Mech.*, 32, 33–53.
- [6] S. Hochstein & R. Blickhan (2010) "Human undulatory swimming: kinematics, flow and mechanical model" In: Kjendlie, P.-L., Stallman, R.K., Cabri, J. (Eds.) *XIth International Symposium for Biomechanics and Medicine in Swimming*, Oslo (Norway), p. 74.
- [7] S. Hochstein, R. Blickhan (2011) "Vortex recapturing and kinematics in human underwater undulatory swimming", *Human Movement Science*, 30(5), 998–1007.

Walking and Running with StarLETH

Marco Hutter, Christian Gehring, Michael Bloesch, Mark Hoepfflinger and Roland Siegwart
Autonomous Systems Lab, ETH Zurich, Zurich, Switzerland
{mahutter, gehrinch, bloeschm, markho, rsiegwart}@ethz.ch

This paper presents the latest advances we made in static and dynamic locomotion with our compliant quadrupedal robot StarLETH. It summarizes the robot design and outlines the different underlying control principles used to achieve sophisticated locomotion performance. The focus of the paper is put on experimental findings which illustrate that the applied actuation and control principles are a valuable approach to bring our robotic devices a step closer to their natural counterparts.

1 Motivation

Legged robotic devices, and in particular quadrupedal systems, have made significant progress in the past years. Such artificial systems have broken records in different areas. For example, Boston Dynamic’s hydraulically actuated Cheetah [4] very recently set the world record in fast running. Last year, the Cornell Ranger [1] was able to walk the Marathon with a cost of transport that is better than a human. This high energetic efficiency was achieved as the robot largely exploits swing leg pendulum dynamics similar to McGeer’s passive dynamic walkers [13]. Going a bit further back in the history of quadrupedal locomotion, different groups participating in the LittleDog challenge (e.g. [11]) pushed the state of the art of climbing in very rough and unstructured terrain using precise foot placement strategies. The large range of motion due to the mechanical design of the robot and advanced motion planning, control and learning algorithms led to remarkable performances of the robots. Other robots like the six-legged robot RHex [12] are able to overcome similar obstacles in a brute force way owing to the inherent robustness of the system design.

Despite these advances in design and control, all existing robotic solutions are still far behind our natural counterparts. Unlike animals and humans, most of the robots lack some of the key characteristics, namely *versatility*, *speed*, *efficiency*, and *robustness*. Vertebrates are able to climb in very difficult environment by carefully selecting the footholds, at the same time they can walk or run nearly effortlessly on less challenging ground while maintaining balance even in case of large external disturbances. On the contrary, man-made machines as previously mentioned are particularly good in

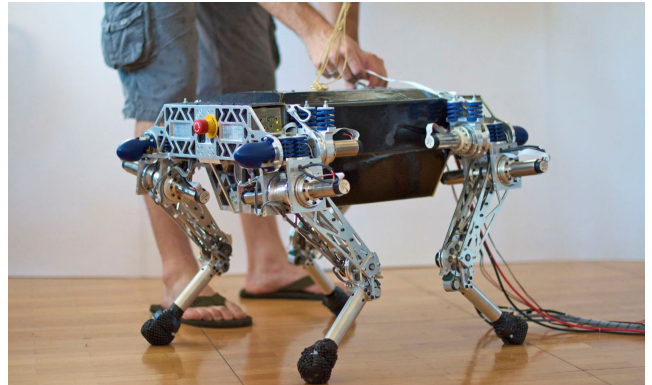


Figure 1: StarLETH: A compliant quadrupedal robot.

a specific domain, but perform poorly regarding at least to one of the other aforementioned key features.

At the Autonomous Systems Lab, we recently developed the quadrupedal robot StarLETH that combines all these features and allows us to investigate different control and planning principles to achieve advanced locomotion skills. In the following section we give an overview of the applied design and actuation principles, followed by an outline of the locomotion control methods. In the experimental part, we illustrate how the robot can statically walk while optimizing energetic efficiency or safety against slippage. We present results of a dynamic trotting gait under substantial external disturbances and summarize some interesting aspects from a bio-mechanical point of view.

2 System Design

StarLETH (Springy Tetrapod with Articulated Robotic Legs) is a fully actuated robot that features four identical, completely symmetric articulated legs connected to a single rigid main body. Each leg has three degrees of freedom (DOF) that are arranged in mammalian-style with successive hip abduction/adduction, hip flexion/extension, and knee flexion/extension. To achieve fast swing leg motion, we put emphasis on a lightweight construction with all actuators tightly integrated at the main body. Using rotational actuators in all joints makes a large range of motion possible, so that the leg can be fully retracted and extended. Having a body length of about 0.5 m, segment lengths of 0.2 m, and a total weight of 23 kg,

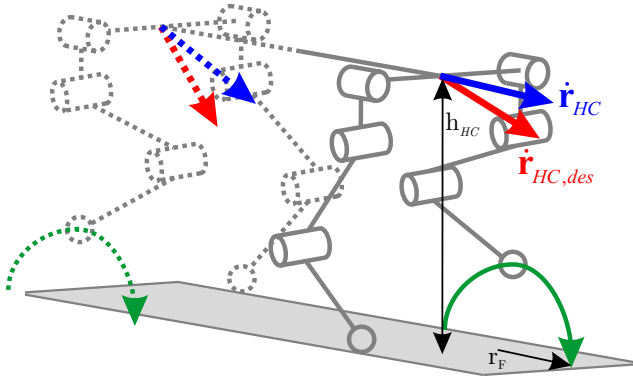


Figure 2: Foothold planning in a dynamic gait.

this robot is comparable to a medium-sized dog.

StarLETH is driven by highly compliant series elastic actuators which have very similar properties of our muscles and tendons. They act as compliant elements to temporarily store a large amount of energy. Mechanical springs decouple the motor and gearbox from the joint to protect the gearbox from impact loads at landing, to intermittently store energy, and most importantly, to allow for high fidelity joint torque control. This opens a very broad spectrum of opportunities to implement novel locomotion control algorithms.

The system is equipped with an inertial measurement unit (IMU) that allows, in combination with the accurate kinematic information from the joint encoders, to precisely estimate the state of the robot [3]. Hence, all maneuvers can be executed without additional perception or using a motion capture system. Differential pressure sensors in the compliant ball feet give reliable feedback about the contact situation of the legs. StarLETH is operated on a large-scale custom made treadmill with the dimensions of about 2.90 m × 1.6 m in most of the experiments presented in this paper.

3 Control Design

We separate locomotion control into three layers such as *motion generation*, *motion control*, and *actuator control*.

3.1 Motion Generation

Motion generation defines the desired foot locations and the motion of the main body. For static walking in rough terrain, such as in the LittleDog challenge (e.g. [11]), the motion of the robot is mainly determined by the available footholds. As soon as it comes to less demanding surfaces, the robot can speed up and switch to dynamic gaits. In that case the desired foothold locations are determined by the desired body velocity as well as the postural control strategy to counteract external disturbances. Following the fundamental principles that can be adopted from the SLIP template [2] respectively the early Raibert controllers [14], we apply

the control framework described in [6]. A predefined gait graph clocks the swing and stance phases of each leg and specifies the foot fall pattern. The stepping position of each leg is computed based on the reference frames in the middle of the front and back leg pair, respectively, as shown in Figure 2. The desired position of the foot is calculated relative to the nominal standing position by

$$\mathbf{r}_F = \frac{1}{2} \dot{\mathbf{r}}_{HC,des} T_{st} + k_R^{FB} (\dot{\mathbf{r}}_{HC,des} - \dot{\mathbf{r}}_{HC}) \sqrt{h_{HC}}, \quad (1)$$

with the velocity at the respective hip center $\dot{\mathbf{r}}_{HC}$, the stance duration T_{st} defined by the gait pattern, the hip height h_{HC} to normalize the feedback contribution [17], and the feedback control gain k_R^{FB} .

3.2 Motion Control

To achieve robust and sophisticated walking, we use a hierarchical task space inverse dynamics control framework [9] that is based on support consistent equations of motion and prioritized least square optimization. The complex behavior of a robotic system evolves from the simultaneous execution of different motion tasks, such as ensuring stability, moving a foot point, or keeping certain posture. At the same time, joint torques and ground contact forces can be optimally distributed, e.g. to guarantee safety against slippage or to minimize the actuator effort. The hierarchical task decomposition ensures that critical tasks are fulfilled by all means while less important ones are only fulfilled as good as possible.

3.3 Actuator Control

We developed two complementary actuator control strategies for torque and position control [10]. To achieve high energetic efficiency and accurate torque control, we designed the mechanical damping in the actuator as low as possible. In return, to achieve fast and precise foot positioning and to suppress undesired oscillations due to the series elasticity, we implemented a position controller that can actively damp out all undesired oscillations.

4 Results

Preliminary performance tests with StarLETH showed a payload capability¹ of 25 kg and a large, passive robustness² against impacts during dynamics maneuvers [8].

4.1 Static Walking

Static walking gaits are used for slow locomotion speed and in particular when it comes to crossing challenging terrain. Static stability can be ensured since at least three legs are in contact with the ground. Moreover, this offers the potential to optimize the contact forces and joint torque distribution, respectively.

¹<http://www.youtube.com/watch?v=ZEZe2w1NUGo>

²<http://www.youtube.com/watch?v=5XLf43GXFxI>

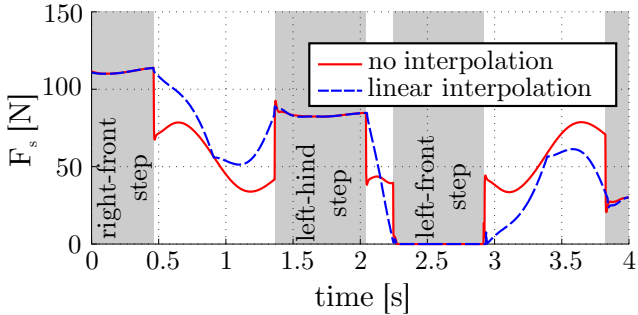


Figure 3: Smooth contact force distribution is achieved by interpolating between subsequent contact situations.

In a first set of experiments, we compared actuator efficiency defined by³

$$E_\tau = \int \boldsymbol{\tau}^T \boldsymbol{\tau} dt, \quad (2)$$

and risk of slippage expressed by the relation between local tangential and normal contact forces:

$$\bar{\mu} = \text{mean} \left(\frac{F_{\text{tangential}}(t)}{F_{\text{normal}}(t)} \right). \quad (3)$$

By minimizing the local tangential forces in contrast to optimizing actuator efficiency, we could lower $\bar{\mu}$ from 0.2 to 0.04. In return, the actuator cost E_τ was increased by about 20% while the executed motion remained exactly equal.

Legged locomotion is accompanied by discrete changes in the contact situation which is often reflected in discontinuous actuator torques and contact force distributions. To compensate for that, we apply an interpolation method between two subsequent contact situation by changing the internal force directions as illustrated in Figure 3.

As soon as it comes to challenging terrain, it is often required to perform climbing maneuvers by clinging to the ground. In case the local contact surface normal directions are known, the proposed optimization routines allow to minimize the local tangential forces and hence to minimize the risk of slippage⁴. We demonstrated this capability by walking on a curved surface shown in Figure 4.

4.2 Dynamic Trotting

Dynamic locomotion is characterized by inherent instability as the robot will fall if the legs are not appropriately positioned. When performing such a gait, the robot can resist external disturbances in two ways. First, it can produce reaction forces with the grounded legs to counteract the perturbations as good as possible. Second, to compensate for disturbances in the

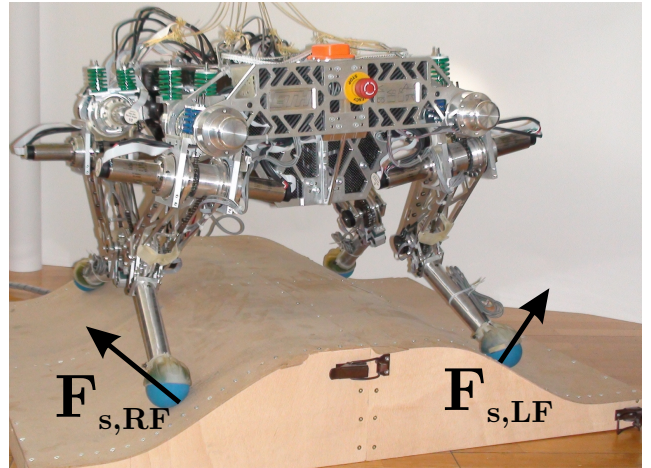


Figure 4: Robust walking on a curved surface is only possible by applying internal contact forces.

underactuated subspace⁵, the subsequent foothold locations of the current swing legs are adapted appropriately. To evaluate the performance of our control approach for dynamic gaits, we performed two experiments with StarLETH trotting at speed in the range of 0.5–0.7 m/s on the treadmill. In the first one, we put unperceived obstacles on the treadmill as shown in Figure 5(a). The robot detects the change in ground elevation by the tactile sensor in the foot element and reacts accordingly⁶. In the second experiment, we kicked the robot from the side while the quadruped was trotting (Figure 5(b)). The robot immediately steps sideways to counterbalance this impulsive disturbance, and finds back to the nominal trotting gait⁷ within two steps.

In order to quantify the energy consumption we conducted a long-term experiment by letting StarLETH trot a distance of 100 m at constant speed. To get comparable values to the metabolic costs found in nature, we measured the electric power delivered at the socket before the AC/DC converter. For a trotting gait with ≈ 0.43 m/s, the robot required an average power of $P_{el} = 360$ W. This results in a dimensionless cost of transport (COT) of about 3.5. The energy losses of all electric components without load amounts to $P_{loss0} \approx 80$ W. We estimated an average positive mechanical power $P_{mech_{pos}} \approx 32$ W by multiplying joint torque with motor speed. This means on one hand that the mechanical COT including all control actions required to stabilize the robot on its nominal walking gait is $COT_{mech_{pos}} = 0.28$. On the other hand, we notice that the efficiency of the overall energy conversion is as low as about 10%. This is reasonable as already the maximal possible efficiency is not more than 55%, which is determined by multiplying the values given by the manufacturer for AC/DC converter ($\eta_{AC/DC} = 90\%$),

⁵for trotting this is the rotation around the line of support

⁶<http://www.youtube.com/watch?v=Wuc7mL0hkGo>

⁷<http://www.youtube.com/watch?v=7F6GRFPkdp0>

³ τ^2 is often use to quantify electric losses in the motor

⁴http://www.youtube.com/watch?v=_OfJoyeveA4

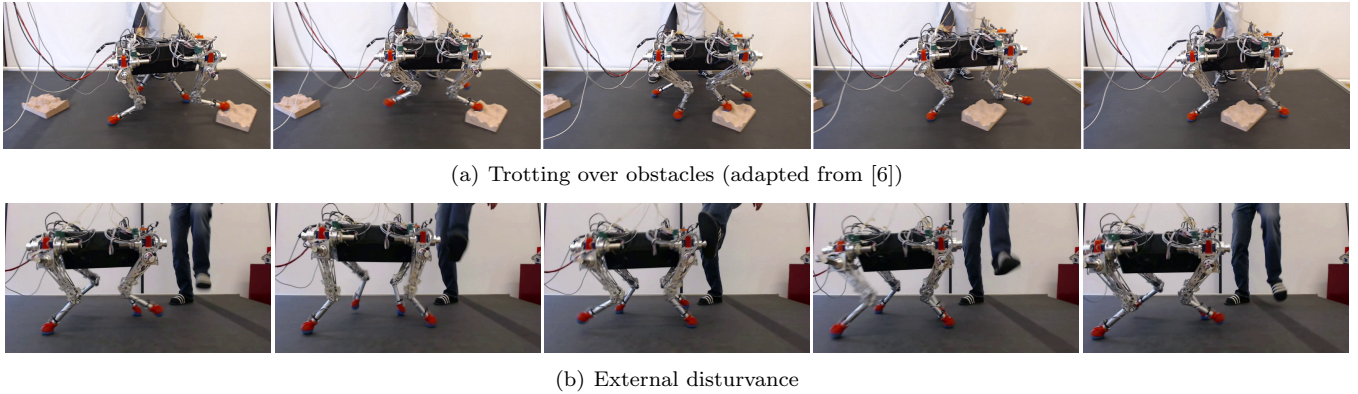


Figure 5: Robust dynamic trotting in 3D under significant external disturbances such as obstacles (a) or a kick (b).

motor controller ($\eta_{EPOS} = 94\%$), motor ($\eta_{mot} = 90\%$), and gearbox ($\eta_{HD} = 75\%$). In particular motor and gearbox efficiencies are significantly lower while walking due to the alternating load direction in every joint.

5 Discussion

In this project, we showcased the applicability of compliant actuation for torque controllable legged devices that can robustly perform different gaits from static climbing in challenging terrain to dynamic trotting. We see a large potential in this actuation principle for legged robots, in particular since the underlying principles are very similar to the muscular tendon system of humans and animals. We revealed in earlier studies that the applied series elastic actuators indeed largely support the passive dynamics of locomotion [10]. We showed that more than 60% of the energy can be passively stored and released while the motors only compensate for the energy loss. Furthermore, the output power and speed of the motor is amplified by a factor four. All these findings show an astonishing level of agreement with biomechanical studies (e.g. [15]).

We are also not that far away from nature in terms of efficiency. A similar sized dog (*canis familiaris*, 18kg) requires for the same locomotion speed a metabolic COT of 0.73 [16]. At first glance, this seems to be an extreme difference. However, considering that motors produce an average mechanical power of about 32W (COT=0.32), there is large potential to optimize the energy consumption of the electronic equipment. Ongoing progress in this field can potentially fully close this discrepancy with respect to efficiency. Comparing only the actuator performance with the biological counterparts unveils that our machines have for instance higher power and torque density (e.g. [7]) as well as a higher control bandwidth than human reflexes (e.g. [5]).

Despite these local advantages, animals still largely outperform our robots and there remains many unanswered research questions before our robots can compete with nature.

References

- [1] P A Bhounsule, J Cortell, and A Ruina. Design and control of Ranger: An energy-efficient, dynamic walking robot. In *International Conference on Climbing and Walking Robots (CLAWAR)*, 2012.
- [2] R Blickhan. The spring-mass model for running and hopping. *Journal of Biomechanics*, 22(11-12): 1217–1227, 1989.
- [3] M Bloesch, M Hutter, M H Hoepflinger, S Leutenegger, C Gehring, C David Remy, and R Siegwart. State Estimation for Legged Robots - Consistent Fusion of Leg Kinematics and IMU. In *Robotics Science and Systems (RSS)*, Sydney, Australia, 2012.
- [4] Dynamics Boston. <http://www.bostondynamics.com>, 2012.
- [5] R C Fitzpatrick, R B Gorman, D Burke, and S C Gandevia. Postural proprioceptive reflexes in standing human subjects: bandwidth of response and transmission characteristics. *The Journal of physiology*, 458:69–83, December 1992.
- [6] C Gehring, Stelian Coros, M Hutter, M Bloesch, M H Hoepflinger, and R Siegwart. Control of Dynamic Gaits for a Quadrupedal Robot. In *IEEE International Conference on Robotics and Automation (ICRA)*, Karlsruhe, Germany, 2013.
- [7] J M Hollerbach, I W Hunter, and J Ballantyne. A comparative analysis of actuator technologies for robotics. *Robotics Review*, 2, 1991.
- [8] M Hutter, C Gehring, M Bloesch, M H Hoepflinger, C David Remy, and R Siegwart. Star-LETH: a Compliant Quadrupedal Robot for Fast, Efficient, and Versatile Locomotion. In *International Conference on Climbing and Walking Robots (CLAWAR)*, pages 483–490, 2012.

- [9] M Hutter, H Sommer, C Gehring, M A Hoepflinger, M Bloesch, and R Siegwart. Hierarchical Task-Space Motion and Force/Torque Control based on Least Square Optimization. *submitted to International Journal of Robotics Research (IJRR)*, 2012.
- [10] Marco Hutter, C. David Remy, Mark A. Hoepflinger, and Roland Siegwart. Efficient and Versatile Locomotion with Highly Compliant Legs. *IEEE/ASME Transactions on Mechatronics*, 18(2):449–458, 2013.
- [11] Mrinal Kalakrishnan, Jonas Buchli, Peter Pastor, Michael Mistry, and Stefan Schaal. Fast, Robust Quadruped Locomotion over Challenging Terrain. In *IEEE International Conference on Robotics and Automation (ICRA)*, Anchorage, AK, 2010.
- [12] D E Koditschek, R J Full, and M Buehler. Mechanical aspects of legged locomotion control. *Arthropod Structure & Development*, 33(3):251–272, 2004.
- [13] T McGeer. Passive Dynamic Walking. *The International Journal of Robotics Research (IJRR)*, 9(2):62–82, 1990.
- [14] Marc H Raibert. *Legged robots that balance*. MIT Press, Cambridge, Mass., 1986.
- [15] Thomas J Roberts. The integrated function of muscles and tendons during locomotion. *Comparative biochemistry and physiology. Part A, Molecular & integrative physiology*, 133(4):1087–99, December 2002.
- [16] C R Taylor, K Schmidt-Nielsen, and J L Raab. Scaling of energetic cost of running to body size in mammals. *The American journal of physiology*, 219(4):1104–7, October 1970.
- [17] Christopher L Vaughan and Mark J O'Malley. Froude and the contribution of naval architecture to our understanding of bipedal locomotion. *Gait & Posture*, 21(3):350–362, 2005.

Humans adapt to a changed arm dynamics always in the same manner - whether visual feedback is given or not

Karl T. Kalveram^{*}, Madelein Georg⁺, Jasmin Kensche⁺, Philipp König⁺, Tim Lauer⁺, Tobias Schröder⁺, Saskia Schwering⁺, Edith Eichhorn[#]

^{*}: Locomotion Laboratory, Technische Universität Darmstadt, Darmstadt, Germany, and Department of Experimental Psychology, Universität Düsseldorf, Duesseldorf, Germany (Concept and methods). ⁺: Department of Psychology, Technische Universität Darmstadt, (Student Researchers. Conduction of the experiment). [#]: Department of Psychology, Technische Universität Darmstadt (Doctoral Student. Organisation, critical discussion). <mailto:kalveram@uni-duesseldorf.de>

Abstract Regarding aiming movements with the arm, roboter and humans both face the problem, how to adapt to externally imposed changes of the arm's dynamical properties, and what kind of information is necessary to succeed? In an experiment, subjects were asked to perform goal directed forearm movement with (N=15) and without (N=15) visual feedback of the actual forearm position. Movements were conducted either unloaded or loaded with viscous (velocity dependent) damping applied via a torque motor. On the load changes, which occurred every 10 movements, the peak velocities showed on average clear transition-effects and re-adapted to the previous state step by step. These effects, however, were independent of the feedback condition. We concluded that humans apply feedforward control through an inverse model of their arm dynamics, which adapts to changes of the actual arm dynamics via the interrelationships within the proprioceptive measurements solely. Simulations conform to these hypotheses. Consequences of these findings for the type of motor learning that humans probably apply are discussed.

1 Introduction

Roboter and humans as well face the same problem when performing aiming movements: How to adapt to externally imposed changes of the arm's dynamical properties, for instance through altered weight, inertia, stiffness or damping? And what information is necessary to succeed? The type of the adaptive mechanism depends, of course, on the type of movement control. Here we insinuate that the human operator applies feedforward control, which includes an inverse dynamics model of the arm (e.g. Kalentscher et al. 2003, Wolpert & Kawato 1998, Kalveram et al. 2005, Miyamoto et al. 1988).

An inverse dynamics model operates by load compensation. Therefore, feedforward control by an already adapted inverse dynamics model would cause a transition-effect (after-effect) in the torque domain, if a load is added to or removed from the limb. Loading with damping, for instance, should diminish the arm's velocity in the next moment, and unloading from damping should

make the arm immediately move faster. The occurrence of a transition-effect and the following piecemeal re-adaptation to the previous balanced state distinguishes a controller as an adaptive feedforward controller applying an inverse dynamics model of the arm. The yet open question is, if successful adaptation is based either on visual, or proprioceptive, or mixed feedback.

2 Method

In a motor learning experiment, we checked whether the adaptation to a changed additional damping load follows the above described pattern, and whether adaptation does require visual feedback of the movement error or does not. For these purposes, the subject's forearm was fixed on a lever driven by a torque motor. The forearm was movable in a horizontal plane, and rotated with respect to the upper arm about the elbow joint. See fig.1 for the experimental setup. The forearm's angular position, referenced to straight ahead, was electronically transposed to the angular position of a lamp, which was located above the subject's head and projected a mark to a flat screen at a distance of $r=3.4\text{m}$ in front of the subject's face. A second projection lamp provided the goal marker the subject was asked to hit with the arm marker if the goal marker changed the position.

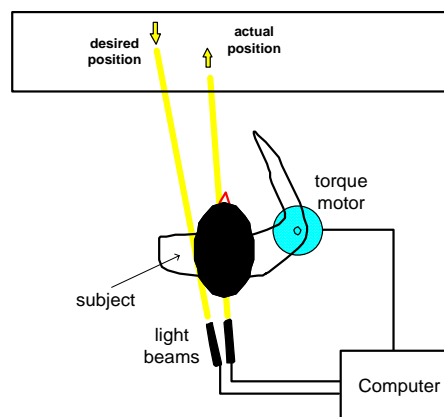


Figure1: Schema of the experimental setup

During movement the arm marker was darkened to avoid visual velocity feedback. At the arm's standstill the feedback marker re-appeared. Each subject performed 5 blocks of 62 trials á 4s. A trial consisted of a goal directed movement either in positive or negative direction. The goals of these 62 trials were randomly chosen from $\{-0.225, -0.2, -0.15, +0.15, +0.2, +0.225 \text{ rad}\}$ with alternating signs. In the 17th and 37th trial, velocity dependent (viscous) damping (coefficient = 3Nms/rad) was applied around the lever axis and remained effective until the 26th or 46th trial respectively. The experimental group experienced all trials with visual positional feedback marker on. The control group saw no visual feedback marker, only the goal marker. We took the absolute peak velocity of the lever's motion during a trial as the dependent variable, because this variable represents best the damping force the subject has to counteract.

3 Results

Results are visualized in Fig.2a (experimental group N=15, visual feedback on) and Fig.2b (control group N=15, visual feedback off). Fig.2c presents the results of a simulation run that mimics the conditions of the human experiment (see discussion in chapter 4).

Under visual feedback, the original peak velocity measurements are on average smaller than those performed without visual feedback. To eliminate this discrepancy, the original velocity measurements v_o were transformed into standardized values v_s using the formula

$$v_s = 0.5 + (v_o - \min) / (\max - \min) \quad (1)$$

This causes the averages to vary between 0.5 and 1.5. In both groups, the standardized mean peak velocities taken over blocks and subjects exhibit clear transition-effects (t-tests, $p < 0.01$) and re-adaptation courses (t-tests, $p < 0.01$) on loading or unloading the arm with damping. Between the groups, however, neither the strengths of the transition-effects nor of the re-adaptation courses differ significantly (t-tests, $p > 0.1$).

The positional errors (absolute difference between goal marker and feedback marker at first stop position), however, exhibit no systematic dependency on the damping condition. Aside from this, the error in the condition with visual feedback off reveals as much greater compared to the condition with visual feedback on. The bifid distribution of the error originates from the subjects' tendency, to confine their movements relative independently of the goal positions to the left side.

4 Discussion, conclusions

Regarding aiming movements, results support the hypothesis, that humans apply feedforward control using an inverse model of the respective limb, and that the respective inverse model adapts online to variations of the limb's dynamics. Results further provide a strong hint that the adaptive process does not rely on the positional error fed back visually, but rather exploits the interrelationships

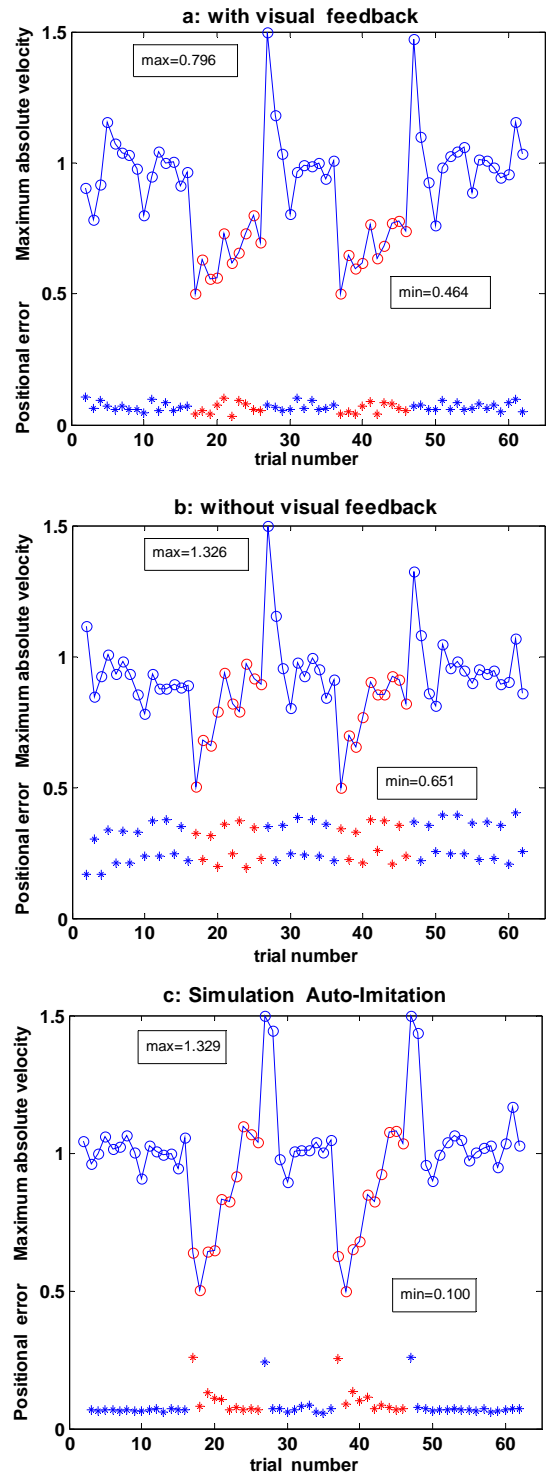


Figure 2: Mean absolute peak angular velocity values (circles) and angular positional errors (stars) in dependency on the trial number - without (blue markers) and with additional damping (red markers). The averages are taken over blocks and subjects. The circles represent standardized averages. Standardizing is based on \max and \min , which denote the maxima respectively minima of the original mean peak angular velocity measurements among the 62 trials (formula see text).

within the proprioceptive (bodily centred) measurements. An inverse model based on those measurements, however, cannot effectively reduce the error defined in exteroceptive (environmentally centred) coordinates. This task needs to hook up the controller by an inverse model that also transforms goals expressed in environmentally centred coordinates into goals expressed in bodily centred coordinates. Given that humans are provided with such an inverse kinematics model, we conclude that the experimental conditions applied in the current investigation prevent an update of this model. Therefore, its output may fluctuate randomly.

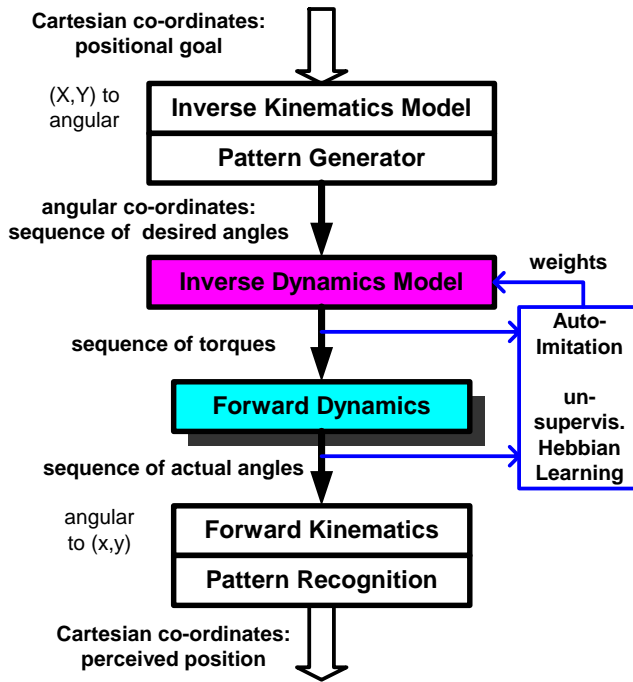


Figure3: Feedforward control of goal directed horizontal movements (see text for more information).

Fig.3 sketches a **control model** that meets the requirements outlined above. The forearm is represented by its forward dynamics described by the differential equation

$$\ddot{\varphi}(t) = \frac{1}{J} \{ Q(t) - B \cdot \dot{\varphi}(t) - K \cdot \varphi(t) \}, \quad (2)$$

where J denotes the inertia, B the coefficient of damping, K the stiffness, Q the external torque, and $\ddot{\varphi}, \dot{\varphi}, \varphi$ the angular kinematics. The inverse dynamics model then reads as

$$J \cdot \ddot{\varphi}(t) + B \cdot \dot{\varphi}(t) + K \varphi(t) = Q(t). \quad (3)$$

In equ.(3), the symbols of course denote neural correlates of the physical magnitudes residing in (2). In the present case, a single artificial neuron with linear input-to-output characteristic principally suffices to represent the inverse model in (3). Its coefficients respectively weights can be by acquired by auto-imitation (Kalveram 2004, Kalveram

& Seyfarth 2010), an un-supervised learning algorithm based on original Hebbian learning (Hebb 1949, Kalveram 1999). The procedure conducted by this learning model resembles the regression of the angular kinematics $\ddot{\varphi}, \dot{\varphi}, \varphi$ on the torque Q . The procedure determines values for J, B and K , which are interpreted as synaptic weights, and transferred to the neuronal network representing the inverse dynamics. So, a change of the arm's damping can quickly be counteracted for through an update of the inverse dynamics model.

To define the measurements of the goals and of the actions of the subjects, we used the angles of the projection lamps and of the lever (see methods, chapter 2). This provides simplified kinematics transformations; but note that formally the **forward kinematics** is given by

$$x = r \cdot \tan \varphi, \quad (4)$$

where x denotes the location of the marker on the screen referred to the midst of the screen located straight ahead (representing $x=0$), r the distance between the projection lamp and the screen at $x=0$, and φ the angle of the projection lamp, which equals the angle of the lever. The inverse kinematics model then reads

$$\varphi = \text{atan } x / r. \quad (5)$$

We guess that it is this relationship that cannot validly be learnt under the circumstances of the present experiment. So the positional error level remains high though the inverse dynamics model adapts.

We checked the control model by generating 15*5 blocks with 62 **simulated movement trials**, using the same series of goals as in the human experiment. In each trial, a random number (normally distributed with mean=0 and SD=0.0075) was superimposed on the output of the inverse kinematics model. This mimicked the fluctuations of the inverse kinematics output as assumed in the subjects. The inertia J of the simulated arm plus lever was set to 0.1 Nm/(rad*s²), and the coefficient of damping B was given the values 1.25 at the no-load condition and 3 Nm/(rad*s⁻¹) at the load condition. K was zeroed. Regarding B , learning rate was set to 7.5. The simulated data were processed in the same manner as in the human experiment. Results of the simulation are shown in fig.2c. They reveal, regarding transition-effects and recovery, essentially the same features as in the human experiment. The courses of human and simulated mean absolute peak velocities even coincide in lots of further details (see fig.2). It obviously are the interactions between the varying goals, the changed damping, the ongoing synaptic adaptation, and the dynamics of the arm plus lever, which shape the course of the peak velocities along the trials.

5 Open questions

In order to simulate the control model of fig.3, we based on auto-imitation, a kind of un-supervised learning. To acquire inverse models, the machine learning community, however, keeps lots of further - supervised as

well as unsupervised - learning techniques at hand (e.g. Nguyen-Tuong & Peters 2011). Which of all these control models has the greatest chance of being functionally applied by humans? To answer this question the test trilogy (Kalveram & Seyfarth 2009) can be used. In the framework of this procedure, the simulation test checks the logical correctness of a model, the hardware test proves its physical feasibility, and the behavioural comparison test compares the results of human experiments with the effects of the thus validated control models on the controlled system, all of this done under the same conditions.

A technical feedforward controller, however, will have problems of getting validated in the sense of the behavioral comparison test, if it has a holistic view on motor control, and/or needs only visual respectively task specific feedback to establish control. This we expect, because our results rather invoke that humans tend to separate inverse dynamics and inverse kinematics, and are reliant on proprioceptive feedback to establish the inverse dynamics model.

References

- Hebb, D.O., The organization of behavior. New York: Wiley & Sons (1949)
- Jordan, M.I., Supervised learning and systems with excess degrees of freedom, *COINS Technical Report*, 88/27 (1988) 1-41.
- Kalenscher, T., Kalveram, K. Th., & Konczak, J., Effects of two different dynamic environments on force adaptation: Exposure to a new force but not the preceding force experience accounts for transition- and after-effects. *Motor Control*, (2003), Vol.7, 242-263.
- Kalveram, K.T.. A modified model of the Hebbian synapse and its role in motor learning. *Human Movement Science*, 18 (1999), 185-199,
- Kalveram, K.T., The inverse problem in cognitive, perceptual, and proprioceptive control of sensorimotor behaviour: Towards a biologically plausible model of the control of aiming movements, *International Journal of Sport and Exercise Psychology*, 2 (2004) 255-273.
- Kalveram, K.T., Seyfarth, A. Learning the Inverse Dynamics of a Robot Arm by Auto-Imitation. In J. Baralt, N. Callaos, H. W. Chu, M. Savoie & C. D. Zinn (Eds.), *Proceedings of The International Multi-Conference on Complexity, Informatics and Cybernetics*, April 6-9 (Orlando, Florida), Vol. I (2010), pp. 230-235: International Institute of Informatics and Systemics (IIIS).
- Kalveram, K.T., Schinauer, T., Beirle, S., Richter, S. and Jansen-Osmann, P., Threading neural feedforward into a mechanical spring: How biology exploits physics in limb control, *Biological Cybernetics*, 92 (2005) 229-240.
- Kalveram, K.T. and Seyfarth, A., Inverse biomimetics: How robots can help to verify concepts concerning sensorimotor control of human arm and leg movements, *Journal of Physiology - Paris*, 103 (2009) 232-243.
- Wolpert, D.M. and Kawato, M., Multiple paired forward and inverse models for motor control, *Neural Netw*, 11 (1998) 1317-1329.
- Miyamoto, H., Kawato, M., Setoyama, T. and Suzuki, R., Feedback-error-learning neural network for trajectory control of a robotic manipulator, *Neural Networks*, 1 (1988) 251-265.
- Nguyen-Tuong, D. and Peters, J., Model learning for robot control: a survey. *Cognitive Processing* 12 (2011), 319-340.

Poppy: a New Bio-Inspired Humanoid Robot Platform for Biped Locomotion and Physical Human-Robot Interaction

Matthieu Lapeyre, Pierre Rouanet and Pierre Yves Oudeyer
Flowers Team, INRIA Bordeaux Sud Ouest, France
matthieu.lapeyre@inria.fr

1 Introduction

Humanoid robots are predicted to play a key role in our everyday lives in the future. Yet, several challenges need to be addressed before this becomes a reality. In particular, biped robots need to be able to locomote robustly in human environments, which includes the ability to keep stability when unpredictable physical contact with humans happens. At the same time, these robots need to be capable of rich and safe social and physical interaction with humans, and to adapt to the behaviour and preferences of each particular user.

We should not only try to solve these challenges through artificial cognitive intelligence but also through body intelligence [1]. On one hand, a way to permit robots to adapt their behaviors to unknown environments is to provide them with learning algorithms based on social guidance [2], or on autonomous self-exploration mechanisms [3, 4]. On the other hand, a part of the computation needed for such adaptation could also be done through the intrinsic mechanics and electronics of the robot, thus providing effective and hyper-responsive reactions while simplifying the algorithms of the different behaviors. Actually, body intelligence, realizing morphological computation, has been argued to facilitate and guide considerably the learning and development of sensorimotor skills [5].

No current platform (Nao [6], Darwin Op [7], Nimbro Op [8], HRP-2, ...) does offer both a bio-inspired morphology optimized for both walking and human physical interaction capability (safe, compliant, playful). To address these challenges, while exploring further approaches to the one elaborated for the Acroban robot [9], we have designed a new bio-inspired humanoid robotic platform, called Poppy, which provides some of the software and hardware features needed to explore physical and social interaction together with biped locomotion for personal robots. It presents the following main features:

- Design inspired from the study of the anatomy of the human body and its bio-mechanic, with an emphasis on leg structure;
- Dynamic and reactive: we try to keep the weight of the robot as low as possible (optimized geometry of the pieces and smaller motors);

- Human interaction: screen for communication and compliant physical interaction;
- Practical platform: low cost, ease of use and easy to reproduce through rapid prototyping techniques;

2 Poppy

Poppy (Figure 1) is a humanoid robot, 84cm tall, and 3 kg. It has a large sensorimotor space including 25 Robotis motors (including MX-28 permitting dynamic compliance control), force sensors under its feet and some extra sensors in the head: 2 HD-wide angle-cameras, a stereo-micro and an inertial central unit (IMU 9DoF) plus a large LCD Screen (4 inch) for visual communication (e.g. emotions, instructions or debug).

The poppy morphology is designed based on important aspects of the actual human body. This inspiration is expressed in the whole structure (e.g. the limb proportions) and in particular in the trunk and legs. The weight of all limbs has been minimized thanks to sophisticated girder like design, which was made possible by the use of 3D printing techniques (all limbs were 3D printed).

Poppy uses the bio-inspired trunk system introduced by Acroban [9]. These five motors allow it to reproduce the main DOFs of the human spine [10]. This feature allows the integration of more natural and fluid motion while improving the user experience during physical interactions. In addition, the spine plays a fundamental role in bipedal walking and postural balance by actively participating in the balancing of the robot.

The legs were designed to increase the stability and agility of the robot during the biped walking by combining bio-inspired, semi-passive, lightweight and mechanical-computation features. The architecture of the hips and thighs of Poppy uses biomechanical principles existing in humans. The human femur is actually slightly bent at an angle of about 6 degrees. In addition, the implantation of the femoral head in the hip is on the side. This results in a reduction of the lateral hip movement needed to move the center of gravity from one foot to another and a decrease in the lateral falling speed. In the case of Poppy, the inclination of its thighs by an angle of 6 degrees causes a gain of performance of more than 30% for the two above mentioned points. Another example is Poppy's feet. Poppy has the particularity of

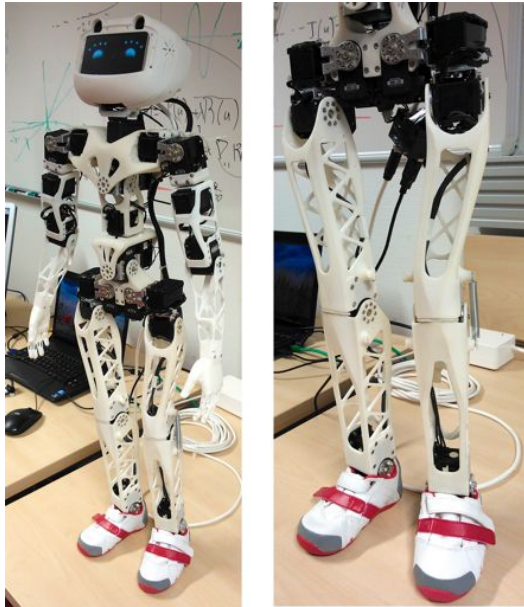


Figure 1: a. Global view of the Poppy platform. b. Zoom on legs design



Figure 2: Poppy feet use actual children shoes combine with a compliant feet, toes (a.) and pressure sensors (b.)

having small feet compared to standard humanoids. It has humanly proportioned feet (ie about 15% of its total size). It is also equipped with toe joint actuated by compliance (see Figure 2.a). We believe that these are two key features to obtain a human-like and efficient walking gait. However, that raises problems regarding balance because the support polygon is reduced. We included pressure sensors under each foot in order to get accurate feedback of the current state of the robot (see Figure 2.b).

3 Open questions

In our current work, we explore the combination of both a bio-inspired body and bio-inspired learning algorithms. We are currently working on experiments involving Poppy to perform skill learning. First we aim at achieving an effective postural balance using the articulated spine, the feet pressure sensors and the IMU. Then, when this is learnt and used as a building block, we will experiment on the learning of biped walking using online and developmental learning

algorithms such as [4] and [11]. We are expecting to clearly reduce the learning time needed and increase the quality of the learned skills thanks to the bio-inspired morphology of Poppy.

We are also studying social physical interactions with non-expert users. We plan to conduct user studies to evaluate how playful physical interactions and emotions could improve learning in robotics. We think that the poppy platform could be very suitable for such studies.

References

- [1] Rolf Pfeifer and Josh C. Bongard. *How the Body Shapes the Way We Think: A New View of Intelligence* (Bradford Books). The MIT Press, 2006.
- [2] A. Billard, S. Calinon, R. Dillmann, and S. Schaal. Robot programming by demonstration. *Handbook of robotics*, 1, 2008.
- [3] A. Baranes and P.Y. Oudeyer. Active learning of inverse models with intrinsically motivated goal exploration in robots. *Robotics and Autonomous Systems*, 2012.
- [4] M. Lapeyre, O. Ly, and P.Y. Oudeyer. Maturational constraints for motor learning in high-dimensions: the case of biped walking. In *Humanoid Robots (Humanoids), 2011 11th IEEE-RAS International Conference on*, pages 707–714. IEEE, 2011.
- [5] P-Y. Oudeyer, A. Baranes, and F. Kaplan. Intrinsically motivated learning of real-world sensorimotor skills with developmental constraints, in. *Intrinsically Motivated Learning in Natural and Artificial Systems*, 2013.
- [6] D. Gouaillier, V. Hugel, P. Blazevic, C. Kilner, J. Monceaux, P. Lafourcade, B. Marnier, J. Serre, and B. Maisonnier. The nao humanoid: a combination of performance and affordability. *CoRR*, vol. abs/0807.3223, 2008.
- [7] I. Ha, Y. Tamura, H. Asama, J. Han, and D.W. Hong. Development of open humanoid platform darwin-op. In *SICE Annual Conference (SICE), 2011 Proceedings of*, pages 2178–2181. IEEE, 2011.
- [8] M. Schwarz, M. Schreiber, S. Schueller, M. Missura, and S. Behnke. Nimbro-op humanoid teensize open platform. In *Proceedings of 7th Workshop on Humanoid Soccer Robots*. IEEE-RAS International Conference on Humanoid Robots, 2012.
- [9] O. Ly, M. Lapeyre, and P.Y. Oudeyer. Bio-inspired vertebral column, compliance and semi-passive dynamics in a lightweight humanoid robot. In *Intelligent Robots and Systems (IROS), 2011 IEEE/RSJ International Conference on*, pages 1465–1472. IEEE, 2011.
- [10] J.C. Ceccato. *Le tronc, de la locomotion à la commande*. PhD thesis, Université Montpellier II-Sciences et Techniques du Languedoc, 2009.
- [11] Thomas Degris, Martha White, and S. Sutton, Richard. Off-Policy Actor-Critic. In *International Conference on Machine Learning*, Edinburgh, Royaume-Uni, 2012.

Stride-to-Stride vs. Step-to-Step Return Maps for Human Running

Manu S. Madhav, M. Mert Ankarali, Shahin Sefati, Jusuk Lee, Julia Choi,
Amy J. Bastian and Noah J. Cowan

Johns Hopkins University

1 Motivation

Several biological behaviors such as locomotion are rhythmic processes which can be modeled as dynamical systems with stable periodic orbits. Examining periodic behaviors from this perspective allows us to distill significant amounts of data into low-dimensional representations that are both descriptive and predictive.

A prevalent hypothesis is that a periodic behavior is characterized by a dynamical system in the neighborhood of a limit cycle. However, given noisy measurements from system outputs comprising a subset of the states, it is not obvious what the dimension of the dynamics should be, much less their structure. Assuming noisy, possibly redundant, full state measurement, what is the maximum dimension of the underlying dynamics (that is, the co-dimension of the noise dynamics) that can be reliably inferred from data? For running, this question is compounded by an important modeling choice: do we treat a human as bilaterally symmetric or do we embrace its asymmetry? If symmetric, we should fit the step-to-step return map, else we should fit the stride-to-stride return map. What are the consequences on the co-dimension of the noise dynamics under these two modeling paradigms? To address these questions we adapt the method of Revzen and Guckenheimer (2011).

2 Previous work

Various template models have been developed for analyzing and studying animal and human locomotion (Blickhan and Full, 1993). Majority of these templates are governed by intuitive mechanical models which can (more or less) accurately describe steady-state center of mass trajectories, ground reaction forces or responses to perturbations.

In contrast, Revzen and Guckenheimer (2011) developed a numerical method to estimate the dimension of the slow dynamics of a periodic system directly from data with no intermediate modeling step. The algorithm is as follows:

1. Estimate the phase of the data.
2. Fit a Fourier approximation of the limit cycle in the measured variables.
3. Estimate return maps between Poincaré sections at specific phases.
4. Compare the eigenvalue distribution of randomly sampled return maps to a null distribution, i.e. eigenvalues of Gaussian random real matrices.
5. From this comparison, construct a heuristic to estimate the dimension of dynamics which can be approximated by the Gaussian noise.
6. Subtract this noise ‘dimension’ from the dimension of measurements to obtain the dimension of slow dynamics.

3 Data

In this work, we seek to identify the dimension of the noise dynamics (the co-dimension of which would correspond to the highest dimension of a model that could be informed by the data at hand) using the methods described above. The system of interest is human treadmill running. We address the question of how the noise dimension changes with the modeling choice of selecting a return map, namely step vs. stride.

The data consist of 3D tracked markers at the toe, foot, knee and hip on each leg. We reduce this data to the three sagittal plane angles and angular velocities for each leg, as well as position and velocity of the

center of mass in Cartesian coordinates. This 16-dimensional dataset is obtained for three subjects, at three different belt speeds (2.4, 2.8, and 3.2 m/s).

4 Phase and limit cycle estimation

The ‘phaser’ algorithm (Revzen and Guckenheimer, 2008) was used to estimate phase from the kinematic data, assuming periodic data with the same fundamental frequency. This frequency corresponds to the derivative of the phase. Once phase was estimated, data was transformed from time to phase coordinates.

The data in phase coordinates were fit to a Fourier series (order 11), with coefficients at the fundamental frequency and its harmonics. Fitting in the Fourier domain ensured that the limit cycle was periodic.

5 Dimension of slow dynamics

Observing the states at a specific Poincaré section (that is, at a particular phase), it is possible to estimate one set of eigenvalues (Floquet multipliers) using all the data available. However, this would not allow statistical estimation of the noise dimension. Instead, we follow Revzen and Guckenheimer (2011) to obtain an empirical return map distribution based on resampling of the available data. Dimension of the highest-dimensional model informed by the data can be defined as the dimensionality that cannot be generated by a null (noise) model. Here, the null model is the set of random matrices whose elements are unit normal random variables. In order to characterize and compare the return map and null distributions, Revzen and Guckenheimer (2011) extract the distributions of ordered eigenvalue magnitudes. Finally they introduce a scale independent error metric based on cumulative densities to estimate the noise dimension.

6 Discussion

The return maps for each step and each stride (2 steps) were computed. The noise co-dimension for the step-to-step fits was typically 5 to 7 compared to only 2 to 3 for stride-to-stride fits. In other words, step-to-step fits can inform a model with roughly twice as many states as a stride-to-stride model indicating that many dimensions of perturbations that could affect running are attenuated below the noise floor within two steps.

This finding highlights an important modeling trade-off. Fitting the dynamics for step-to-step transitions provides much greater modeling fidelity at the expense of making a strong assumption about bilateral symmetry.

References

- R. Blickhan and R. J. Full. Similarity in multilegged locomotion: Bouncing like a monopode. *J. Comp. Physiol. A*, 173(5):509–517, 1993.
- R. J. Full and D. E. Koditschek. Templates and anchors: neuromechanical hypotheses of legged locomotion on land. *J. Exp. Biol.*, 202(23):3325–3332, 1999.
- J. Lee. *Identifying Feedback Control Strategies of Running Cockroaches and Humans*. PhD thesis, Johns Hopkins University, Jan. 2009.
- S. Revzen and J. M. Guckenheimer. Estimating the phase of synchronized oscillators. *Phys. Rev. E*, 78(5 Pt 1):051907–051918, 2008.
- S. Revzen and J. M. Guckenheimer. Finding the dimension of slow dynamics in a rhythmic system. *Journal of The Royal Society Interface*, 2011.

7 Format

Talk preferred

8 Travel Grant

Manu S. Madhav would like to request travel support to attend the conference.

Running across visible and non visible changes in ground level

Roy Müller, Michael Ernst and Reinhard Blickhan

Lehrstuhl für Bewegungswissenschaft, Institut für Sportwissenschaft, FSU Jena, Jena, Germany
{roy.mueller, michael.ernst, reinhard.blickhan}@uni-jena.de

1 Motivation and State of the Art

During running in a natural environment, humans must routinely negotiate varied and unpredictable changes in ground condition (e.g. stiff and compliant forest trails, asphalt partially covered with snow or uneven pavement and roots). Nevertheless, it seems that they handle such irregularities with ease.

Recent studies have shown that humans adapt their leg properties (e.g. leg stiffness, orientation, length) to changing ground conditions [1, 2, 3, and 4]. These adaptations take place within the descriptive realm of a spring-mass model and help to stabilize the locomotion in part passively. Current records of muscle activation during running across uneven ground suggest that the observed leg stiffness adjustment (during ground contact) is introduced by an altered pre-activation pattern (during flight before ground contact) of the *m. gastrocnemius medialis* [5]. The visual perception of the perturbation allows an adaptation of the motor program prior to the perturbation, overlapping a purely passive response. Such a visually guided pre-adaptation is not possible in experiments where the changes in ground level are invisible due to camouflage and occur by chance. However, until recently it was not known how human runners react if they encounter an unexpected drop and if they alter their strategies compared to running on uneven ground with visible ground level changes.

2 Own approach

For eleven subjects we investigated two consecutive contacts during running across visible and camouflaged changes in ground level [6]. After running on the unperturbed flat track, in a first set-up the variable-height force plate at perturbed second contact (first contact remains unchanged) was set down to an elevation of -5 cm and -10 cm, respectively. After the visible trials, in a second set-up, the variable height force plate was camouflaged with a non-transparent paper and randomly set to an elevation of 0 cm or -10 cm (Figure1).

For both situations (visible, camouflaged), we found significant variances in their leg parameters and ground reaction forces (GRF) during the perturbed second contact but also one step ahead, in the unperturbed first contact. At visible first contact, humans linearly adapt their GRF to

lower their center of mass. During the camouflaged situation, the GRF decreased too, but it seems that the runners anticipate a drop of about 5-10 cm. During the visible perturbed second contact the GRF increased with drop height. At the camouflaged second contact, GRF differ obviously from the observed reaction when crossing a similar visible drop, the contact time decreases and the initial impact peak increases (Figure1).

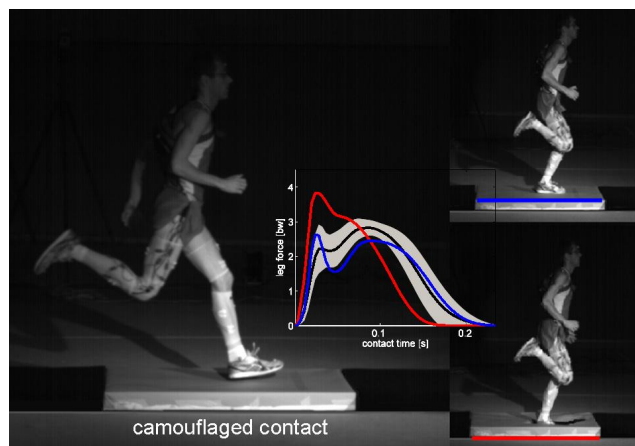


Figure1 Side view of the runway with camouflaged second contact. The force plate on second contact was set on two different elevations of 0 cm (upper right) and -10 cm (lower right). The initial impact peak increases in both situations.

3 Discussion and Open questions

Runners encountering camouflaged drops are able to cope with the situation but at the cost of a reduced performance which become visible in the increased impact peak. It is arguable whether this increased impact peak can be interpreted as a purely mechanical contribution to cope with the event or whether it can be attributed to a mismatch between the produced and required muscle force at the moment of impact (caused by the vague visual perception).

Furthermore, we observed increased angle of attack and leg length with drop height for both situations. This is in accordance with the results observed in birds running over a track with an unexpected drop [7]. Daley et al. showed that guinea fowls can easily negotiate drops of 8.5 cm (40% of their standing hip height). If we scale this

into human size, it would be hardly feasible. So, what is the different between human and avian locomotion?

References

- [1] Ferris, D. P., Liang, K., & Farley, C. T. (1999). Runners adjust leg stiffness for their first step on a new running surface. *Journal of Biomechanics* 32(8), 787-794.
- [2] Grimmer, S., Ernst, M., Günther, M., & Blickhan, R. (2008). Running on uneven ground: leg adjustment to vertical steps and self-stability. *Journal of Experimental Biology* (211), 2989-3000.
- [3] Kerdok, A. E., Biewener, A. A., McMahon, T. A., Weyand, P. G., & Herr, H. M. (2002). Energetics and mechanics of human running on surfaces of different stiffnesses. *J Appl Physiol*, 92(2), 469-478.
- [4] Müller, R., & Blickhan, R. (2010). Running on uneven ground: Leg adjustments to altered ground level. *Human Movement Science*, 29(4), 578-589.
- [5] Müller, R., Grimmer, S., & Blickhan, R. (2010). Running on uneven ground: Leg adjustments by muscle pre-activation control. *Human Movement Science*, 29(2), 299-310.
- [6] Müller, R., Ernst, M., & Blickhan, R. (2012). Leg adjustments during running across visible and camouflaged incidental changes in ground level. *Journal of Experimental Biology*, 215(Pt 17), 3072-3079.
- [7] Daley, M. A., Usherwood, J. R., Felix, G., & Biewener, A. A. (2006). Running over rough terrain: guinea fowl maintain dynamic stability despite a large unexpected change in substrate height. *Journal of Experimental Biology*, 209(Pt 1), 171-187.

Maximizing Energy Efficiency of the Robot Hopping based on Free Vibration

Xiaoxiang Yu^{*'***} and Fumiya Iida^{*}

^{*} Bio-Inspired Lab, ETH Zurich, Zurich, Switzerland

{*xiaoxiang.yu, fumiya.iida*}@mavt.ethz.ch

^{**}Artificial Intelligence Lab, University of Zurich, Zurich, Switzerland

yuxiaoxiang@ifi.uzh.ch

1 Introduction

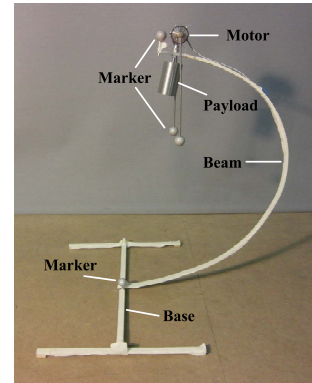
Despite legged robot locomotion has been studied by many researchers for long time, there are still a number of challenges remained. The energy efficiency of legged robot locomotion is still low if compared to the biological system. In order to improve the energy efficiency, our legged robots usually have complex mechanical designs, lack of locomotion patterns, and limited scalability in terms of weights and size [1][2][3]. From this perspective, we have been exploring the design strategy of a legged robot which achieves a high energy efficiency of locomotion and capability of variation in the weight and size.

Previously many researches attempted to introduce compliant elements into robot structures, since the spring-like system can store the kinematic energy and release it when necessary. One of the energy efficient legged robots is the Passive Dynamic Walker, which makes use of the passive dynamics of swing and stance legs to achieve natural bipedal locomotion with the energy efficiency similar to the human walk (specific energetic cost of transport (COT) at 0.2) [4]. The other robot is ARL Monopod. By optimizing many parameters, the robot can achieve the COT of 0.2 at 1.2m/s [5]. However, our robots still have limited speed, behavioral variations or more complex design. Furthermore, the design strategy does not scale to different sizes and body weights.

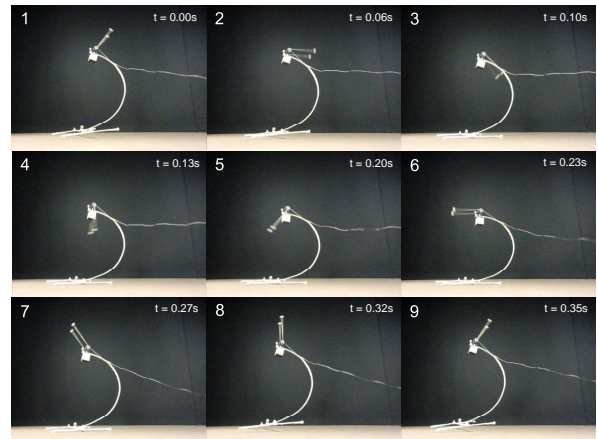
2 Curved beam robot based on free vibration

To achieve the energy efficient robot locomotion, we have been investigating the use of free vibration. Free vibration designates oscillatory motion patterns of an elastic mechanical structure when actuated at the resonance frequencies. The energy efficiency of locomotion can benefit from free vibration in many ways [6]. First, the mechanical design of the robot is simple since the free vibration does not need many motors or sensors that consume energy. Second, the leg can be made by a simple elastic structure that leads to a light weight of the leg. As a result, the energy loss in the collision with the ground is low. Third, the free vibration is induced simply by resonance frequencies instead of large actuation forces that consume a great deal of energy.

In our previous works, we made use of elastic curved



(a)



(b)

Figure 1: (a) The curved beam robot. (b) Time series photographs for one cycle stable vertical hopping of the curved beam robot. The time is shown at the upper right of each snapshot. The upper left numbers index the order. The rotation direction of the motor is clockwise. The snapshots 3 and 7 show the moments when the robot touches down and takes off the ground.

beams to achieve the free vibration. When an elastic curved beam is structured properly, a near-to resonance frequency from the motor can induce self-excited vibration which is exploited for the locomotion behavior. The curved beam is not only easy to manufacture but also low-cost and light-

weight. Moreover, the low damping of the curved beam is helpful to improve the energy efficiency of locomotion. From these perspectives, several different curved beam robots have been developed. Because of different designs of beam structures, each robot has a specific locomotion mode (e.g. hopping and running) [7]. These curved beam robots have shown high energy efficiency in the robot locomotion. In addition, one robot can exhibit various gait patterns (e.g. hopping and running) that can be controlled by regulating the actuated frequencies [8].

In this article, we introduce a hopping robot and discuss the further method of improving its energy efficiency in hopping locomotion. The robot is shown in Fig. 1a. It consists of a body made by an elastic curved beam, a foot base, a payload, a DC motor and two rotating masses. The curved beam is made of aluminum and structured into a C-shape, which provides certain elasticity. The foot base is also made of aluminum and has an H-shape structure to provide basic stability during locomotion. The DC motor drives the rotating masses around the shaft with approximately constant speed and this rotation induces centripetal force. By increasing angular velocity of these rotating masses, the whole system oscillates with larger amplitude, and at a certain frequency, the base takes off from the ground and the robot starts hopping. If the curved beam is structured into a certain shape, this hopping behavior occurs mainly along the vertical direction as shown in Fig. 1b.

The current robot can achieve an energetic cost of transport of 0.4 without optimization [6], so there is still room to improve the energy efficiency of the robot hopping. Moreover, it is not clarified whether the energy efficiency of locomotion can be maintained at the same level when the hopping robot changes its size and weight. Although the numerical simulations have proved that the high locomotion energy efficiency can be still achieved for the robot with a changing size, we are exploring the development of the hopping robot with the large size and heavy weight

During the manufacture, we need to carefully consider two points. The first one is the selection of the material that constructs the beam. The material needs to be strong and light. Furthermore, the damping in the beam should be also considered when the size and weight of the beam are changed. We will systematically explore some materials including glass-reinforced plastic and carbon fiber springs, and investigate their properties. The second one is the design of robot beams. We will adopt optimization methods to obtain certain number of optimized parameters for the energy efficient hopping, e.g. the shape, thickness and width of the elastic curved beam.

3 Open questions

There are three challenging questions in this project. First, it is not clarified the robot with large size and heavy weight can actually reach the high energy efficiency in hopping. Although we carefully set up a development plan,

there are still potential risks that we have not realized. Thus we expect several iterations of design and manufacture of the large hopping robot. Second, we lack effective methods to systematically analyze the stability of hopping, although there are some initial results that show the hopping robot is able to exhibit a certain ability of self-stabilizing in the hopping. Third, it is not fully understood how to design and control a set of desired locomotion patterns in different environments. It is particular challenging to investigate how to achieve the trajectory control in the hopping robot based on free vibration.

Acknowledgment

This research was funded by the Swiss National Science Foundation through the National Centre of Competence in Research Robotics.

References

- [1] G. Gabrielli and T. Von Karman, "What price speed? specific power required for propulsion of vehicles," *Mechanical Engineering*, vol. 72, pp. 775–781, 1950.
- [2] V. Tucker, "Energetic cost of locomotion in animals," *Comparative Biochemistry and Physiology*, vol. 34, no. 4, pp. 841–846, 1970.
- [3] A. D. Kuo, "Choosing your steps carefully: Trade-offs between economy and versatility in dynamic walking bipedal robots," *IEEE Robotics & Automation Magazine*, vol. 14, no. 2, pp. 18–29, 2007.
- [4] S. Collins, A. Ruina, R. Tedrake, and M. Wisse, "Efficient bipedal robots based on passive-dynamic walkers," *Science*, vol. 307, no. 5712, pp. 1082–1085, 2005.
- [5] M. Ahmadi and M. Buehler, "The arl monopod ii running robot: control and energetics," in *Proc. IEEE International Conference on Robotics and Automation*, vol. 3, 1999, pp. 1689–1694.
- [6] M. Reis and F. Iida, "An energy-efficient hopping robot based on free vibration of a curved beam," *IEEE/ASME Transactions on Mechatronics*, in press.
- [7] F. Iida, M. Reis, N. Maheshwari, K. Gunura, and S. Hauser, "Legged robot locomotion based on free vibration," in *Proc. IEEE International Workshop on Advanced Motion Control*, March 2012, pp. 1–6.
- [8] M. Reis, X. Yu, N. Maheshwari, and F. Iida, "Morphological computation of multi-gaited robot locomotion based on free vibration," *Artificial Life*, vol. 19, no. 1, pp. 97–114, 2012.

Poster Presentations

Data-driven Extraction of Drive Functions for Legged Locomotion: A Study on Cheetah-cub Robot

Mostafa Ajallooeian, Alexander Sproewitz, Alexandre Tuleu and Auke J. Ijspeert
Biorobotics Laboratory, École Polytechnique Fédérale de Lausanne (EPFL), Switzerland
{*first.last*}@epfl.ch

1 Introduction

The process of finding working gaits for legged robots always, to different extents, includes manual tuning, systematic search, or optimization of control parameters. This process populates a dataset of control parameter vectors and respective robot behavior factors including body rotations, speed, duty factor, etc. Normally, targeting actuated robots and not simulated ones, these datasets are sparse, unless systematic search with small parameter changes is applied.

The dataset obtained from a tuning process can include many gaits which share a similar performance in one behavior factor, e.g. speed, but differ in the control parameter vectors used. Our question here is, using the tuning dataset, how a continuous drive function can be calculated which takes the desired behavior, e.g. speed, and maps that to a control parameter vector¹. If this question is answered properly, then the robot operator (or a higher level controller) will have a single control knob to continuously change the desired behavior factor. Here in this contribution we address the case where a Central Pattern Generator (CPG) [3] is used as the locomotion controller and the desired behavior factor to control is the locomotion speed.

There are model-based approaches like [4, 5, 6] which explore speed control using closed-loop control of the step length. We address the question of the speed drive function from a model-free open-loop² control perspective when a parameter-speed dataset is given. We do our experiments with the compliant quadruped robot Cheetah-cub (Figure 1) [7], use trot gaits, and go up to a speed of more than 4 BodyLength/s which gives dynamic locomotion with a froude number $fr \approx 1$.

2 Drive function extraction

Our hypothesis is that if the desired continuous change in the behavior is small, then the change in control parameter vector should be small as well. So, using the collected tuning dataset, one should choose an array of parameter vectors such that the successive changes between them are minimal and results in a small change in the desired behavior factor

¹This is different from experiment design approaches like Doehlerters [1, 2] where prior knowledge about the form of the drive functions and independence of control parameters is available.

²no sensing other than for low-level motor control.

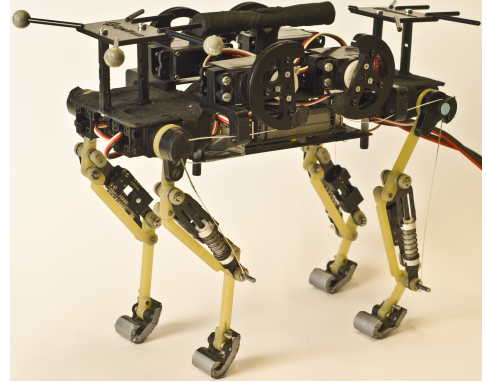


Figure 1: Cheetah-cub robot

(e.g a small increase in speed). Then function approximation tools can be used to fit continuous functions on the chosen parameter vectors.

We cluster all the control parameter vectors based on the speed that they give to the robot in equally spaced bins. So the i -th bin \mathcal{B}_i contains:

$$\mathcal{B}_i = \{\mathbf{x}_k : \|v(\mathbf{x}_k) - v_i\| < \delta\} \forall k = 1..K \quad (1)$$

where K is the number of control parameter vectors, \mathbf{x}_k is the k -th parameter vector, $v(\cdot)$ is the obtained speed, and v_i values are the center of the bins equally space on the speed axis and δ determines the bin width. Now if one candidate is chosen from each bin, then the total length of the multi-segment line passing through all candidates is:

$$d = \sum_{i=1}^{N-1} \|\mathbf{x}_{k_i} - \mathbf{x}_{k_{i+1}}\| \quad (2)$$

Table 1: CPG parameters and the obtained drive functions

Name	Param.	Obtained drive function
Frequency	f	$-1.7v^2 + 4.7v + 0.3$
Desired duty factor	D	$-0.18v + 0.66$
Fore/hind hip amplitude	A_H	$12v^3 - 9.3v^2 + 48v + 19$
Fore knee swing amplitude	A_{FK}	$-0.74v^3 + 2.3v^2 - 1.4v + 0.71$
Hind knee swing amplitude	A_{HK}	$-0.44v^3 + 1.7v^2 - 1.2v + 0.71$
Fore hip offset	O_{FH}	$1.8v^3 - 6.8v^2 + 5v + 14$
Hind hip offset	O_{HH}	$4.4v^3 - 17v^2 + 12v + 13$
Fore knee offset	O_{FK}	$-0.14v^2 + 0.12v + 0.38$
Hind knee offset	O_{HK}	$-0.28v^2 + 0.24v + 0.16$

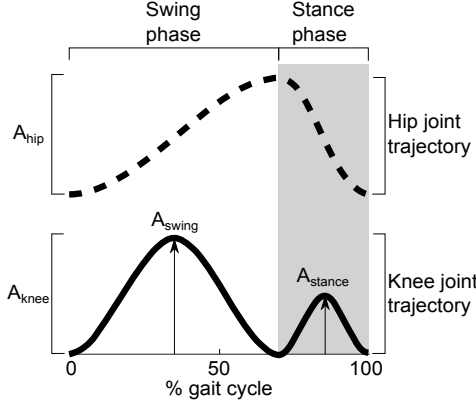


Figure 2: Parametric joint angles profiles generated by CPG.

with N being the number of bins, and \mathbf{x}_{k_i} the k -th member of the i -th bin. Finally, the problem of finding the drive function knot points can be formalized as:

$$\min_{k_i, i=1..N} d \quad (3)$$

Solving the aforementioned problem, we obtain an array of control parameter vectors with respectively increasing robot speeds, which then should be approximated by fitting tools to obtain the drive functions.

3 Results

We implemented our approach on the Cheetah-cub robot, a small ($\sim 1Kg$) quadruped robot with compliant pantograph legs (Figure 1). In order to find working gaits for Cheetahcub, a series of manual trials was done to find working gaits. A collection of 110 control parameter vectors and respective locomotion speeds was obtained from the manual tuning process, which includes only the cases where the robot did not fall during locomotion on a flat terrain. This data collection is depicted in Figure 3 (cross markers).

The CPG model used for the control of locomotion is defined by four coupled phase oscillators generating the desired joint angles profiles for hip and knee joints, depicted in Figure 2. The hip joint angle profile is a skewed sine (skewed based on the desired duty factor), and the knee joint angle profile consists of a flexion during the swing phase (to obtain foot clearance), and an additional flexion during the stance phase to actively control the leg length. The CPG control parameters are given in Table 1.

Solving³ the problem in equation (3) gave the selection of the knot points per bins which are depicted with bold markers in Figure 3. We then used first to third order polynomials to fit a function on these points and thus obtained the drive functions as depicted in Figure 3 and given in Table 1.

³Using brute force and checking all possible solutions. This takes about five minutes using MATLAB running on a quad-core PC. For bigger datasets, one can instead use discrete valued optimization techniques like Genetic Algorithm or [8].

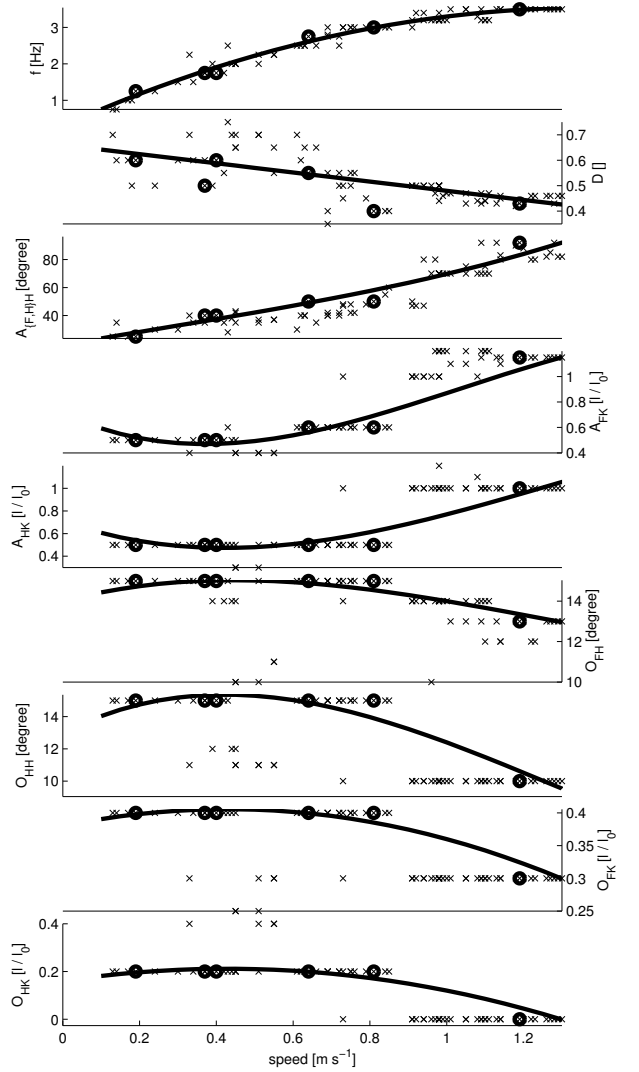


Figure 3: The tuning dataset (cross markers), selected candidates (bold markers), and the calculated drive functions. Bin parameters are $v_i = 0.1 + 0.2i$, $i = 0..6$ and $\delta = 0.1$.

We interpolated the obtained drive functions in the speed range of $v = 0.1 + 0.1i[m/s]$, $i = 0..12$ and extracted the respective control parameter vectors. Then we ran the robot with these parameter vectors (5 runs for each parameter vector) and recorded the locomotion speed. Results of these evaluation runs are depicted in Figure 4. No post-processing was done on the obtained drive functions. The robot did not fall in any of these experiments, and the average pitch and roll angles were always less than 10 degrees.

4 Discussion

We proposed a simple way to extract drive functions from existing data obtained from manual tuning of a robot's locomotion controller. These drive functions act as a single control knob which give the proper control parameters for a certain desired behavior (speed in this paper). The introduced method differs from a model fitting on the whole dataset which is not the proper way to extract the drive func-

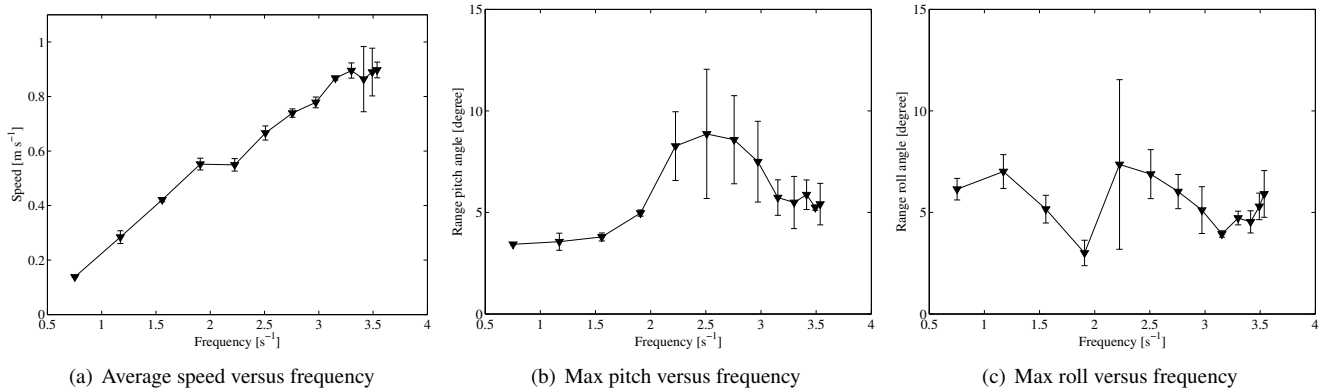


Figure 4: Evaluation of the obtained drive functions. The error bars show the minimum and maximum values.

tions because it will average different trails out instead of finding a correct path along them. We believe that the introduced drive function extraction method is useful in many cases where robots are going through a tuning process and a dataset of behavior versus control parameters is collected.

The introduced approach is not dependent to the meaning of the control parameters. One can use a different control strategy, like a different CPG controller, or even a model-based controller, and obtain a parameter-behavior dataset while tuning the robot’s locomotion. Such dataset can then be utilized to obtain a data-driven drive function using the method introduced in this paper.

Our drive-function experiments with the cheetah-cub robot were limited to testing the obtained parameter vectors one at a time, and we have not yet explored the online change of the control parameters during locomotion. We expect a slow change of the control parameters to give a smooth change in the locomotion speed, but this has to be further tested, especially to inspect the transient behavior and balance of the robot during the parameter change.

There are a number of open questions that we aim to explore in the future: 1) Is there a common parametric representation of the drive functions for a class of similar quadrupeds? 2) Can we also extract drive functions for all control parameters including both feedforward and feedback parameters? 3) Can we use the method here to extract drive functions at a different level of control, e.g. at the muscle activation level?

References

- [1] D. Doehlert, “Uniform shell designs,” *Applied statistics*, pp. 231–239, 1970.
- [2] D. Vojnovic, D. Chicco, and H. El Zenary, “Doehlert experimental design applied to optimization and quality control of a granulation process in a high shear mixer,” *International journal of pharmaceuticals*, vol. 145, no. 1, pp. 203–213, 1996.
- [3] A. Ijspeert, “Central pattern generators for locomotion control in animals and robots: A review,” *Neural Networks*, vol. 21, no. 4, pp. 642 – 653, 2008.

tion control in animals and robots: A review,” *Neural Networks*, vol. 21, no. 4, pp. 642 – 653, 2008.

- [4] J. Hodgins and M. Raibert, “Adjusting step length for rough terrain locomotion,” *Robotics and Automation, IEEE Transactions on*, vol. 7, no. 3, pp. 289–298, 1991.
- [5] A. Kuo, “A simple model of bipedal walking predicts the preferred speed–step length relationship,” *Ann Arbor*, vol. 1001, pp. 48109–2125, 2001.
- [6] S. Pouya, M. Ajallooeian, and A. Ijspeert, “a closed-loop optimal control approach for online control of a planar monopod hopper,” in *15th International Conference on Climbing and Walking Robots (CLAWAR 2012), USA*, 2012.
- [7] A. Sproewitz, A. Tuleu, M. Vespignani, M. Ajallooeian, E. Badri, and A. Ijspeert, “Towards dynamic trot gait locomotion – design, control, and experiments with a compliant quadruped robot,” *International Journal of Robotics Research (IJRR)*, 2012, Submitted.
- [8] J. Kennedy and R. Eberhart, “A discrete binary version of the particle swarm algorithm,” in *Systems, Man, and Cybernetics, 1997. Computational Cybernetics and Simulation., 1997 IEEE International Conference on*, vol. 5, pp. 4104–4108, IEEE, 1997.

Terrestrial locomotion of the common quail: one leg function for all gaits?

Emanuel Andrada*, John Nyakatura**, Stefan Hochstein*, and Reinhard Blickhan*

* Motion Science, Friedrich-Schiller-Universität Jena, Jena, Germany.

** Institut für Spezielle Zoologie und Evolutionsbiologie mit Phyletischem Museum,
Friedrich-Schiller-Universität Jena, Jena, Germany.

{*emanuel.andrada, john.nyakatura, reinhard.blickhan*}@uni-jena.de

1 Motivation & State of the Art

When birds increase speed during terrestrial locomotion, they change gait. At slow speeds, birds walk. With increasing speed they gradually change to grounded running (a running gait without aerial phases [1, 2]). At higher speeds many species change from grounded running to aerial running. Gait changes appear to not always be correlated to changes in the metabolic energy consumption, but specialized walking/running birds utilize specific gaits at given speeds on a treadmill in correlation to energetic minima [1, 5]. So far, studies on avian gait transitions mostly focus on i) variations of spatio-temporal parameters as the speed increases ii) leg joint amplitudes related to speed, and iii) the gradual shift from vaulting mechanics towards bouncing mechanics of the center of mass (CoM) [1, 3-6]. Although these studies provided important insight into speed related changes of avian terrestrial locomotion, we still know surprisingly little about how template parameters related to the SLIP (spring loaded inverted pendulum) vary with gait changes, and thus how their tuning impacts gait and motor control strategies. Template related parameters describe biomechanical systems as a whole. In the case of avian terrestrial locomotion by reducing the hindlimb to a "virtual leg" linking the hip or the CoM with the center of pressure (CoP). Parameters of the SLIP model are the leg stiffness k , touch-down angle α , mass m , and rest length l_0 . Experimental determination of k and l_0 are challenging, especially for small animals.

In the present work we aim to study how the template parameters k and l_0 in a small predominantly terrestrial bird change with speed and gait.

Our main hypothesis is that at the global virtual leg function approximates a spring-mass behavior for all gaits. Contrary to humans or large animals which walk with extended legs, and thus with high leg stiffness (e.g. humans, [7]), the crouched posture observed in small animals may enable spring-like locomotion even at lower speeds.

2 Own approach

Eight adult common quails were motivated to move across

a 3 m long walking-track at their preferred speeds. The track was covered with sand paper to reduce slipping. We simultaneously recorded kinematics (biplanar X-ray videography) and ground reaction forces (GRFs).

We calculated the instantaneous position of the body's CoM from kinematic data (X-ray motion analysis data of the limbs, additional kinematic data of digitized head, neck and torso landmarks, and each element's CoM position) as presented in [6]. CoM's motions and speed were used to obtain the fluctuation of the potential (E_p) and kinetic energy (E_k). Then, we relied on the percentage of congruity, as proposed by [8], between E_p and E_k to discriminate bouncing (running) from vaulting (walking) mechanics.

We computed the instantaneous virtual leg length as the distance between CoM and CoP. As leg length usually is non-symmetrical relative to touch-down (TD) and take-off (TO) events, we averaged relative virtual leg lengths in order to determine the leg stiffness k from kinetic data. We computed k as $k = GRF_{midstance} / \Delta l$, where $\Delta l = (l_{leg_TD} + l_{leg_TO}) / 2 - l_{leg_midstance}$. Note that $l_0 = (l_{leg_TD} + l_{leg_TO}) / 2$ is the rest length of the spring. Dimensionless leg stiffness was defined as $\hat{k} = kl_0 / mg$, where m is the mass of the bird and g gravity. The dimensionless leg compression (ψ) related to the compression of the spring at midstance is equal to the GRF in body weight ($\psi = GRF / mg = k(l_0 - l) / mg$; see [2]).

3 Results and Discussion

Globally, quail locomotion displays a surprisingly linear-like spring-like behavior at all investigated gaits (walking, grounded running, and running) in accordance to the SLIP model. However, contrarily to the telescopic expectation of the SLIP model, GRFs are more vertically oriented; highlighting that trunk balance during all gaits seems to be a mandatory issue.

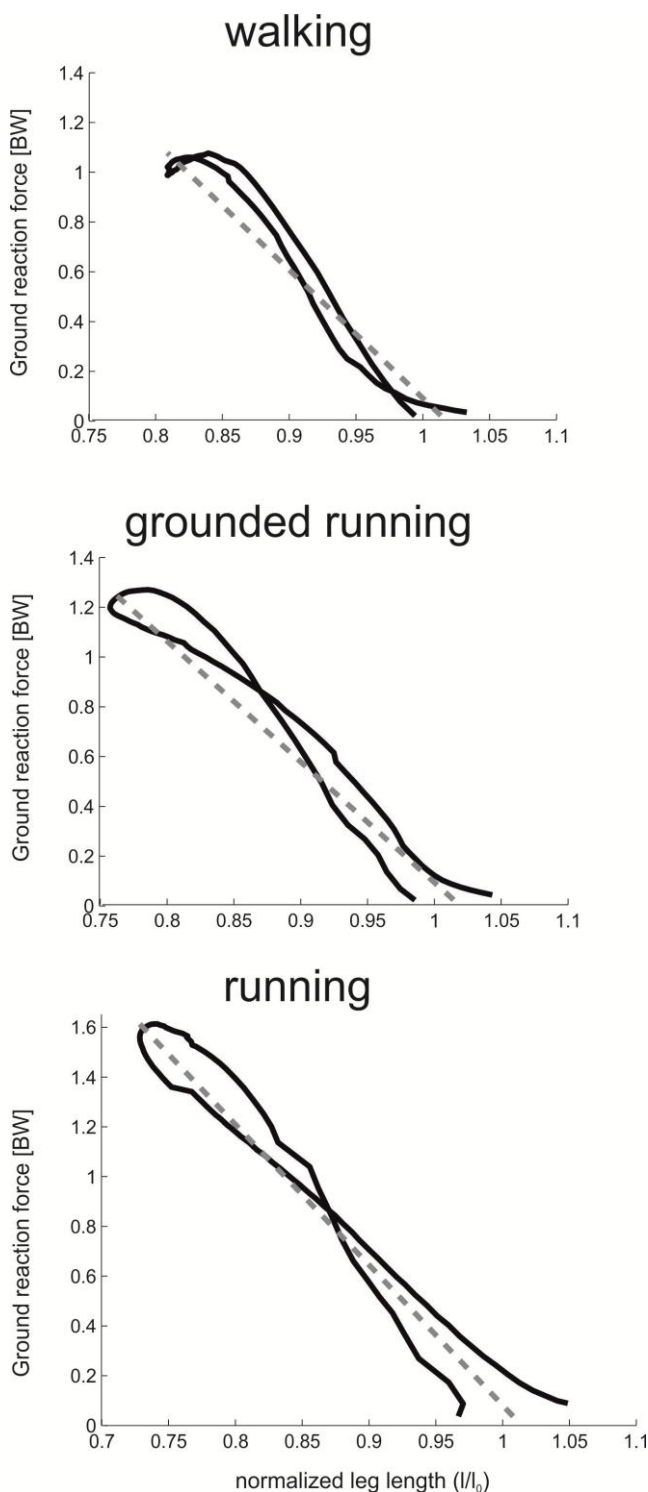


Figure 1 Virtual leg-function at different gaits (force-length plots). Results are presented as mean (walking, $n=32$ strides; grounded running, $n=34$ strides; running, $n=8$ strides)

Our results show that between walking and grounded running the leg stiffness decreases (w. $\hat{k} = 5.77 \pm 1.25$; g.r.

$\hat{k} = 4.99 \pm 0.67$). Accordingly, increased leg compression resulted in higher vertical GRFs at midstance during grounded running compared to walking. When quails run, higher leg compression permits them to introduce aerial phases, and leg stiffness is increased (to values not significantly different to those obtained during walking; $\hat{k} = 6.15 \pm 0.62$) to the cope with the decreasing contact times. The value $l_0 [m]$, associated with the rest length of the spring in the SLIP model, was similar for walking and grounded running, but significantly longer for running (w. 0.0872 ± 0.0087 ; g.r. 0.0886 ± 0.007 ; r. 0.0956 ± 0.009). We hypothesize that a more extended leg at touch-down, controlled by the joint angles in knee and intertarsal joints, has an important influence in the leg stiffness adjustment process during running.

4 Open questions

How does real local leg control contribute to a global linear-like spring-like behavior?

Do small birds always use the same leg function despite gait and speed?

References

- [1] Rubenson, J., Heliams, D. B., Lloyd, D. G., Fournier, P. A., Gait selection in the ostrich: mechanical and metabolic characteristics of walking and running with and without an aerial phase. *Proc R Soc Lond, B* 271, 1091-1099, 2004.
- [2] Andrada, E., Nyakatura, J., Müller, R., Rode, C., Blickhan, R., Grounded Running: An Overlooked Strategy for Robots. *Autonomous Mobile Systems*. Springer Berlin Heidelberg, pp. 79-87, 2012
- [3] Gatesy SM, Biewener AA., Bipedal locomotion: effects of speed, size and limb posture in birds and humans. *J Zool* 224(1): 127-147, 1991.
- [4] Abourachid A, Renous S., Bipedal locomotion in ratites (Paleognathiform): examples of cursorial birds. *Ibis* 142:538-549, 2000.
- [5] Nudds RL, Folkow LP, Lees JJ, et al., Evidence for energy savings from aerial running in the Svalbard rock ptarmigan (*Lagopusmutahyperborea*). *Proc R Soc B Biol Sci* 278(1718): 2654-2661, 2011
- [6] Nyakatura, J. A., Andrada, E., Grimm, N., Weise, H., Fischer, M. S., Kinematics and Center of Mass Mechanics During Terrestrial Locomotion in Northern Lapwings (*Vanellus vanellus*, Charadriiformes). *J Exp Zool Part A: Ecological Genetics and Physiology*, 317(9):580-94, 2012.
- [7] Lipfert, S. W., Günther, M., Renjewski, D., Grimmer, S., Seyfarth, A., A model-experiment comparison of system dynamics for human walking and running. *Journal of Theoretical Biology* 292, 11-17, 2012.
- [8] Ahn AN, Furrow E, Biewener AA., Walking and running in the redlegged running frog, *Kassina maculata*. *J Exp Biol* 207(3): 399-410, 2004.

Friction Compensation and Stiffness Evaluation on a Variable Torsion Stiffness

P. Beckerle *, F. Stuhlenmiller, J. Schuy *, J. Wojtusch **, S. Rinderknecht *, and O. v. Stryk **

* Institute for Mechatronic Systems (IMS) — ** Simulation, Systems Optimization and Robotics (SIM)
 {lastname}@{ims/sim}.tu-darmstadt.de — Technische Universität Darmstadt, Germany

1 Introduction

With safety aspects due to closer human-robot interaction and increased requirements in energy efficiency due to mobile applications, series elastic joint concepts receive high priority in contemporary robotics. Beyond making robots more safe and flexible, such concepts can store energy and thus optimize the energetic efficiency of the robot's motion. Therefore adjusting the stiffness is advantageous, since the natural frequency of the drive train and the frequency of the desired trajectory can be matched [1, 2].

2 State of the Art

Introduced in the 1990s, the Series Elastic Actuator (SEA) [1] and the Mechanical Impedance Adjuster (MIA) [3] pathed the way for series elastic actuation and variable compliance in robotic joints. The majority of concepts developed since then can be categorized in four groups considering the principle of stiffness variation [4]. Those are equilibrium-controlled, antagonistic-controlled, structure-controlled and mechanically controlled stiffness. As the original SEA changes the equilibrium position of a spring, it belongs to the first group. Antagonistic-controlled approaches utilize actuators working against each other as in AMASC [5]. Although both groups allow for stiffness variation, energy is dissipated during operation in both: The equilibrium-controlled solutions require power to simulate a virtual spring while the actuators work against each other in the antagonistically-controlled ones. Thus, many contemporary variable stiffness designs belong to structure-controlled and mechanically controlled solutions. Structure-controlled devices change stiffness by a modification of an elastic element's structure as in MIA. Mechanically controlled ones like MACCEPA [2] adjust the system stiffness by pre-tension.

3 Concept and Implementation

The authors' approach based on variable torsion stiffness (VTS) aims at biomechanically inspired robotic joints [6]. As described there and shown in Figure 1, actuator 1 applies an input torque τ_i to the torsional elastic element to move the link. For the adjustment of the torsional stiffness $k_{vts}(x)$, the active length x of an torsional elastic element is varied by changing the position of counter bearing

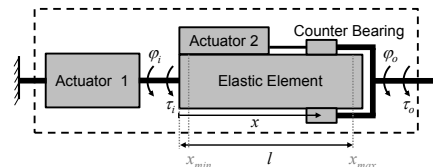


Figure 1: Concept of variable torsion stiffness [6]

ing using actuator 2. Hence, this concept belongs to the structure-controlled group. Since the joint driving and the stiffness control actuator are separated, the adjustment of the stiffness does not depend on the joint position. For the im-



Figure 2: Implementation of the elastic element

plementation of the elastic element, a hollow cylinder with outer radius $R = 11.0\text{mm}$ and inner radius $r = 8.7\text{mm}$ and a length of $l = 0.16\text{m}$ is chosen due to [6]. The realized version manufactured from polyamide is presented in Figure 2. A flange on the left connects the element to actuator 1, while six evenly distributed fitting rails are used to transmit the torque from the tube to the output side. Due to the deviations in material and geometry compared to the ideal cylinder proposed in [6], the stiffness characteristics might not fit perfectly the requirements given there. Thus, the influence of those deviations is investigated experimentally in this paper. To realize the experimental evaluation



Figure 3: Test rig for experimental investigations

of the stiffness characteristics, a friction compensation is

realized. As most of the friction is due to the motor-gear unit, only this is investigated. In the experiment, the motor torque is increased linearly from 0Nm to ± 10 Nm. Figure 4

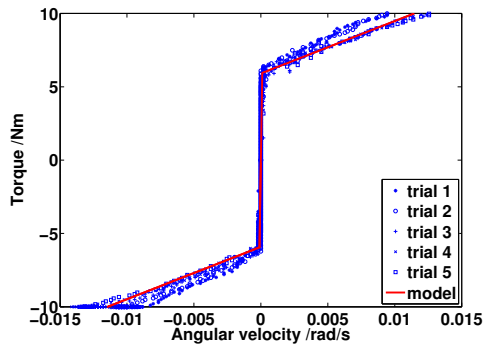


Figure 4: Friction characteristics and model

shows the data measured in 5 trials for each direction and the model fitted with least squares regression. With this, the friction torque is compensated by feedforward control of the model $\tau_f = 5.9\text{Nm}\text{sign}(\dot{\phi}_i) + 357.1\text{Nms/rad}\dot{\phi}_i$.

4 Stiffness Characteristics

The stiffness characteristics of the element are investigated in a static experiment. Therefore, the active length x of the elastic element is set to values between 0.011m and 0.151m in steps of 0.02m and a final step at $x = 0.166$ m. As these settings should refer to different stiffness values, the pendulum is positioned at specific angles statically and the input and output angles are measured. Further, the torque τ_g resulting from gravity is determined. With the models given in [6], the stiffness k_{vts} at a specific length x can be determined by

$$k_{vts} = \frac{\tau_g}{\phi_i - \phi_o}, \quad (1)$$

and is parameterized by a least squares regression. The stiffness characteristics determined in this experiments are shown in Figure 5. It becomes distinct that the stiffness

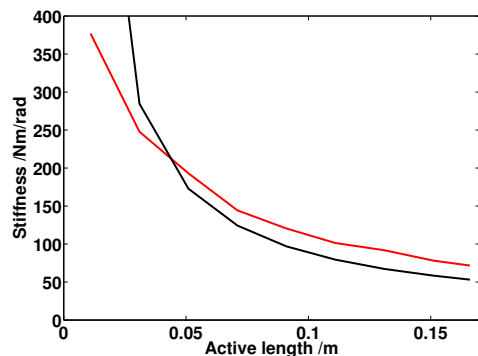


Figure 5: Experimentally determined stiffness characteristics

determined in the experiment on the test rig plotted in red

shows higher values than expected from the analytical model plotted in red. Only for an active length below $x = 0.04$ m the analytical solution exceeds the experimentally obtained results. This is due to the reason, that the analytical solution converges to infinity, while the real system is constrained to finite stiffness. The increased stiffness of the experimental measurement is caused by the implementation, as the fitting rails reinforce the elements structure.

5 Discussion and Conclusion

Regarding the friction characteristics, the influence of static friction (5.9Nm) is higher than the one of gravity (4.1Nm for $\phi_o = 10^\circ$) and has to be compensated. Further, a confirmation of the friction compensation in the complete test rig should be performed before testing in dynamic scenarios. For the stiffness characteristics, the evaluation shows that the implemented elastic elements have comparable behaviour as the analytical model predicts. Anyhow, the real element geometry should be considered during design to achieve a better consistency - e.g., by finite element simulation.

6 Open Questions

One open question for future research is the investigation of alternative design of the elastic element. Further, the structural integrity of the elastic element is a key issue due to the high loads and stresses that can be expected during dynamic operation. As for the current implementation stiffness control is performed manually, an appropriate actuation is to be determined for a complete realization of the concept.

References

- [1] G. A. Pratt and M. M. Williamson, "Series elastic actuators," in *Proceedings of the 1995 IEEE/RSJ International Conference on Intelligent Robots and Systems*, 1995.
- [2] B. Vanderborght et al., "Comparison of Mechanical Design and Energy Consumption of Adaptable, Passive-compliant Actuators," *The International Journal of Robotics Research*, vol. 28, pp. 90–103, 2009.
- [3] T. Morita and S. Sugano, "Design and development of a new robot joint using a mechanical impedance adjuster," in *1995 IEEE International Conference on Robotics and Automation*, 1995.
- [4] R. Van Ham et al., "Compliant Actuator Designs Review of Actuators with Passive Adjustable Compliance/Controllable Stiffness for Robotic Applications," *IEEE Robotics & Automation Magazine*, vol. 16, pp. 81–94, 2009.
- [5] J. W. Hurst et al., "An actuator with physically variable stiffness for highly dynamic legged locomotion," in *2004 IEEE International Conference on Robotics and Automation*, 2004.
- [6] J. Schuy et al., "Conception and Evaluation of a Novel Variable Torsion Stiffness for Biomechanical Applications," in *IEEE International Conference on Biomedical Robotics and Biomechatronics*, 2012.

Mechanical Influences on the Design of Actuators with Variable Stiffness

P. Beckerle *, J. Wojtusch **, S. Rinderknecht *, and O. v. Stryk **

* Institute for Mechatronic Systems (IMS) — ** Simulation, Systems Optimization and Robotics (SIM)
 $\{lastname\}@ \{ims/sim\}.tu-darmstadt.de$ — Technische Universität Darmstadt, Germany

1 Introduction

In the 1990s compliant joint actuation was introduced to robotics with the Series Elastic Actuator [1] and the Mechanical Impedance Adjuster [2]. Such concepts provide safer human-robot interaction, can store energy and decrease force control effort [1]. In the following decades, energy efficient actuation with such concepts had high impact in mobile applications such as bipedal robots, since the stiffness adjustment can be utilized to match the natural frequency of the drive train to the frequency of the desired trajectory [1, 3]. A review on designs of actuators with variable elasticity between drive and link is given in [4] and followed by an energetic examination of specific concepts in [3].

Early solutions for actuators with variable stiffness are designed focusing on the drive side and hence only the input inertia of the drive train is considered as in [1]. Although the input and output inertia of the drive train were included in models of the complete robotic application according to [5], the dynamic interaction of those inertias is not considered for drive train design sufficiently [2]. In contrast to this, input inertia is not considered appropriately in the dimensioning of recent approaches due to the assumption that drives represent ideal torques or position generators [6, 7, 8, 9]. Further, the analysis of power consumption in [3] is based on the same assumptions and hence does not regard the inertia interaction during dynamic operation. So far, the influence of more than one inertia is mainly considered in complex antagonistically-controlled concepts as AMASC [10] and VSA [11]. While the influence of interaction does not show significant influence on the characteristics of AMASC, its impact is not examined in the case of VSA. In the structure-controlled and comparable complex VSJ [12], the interaction influence is rather low as in AMASC.

Yet, this is not the case in general applications and thus both inertias and their interaction should be considered, as this has strong impact on the drive train dynamics and hence its dimensioning as well as an energy-efficient strategy for stiffness variation. This paper investigates those influences on a linearized model of a generic actuator with variable stiffness based on the parameters of VTS [13].

2 Modelling

To investigate the mechanical influences of input inertia, output inertia and their interaction, simple dynamic models

of serial elastic drives are used. Their basic structures are given in Figure 1. While the upper model considers the out-

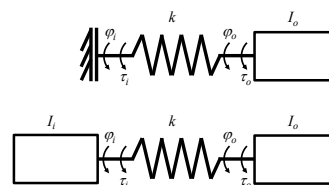


Figure 1: Investigated drive train models

put inertia I_o only, the one depicted below can be used to examine the interaction of the inertias. Both are investigated with and without the torque $m_o g l \sin(\varphi_o)$ at the link due to gravity. The dynamics of those can be represented by their equations of motion: Considering the output inertia only, this is given by the one from [13], while the extended model is given by the equations from [5]. After linearization at equilibrium position, these are transformed to the frequency domain. Thus, the first model with gravity is described by

$$\frac{\varphi_o(s)}{\tau_i(s)} = \frac{1}{I_o s^2 + k + m_o g l}, \quad (1)$$

while the transfer function of the extended model is

$$\frac{\varphi_o(s)}{\tau_i(s)} = \frac{k}{I_o I_i s^4 + ((I_i + I_o)k + I_i m_o g l) s^2 + k m_o g l}. \quad (2)$$

In both models, φ_i and φ_o represent the input and output position, while τ_i and τ_o are the corresponding torques. The stiffness k is treated as a variable parameter to examine the impact of stiffness variation on the mechanical influences.

3 Mechanical Influences

The system dynamics of all four systems - with/without I_i and with/without g - are given in the bode plots shown in Figure 2. Compared to the simple model plotted in blue, significantly higher natural frequencies can be observed for all other models. For the green plot, this is due to an increased stiffness caused by the gravity term, which also leads to an increased static gain. By considering I_i , the integral behaviour of a rigid body mode can be observed in addition to a higher increase of the natural frequency in the red plot. For the cyan plot, this

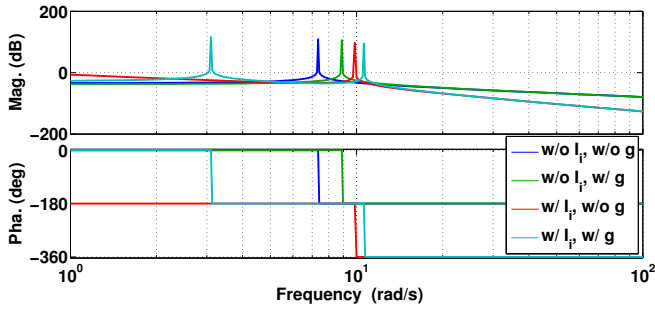


Figure 2: Mechanical influences on drive train dynamics

rigid body mode is transformed to an elastic mode with higher frequency due to the fixation introduced by gravity and the elastic mode increases in frequency. In Figure 3, the

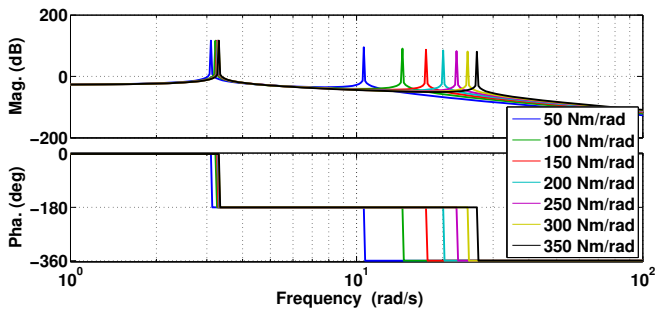


Figure 3: Impact of stiffness variation

impact of stiffness variation is presented for the extended model. With increasing stiffness, both natural frequencies increase, where the influence is stronger for the second one.

4 Discussion and Conclusion

As the natural frequencies of actuators with variable serial stiffness should be optimized to the specific task for energy-efficient operation, an holistic modelling of the basic mechanical system is required for design. Thus, the mechanical influences of input inertia and gravity should not be neglected in general applications, since the reflected inertia on the input can be comparable to output inertia due to the gear ratio and gravity introduces a virtual fixation. Although drive and link are not rigidly coupled, the reflected inertia is fully present at the input and influences the system dynamics significantly. By considering those mechanical effects, an investigation of power consumption should show two areas with minimum power due to the two natural frequencies. This also has impact on the stiffness variation strategy, since other stiffness values have to be chosen to match the frequencies of actuator and trajectory.

5 Open Questions

Future work should focus on the investigation of the influence of damping as well as analyses of the eigenvectors,

which are defining the relative motion, and the power consumption of the system.

References

- [1] G. A. Pratt and M. M. Williamson, "Series elastic actuators," in *Proceedings of the 1995 IEEE/RSJ International Conference on Intelligent Robots and Systems*, 1995.
- [2] T. Morita and S. Sugano, "Development and evaluation of seven-d.o.f. mia arm," *Proceedings of the 1997 IEEE International Conference on Robotics and Automation*, pp. 462 – 467, 1997.
- [3] B. Vanderborght et al., "Comparison of Mechanical Design and Energy Consumption of Adaptable, Passive-compliant Actuators," *The International Journal of Robotics Research*, vol. 28, pp. 90–103, 2009.
- [4] R. Van Ham et al., "Compliant Actuator Designs Review of Actuators with Passive Adjustable Compliance/Controllable Stiffness for Robotic Applications," *IEEE Robotics & Automation Magazine*, vol. 16, pp. 81–94, 2009.
- [5] A. W. Spong, "Modeling and control of elastic joint robots," *Journal of Dynamic Systems, Measurement, and Control*, vol. 109, pp. 310–318, 1987.
- [6] A. Jafari et al., "AwAS-II: a new actuator with adjustable stiffness based on the novel principle of adaptable pivot point and variable lever ratio," in *2011 IEEE International Conference on Robotics and Automation*, 2011.
- [7] K. W. Hollander et al., "Adjustable robotic tendon using a 'jack spring'TM," *Proceedings of the 2005 IEEE 9th International Conference on Rehabilitation Robotics*, pp. 113 – 118, 2005.
- [8] J. S. Sulzer et al., "MARIONET: an exotendon-driven rotary series elastic actuator for exerting joint torque," in *9th International Conference on Rehabilitation Robotics*, 2005.
- [9] S. Wolf and G. Hirzinger, "A new variable stiffness design: Matching requirements of the next robot generation," in *2008 IEEE International Conference on Robotics and Automation*, 2008.
- [10] J. W. Hurst et al., "An actuator with physically variable stiffness for highly dynamic legged locomotion," in *2004 IEEE International Conference on Robotics and Automation*, 2004.
- [11] G. Tonietti et al., "Design and control of a variable stiffness actuator for safe and fast physical Human/Robot interaction," *Proceedings of the 2005 IEEE International Conference on Robotics and Automation*, vol. 1, pp. 526–531, 2005.
- [12] J. Choi et al., "Design of a robot joint with variable stiffness," in *IEEE International Conference on Robotics and Automation*, 2008., 2008.
- [13] J. Schuy et al., "Conception and Evaluation of a Novel Variable Torsion Stiffness for Biomechanical Applications," in *IEEE International Conference on Biomedical Robotics and Biomechatronics*, 2012.

Active shifting of center-of-mass in quadruped bounding robot

Jorgen Christian Larsen, Kasper Stoy
University of Southern Denmark, Maersk Mc-Kinny Moller Institute
{*jcla, kaspers*}@mmmi.sdu.dk

1 Motivation

The locomotion gaits of animals are elegantly supported by the mechanisms, materials and physical properties of their bodies. In every stride, the body supports the movement of the animal to make every single step as seamless as possible. The cheetah is e.g using its tail to steer its body during running. The number of examples where the body of an animal is used to support its movements are countless. If we compare what is observed in nature with a large range of “state of the art robots”, some differences are noticed. The body of the robot is often stiff and inflexible, and does therefore not support the dynamics of the robots during locomotion. The brain is controlling the robot in the classical way, where every movement of the robot is planned, and very little influence have been left for the dynamics of the body. The body is so to speak ”under total control”. A reason is that, this is the general way of designing robots, firstly because creating mechanics with the same abilities as we seen in nature is an difficult engineering problem, but also because it offers several advantages such as making the system easier to model and allows for more precise control. However, this approach is maybe limiting the results that can be achieved in the area of locomotion. In contrast, we will describe experiments done on a robot build from the robotic toolkit, LocoKit. The robot is quadruped, with a flexible body, and with a added mass on top of the robot that can be shifted between front and back on the robot during locomotion in order to control the center-of-mass (COM) on the robot, *Figure 1*. In the spirit of embodied artificial intelligence (Pfeifer R.), we aim to improve the robustness, efficiency, and versatility of robot locomotion by controlling the physical properties of the robot’s body.

2 State of the art

In the past years, there have been put a lot of effort into studies of animal locomotion. Some of these studies have been concentrating on the mass distribution [1], others on the movements of the body center of mass [2]. On robots, some experiments have been made with robots either able to walk or jump, by using an actuated lever mechanism to actuate the body, [3], [4].

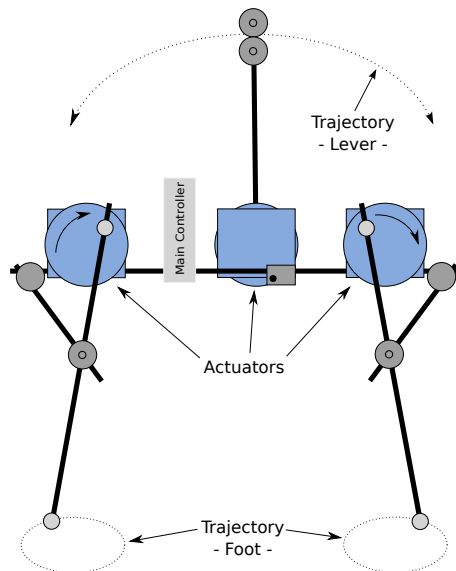
3 Approach

To construct the robot used in these experiments, we have used the LocoKit robotic toolkit [5]. The dimensions of the robot is W27xD18.5xH21cm, one motor per leg and one motor used to move the COM. The motors for the four legs are placed next to the legs on the body of the robot and the motor for moving the COM is positioned slightly towards the hind, holding an arm with a weight in the end. This arm is used to move the center of mass (COM) during locomotion. The control of the robot is done in two separate functions; the control of the legs, and the control of the lever arm. The legs on the robot are controlled in a simple feed-forward open loop. The legs are synchronized with each other, to make sure that the two leg pairs, front and hind, always have the same phase shift between them. The lever arm is either controlled by using feedback control using the tilt of the robot as input or open-looped control synchronizing the arm with the movement of the legs with a specific phase shift. During all experiments the robot have been programmed for a bounding gait.

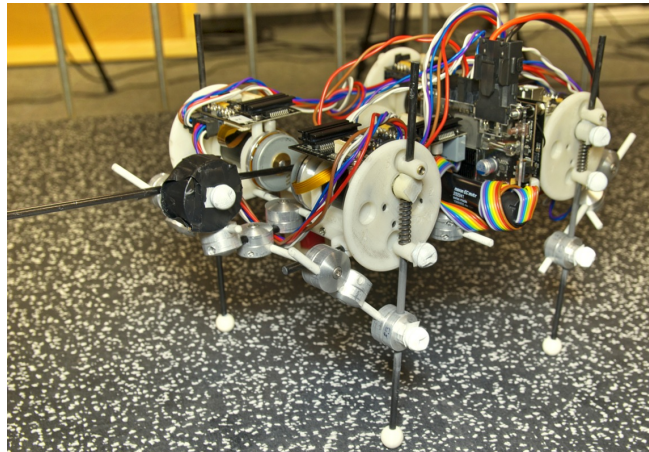
4 Discussion outline

Shifting the COM during locomotion have a big impact on the locomotive abilities of our robot. It opens up a number of interesting research questions that we would like to address. What makes these studies even more interesting is that they can be focused on multiple questions like the control of the lever arm, the embodiment of the arm, locomotive skills of the robot etc. The following list is to name but a few:

- Can moving the COM improve the locomotive abilities like speed, energy efficiency, gait stability etc.?
- Can the locomotion be made more stable?
- Can the lever arm be used to increase mobility in uneven terrain?
- Which control schema is most fruitful. Having the lever arm coupled to the body or the legs?
- What is the optimal moment that the lever arm have to produce to make body steady during bounding?



(a) Schematic of the robot for testing the impact of using an actuated lever arm.



(b) Actual robot build from LocoKit.

Figure 1: Figure (a) shows the schematics of the robot used during all the experiments. The robot is quadruped, and has an actuated lever positioned slightly towards the hind of the robot. The weight on the lever can be adjusted during the experiments. In the right figure (b) the final robot build from LocoKit is shown.

To get a deep insight into the dynamics of the robot, we are measuring the kinematics of the robot during experiments with 9 high speed cameras (Oqus series, Qualisys, Gothenburg, Sweden) at 250Hz, as well as the forces created by the robot using a force plate (Kistler, Winterhut, Switzerland). Combining these data will provide us with great insight into the dynamics of the complete system as it acts in the real world.

5 Acknowledgments

The research leading to these results has received funding from the European Community's Seventh Framework Programme FP7/2007-2013 - Future Emerging Technologies, Embodied Intelligence, under grant agreement no. 231688.

References

- [1] David V. Lee, John E. A. Bertram and Rory J. Todhunter, "Acceleration and Balance in Trotting Dogs," *The Journal of Experimental Biology* 202, 35653573 (1999).
- [2] Thilo Pfau, Thomas H. Witte, and Alan M. Wilson, "Centre of mass movement and mechanical energy fluctuation during gallop locomotion in the Thoroughbred racehorse," *The Journal of Experimental Biology* 209, 3742-3757, Published by The Company of Biologists 2006
- [3] Fumiya Iida, Raja Dravid, Chandana Paul "Design and Control of a Pendulum Driven Hopping Robot," *Intelligent Robots and Systems*, 2002. IEEE/RSJ International Conference on Intelligent Robots and Systems.

- [4] Ryota Hayashi and Showzou Tsujio "High-performance Jumping Movements by Pendulum-type Jumping Machines," *Proceedings of the 2001 IEEE/RSJ International Conference on Intelligent Robots and Systems Maui, Hawaii, USA, Oct. 29 -Nov. 03,2001*

- [5] Jorgen Christian Larsen, David Brandt, Kasper Stoy "LocoKit: A Robot Construction Kit for Studying and Developing Functional Morphologies," *From Animals to Animats 12, Lecture Notes in Computer Science Volume 7426*, 2012, pp 12-22

Different strategies for different situations? Adaptations of the CoM-trajectories to visible and camouflaged ground level changes in human running.

Michael Ernst, Martin Götze, Roy Müller and Reinhard Blickhan
Institute of Sport Science, Friedrich-Schiller-University, Jena, Germany
{michael.ernst, martin.goetzel, roy.mueller, reinhard.blickhan}@uni-jena.de

1 Motivation

While jogging or running in an urban environment or on nature trails, humans face major and minor disturbances requiring quick reactions and adaptations. For example, we actively initiate turning, sidestepping pedestrians, or jumping over obstacles. On the other hand, minor disturbances such as sudden moderate changes in ground level or stiffness can be compensated passively (e.g. [1, 2]). Investigating the kinematics of the runner's center of mass (CoM) in such situations can unravel which global locomotion control strategies humans use and help to distinguish between willingly initiated (and actively controlled) or mechanical (passively controlled) reactions. Such insights not only help toward a more complete understanding of the locomotion but may also find application in the control of bipedal robots.

2 State of the art

It is well known that human runners show adaptations in their kinematics and dynamics if they face disturbances on the path. These adaptations are visible in the global (leg stiffness, orientation and length – referring to the spring-mass model [3]) and local leg parameters (leg joint angles). For example, for running on surfaces with altered ground stiffness it could be shown that humans adapt the leg stiffness to compensate for changes in the ground stiffness [1, 4, 5]. These adaptations in leg stiffness correlate with a nearly unaffected CoM deflection for both known and unknown changes in ground stiffness. From this, the researchers inferred that the control of the CoM trajectory might be a general principle in running and that adaptations of leg stiffness are utilized to achieve this [4, 5]. Runners encountering ground level changes adapt leg stiffness too [2, 6, 7]. But they also alter leg orientation and length. Using numerical modeling (spring-mass model) it could be demonstrated that the adaptation process is able to stabilize running [2, 8]. However, until now it is not clear what kind of CoM strategies humans use while running on uneven ground. For example, do they use controls keeping the CoM trajectory nearly unchanged [9, 10] similar to the findings for ground stiffness changes or do they prefer controls maximizing gait stability [11, 12]?

3 Own approach

To shed light on the strategies human runners use we first analyze adaptations of the CoM for different ground level changes and second discuss these findings with respect to recently proposed theoretical strategies.

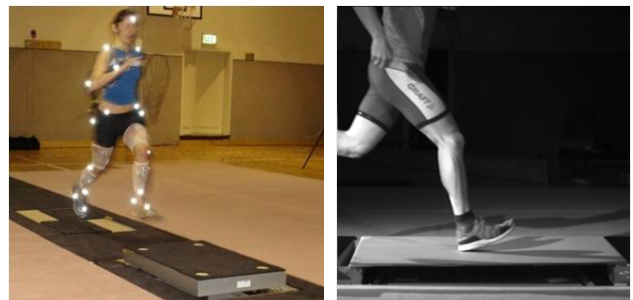


Figure 1 Different ground level situations (left) running on a visible single step of 10 cm and (right) running across a camouflaged drop of 10 cm.

For the experimental part, we studied running on visible single or permanent steps (10 cm and -10 cm, see [6]) and running across camouflaged drops (which occurred by chance, 10 cm depth, see [7] and fig.1). For both studies, the relative adaptations in the vertical oscillation of the CoM compared to the undisturbed situation were analyzed. We found that the runners adapted their CoM in preparation for a visible step up or down by lifting it about 50% of step height or lowering it by about 40% of drop height. After contact on the changed ground level, different adaptations depending on the situation occur (about 100% for plateau up/down, about 60% for single step up/down, fig.2A&B).

We also found adaptations in preparation for the camouflaged step which are similar to the adaptations for a visible step down. The runners lowered their CoM (about 25% of the possible drop height) equally whether a drop occurred or not (fig.2C). However, the height of the CoM in the subsequent flight phase depends on the situation which actually occurred (drop or not). In case the runners encountered the drop, the CoM was lowered about 90% of

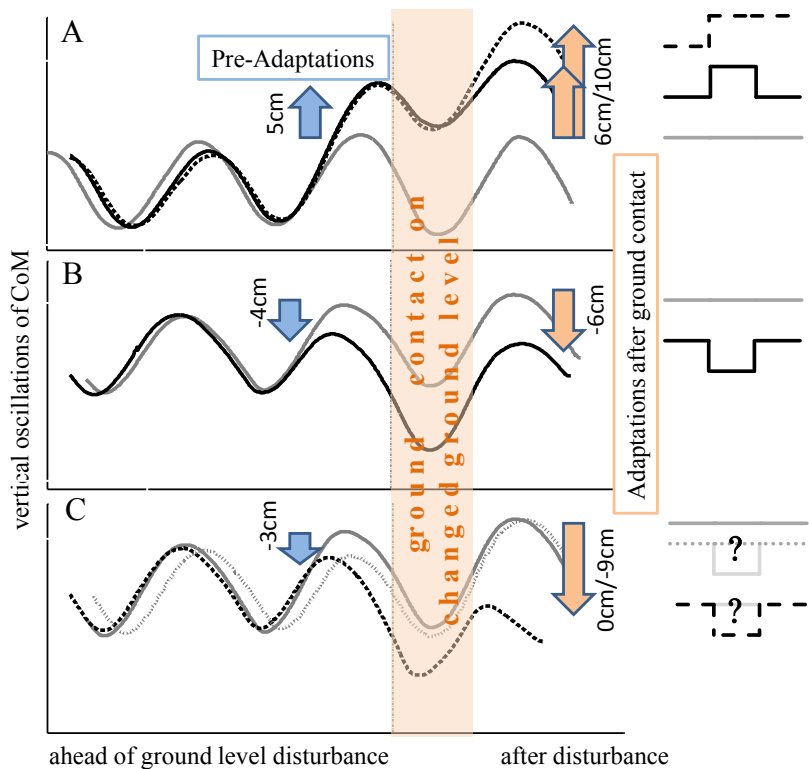


Figure 2 Vertical oscillations of the CoM of a typical runner for: (A) running up a visible single step of 10 cm (black-solid) and a visible permanent elevated track step of also 10 cm (black-dashed), (B) running down a single visible 10 cm drop (black-solid), and (C) for running across a camouflaged area where drops of 10 cm occurred by chance (black-dashed for the 10 cm drop, grey-dotted for an unchanged ground level). The grey-solid lines represent the reference trails i.e. running on even ground. The adaptations of the vertical deflection of the CoM are highlighted with thick arrows (blue – ahead of a (possible) ground level change, orange – in the subsequent flight phase after a ground level disturbance).

drop height, and in case the runners encountered an even ground, their CoM height was almost unaffected (fig.2C).

4 Discussion and open questions

Adaptation to visible ground level changes

If human can see the disturbances they adapt their global leg parameters not only on the disturbed step but also in advance of a step ahead. These adaptations change the height of the center of mass with respect to the actual ground level and achieve a smooth, not abruptly changed ride of the CoM. Also, it shows that runners prefer two or more steps to compensate for a visible ground level disturbance, regardless of whether it is a single step up or permanently altered ground level.

The finding that human runners alter their CoM height when running on uneven ground suggests that they do not use strategies keeping the CoM trajectory unchanged [4, 9, 10], even if the disturbance in ground level is only short and temporary (single step up or down). Such adaptations were expected for a permanently altered ground level where runners have to adapt their CoM in order to perform a normal running gait, but not necessarily for a single step. This raises the question why human runners use the observed strategies?

Aspects influencing the CoM-strategies

The observed strategies may represent a compromise with respect to energy consumption, safety, and/or comfort (see also [13]). In our experiment, the visual perception of the mechanical disturbance largely influences the reaction

of the system and makes it difficult to distinguish between active (feedback) and passive (self-stabilizing feedforward) strategies. We think experiments with camouflaged disturbances, where runners cannot predict whether a disturbance occurs or not, lead to a more complete understanding of the strategies in human running. Furthermore, it can help to unravel to which extent the locomotion control rely on active and passive parts.

Strategies for running across camouflaged disturbances

The adaptations to the CoM height which we found for the camouflaged situation (drop or even ground) are in part different to the same, visible situation. The pre-adaptation in front of the camouflaged step with the potential disturbance are of the same size as for a 5 cm drop [7]. Because the runners are aware that the next step might be a drop they lower their CoM ahead, probably with the aim to reduce the peak ground reaction forces (safety and comfort). In the subsequent flight phase after the camouflaged step, the runners CoM height depends on the encountered situation (drop or even ground, fig. 2C). We found that the height difference between these two situations equals almost the drop height. Numerical modeling (spring-mass model) revealed that such a height difference is characteristic for a dead-beat control maximizing gait stability [11, 12].

Open questions and future work

The observations suggest that humans rely on CoM-strategies which support sufficient and situation-dependent gait stability. Until now, it could not be conclusively

unraveled to which extend active or passive parts contribute to the control. For the different studies the EMG-pattern of the leg muscles were recorded and will be analyzed in the future. They might reveal whether humans rely mainly on reflexes (e.g. positive force feedback) or on feedforward strategies (e.g. use a predetermined EMG pattern set ahead of the disturbance), or of both when altering the leg parameters for the compensation of a disturbance and stabilization of the movement.

Acknowledgment - This project was supported by the German Research Foundation (DFG: Bl 236/21).

References

- [1] Ferris, D. P., Louie, M., and Farley, C. T., 1998, "Running in the real world: adjusting leg stiffness for different surfaces," *Proc Biol Sci*, 265(1400), pp. 989-994.
- [2] Grimmer, S., Ernst, M., Gunther, M., and Blickhan, R., 2008, "Running on uneven ground: leg adjustment to vertical steps and self-stability," *J Exp Biol*, 211(Pt 18), pp. 2989-3000.
- [3] Blickhan, R., 1989, "The spring-mass model for running and hopping," *J Biomech*, 22(11-12), pp. 1217-1227.
- [4] Ferris, D. P., Liang, K., and Farley, C. T., 1999, "Runners adjust leg stiffness for their first step on a new running surface," *J Biomech*, 32(8), pp. 787-794.
- [5] Kerdok, A. E., Biewener, A. A., McMahon, T. A., Weyand, P. G., and Herr, H. M., 2002, "Energetics and mechanics of human running on surfaces of different stiffnesses," *J Appl Physiol*, 92(2), pp. 469-478.
- [6] Müller, R., and Blickhan, R., 2010, "Running on uneven ground: Leg adjustments to altered ground level," *Hum Mov Sci*, 29(4), pp. 578-589.
- [7] Müller, R., Ernst, M., and Blickhan, R., 2012, "Leg adjustments during running across visible and camouflaged incidental changes in ground level," *J Exp Biol*, 215(17), pp. 3072-3079.
- [8] Seyfarth, A., Geyer, H., and Herr, H., 2003, "Swing-leg retraction: a simple control model for stable running," *J Exp Biol*, 206(Pt 15), pp. 2547-2555.
- [9] Ernst, M., Geyer, H., and Blickhan, R., 2009, "Spring-Legged Locomotion on uneven Ground: A Control Approach to keep the running Speed constant," *Proceedings of the 12th CLAWAR*, pp. 639-644.
- [10] Koepf, D., and Hurst, J., 2011, "Force control for planar spring-mass running," *Intelligent Robots and Systems (IROS)*, 2011 IEEE/RSJ International Conference on, pp. 3758-3763.
- [11] Seyfarth, A., and Geyer, H., 2002, "Natural control of spring-like running -- optimized self-stabilization," *Proceedings of the 5th CLAWAR*, pp. 81--85.
- [12] Ernst, M., Geyer, H., and Blickhan, R., 2012, "Extension and customization of self-stability control in compliant legged systems," *Bioinspiration & Biomimetics*, 7(4), p. 046002.
- [13] Blickhan, R., Ernst, M., Koch, M., and Müller, R., accepted, "Coping with disturbances," *Hum Mov Sci*.

Measurement of 3D human foot deformation during walking by digital image correlation method

Ikumi Fujiwara*, Naomichi Ogihara*, Koh Hosoda**, Takeo Nagura***, Toshiyasu Nakamura***

*Department of Mechanical Engineering, Keio University, Yokohama, Japan

**Graduate School of Information Science and Technology, Osaka University, Suita, Japan

***School of Medicine, Keio University, Tokyo, Japan

ogihara@mech.keio.ac.jp

1 Introduction

The anatomical structure of the human foot is known to be substantially different from those of other primates owing to its adaptation to bipedal locomotion. For examples, the human foot possesses the longitudinal arch and the unique structure of the calcaneocuboid joint that are not present in the other primate feet[1]. As human walking is a mechanical phenomenon to move the center of body mass forward without falling by appropriately generating the ground reaction forces acting onto the foot, it is anticipated that mechanical characteristics of the human foot embedded in its anatomical design may contribute to realize appropriate physical interaction between the body and the ground, and hence facilitate generation of robust human bipedal walking. However, how the human foot physically interacts with the ground during bipedal walking has not been fully investigated. In this study, we therefore attempted to clarify the deformation of the human foot during bipedal walking by means of digital image correlation method.

2 Methods

The digital image correlation method is an optical method to measure 3D deformation of an object surface by using the stereo-triangulation and the correlation of the speckle pattern on the surface[2]. In this study, we sprayed the right foot of an adult male participant with aqueous black ink to draw the speckle pattern on the foot surface. The participant was then asked to walk at self-selected speed. The dorsolateral surface of the foot from heel-contact to toe-off was filmed at 30 Hz by two manually-synchronized digital cameras as shown in Figure 1. The image size of the camera was 1920 x 1080 pixels. We used digital image correlation software Vic-3D (Correlated Solutions, Columbia, SC, USA) for quantification of the foot deformation during walking.

3 Results & Discussion

Figure 1 shows dynamic changes in the distribution patterns of the magnitudes and directions of the principal strain on the dorsolateral surface of the foot during walking.

In the present study, the skin strain distribution was calculated assuming that the foot shape at the mid-stance phase is the reference shape configuration. Therefore, the color contour map in Figure 1 illustrated how each location on the foot surface was stretched or contracted from the mid-stance phase.

As shown in Figure 1, at the heel contact, the anterior surface around the ankle was stretched and the dorsomedial surface corresponding to the distal end of the first metacarpals was contracted, since the ankle joint was comparatively plantarflexed and the first metatarsophalangeal joint was dorsiflexed (Fig 1.A). When the heel was lifted, the lateral surface corresponding to the fifth metatarsal was stretched in the anteroposterior direction (Fig 1.E), suggesting that the lateral longitudinal arch started to flatten at this time. However, this region was then stretched in the dorsopalmar direction at the time of toe-off (Fig 1.F), possibly because the transverse arch flattened as the toe pushed off the ground and the tuberosity of the fifth metatarsal was projected out laterally.

4 Open questions

Detailed understanding of the deformation of the foot during locomotion is important for elucidating how the design and architecture of the human foot contribute to generation of adaptive bipedal walking in humans. We would like to discuss with the other participants of the AMAM meeting during poster presentation how the extracted deformation characteristics of the human foot during walking may contribute to the facilitation of balance control in human walking.

References

- [1] L. Aiello, C. Dean, An Introduction to Human Evolutionary Anatomy : Academic Press, 1990.
- [2] M.A. Sutton, J.J. Orteu, H.W. Schreier, Image Correlation for Shape, Motion and Deformation Measurements : Springer, 2009.

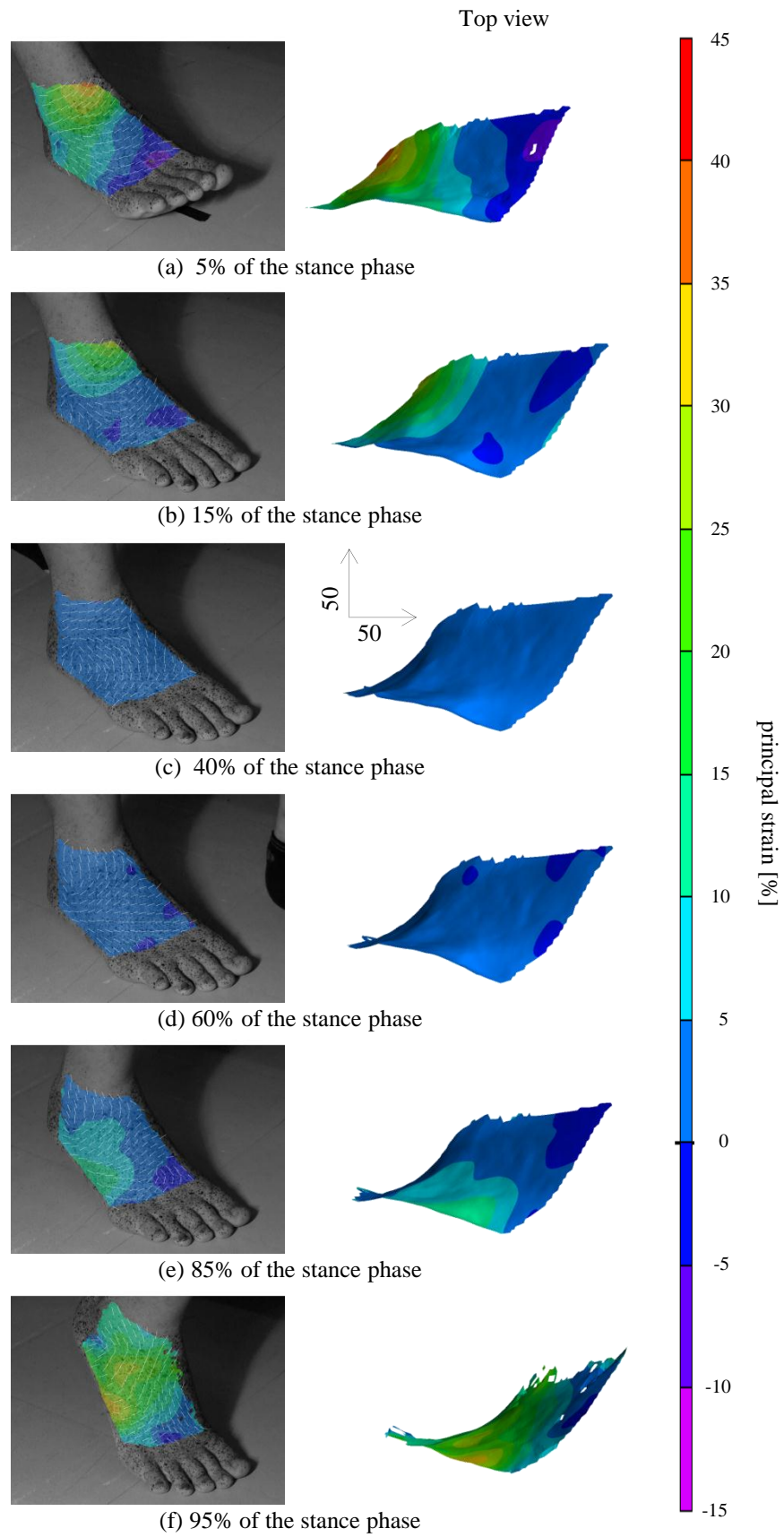


Figure1 Principal strain distribution on the dorsolateral surface of the human foot during walking.

Transitional Buckling Model for Active Bending Effect in Pole Vault

Toshihiko Fukushima*, Satoshi Nishikawa*^{***}, Kazutoshi Tanaka* and Yasuo Kuniyoshi*

*Intelligent Systems and Informatics Lab., The University of Tokyo, Tokyo, Japan

**Research fellow of the Japan Society for the Promotion of Science

{*fukushima, nisikawa, tanaka, kuniyosh*}@isi.imi.i.u-tokyo.ac.jp

1 INTRODUCTION

Tool-use enables humans to accomplish tasks that cannot be realized solely with the human body. In the robotic motion, tools can be used to extend the robot's body, allowing it to achieve tasks that would be otherwise impossible to complete [1]. That is to say, skillful tool-use dramatically improves the robot's performance of locomotion. In those skill, a particularly interesting task is the pole vault, in which the athlete's movement dynamically changes depending on the way the pole is manipulated.

It is important for improving the vaulting performance that the athlete suspending from the pole actively manipulates the pole. In fact, it is known that the athlete's total energy when crossing the bar can exceed 120% of the initial energy at takeoff [2]. Many previous studies have measured the athlete's mid-flight behavior. For example, Frère *et al.* took electromyograms of the muscles in upper limbs and analyzed the role of each muscle in the overall action [2]. Other studies such as McGinnis *et al.* used inverse kinematics to calculate the moment exerted by the athlete mid-flight [3]. These studies have focused on measuring the athlete's behavior. However, they have not explicitly addressed the how the athlete's manipulation of the pole contribute to his overall performance.

Therefore, in this study, we try to analyze the active bending effect to the vaulting performance proposing "Transitional Buckling Model". This proposed model accounts for the athlete's active bending on the pole. In addition, we find out how the robot should actuate the pole. Accordingly, we present one of the way to skillfully use the flexible and complex tools.

2 MODEL

2.1 Active Bending of the Pole

In a pole vault, it is known that the athlete's body movements have a significant impact on the pole. Based on previous works which use EMG signals from upper limbs [2] or use inverse kinematics [3] to analyze the athlete's actions, it is known that an experienced athlete bends his pole as follows (Fig.1).

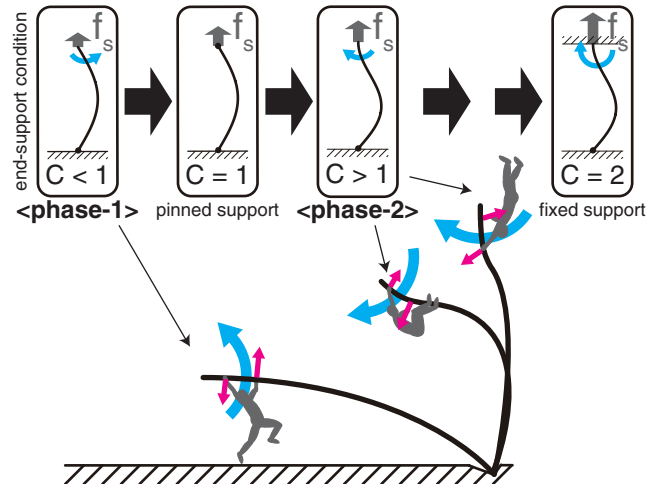


Figure 1: Transitional Buckling Model. Pink linear arrows are forces from arms. Blue curved arrows are input bending moments from arm forces.

Phase 1: Pole-plant and pole-bending phase

By applying an upward force on the lower hand-grip of the pole, the athlete bends the pole in such a way as to increase the pole curvature.

Phase 2: Pole-straightening phase

By doing a handstand mid-flight, the athlete bends the pole in such a way as to reduce the pole curvature.

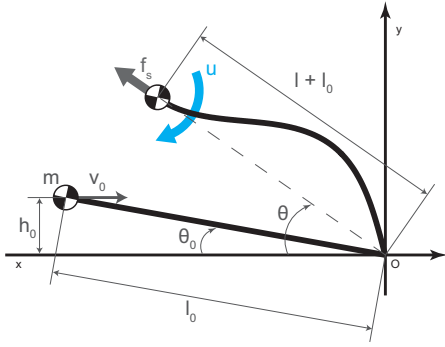
It has enough studied that how the athlete action, but not enough studied that how the action affect vaulting performance. Thus, there is a need to model a system including both the human and the pole.

2.2 Transitional Buckling Model for Active Bending

First, we modeled the overall pole vault motion illustrated in Fig.2. It was quite difficult to model the system containing flexible pole so that we modeled the system by Euler buckling model. Euler buckling model can treat the force exerted by the flexible pole as a simple constant force and is generally used for analysis of the pole vault. Besides, we treated vaulter and vaulter's

Table 1: Simulation parameter

parameter	description	experiment1	experiment2
θ	elevation angle of mass	variable	\rightarrow
l	displacement from pole length	variable	\rightarrow
θ_0	initial angle	$\sin^{-1}(l/h_0)$	\rightarrow
l_0	pole length	3-5[m]	\rightarrow
h_0	initial height	2.0[m]	\rightarrow
v_0	initial velocity	6-9[m/s]	9[m/s]
m	mass of vaulter	80[kg]	\rightarrow
g	acceleration of gravity	9.8[m/s ²]	\rightarrow
E	Young's modulus	70[GPa]	\rightarrow
I	second moment of area	5[cm ⁴]	\rightarrow
f_s	exerted force from the pole	-	\rightarrow
u	input bending moment	-	\rightarrow

**Figure 2:** Pole suspending one point mass model.

motion as the mass point and bending moment. Therefore, the equation of motion is represented as:

$$\frac{d}{dt} \begin{pmatrix} \theta \\ \dot{\theta} \\ l \\ \dot{l} \\ i \end{pmatrix} = \begin{pmatrix} \dot{\theta} \\ -\frac{1}{l+l_0}(2l\dot{\theta} + g \cos \theta) \\ i \\ -(l+l_0)\dot{\theta}^2 + g \sin \theta \end{pmatrix} + \begin{pmatrix} 0 \\ 0 \\ 0 \\ 0 \\ \frac{f_s}{m} \end{pmatrix}, \quad (1)$$

$$\text{where } f_s = C \frac{\pi^2 EI}{l_0^2} = (\text{const.}).$$

Here, C is the end-support condition coefficient, E is Young's modulus, and I is second moment of area. The mass point has horizontal initial velocity v_0 and the pole applies the exerted force f_s on the mass point. The exerted force f_s can be represented by Euler buckling load. According to the Euler buckling model, as long as the end-support condition of the pole remains constant, f_s remains constant regardless of pole deformation. In the Euler buckling model, the coefficient C is determined by the end-support condition (Fig.1). The exerted force f_s is constrained by the coefficient C .

Second, we represent active bending effect presented in Sec.2.1 as the extended Euler buckling model. Most previous pole vault models have treated both the top and bottom end of the pole as pinned support, and C

has been usually set to constant as $C = 1$ [4] [5]. In contrast, our proposed model also treats the bottom end of the pole as pinned support, while it differently treats the top end of the pole as variable support transitioning as a function of input bending moment u (Fig.1). Thus C is set to variable $C = C(u)$. The exerted force f'_s is represented as:

$$f'_s = C(u) \frac{\pi^2 EI}{l_0^2}. \quad (2)$$

Therefore, to substitute f'_s for f_s in Eq.(1) properly accounts for bending moment influence. We call this proposed model the Transitional Buckling Model (TBM). The relationship between the active bending action and $C(u)$ is as follows.

Phase 1: $C(u) < 1$

Force received from the pole f'_s is small, so that the pole can be bent with a larger curvature than in $C = 1$.

Phase 2: $C(u) > 1$

Force received from the pole f'_s is large, so that the mass point can reach a greater height.

3 SIMULATION EXPERIMENTS

We focused on the advantage of input bending moment. To compare that we conducted follow experiment. First, we experimentally compared the original buckling model treating C as constant and the Transitional Buckling Model treating $C(u)$ as variable. Second, in Transitional Buckling Model, we experimentally explored the vaulting performance shifting the timing and change rate of the transition of $C(u)$.

3.1 Experimental Setup

We simulated the pole vault by use of numerically-solving ordinary differential equation eq.(1) with a step time of 1[ms]. Simulation parameters was determined

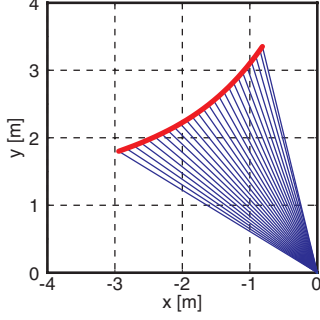


Figure 3: Trajectory of the mass point while the mass point contacts with the pole. Red heavy line is the trajectory of the mass point. Blue thin line is the segment from origin to the mass point. $l_0 = 3.5[\text{m}]$, $v_0 = 9.0[\text{m/s}]$.

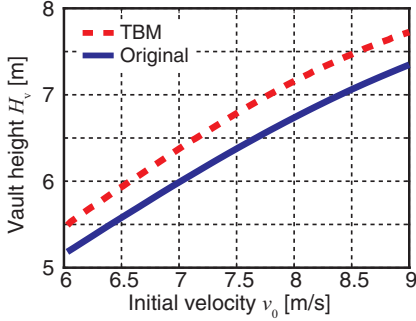


Figure 4: Vault height at each initial velocity. 'original' does not include active bending, and 'TBM' includes it.

referring to an actual athlete's data (Table1). Vault height H_v is a maximum height of the trajectory of the mass point. The mass point lets go of the pole when the pole straightens, so that it takes off in a projectile motion.

3.2 Experiment1: Active Bending Effect

In original Euler buckling model, C is constant as $C = 1$. In Transitional Buckling Model (TBM), $C(u)$ is linearly changed from $C_0 = 0.8$ to $C_1 = 1.2$. We changed initial velocity from $6.0[\text{m/s}]$ to $9.0[\text{m/s}]$. In TBM, vault height H_v at each initial velocity was larger than in the original model (Fig.4). Here, H_v is a maximum height of the trajectory of the mass point. The mass point lets go of the pole when the pole straightens, so that it takes off in a projectile motion. Thus, input bending moment affects the vaulting performance.

3.3 Experiment2: How to Change Input Moment

In TBM, we analyzed the effect of how $C(u)$ changes from C_0 to C_1 . Vault height H_v map show that H_v took a high value around $\dot{l} = 0$ and sharp increase area

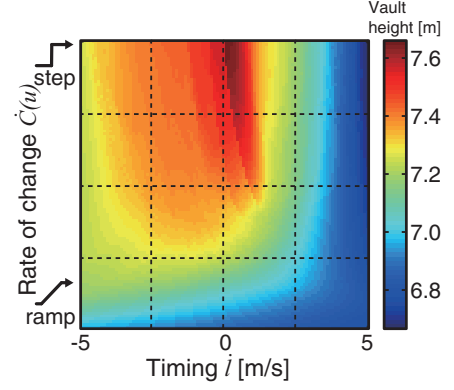


Figure 5: Vault height map by the transition timing and the rate of change with end-support condition coefficient $C(u)$. Horizontal axis is the transition timing normalized by \dot{l} . When $\dot{C}(u)$ is large, input bending moment is like a step input.

(Fig.5). The point of $\dot{l} = 0$ is the point of minimum l , which is the timing at which the pole is maximally bent. Therefore, the robot should change the direction of the bending moment like a step input at the time when the pole is maximally bent.

4 CONCLUSION

In this paper, we analyzed the active bending effect to vaulting performance proposing a model that the pole's end-support condition varies with input bending moment. We showed that input bending moment improved the vaulting performance. In addition, we analyzed the best timing and the change rate at which the bending moment direction to improve the vaulting performance. We found that the robot should change the direction of bending moment like a step input at the time when the pole is maximally bent. Accordingly, we inspire the way of skillfully using complex flexible tools.

In the future, we will implement the above model in a control theory of a pole vaulting robot.

5 OPEN QUESTIONS

The equation for input bending moment u and end-support condition coefficient $C(u)$ is still an open question.

6 ACKNOWLEDGEMENT

We thank Yuko Hara for her valuable comments on the draft of the manuscript. This work has been supported by MEXT/JSPS KAKENHI Grant Number 22240015.

References

- [1] C. Nabeshima, Y. Kuniyoshi, and M. Lungarella, "Towards a model for tool-body assimilation and adaptive tool-use," in *IEEE 6th International Conference on Development and Learning*, pp. 288–293, 2007.
- [2] J. Frère, B. Göpfert, J. Slawinski, and C. Tourny-Chollet, "Effect of the upper limbs muscles activity on the mechanical energy gain in pole vaulting," *Journal of Electromyography and Kinesiology*, vol. 22, no. 2, pp. 207–214, 2012.
- [3] P. M. McGinnis and L. A. Bergman, "An inverse dynamic analysis of the pole vault," *International Journal of Sport Biomechanics*, vol. 2, no. 3, pp. 186–201, 1987.
- [4] N. Linthorne, "Energy loss in the pole vault take-off and the advantage of the flexible pole," *Sports Engineering*, vol. 3, no. 4, pp. 205–218, 2001.
- [5] G. Liu, S. Nguang, and Y. Zhang, "Pole vault performance for anthropometric variability via a dynamical optimal control model," *Journal of Biomechanics*, vol. 44, no. 3, pp. 436–441, 2011.

Simulation study of human slope walking gait based on a musculoskeletal model

Vincent Godivier, Naomichi Ogihara

Department of Mechanical Engineering, Faculty of Science and Technology, Keio University
ogihara@mech.keio.ac.jp

1 Introduction

Humans can walk without tumbling by coordinated control of muscles in the musculoskeletal system. Numerous studies have been conducted to understand the mechanism underlying the generation of human walking (Aoi et al. 2008). However the changes of control strategies of human walking to adapt on slopes remain unknown. A few experimental studies have been conducted to gain some insight on the effect of the slope on the kinematic of the body and the activation signals of the muscles (Lay et al. 2006). However, no simulation study has yet managed to represent stable walking gait on various inclined grounds.

A better knowledge on how the nervous system manages to deal with the change of inclination of the ground would have very practical applications. It could be used for implementing new control laws for biped robots to deal with sloped grounds in an energetically optimized way. Moreover, lower limb amputees using prosthetic feet have difficulty walking on slopes. Biomechanics could then be used for the design of lower-limb prostheses that would automatically adapt to the terrain.

In this abstract, we will describe our approach to create an anatomically based human walking simulation on various inclined grounds which would help us to better understand the mechanisms of the nervous system to deal with the change of the environment.

2 Musculoskeletal and nervous system model

We constructed a two-dimensional anatomically based musculoskeletal model composed of seven rigid links: the HAT (head, arms, and trunk), thighs, shanks, and feet; and nine muscles: Gluteus Maximus, Iliopsoas, Biceps Femoris Long Head, the Biceps Femoris Short Head, Vastus, Rectus Femoris, Gastrocnemius, Soleus and Tibialis Anterior. All the anatomical parameters are chosen to create a model very similar to the average Japanese man (Ogihara and Yamazaki 2001). The model is constructed using Open Dynamics Engine's library.

Physiological studies suggest that the central pattern generators (CPGs) located in the spinal cord would contribute to rhythmic limb movement, such as locomotion. We decided to base the control system of our simulation on a model of the Central Pattern Generator model composed two hierarchical networks: a rhythm generator (RG) and a

pattern formation network (PF) (Fig.1). The RG network generates the basic rhythm and alters it by producing phase shift and phase resetting based on sensory feedbacks. We model it using two simple oscillators including a phase resetting system at each heel contact. The phase produced by this network can be written:

$$\begin{aligned}\dot{\varphi}_R &= \omega - K_\varphi \sin(\varphi_R - \varphi_L - \pi) - (\varphi_R - \varphi^{contact}) \delta(t - t_R^{contact}) \\ \dot{\varphi}_L &= \omega - K_\varphi \sin(\varphi_L - \varphi_R - \pi) - (\varphi_L - \varphi^{contact}) \delta(t - t_L^{contact})\end{aligned}\quad (1)$$

where φ_R and φ_L are respectively the phases of the right and of the left leg, $\omega = 2\pi/T$ is the basic frequency, $T = 1.1$ s being the period of a gait cycle and $K_\varphi = 10$ the gain parameter, where $\delta(\cdot)$ is Dirac's delta function, $t_i^{contact}$ ($i = \text{left, right}$) is the time when the foot lands on the ground, $\varphi^{contact}$ is the phase value to be resetted when the foot touches the ground.

Ivanenko et al. discovered that the activation patterns of the muscles during human locomotion can be accounted to only five basics patterns. In our simulation, we thus use the rhythm of locomotion generated in the RG in the Pattern Formation network to determine the activation signals of the muscles using combination of five basics Gaussian shaped signals.

The activation signal of muscle m can thus be written:

$$a_m(\varphi) = \sum_{i=0}^5 K_{i,m} \frac{1}{\sigma_i \sqrt{2\pi}} \exp\left(-\frac{(\varphi - \mu_i)^2}{2\sigma_i^2}\right) \quad (2)$$

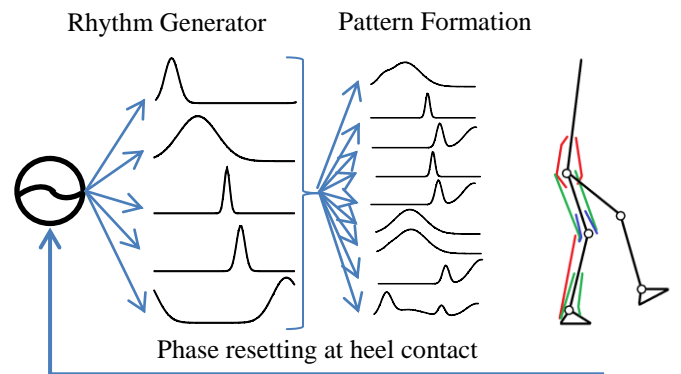


Figure 1 Nervous system model

where $K_{i,m}$ the weight coefficient of the Gaussian i for the muscle m and μ_i and σ_i are the coefficients of the Gaussian i . A PD control of the hip muscles is also included for postural control of the trunk.

In order to generate bipedal locomotion, one must thus determine the shapes of the five basic Gaussian signals (10 parameters) and the dependency relationships between the muscle activations and basic signals (45 parameters). In this study, we decided to use a genetic algorithm for tuning the parameters in order to maximize walking distance and to minimize energy expenditure. We first realized a PD controlled simulation on a flat ground to approximate the shapes of the activation signals to be input as initial conditions for the Genetic Algorithm searching. We then obtained a stable walking pattern for a flat ground and we used the corresponding muscle's parameters as initial conditions for a new Genetic Algorithm searching, this time on a slope.

3 Results and Discussion

As illustrated in Figure 2, the genetic algorithm searching allowed us to determine the parameters of the muscle activation resulting in a stable walking gait for the level ground as well as for a sloped ground. The amount of the inclination of the ground chosen for this simulation is relatively small (2 degrees) but is still encouraging for future parameter searching on more inclined surfaces. Looking at the stick diagrams, the gait obtained for the level ground is very similar to normally observed experimental data. Then, on the slope, we can notice that the trunk seems to be a bit more bent forward compared to the result on the level ground. It seems to indicate that the model is naturally moving the center of gravity forward in order to keep its balance when walking on the slope. The swinging leg also seems to reach a higher position, compared to the position reached on the level ground, at the end of the swing phase. This allows the model to finish the swing phase without the foot touching the ground prematurely, which would result on the model falling down.

The generated muscle forces obtained also seems encouraging. On the flat ground, the amplitudes of the muscles are consistently similar to experimental data and we can observe most of characteristic behaviors of the muscles during locomotion. We can note the activation of

the Gluteus Maximus and of the Biceps Femoris Long head during the double support phase. We can also observe the activation of the Soleus and the Gastrocnemius during the swing phase and the activation of the Tibialis Anterior right before heel contact.

On the slope, we can observe that the amplitude and the duration of activation of some muscles are significantly different to the result on the flat ground. This observation is quite consistent with the experimental findings of Lay et al. publishing EMG data on downhill, level and up uphill walking. We can notice for example that, as observed on EMG data, the amplitude and the duration of the activation of the Vastus, the Gluteus Maximus and the Biceps Femoris Long Head is significantly increased during the early stand phase. The amplitude of the Rectus Femoris, the Gastrocnemius and the Soleus are also slightly bigger which seems natural since, as noted previously, the model tends to reach a higher position of the leg at the end of the swing phase. Higher energy expenditure during the swing phase was thus to be expected to avoid a premature foot contact. Finally, the activation profiles of the Iliopsoas, the Biceps Femoris Short Head and the Tibialis Anterior don't seem to be affected much by the change of the inclination of the ground. This result is still to be confirmed with other runs of the Genetic algorithm for various inclinations.

4 Perspectives

The results obtained after the Genetic Algorithm searching on a slope are encouraging since they correspond quantitatively to the observation of EMG data. However, they can still be improved to be more similar to human walking by for instance reducing the energy expenditure of the muscles. New parameters searching for a large number of different inclinations of the ground (uphill as well as downhill) are also planned in order to have a more quantitative approach of the influence of the slope for different surfaces.

The understanding of the relationships between muscle activity and mechanics during challenging tasks would provide insight on how the neural control strategies adapt to the changes of the environment and could open new possibilities for artificial control systems to deal with change of the terrain.

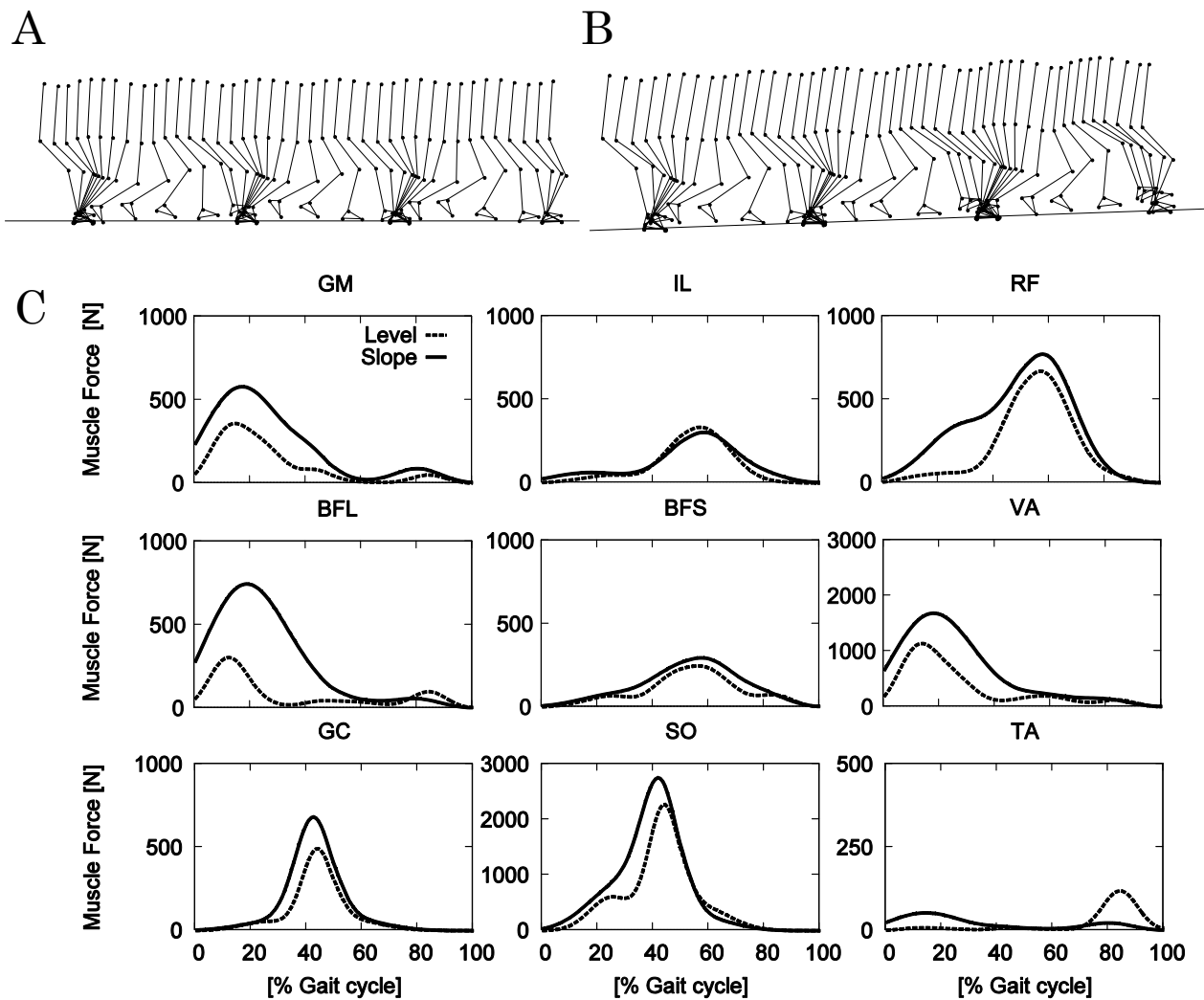


Figure 2 A: Stick diagram of the gait obtained for a flat ground, **B:** Stick diagram of the gait obtained for a slope of 2 degrees, **C:** Muscle activation patterns

References

- [1] Aoi S, Ogihara N, Sugimoto Y, Tsuchiya K. Simulating adaptive human bipedal locomotion based on phase resetting using foot-contact information. *Advanced Robotics*, 22:1697–1713, 2008
- [2] Ivanenko YP, Poppele RE, Lacquaniti F. Five basic muscle activation patterns account for the muscle activity during human locomotion. *J Physiol* 556.1 pp267-282, 2004
- [3] Lay A.N, Hass C.J, Nichols T.R, Gregor R.J. The effects of sloped surfaces on locomotion: an electromyographic analysis. *Journal of Biomechanics* 2007, 40:1276–1285, 2006
- [4] Ogihara N, Yamazaki N. Generation of human bipedal locomotion by a bio-mimetic neuro-musculo-skeletal model. *Biological Cybernetics*, 84:1–11, 2001

Prediction of Self-induced Mechanoreceptive Sensor Readings in An Insect-inspired Active Tactile Sensing System

Nalin Harischandra* and Volker Dürr**

* Department of Biological Cybernetics, Faculty of Biology, Bielefeld University
Bielefeld, Germany

{*nalin.harischandra, volker.duerr*}@uni-bielefeld.de

** Cognitive Interaction Technology- Center of Excellence, Bielefeld University
Bielefeld, Germany

1 Introduction

Many animals use actively moveable tactile sensors to explore the near-range space. While mammals like rats and cats use active whisker movements to detect and scan objects in the vicinity of the body, insects and crustaceans use antennae (or feelers) for obstacle localization, orientation and pattern recognition [1]. Compared to vision-based sensors, the tactile sense is independent of light conditions, it works at day and night. Recently, a number of artificial tactile sensing systems have been developed that were inspired by insect antennae or mammal whiskers. Insect antennae are highly sensorized and multimodal limbs of the head. As actively moving sensory organs, they are subject to self-stimulation, particularly of their mechanoreceptors. For an animal to adapt its behaviour to environmental conditions, it is important to identify external cues, e.g., true touch events, from self-stimulation during self-motion.

Here we use a bionic tactile sensor inspired by the antenna of the stick insect, *Carausius morosus*. It consists of an acceleration sensor mounted to the tip of an otherwise unsensorized probe, and is capable of near-range tactile localization and material classification [2]. However, if the tactile system is attached to a moving body, with each sensor being moved relative to the body, the mechanosensory signal will be corrupted by self-induced motion artefacts. Self-stimulation is a general problem of sensory systems on moving bodies, and of moving mechanoreceptors in particular. In [2], state-dependent modulation of input signals was used to suppress the detrimental effects of robot velocity on the antennal dynamics. Rather than modulating the input signal, [3] applied a forward model based on Echo State Networks (ESN) for predicting the expected sensory reading. The goal was to tell true contact events from false positives as the robot was moving along a path with bumps. Here, we expand this system to two antennae with 2 degrees of freedoms each, executing a complex sampling pattern in three dimensional (3D) space. Additionally, we have tested the prediction system in different scenarios (see section 2.1) which included not only different acceleration profiles of the robot, but also rhythmic perturbation by a spiked wheel, simulating rhythmic impacts of the feet of a legged robot.

In physiological motor control, a forward model is an internal approximation of the motor system that uses the current state of the system and the motor command (*efference copy*) to predict the next state [4]. The state affects the processing of sensory signals. Therefore, the forward model can be used to estimate the sensory consequences of a motor command. Self-induced movements can produce sensory inputs (*reafference*) that are indistinguishable from inputs caused externally (*afference*). A forward model can be used to cancel the reafferent signal (*corollary discharge*), and thus allow the external signals to be recovered [4, 5].

The forward model described here is based on an Echo State Network (ESN), a special type of artificial neural network. It has been shown that ESNs are suitable for chaotic time series predictions with a comparatively high accuracy [6]. In general, ESNs have a large, fixed, randomly initialized reservoir of recurrently and sparsely connected neurons. The output of the ESN is read out through a *linear* layer and the training of the output weight matrix is a linear regression task which is straightforward and fast compared to classical, gradient-based training methods. Here, inputs to the ESN are the motor commands which set the positions of the antennae, and a local proprioceptive signal which measures the vibrations of the robot platform.

The next section briefly describes the experimental setup, our approach, and the test scenarios. For more details of the experimental setup, see [3]. In section 3, the results are shown and discussed briefly. Then a summary of findings and contributions of our investigation are given. Finally, open questions will be discussed.

2 Approach

The data for training the ESN were obtained from several trials carried out with the moving robot (Erratic base, ERA-*Videre Design LLC*). The two antennae were mounted onto two pan-tilt-units, each allowing active rotation around two orthogonal axes, controlled via *servo* motors (HiTEC HS-755MG, see Figure 1a). Each antenna carried a 2-axes

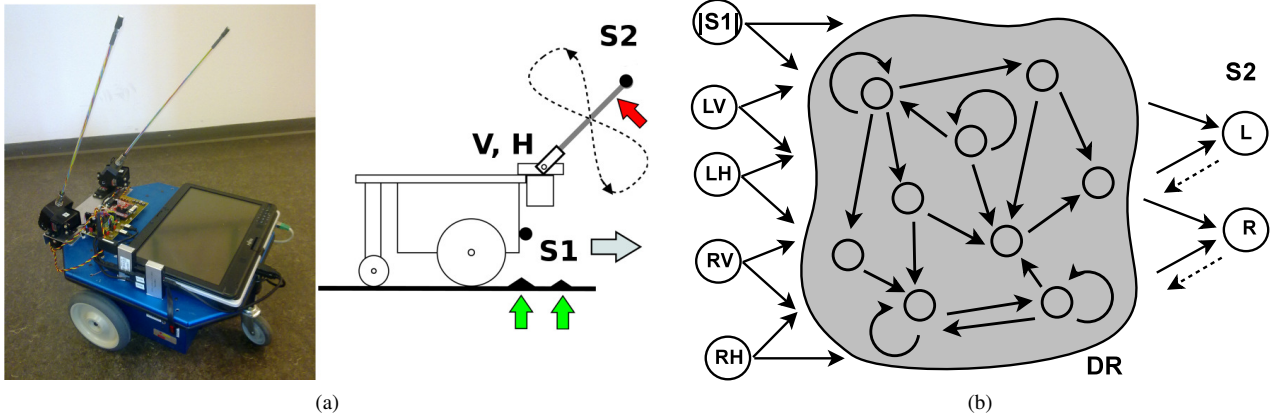


Figure 1: (a): Experimental set-up showing the ERA robot and the positions of the sensors. S1 and S2 are the acceleration sensors mounted to the robot platform and to the tip of the antenna, respectively. Arrows correspond to possible causes of events, touch (red) and disturbances (green), recorded by S2 sensor signal. (b): Echo State Network showing the inputs, S1 and antennal servo commands (LV, LH, RV, RH), Dynamical reservoir (DR), and the outputs S2. L and R represent left and right antennae. V and H suffixes stand for vertical and horizontal.

accelerometer (ADXL321) mounted at the tip of a 40 cm poly-acrylic tube. Both antennae were moving in an “8”-shaped pattern with an approximate frequency of 0.56 Hz. The working-range of each antenna was about 100 degrees in both the vertical and horizontal planes. An Inertial Measurement Unit (x-IMU, from *x-io Technologies Ltd.*, which includes a 3-axes acceleration sensor) was mounted on the robot (S1) in order to measure the vibration of the robot base while moving. The readout for the acceleration sensors was implemented on a micro-controller (ATMEL AT90CAN128) and the raw sensor signals were transferred to a notebook via serial interface (RS232/USB) for storage and further processing in Matlab (7.9.0-R2009b). All the devices were integrated into a common framework for easy communication.

The servo position commands and both acceleration data were preprocessed in order to remove the DC-bias. Furthermore, the two components of S2 (X, Y) and the components of S1 (X, Y, Z) were combined according to the *Euclidean norm* before being fed into the ESN model. As shown in Figure 1b, a single network was used to predict the accelerometer readings of both antennae.

The Matlab ESN toolbox created by D. Popovici (revised by H. Jaeger) was used to implement the ESN [7]. The parameters, such as size of the dynamic reservoir (DR), spectral radius (SR) and input scaling factor (ISF) were systematically varied in order to find a suitable set for the ESN. The normalized root mean square error (NRMSE) between the predicted and actual time series was used as the performance measure. Then, the trained network was used as the forward model in the proposed method for detecting true touch events to the antennal system (see Figure 2 and section 3).

2.1 Experiments

The forward-model-based prediction system was tested in three different scenarios:

- **Straight motion** - The robot was moving straight on a flat surface with a constant velocity of 0.3 ms^{-1} . Obstacles or bumps (5 mm height) were placed along the robot’s pathway to generate disturbances. A wooden stick was used as the contact object presented to the antennae.
- **Curve motion** - In separate trials, the robot was set to move on a curved path in clockwise or in anti-clockwise direction. Here, the linear and angular velocities were about 0.15 ms^{-1} and 0.5 rads^{-1} (approximately 30 *degrees/s*) respectively. The bumps and contact objects were introduced as in the previous case.
- **Spiked wheels**: A small rubber protrusion (about 1 cm x 1 cm x thickness of the wheel) was attached to each of the front wheels of the ERA robot with a phase shift of 180 degrees. When the robot moved forward, the wheels alternatingly generated rhythmic impacts. With this experiment, we were able to estimate the performance of an active tactile system mounted to a walking robot with rhythmic impacts, as caused by the limbs touching the ground. Here, the robot was moving straight with a constant velocity of approximately 0.2 ms^{-1} .

3 Results and Discussion

When the wheeled robot drove across bumps, the impact caused vibrations, thus affecting the tactile sensor reading (S2). We refer to these unwanted sensory readings as

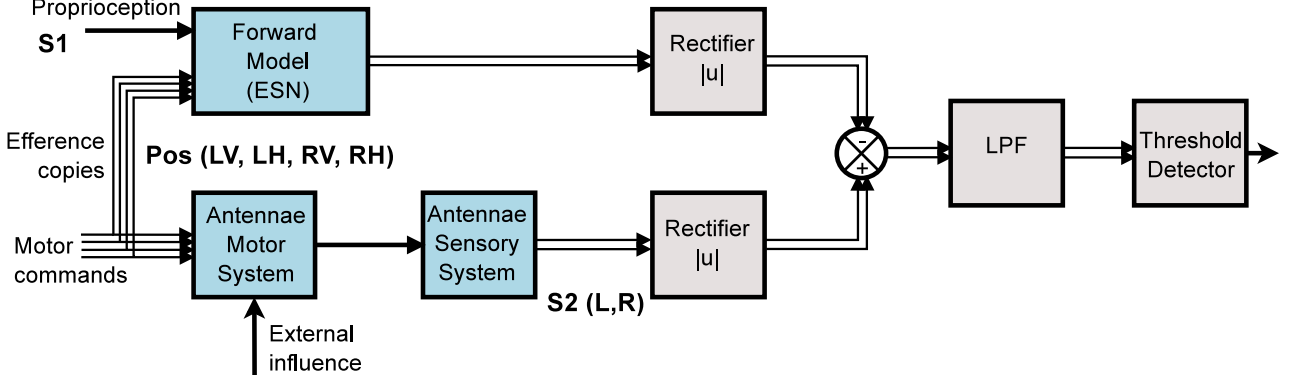


Figure 2: Our approach for the detection of true touch events to the antennae. An ESN-based forward model is used to predict the expected sensory reading of S2 due to ego motion. Rectifiers are used for obtaining absolute values of the signals. S1, S2 and the position or motor commands, LV, LH, RV and RH have the same meanings as in Figure 1b. LPF: Low Pass Filter.

disturbances. On the other hand, the antennal sensors (S2) were capturing direct contacts (touch events) to the antennae. Owing to the similar magnitude of these two types of responses, we could not directly use a threshold on the S2 signal since that would have caused miss-classification of disturbances as touch events. Therefore, we applied the forward model for predicting the expected S2 sensory reading and then the reading was compared with the actual value for peak cancellation. A small but variable phase difference could be seen between the *actual* and the *predicted* signals. Therefore, simple subtraction of the predicted signal from the actual traces did not cancel all unwanted peaks in the original signal. As shown in Figure 2, both signals were first *rectified*, then subtracted and finally filtered with a first-order low-pass filter (LPF). In fact, for a linear filter, this is same as taking the envelopes before the subtraction. We tested the model performance for LPFs with different cut-off frequencies (ω_c): 100, 50, 20 and 10 Hz. Table 1 summarizes the number of total false predictions in the three scenarios used, i.e., *straight* and *curved* trials with bumps on the floor, and straight trials with *spiked* wheels (see section 2.1). With cut-off frequencies 100 and 50 Hz, the prediction system was able to correctly identify the true touch events, i.e., without false negatives. However,

No.Trials		No. of Events		ω_c [Hz]			
				100	50	20	10
Straight n = 16	L	16	44	26	14	3	11
	R	11	44	27	14	0	6
Curve n = 10	L	13	35	18	11	4	9
	R	13	35	17	10	1	2
Spiked n = 3	L	0	47	28	22	1	2
	R	0	47	31	14	3	1
Total		53	252	147	85	12	31

Table 1: Total number of false predictions in each scenario

some of the the disturbances were misclassified as touch events (false positives). In summary, we found that a cut-off frequency of 20 Hz allowed the forward model to distinguish 53 touch events from 252 other disturbances with a success rate of about 96%. Note that the touch events occurred at different positions along the each antenna covering approximately 20-90% (proximal to distal) of its length. For a lower ω_c , e.g., $\omega_c = 10$ Hz, false negatives occur owing to stronger smoothing of the input signal. Given the high performance for single contact events, we conclude that our method provides an appropriate means of eliminating self-stimulation of a tactile sensor on a moving body. Its neural network implementation makes the forward model a good candidate for prediction and elimination of self-induced stimulation of mechanosensors in general, but also for sensors in other modalities.

Our approach implements a forward model using efference copies (LV, LH, RV, RH) and a local proprioceptive signal (S1) as inputs. It is interesting to compare the importance of each signal as an input to the model. Therefore, we conducted simulated *lesion experiments* and compared how the individual inputs affect the prediction performance. In each trial, at first, the ESN was trained using both signals as inputs. Then the prediction task was carried out with the model receiving only one input, i.e., either the local proprioception or the efference copies (all four) were set to zero or to a constant value. Table 2 lists the number of false predictions that occurred in each scenario. Two cases are compared; one, where the efference copies were set to 0.5 and one where they were set to zero. Thus, the only varying input available to the ESN was the local proprioception from S1. In both cases, the lowest number of misclassifications increased compared to the full model, and the prediction performance declined by about 7.5 or 5.0%, depending on whether the ECs were non-zero or zero. The minimum occurred for $\omega_c = 10$ or 20 Hz respectively. On the other hand, without the S1 signal (after setting it to either 0.0 or 0.5), the ESN was completely unable to predict

No.Trials		ω_c [Hz]							
		100		50		20		10	
EC \Rightarrow		0.5	0	0.5	0	0.5	0	0.5	0
Straight n = 16	L	35	25	23	16	12	8	10	11
	R	36	31	26	16	9	4	7	6
Curve n = 10	L	23	16	18	11	8	4	8	7
	R	22	14	14	8	6	2	6	3
Spiked n = 3	L	24	23	19	18	8	6	3	4
	R	22	19	18	18	4	2	1	1
Total		162	128	118	87	47	26	35	32

Table 2: False predictions of the model with efference copies (normalized EC) set to either 0.5 or 0.0

the effect on the S2 sensors due to disturbances. Hence, the proposed method (see Figure 2) failed to distinguish touch events to the antennae from other disturbances. Therefore we conclude that, in the current experimental setup, both the local proprioceptive signal and the efference copies are useful but only the proprioceptive signal is necessary. Nevertheless, the efference copy is a *necessary* input to the ESN in order to predict the induced accelerations due to self-motion (oscillatory movements when sampling the 3D space) of the active tactile system.

4 Summary

In this study, we expand our work on Echo State Network (ESN) based forward models for predicting the expected sensor reading of an insect-inspired active tactile sensor system on a mobile robot [3]. ESNs are a special kind of recurrent artificial neural networks that are suitable for chaotic time series prediction. Inputs to the forward model are the motor commands which set the positions of both antennae, and a local proprioceptive signal which measures the vibrations of the robot platform. The model was successfully used to detect tactile events on each antenna while the robot, is either moved on a straight or curved path with bumps on the floor, or moved with spiked wheels. The latter scenario was chosen to estimate the performance of an active tactile system mounted to a walking robot with rhythmic impacts caused by the legs touching down. By simulated lesion experiments, we found that the local proprioceptive signal plays a major role in discriminating disturbances from tactile events in the proposed forward model. We conclude that such an ESN-based forward model is suitable for prediction and elimination of self-induced stimulation of sensors, in particular of mechanosensors.

5 Open Questions

In this study, we have tested the model on real measured data that were analyzed offline. Online implementation will require real-time control and computational efficient libraries for ESN etc. Also, putting controllers and the forward model

into a single embedded system would be advantageous. Another point to discuss is the selection of the cut-off frequency (ω_c), which has a crucial role for the overall performance, of the LPF. It is known that the decay time of the antennal oscillations depend on the contact position along the antenna [2]. Therefore, the use of an adaptive ω_c as opposed to a globally fixed value could be advantageous. Furthermore, we know that the signal to be predicted (S2) has both fast and slow dynamics. In general, the spectral radius (SR) of the ESN should be small for the fast dynamics and large for the slow dynamics. Hence, finding a single SR value that is equally well suited for different frequency components is difficult. Recently, [8] introduced a modular ESN architecture comprising a combination of local expert ESNs with different SR values and one special gating ESN. Such a method will also serve to improve the performance of the forward model discussed here. Moreover, the adaptation of the method to other sensory modalities, such as vision, may be considered.

Acknowledgments

The authors would like to thank Peter Iseringhausen for his valuable technical assistance, and Prof. Josef Schmitz for many helpful suggestions and support on various technical problems. Financially, this work was supported by EU grant EMICAB (FP7-ICT, grant no. 270182) to Volker Dür.

References

- [1] E. Staudacher, M. Gebhardt, and V. Dür, "Antennal movements and mechanoreception: neurobiology of active tactile sensors," *Advances in Insect Physiology*, vol. 32, pp. 49–205, 2005.
- [2] L. Patanè, S. Hellbach, A. Krause, P. Arena, and V. Dür, "An insect-inspired bionic sensor for tactile localization and material classification with state-dependent modulation," *Frontiers in Neurorobotics*, vol. 6, no. 8, 2012.
- [3] N. Harischandra and V. Dür, "A forward model for an active tactile sensor using echo state networks," in *Robotic and Sensors Environments (ROSE), 2012 IEEE International Symposium on*, pp. 103–108, 2012.
- [4] R. Miall and D. Wolpert, "Forward models for physiological motor control," *Neural networks*, vol. 9, no. 8, pp. 1265–1279, 1996.
- [5] T. Crapse and M. Sommer, "Corollary discharge across the animal kingdom," *Nature Reviews Neuroscience*, vol. 9, no. 8, pp. 587–600, 2008.
- [6] H. Jaeger and H. Haas, "Harnessing nonlinearity: Predicting chaotic systems and saving energy in wireless communication," *Science*, vol. 304, no. 5667, pp. 78–80, 2004.
- [7] H. Jaeger, M. Lukosevicius, D. Popovici and U. Siewert, "Optimization and applications of echo state networks with leaky-integrator neurons," *Neural Networks*, vol. 20, no. 3, pp. 335–352, 2007.
- [8] Š. Babinec and J. Pospíchal, "Modular Echo State Neural Networks in Time Series Prediction," *Computing and Informatics*, vol. 30, no. 2, pp. 321–334, 2011.

Quantifying dynamic stability in healthy and pathological human locomotion

Khai-Long Ho Hoang^{***}, Katja Mombaur^{*} and Sebastian I. Wolf^{**}

^{*} Optimization in Robotics and Biomechanics Group,
Interdisciplinary Center for Scientific Computing, University of Heidelberg, Germany

{*KhaiLong.HoHoang, Katja.Mombaur*}@iwr.uni-heidelberg.de

^{**} Motionlab, Department of Orthopaedic and Trauma Surgery,
Heidelberg University Clinics, Heidelberg, Germany

Sebastian.Wolf@med.uni-heidelberg.de

1 Introduction

Stability and safety are of major interest when it comes to walking with lower-limb prostheses. Enhanced mobility is one of the most important features offered by adaptive and active prosthetic limbs challenging the recent understanding of stability in human walking. Recently, highly versatile exo-prostheses have emerged enabling an amputee patient to master various difficult gait situations, e.g. walking at different gait speeds, ascending and descending slopes, and walking on uneven terrain. With micro-processor assisted prosthetic devices that make use of sensoric information and passive-adaptive mechanical elements, dynamic locomotion became possible for the patient and mobility could be enhanced. Nevertheless, stable walking is still challenging for above-knee amputee patients due to the absence of active control possibilities over the knee and ankle joint of the prosthetic devices. Understanding the strategy of healthy humans in maintaining balance while performing dynamic locomotion is a key-task to develop more versatile and safe prosthetic components. Analytical stability criteria need to be established to exploit the potential given by controlled prosthetic devices.

To quantify dynamic stability of walking on two legs and particularly to address the increasing dynamics within prosthetic walking we combine the methods of multiple-shooting algorithms in optimal control [2, 8] and N-Step Capturability in humanoid robotics [6]. Kinematic data of healthy human gait on level ground were gathered in the gait lab. The human body was modeled as a multi-body system composed of eight rigid bodies that represent the pelvis and three-segmented legs as well as the upper body. The trajectory of the Instantaneous Capture Point (ICP) was computed using the kinematic and kinetic data of the multi-body model that derived from the solution of our optimal control problem. The results show that the swing foot directly approaches the ICP during swing phase and suggest a correlation between the foot placement strategy in human walking and N-Step Capturability.

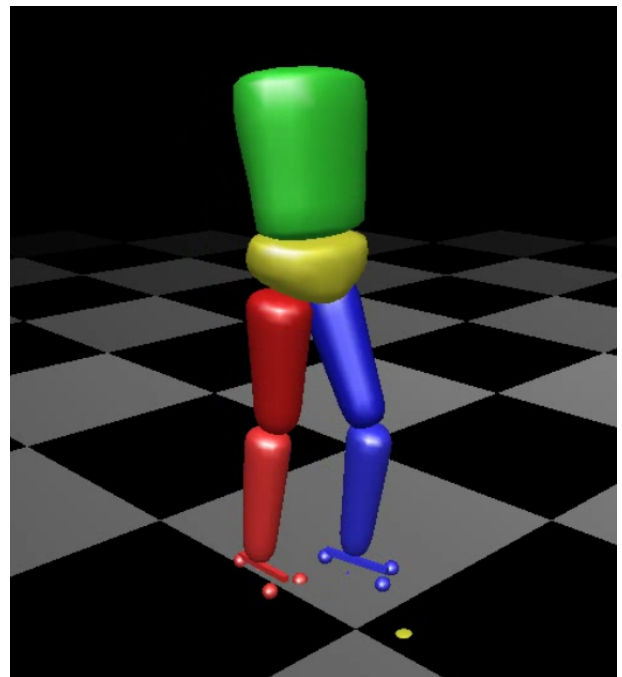


Figure 1: Dynamic simulation of the Instantaneous Capture Point behavior in human walking. The Instantaneous Capture Point is visualized as a yellow dot on the ground.

2 Experiments and Modelling

The experiments in the gait laboratory involved healthy subjects walking on level ground recorded by an image-based motion capture system. Data from one subject (male, 30 years, 1.87 m, 86 kg) walking on level ground (walking speed: $v = 1.5$ m/s, step length $l_s = 0.83$ m) were further processed to obtain the joint-angles for all degrees of freedom (DoF) of our model.

2.1 Multi-body representation of the human body

The parts of the body relevant for walking motions are represented by rigid bodies connected to each other by ball joints allowing three rotational degrees of freedom in each

joint. For the upper body we consider the head, arms and trunk combined in a single rigid body which, accordingly, is named the *HAT*-segment (*Head, Arms, Trunk*). The multi-body model of the human body is comprised of eight rigid bodies representing the segments HAT, pelvis, right and left thigh, right and left shank, and right and left foot. These segments are connected by seven joints representing the lumbosacral joint, the right and left hip, right and left knee, right and left ankle. The resulting 27 DoF of the model are composed of 3 translational and 3 rotational DoF for the pelvis segment which are relative to the global frame and 7×3 rotational DoF that specify the rotation of a more distal segment relative to the next proximal one with the pelvis being the most proximal segment. The anthropometric data of the subject which will be set as model parameters in our multi-body model are obtained using regression equations by de Leva [3] that receive the subject's total mass and total height as input.

2.2 Equations of motion

The dynamics of the multi-body model are described by equations of motion generated using the modeling tool RigidBodyDynamicsLibrary [12]. Since our model is formulated with generalized coordinates q , the equations of motion can be expressed as

$$M(q)\ddot{q} + N(q, \dot{q}) = \tau \quad (1)$$

where $M(q)$ is the symmetric positive definite 27×27 -mass-matrix, $N(q, \dot{q})$ the 27×1 -vector of generalized non-linear effects that contains the coriolis, centrifugal and gravitational forces, and τ the 27×1 -vector of generalized torques. We compute $M(q)$ in a highly efficient way using the *Composite Rigid Body Algorithm* (CRBA) and $N(q, \dot{q})$ using the *Recursive Newton Euler Algorithm* (RNEA) [4].

2.3 Ground contact model

The contact between the model and the ground is modeled as a rigid three point contact at each foot where the three contact points are located at the *Calcaneus* (heel), the *medial Metatarsal Phalangeal Joint* and the *lateral Metatarsal Phalangeal Joint*. In the event of ground contact the vertical position of the contact points in touch with the ground are restricted to the ground by algebraic equality constraints. Furthermore, the horizontal accelerations of the contact points are restricted to zero.

Using the ground contact model we receive the Index 1-*differential algebraic equation*

$$M(q)\ddot{q} = \tau - N(q, \dot{q}) + G(q)^T \lambda \quad (2)$$

$$G(q)\ddot{q} = -\gamma(q, \dot{q}), \quad (3)$$

or in matrix notation

$$\begin{pmatrix} M & G^T \\ G & 0 \end{pmatrix} \begin{pmatrix} \ddot{q} \\ -\lambda \end{pmatrix} = \begin{pmatrix} \tau - N \\ -\gamma \end{pmatrix}. \quad (4)$$

where G are the point jacobians of the contact points, λ the contact forces and γ the generalized acceleration independent part of the contact point accelerations.

In human walking, the occurrence of contact is subject to an impact and leads to discontinuities in the generalized velocities \dot{q} . We compensate these by introducing events of infinitesimal length where we apply the system of equations

$$\begin{pmatrix} M & G^T \\ G & 0 \end{pmatrix} \begin{pmatrix} \dot{q}_+ \\ -\Lambda \end{pmatrix} = \begin{pmatrix} M\dot{q}_- \\ 0 \end{pmatrix}, \quad (5)$$

where Λ refers to an inelastic impulse, \dot{q}_+ denotes the generalized velocities right after the impact and \dot{q}_- the generalized velocities right before the impact, respectively.

With every change in $G(q)$ that arises due to changing ground contact properties we formulate a separate model stage and create a new set of equations of motion (4). Simulating the typical sequence of human gait with our three-point foot model leads to six different stages regarding the ground collision and lift-off of the contact points. This number of stages also includes transition stages that are needed to compensate impacts due to a touch-down of a contact point using (5).

3 Stability, Balance and Capturability

Considering strictly periodic motions, self-stable open-loop gait had been simulated exploiting Lyapunov's first method as a mathematical definition of stability [8].

A very popular criterion to ensure balance of biped robots is known as the *Zero Moment Point* (ZMP) which is defined as the ground-reference point where the net moment generated from the ground reaction forces vanishes for the two axes that span the ground plane [13]. In humanoid robotics the dynamic feasibility of desired trajectories is usually ensured as long as the ZMP lies well within the borders of the *base of support* (BoS) but cannot be guaranteed if the ZMP lies on the edge of the BoS [10].

Balance of a biped walking system can also be quantified using the rate of change of angular momentum at the systems's center of mass (CoM) [5]. This method refers to the preservation of rotational stability and considers a biped walking system to be rotational stable if the external forces and moments sum up to a zero centroidal moment. According to the fundamental principles of mechanics this leads to a minimization of the rate of change of angular momentum.

Push recovery, i.e. enabling a humanoid robot to recover itself from a sudden arbitrary push to avoid falling down, led to the concept of *N-Step Capturability* with the main idea represented by the *Capture Point* [11]. The Capture Point (CP) is defined as the ground-reference point indicating the position where a biped walking system would have to step on to come to a complete stop. Assuming that the CP can be reached instantaneously and neglecting the time that is needed to swing the foot forward leads to the *Instantaneous Capture Point* (ICP). Since, as mentioned earlier, we regard human walking motion as a sequence of falling and catching, we hypothesize that walking can be described related to

push recovery and exploiting the concept of N-Step Capturability. We try to find a correlation between the position of the ICP and the actual foot placement during human walking in order to quantify stability in human locomotion.

4 Optimal control problem

We intend to find joint angle trajectories $x(t)$ and joint torques $u(t)$ for our multi-body model that best fit the experimental data Φ_{exp} using *least-squares algorithms (LSQ)* while considering given constraints. Considering also the contact properties as previously discussed this leads to a multi-stage optimal control problem of the following form:

$$\min_{x(\cdot), u(\cdot), t_i} \int_0^{t_f} \|\Phi_{exp}(t) - \Phi_{opt}(t, x(t))\|_2^2 dt \quad (6)$$

$$\text{subject to: } \dot{x}(t) = f_i(t, x(t), u(t)) \text{ or DAE} \quad (7)$$

$$x(\hat{t}_i^+) = h(x(\hat{t}_i^-)), \quad (8)$$

$$g_i(t, x(t), u(t)) \geq 0, \quad (9)$$

$$\text{for } t \in [\hat{t}_{i-1}, \hat{t}_i], i = 1, \dots, n_{ph}, \hat{t}_0 = 0, \hat{t}_{n_{ph}} = t_f$$

$$r^{eq}(x(0), \dots, x(t_f)) = 0, \quad (10)$$

$$r^{ineq}(x(0), \dots, x(t_f)) \geq 0, \quad (11)$$

where we minimize the *objective function* (6) by modifying the *states* $x(t) = (q(t), \dot{q}(t))$ and the *controls* $u(t) = \tau(t)$. In (7) we find the right hand side of the set of equations of motion that are formulated separately for each of the n_{ph} model stages. With (8) stage transitions are modeled considering (5). The *path constraints* (9) define general limits to the states that are given by physiological constraints such as maximum joint angles. The equality constraints (10) and inequality constraints (11) ensure stage-wise general non-linear constraints such as contact point position at ground contact or positive contact forces.

This optimal control problem is solved using the *direct multiple-shooting method* that is implemented in the optimal control code MUSCOD-II [2, 7, 9]. This method uses a piecewise constant control discretization as a direct method for the discretization of the optimal control problem. Furthermore, the original boundary value problem is transformed into a set of initial value problems with corresponding continuity and boundary conditions by the multiple shooting state parameterization.

With identical grids for the multiple-shooting state parameterization and the direct method, this leads to a non-linear programming problem. This discretized problem can be efficiently solved with *SQP* algorithms adapted to the structure of the problem [7] as well as fast and reliable integration of the trajectories on the multiple-shooting intervals with regard to sensitivity information [1].

5 Results

In the first two plots of Figure 2 the displacement in x and y -direction (in walking direction and to the left) of the

ICP is depicted together with the displacement of the projection of the left and right ankle on the xy -plane for the whole step. The third plot shows the absolute distance from the ankle projections to the ICP. In x -direction the ICP trajectory is greater than the trajectory of both feet for the whole step with the position of the swing foot (*left*) converging to the ICP position during the swing phase. At the end of the swing phase when the left heel gains ground contact, the x -position of the left ankle is 0.089 m less than the ICP x -position. In y -direction the ICP position is less than the left ankle position but greater than the position of the right ankle for the whole step with the swing foot position converging to the ICP position as close as 0.091 m. The absolute distance of the swing foot to the ICP is strictly monotonic decreasing during the swing phase indicating that the ICP is directly approached by the swing foot. The fact that the swing foot strikes behind the ICP also holds for the stance phase can be interpreted as a strategy in human walking to intentionally risk the ability to come to a stop after each step.

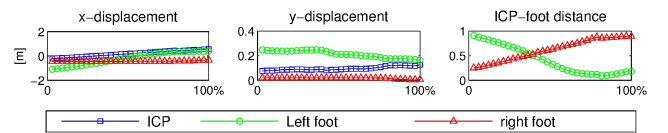


Figure 2: The first two plots show the displacement of ICP and left and right ankle projection on the ground (xy -plane) in x and y -direction during the left step. The third plot shows the absolute distance from right and left foot to the ICP.

6 Discussion

Our investigation was motivated by the need to understand the stability mechanisms of human walking in order to enhance stability in prosthetic devices. We hypothesize a correlation between the stability of human walking and the Instantaneous Capture Point. Using optimal control methods, joint angle trajectories of the multi-body model were generated that best fit the experimental data in a least-squares sense while considering the kinematic and physiological constraints of the human body. The trajectory of the ICP was computed using the kinematic and kinetic data of the multi-body model that derived from the solution of our optimal control problem. The trajectory of the ground projection of the swing foot ankle was found to converge to the trajectory of the ICP. This suggests that the ICP trajectory can be used to compute the location of the foot position.

7 Conclusion

Due to the limited ability to actively control the prosthetic limb and the reduced degrees of freedom, stable walking and avoiding to fall is challenging in prosthetic walking. Unfortunately, a measure to reliably define the stability of gait and how well falling is avoided in a particular walking situation has not been formulated yet. In order to quantify stability and eventually be able to compare stability of dif-

ferent walking strategies, prosthetic setups or gait situations we use N-Step Capturability as a velocity-based concept that closely regards foot placement after swing phase.

8 Open questions

To identify Capture Regions, one needs to consider the physiological abilities of the walker, namely the maximum step length and the minimum step time. While the maximum step length of a subject is rather simple to determine, the minimum step time is highly individual and depends on properties that are difficult to obtain such as reaction time and the configuration of the subject's musculo-skeletal system. Methods to reliably predict these parameters should be part of future investigations.

Furthermore, it is important to predict to which extent upper-body movement can contribute to regaining stability once a critical state has been reached. We will address this question in our future work.

References

- [1] Bock, H.G.: Randwertproblemmethoden zur Parameteridentifizierung in Systemen nichtlinearer Differentialgleichungen. Bonner Mathematische Schriften 183 (University of Bonn, 1987).
- [2] Bock, H. G., Plitt, K.-J.: A multiple shooting algorithm for direct solution of optimal control problems. 9th IFAC World Congress, Budapest. International Federation of Automatic Control, 242-247 (1984)
- [3] de Leva, P.: Adjustments to Zatsiorsky-Seluyanov's segment inertia parameters. *Journal of Biomechanics* **29(9)**, 1223–1330 (1996)
- [4] Featherstone, R.: *Rigid Body Dynamics Algorithms*. Springer, New York (2007)
- [5] Goswami A. and Kallem, V.: Rate of Change of Angular Momentum and Balance Maintenance of Biped Robots. International Conference on Robotics and Automation (2004)
- [6] Koolen, T., de Boer, T., Rebula, J., Goswami, A. and Pratt, J. E.: Capturability-based analysis and control of legged locomotion, Part 1: Theory and application to three simple gait models. *Journal of Biomechanics* **31(9)**, 1094–1113 (2012)
- [7] Leineweber, D. B.: Efficient Reduced SQP Methods for the Optimization of Chemical Processes Described by Large Sparse DAE Models. PhD thesis, VDI-Fortschrittbericht, Reihe 3, No. 613, University of Heidelberg (1999)
- [8] Mombaur, K.: Using optimization to create self-stable human-like running. *Robotica* **27**, 321–330 (2009)
- [9] MUSCOD-II - A Software Package for Numerical Solution of Optimal Control Problems involving Differential-Algebraic Equations (DAE). IWR-SimOpt
- [10] Pratt, J. E. and Tedrake, R.: Velocity-Based Stability Margins for Fast Bipedal Walking. *Fast Motions in Biomechanics and Robotics* (2006)
- [11] Pratt, J. E., Carff, J., Drakunov, S. and Goswami, A.: Capture point: A step toward humanoid push recovery. 6th IEEE-RAS International Conference on Humanoid Robots (2006)
- [12] Felis, M. L.: RBDL - Rigid Body Dynamics Library. <http://rbdl.bitbucket.org/>. Cited January 30, 2013
- [13] Vukobratovic, M., Branislav, B.: Zero Moment Point - Thirty Five Years Of Its Life. *International Journal of Humanoid Robotics* **1(1)**, 157–173 (2004)

Minimalistic Decentralized Modeling of a Skeletal Muscle Force based on Stochastic Resonance

Shuheiki Ikemoto*, Yosuke Inoue*, Masahiro Shimizu* and Koh Hosoda*

* Multimedia Engineering Laboratory, Osaka University, Osaka, Japan

{*ikemoto, inoue.yosuke, m-shimizu, koh.hosoda*}@ist.osaka-u.ac.jp

1 Introduction

A skeletal muscle has a distinctive hierarchical structure consisting of many minimalistic functional units, which can only contract and relax in response to changes in Ca^+ concentration, called sarcomere. More specifically, sarcomeres constitute a skeletal muscle by sequentially building larger structures in the order corresponding to myofibrils, muscle fibers and muscle fiber bundles. In particular, it has been focused how the system efficiently expresses continuous output force based on many binary elements in engineering.

Ueda et al. developed a cellular actuator which consists of a number of small ON-OFF piezoelectric elements[1]. Their main focus is the decentralized control for the cellular actuator, which needs only one common scalar input signal for all ON-OFF elements, called broadcast feedback. In their method, each element is stochastically changing its binary state according to a Markov decision process which consists of two states corresponding to the ON-OFF states. In addition, the muscle activation is decided by the rate of elements which are the ON. The common scalar input signal is used to adjust the transition probability from one state to the other for all elements. Because the expected value, how much the rate of activated elements is, is given as the stationary distribution of the Markov decision process, the scalar value determines the activation rate of the cellular actuator. The broadcast feedback is much simpler and more biologically plausible than a centralized control that deterministically selects ON-OFF states of all elements. In addition, in recent years, biological muscles are also being focused for their use as actuators[2]. To employ simple muscle modeling and to investigate how the system can be controlled is also beneficial for this kind of works.

In this research, we propose a minimalistic decentralized modeling of a skeletal muscle consisting of many binary elements in which the muscle activation is determined by their summation. Each element, instead of having an explicit probabilistic model as in [1], has only a threshold in this modeling. The main idea is to enable threshold elements to stochastically express a magnitude information of an input signal by adding a noise. This phenomenon is well-known as stochastic resonance and the details are explained in the next section. In this paper, we show that this simplest modeling is still able to control the activation continuously.

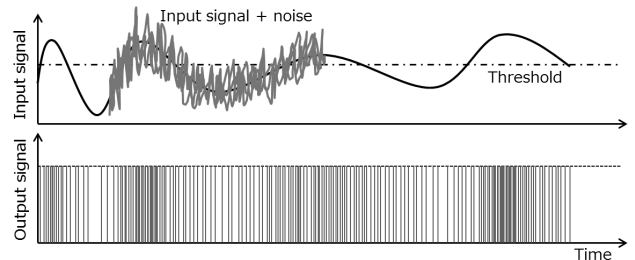


Figure 1: A simplest example of SR in a threshold element.

2 Stochastic Resonance

Stochastic resonance(SR) is a phenomenon, by which the addition of noise can enhance the response of a nonlinear system, proposed to explain the periodic occurrence of ice ages[3]. Since then, SR has been intensively studied for wide variety of problems[4][5].

The simplest example of SR among a number of systems that exhibit SR can be seen in a threshold element as shown in Fig.1. If a system applies a threshold to a received input signal and makes it binary, the magnitude information will be lost. However, when an additional noise is applied to the input signal, the input can stochastically exceed the threshold. In this situation, the probability relates not only the noise variance but also the difference between the input signal and the threshold. As the result, the output signal stochastically expresses the magnitude information of the input signal. Because the output signal will be completely random if the noise variance is unreasonably large, it can be easily estimated that there is a specific noise variance that can maximize the magnitude information of the input signal contained in the output signal. In the minimalistic decentralized modeling, SR enables each threshold element to stochastically express the input signal's magnitude information and to realize the continuous control.

3 Minimalistic Decentralized Modeling

Fig.2 shows the structure of the proposed decentralized modeling of a skeletal muscle. The system is structured by a number of threshold elements that receive independent noises which and that have binary states corresponding to the contract and relax states. For simplicity, we employ the

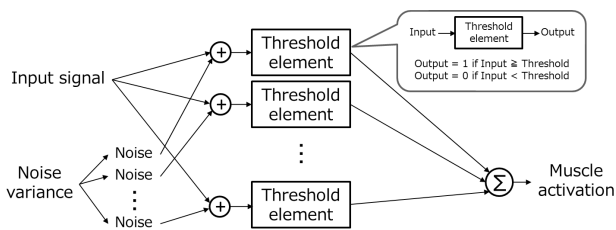


Figure 2: Minimalistic decentralized modeling of a skeletal muscle based on stochastic resonance.

same threshold value and noise variance for all elements. In addition, all elements receive the same input signals and the entire activation of the system is determined as the summation of the element output signals. Therefore, this indicates that all elements contract when the input signal exceeds the threshold value when no noise is added. As explained in previous section, adding a non-zero and adequate level of noise will cause SR and statistics of the binary states will express richer information about the input signals.

Although we assume that the threshold element and the entire system are corresponding to the sarcomere and the skeletal muscle, respectively, several distinctive structures such as myofibril, muscle fiber and muscle fiber bundle are not considered. In other words, we assume that force outputs of myofibrils, muscle fibers, muscle fiber bundles and a skeletal muscle are expressed by linear sum of force outputs of sarcomeres, myofibrils, muscle fibers and muscle fiber bundles, respectively. Because the assumption is not much different to that in biological models, it is valuable to present that the very simple system with very simple decentralized control can still express the input information as statistics of many composing elements by the effect of SR.

4 Simulation

In this section, we confirm that the proposed system can show SR and that it can be exploited by tuning the input signal intensity relative to the environmental noise. In the simulation, the number of elements is 10,000 and the threshold is configured to be the same to the average of the input signal. The input signal is a sinusoidal signal and the amplitude is a parameter to be optimized. In addition, the environmental noise variance is also widely varied to evaluate the effect to change the input amplitude relative to the noise variance.

Fig.3 depicts mutual information between the input signal and the muscle activation, which is the summation of all binary output signals as written in Fig.2, obtained by changing the sinusoidal input signal amplitude and the variance of the environmental noise in the system. From this figure, the occurrence of SR can be confirmed because maximum mutual information when the input amplitude was determined was obtained at a specific size of noise variance. At the same time, a specific amplitude of the input amplitude maximizes the mutual information when the noise variance is

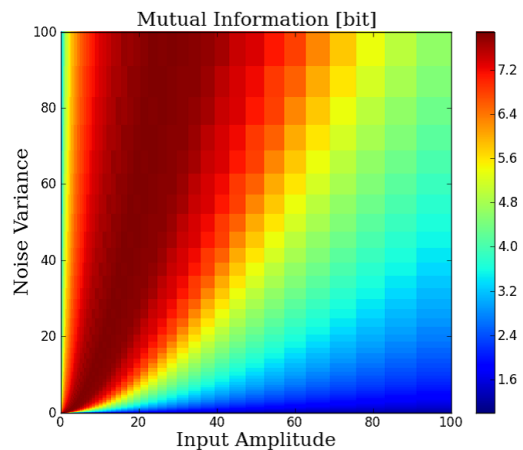


Figure 3: Mutual information between the input signal and the muscle activation.

determined. One of the most suggestive points is that enhancing the input signal intensity does not indicate directly to increase the signal contained in output signals. As the consequence, it can be confirmed that the proposed system can undergo SR and that the performance can be optimized by tuning the input signal intensity relative to the environmental noise.

5 Open questions

In this research, we proposed a minimalistic decentralized modeling for a skeletal muscle based on SR. In our presentation, we wish to discuss wide-ranging topics about both artificial and biological skeletal muscle modeling which have hierarchical structures.

References

- [1] J. Ueda, L. Odhner, and H.H. Asada. Broadcast feedback of stochastic cellular actuators inspired by biological muscle control. *The International Journal of Robotics Research*, 26(11-12):1251–1265, 2007.
- [2] M. Shimizu, S. Yawata, K. Miyamoto, K. Miyasaka, T. Asano, T. Yoshinobu, H. Yawo, T. Ogura, and A. Ishiguro. Toward biorobotic systems with muscle cell actuators. In *In the Proc. of AMAM2011*, pages 87–88, 2011.
- [3] R. Benzi, A. Sutera, and A. Vulpiani. The mechanism of stochastic resonance. *Journal of Physics A: Mathematical and general*, 14:453–457, 1981.
- [4] K. Wiesenfeld and F. Moss. Stochastic resonance and the benefits of noise: from ice ages to crayfish and SQUIDS. *Nature*, 373(6509):33–36, 1995.
- [5] S. Ikemoto, F. DallaLibera, K. Hosoda, and H. Ishiguro. Minimalistic behavioral rule derived from bacterial chemotaxis in a stochastic resonance setup. *Phys. Rev. E*, 85:021905, Feb 2012.

Toward unified understanding of inter-limb coordination mechanism underlying multi-legged locomotion

Akio Ishiguro^{*,**}, Takeshi Kano^{*} and Dai Owaki^{*}

^{*}Research Institute of Electrical Communication, Tohoku University, Japan

{*ishiguro, tkano, owaki*}@*riec.tohoku.ac.jp*

^{**}Japan Science and Technology Agency, CREST, Japan

1 Introduction

Legged animals exhibit versatile gait patterns in response to their locomotion speed and environmental conditions. These locomotor patterns are generated via the coordination of limb movements, i.e. inter-limb coordination. However, the inter-limb coordination mechanism responsible for the generation of such locomotor patterns is largely unknown. Thus, further clarification of this mechanism is required in order to design an adaptable and multifunctional legged robot as well as to understand the fundamental mechanism responsible for the remarkable abilities of legged animals [1][2][3][4][5][6].

In order to elucidate the mechanism underlying the ability of animals to generate adaptive inter-limb coordination, we have recently proposed an unconventional CPG model by focusing on the physical interaction between the legs taking as a quadruped locomotion as a practical example [7]. The CPG was modeled by using phase oscillators that were completely decoupled. Instead, their phases were modified according to the ground reaction forces on the legs. This local force feedback mechanism enabled physical interaction between the legs. Our robot exhibits good adaptability to changes in weight distribution and walking speed simply by responding to local sensory feedback, even in the absence of a “direct neural connection” between the different limb oscillators, and it can reproduce many aspects of the walking patterns of actual quadrupeds. Representative experimental results are shown in Fig.1. As the figure illustrates, the proposed CPG model self-organizes a totally different gait pattern depending on the bodily changes.

Our proposed CPG-based control method suggests that “physical communication” between legs during movements is essential for the inter-limb coordination in quadruped walking. Now a question arises: to what extent is this CPG model applicable to the generation of adaptive locomotion under different number of legs? To put it differently, what is the design principle underlying multi-legged locomotion? As a first step toward a unified understanding of inter-limb coordination mechanism underlying multi-legged locomotion, in this study, we investigate the applicability of our CPG model to hexapod locomotion.

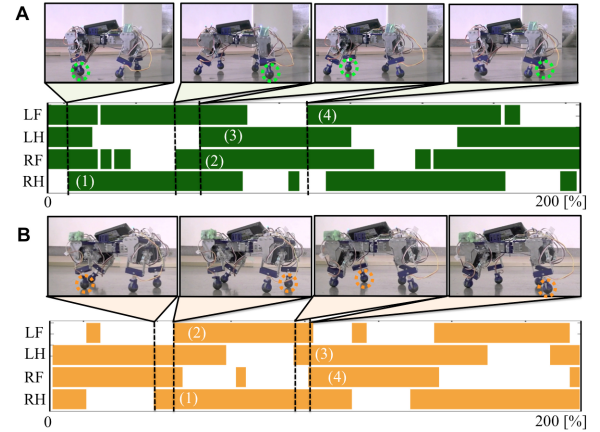


Figure 1: Experimental results of the gait for changes in body properties. (A) With a load of 0.12 kg on the fore legs, and (B) with a load of 0.29 kg on the hind legs. The duty factors of the legs bearing the load (the fore legs in A and the hind legs in B) are larger than those of the legs without a load.

2 The CPG model

We describe each phase oscillator that constitutes the CPG as follows:

$$\dot{\phi}_i = \omega - \sigma N_i \cos \phi_i \quad (1)$$

where ω is the intrinsic angular velocity, and the second term expresses the local sensory feedback in terms of the parameter σ , which is a positive constant describing the magnitude of the feedback to the corresponding oscillator, N_i is the ground reaction force (GRF) acting on the i th leg, which is detected by the pressure sensor in each foot. The i th leg is actively controlled according to the corresponding phase ϕ_i such that the i th leg is in the swing phase when $0 \leq \phi_i < \pi$, the stance phase when $\pi \leq \phi_i < 2\pi$.

We designed the local sensory feedback such that a leg remains in the stance phase while supporting the body ($N_i > 0$). With respect to Eq. (1), we note that the phase is mainly modulated to pull toward $3\pi/2$ in the stance phase when $N_i > 0$ because of the influence of the local sensory feedback. For example, if a leg continues to bear a load ($N_i > 0$) at the end of its stance phase ($\phi_i \approx 2\pi$), a phase delay is introduced in response to the magnitude of N_i . This

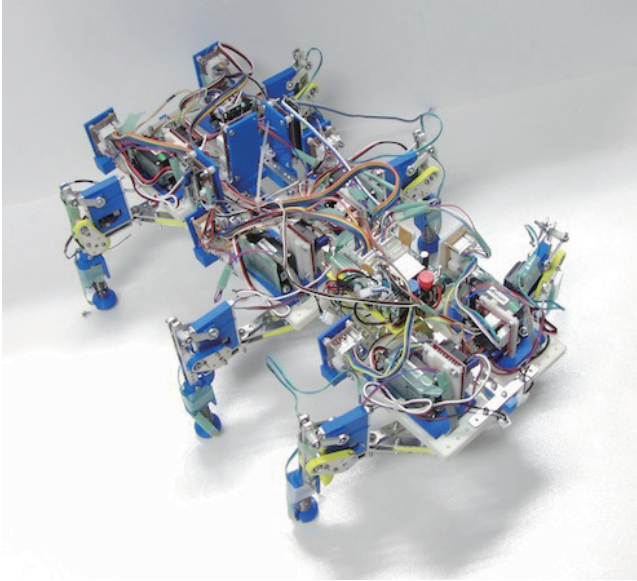


Figure 2: Hexapod robot as a platform for investigating the applicability of our CPG model designed for quadruped locomotion.

phase delay, which is introduced when $-\sigma N_i \cos \phi_i < 0$, allows time for another leg to enter the stance phase. As the other leg begins to support the body, the load on the leg decreases; consequently, the feedback decreases in magnitude, allowing the leg to enter the swing phase. Therefore, the local sensory feedback, which allows the legs to maintain the stance phase by exploiting only the local force sensory information N_i from the foot, governs the appropriate relationship between the phases of the decoupled oscillators and the leg movements.

3 Preliminary results

We have implemented our CPG model to a hexapod robot shown in Fig.2. The obtained gait diagram is illustrated in Fig.3. As the figure explains, the robot successfully self-organizes stable walking pattern called the metachronal wave gait. This suggests that “physical communication” between the limbs plays an essential role in the inter-limb coordination of hexapod locomotion rather than “neural communication”.

4 Open questions

We have demonstrated that the physical communication between the limbs plays a crucial role in hexapod locomotion as well as quadruped locomotion. However, we have observed that the gait pattern did not converge to a stable gait, rather it changed to a slightly different gait pattern over time. Therefore, at present it is still unclear that the inter-limb coordination in hexapod locomotion additionally requires “neural communication” between the limbs for stable and rapid coordination. We will further investigate this point.

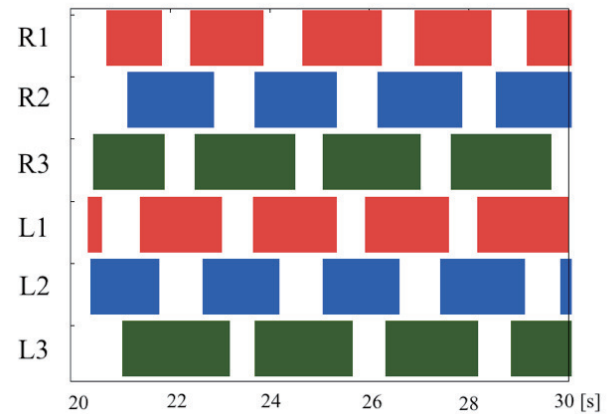


Figure 3: The gait diagram obtained. R1, R2, R3, L1, L2, and L3 represent right fore, right middle, right hind, left fore, left middle, and left hind limb, respectively. The colored area indicates that the corresponding leg is in the stance phase.

5 Acknowledgment

We thank Ken Nakamura and Eishin Endo of Tohoku University for their great help in building the experimental robot.

References

- [1] Hoyt, D. F. and Taylor, R. 1981 Gait and the Energetics of Locomotion in Horses. *Nature*, 292, 239–240.
- [2] Ijspeert, A.J. 2008 Central pattern generators for locomotion control in animals and robots: A review. *Neural Networks*, 21, 642–653.
- [3] Golubitsky, M., Stewart, I., Buono, P. L., Collins, J. J. 1999 Symmetry in locomotor central pattern generators and animal gaits. *Nature*, 401, 693–695.
- [4] Tsujita, K., Tsuchiya, K., Onat, A. 2003 Decentralized autonomous control of a quadrupedal locomotion robot using oscillators. *Artif. Life and Robotics*, 5, 152–158.
- [5] Kimura, H., Fukuoka, Y., Cohen, A.H. 2007 Biologically inspired adaptive walking of a quadruped robot. *Phil. Trans. R. Soc. A*, 365, 153–170.
- [6] Cruse, H., Dürr, V. and Schimitz, J. 2006 Insect walking in based on a decentralized architecture revealing a simple and robust controller. *Phil. Trans. R. Soc. A*, 365, 221–250.
- [7] Owaki, D., Kano, T., Nagasawa, K., Tero, A., and Ishiguro, A. 2012 Simple robot suggests physical interlimb communication is essential for quadruped walking, *J. Roy. Soc. Interface*, doi: 10.1098/rsif.2012.0669.

Three dimensional reconstruction of foot skeletal movement using biplanar fluoroscopic system

Kohta Ito*, Naomichi Ogihara*, Koh Hosoda**, Takeo Nagura***, Toshiyasu Nakamura***, Nobuaki Imanishi***, Sadakazu Aiso***, and Masahiro Jinzaki***

*Department of Mechanical Engineering Keio University, Yokohama, Japan

**Graduate School of Information Science and Technology, Osaka University, Suita, Japan

***School of Medicine, Keio University, Tokyo, Japan

ogihara@mech.keio.ac.jp

1 Introduction

Quantifying skeletal movement of the human foot is crucial for understanding biomechanical function of the complex foot musculoskeletal systems consisting of many bones, ligaments and muscles that mechanically interact to one another and to the ground. Many studies have employed marker-based motion capture system for the measurement of the 3D kinematics of the foot bones in motion, but such quantification is less accurate because of skin movement artifacts[1]. Recently, X-ray fluoroscopy is used to directly quantify the 3D skeletal movements. In these studies, the 3D surface models of the bones are manually matched to single-plane fluoroscopic images frame-by-frame to quantify the dynamic changes in their positions and orientations in the 3D space. However, extracting 3D kinematics data from a single-plane fluoroscopy is notoriously difficult and the measurement for translation along the projection axis is less accurate.

Towards gaining insights about the foot mechanics based on cadaveric experiments, we recently developed a biplanar dynamic X-ray fluoroscopic system with Shimadzu Corporation, Kyoto, Japan. In this study, we aimed to develop an automatic registration method of the bone models to biplanar fluoroscopic images for measuring human foot skeletal movements in our future cadaveric studies.

2 Method

The biplanar fluoroscopic system is shown in Figure 1. The flat panels consist of a precision amorphous silicon metal-insulator semiconductor sensor and thin film transistor array with a field size of 17 in x 14 in and a detector matrix of 2688 x 2208 pixels. Dynamic images of a human foot were acquired at 15 Hz using this biplanar fluoroscopic system (Fig. 1A).

In this study, we attempted to register 3D surface model of a target bone with the two fluoroscopic images to calculate the time changes in the position and orientations of the bone in the 3D space. For this, we firstly constructed the 3D surface models of the human foot bones based on the computed tomography (CT). Each of the bones was extracted from the CT data of the same foot and their surface models were generated by the marching cube

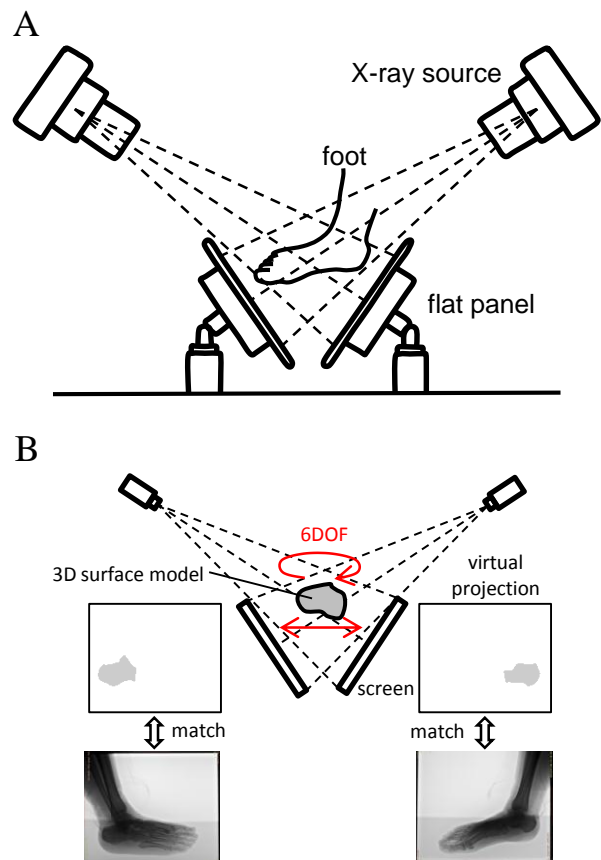


Figure.1 A : Biplanar fluoroscopic system, B : Registration method

method.

To reconstruct the 3D movements of the bones from the 2D images, spatial calibration of the biplanar fluoroscopic system is necessary. We used two calibration objects (an L shaped and a wand) to obtain the projection geometry of the biplanar fluoroscopic system. Using this projection geometry, the extracted bones were virtually projected onto the flat panels and virtual projection images were generated (Fig. 1B). On the other hand, the edge-enhanced images of the actual fluoroscopic images were also generated using the Canny edge detection algorithm. The contour matching

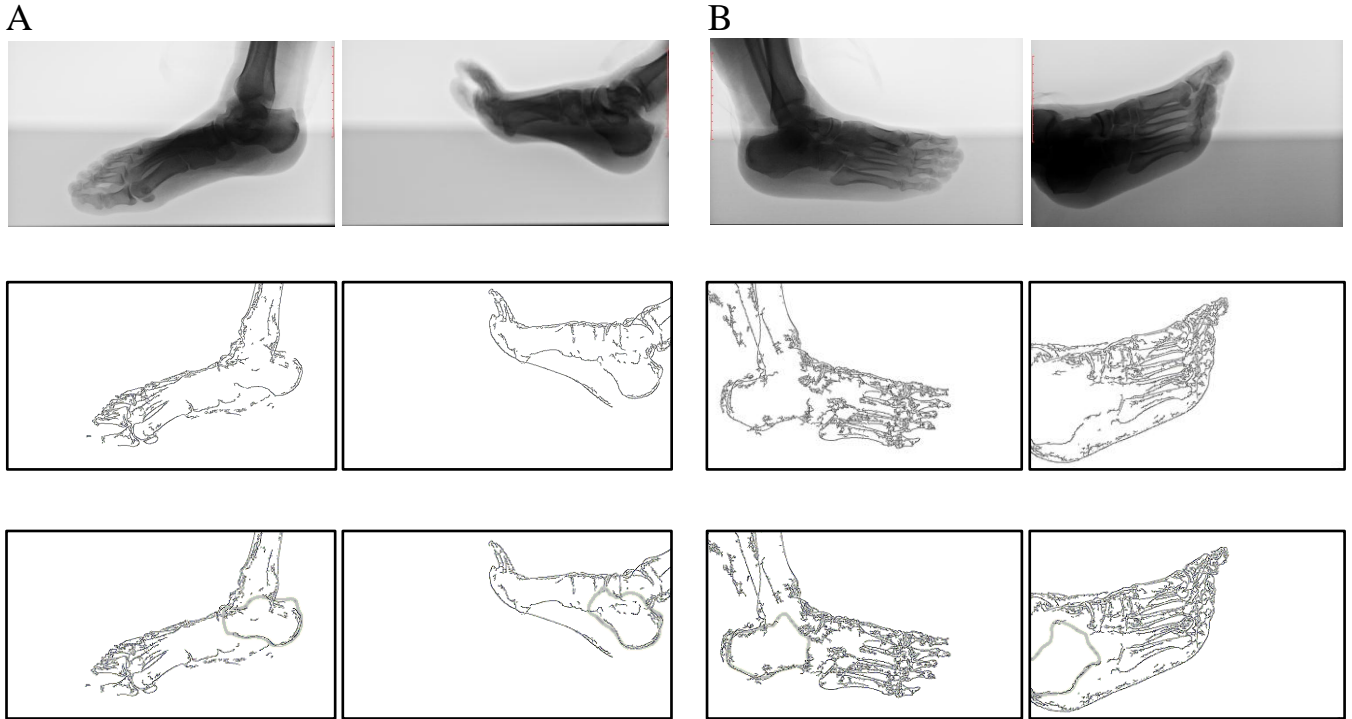


Figure.2 3D reconstruction of calcaneus movement A : Images obtained from left screen, B : Images obtained from right screen. Top: Fluoroscopic images, Middle: Edge-enhanced fluoroscopic images, Bottom : Registration results.

score was used as an objective function to calculate for the position and orientation of the bone that maximize the similarity of the fluoroscopic and the virtually projected images [2]. Let $F(x,y)$ and $V(x,y)$ be brightness values of the edge-enhanced images of the actual fluoroscopic images (Fig.2B) and the virtual fluoroscopic images (gray lines in Fig.2C) respectively, and x and y indicate coordinates of the pixel on each of the images. The contour matching score S is calculated as

$$S = \sum_{(x,y)} F(x,y)V(x,y) / \sum_{(x,y)} V(x,y)$$

This score is similar to a cross correlation between the two edge-enhanced images. To solve for the six degrees of freedom (translation and orientation) of the target bone that maximize the contour matching score, we used the quasi-Newtonian method.

3 Result and Discussion

In our preliminary analysis we choose the calcaneus as the target bone to be matched and its translation and orientation were quantified using the biplanar fluoroscopic system. Figure 2 shows our preliminary results of the automatic registration. Gray lines show edge-enhanced virtual projection images of the 3D calcaneus model. As the figure illustrated, using the optimization technique, the virtual projection images were successfully matched with the corresponding edge-enhanced fluoroscopic images. The present methodology must be undergone further

evaluation, but we believe the proposed framework will serve as an effective tool for understanding the morphofunctional relationships of the human foot.

4 Open questions

Quantification of precise deformation of foot kinematics is important not only for clinical applications but also for science of human walking. While poster presentation, we would like to discuss how our future cadaveric studies using the biplanar fluoroscopic system should be designed towards better understanding of the human foot mechanics.

References

- [1] Shultz, R., Kedgley, A.E., Jenkyn, T.R., Quantifying skin motion artifact error of the hindfoot and forefoot marker clusters with the optical tracking of a multi-segment foot model using single-plane fluoroscopy, *Gait & Posture*, Vol.34, pp.44-48, 2011
- [2] Mahfouz, M.R., Hoff, W.A., Komistek, R.D., Dennis, D.A., A Robust Method for Registration of Three-Dimensional Knee Implant Models to Two-Dimensional Fluoroscopy Images, *IEEE Transactions on Medical Imaging*, Vol. 22, No. 12, pp.1561-1574, 2003

From Walk to Trot to Bound: Quadruped Gait Transition Induced by Simple Local Force Feedback Mechanism

Takeshi Kano*, Dai Owaki*, and Akio Ishiguro**

*Research Institute of Electrical Communication, Tohoku University, Japan

{tkano,owaki,ishiguro}@riec.tohoku.ac.jp

**Japan Science and Technology Agency, CREST, Japan

1 Introduction

Quadrupeds exhibit versatile gait patterns in response to their locomotion speed and environmental conditions [1]. Typically, their gait pattern changes from walk to trot (or pace) to bound as their locomotion speed increases. Clarification of this mechanism will help us to design an adaptable and multi-function robot, as well as to understand the fundamental mechanism underlying versatile animal locomotion. Well-known experiments that used decerebrate cats [2] suggested that this gait transition is caused in part by an intraspinal neural network called the central pattern generator (CPG), which is capable of self-organizing coordinated movement patterns between the legs. Thus, various types of CPG neural network models have been proposed to elucidate the gait transition mechanism [3, 4]. Meanwhile, several researchers have claimed that “physical interaction” between the legs is more essential for the gait transition than is the CPG network topology [5, 6]. Thus, a complete and unified understanding of the gait transition mechanism has not yet been gained.

In our previous work, we employed a minimalist approach and proposed an unconventional CPG model by focusing on the physical interaction between the legs [7]. In this model, we considered a simple body consisting of a trunk and four legs with no knee and ankle joints. The CPG was modeled by using phase oscillators that were completely decoupled. Instead, their phases were modified according to the ground reaction forces on the legs. This local force feedback mechanism enabled physical interaction between the legs. Our model could reproduce many aspects of quadruped locomotion, such as the gait transition from walk to trot and the adaptability to changes in body properties.

However, our previous model could not reproduce the “bound” gait observed in high-speed locomotion. In part, this was because neither a knee nor an ankle joint was implemented in each leg. Accordingly, in this study, we improve our previous model. We describe the body two dimensionally for simplicity and add a prismatic knee joint to each leg. We show via a simulation that the improved model can successfully reproduce the gait transition from walk to trot to bound. This result strongly supports the validity of the local force feedback mechanism that we previously proposed and suggests that the physical interaction between the legs plays a crucial role in realizing quadruped gait transition.

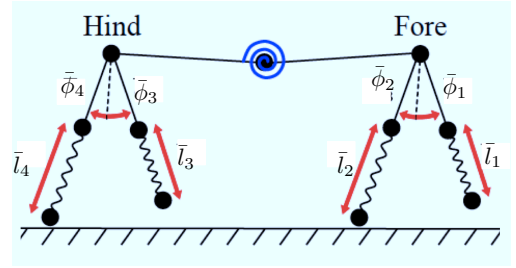


Figure 1: Schematic of model.

2 Model

A schematic of the quadruped model is shown in Fig. 1. Although quadrupeds exhibit three-dimensional motion, we model the body two dimensionally for simplicity. Each leg is described by a rigid link and prismatic knee joint, with which the latter composed of a parallel combination of a real-time tunable spring (RTS) and damper (an RTS is a spring whose natural length can be actively changed [8]). The fore and hind legs are connected via a backbone that includes a joint with an embedded torsional spring and damper.

The CPG is modeled by using phase oscillators, with one oscillator implemented in each leg. The hip (shoulder) joints are actively controlled via proportional-derivative (PD) control, and their target angles are determined according to the corresponding oscillator phases. More specifically, the target angle of the hip (shoulder) joint in the i th leg, $\bar{\phi}_i$, is set to

$$\bar{\phi}_i = \phi_0 \cos \theta_i, \quad (1)$$

where ϕ_0 is a positive constant and θ_i is the i th oscillator phase. The natural length of the RTS in the i th leg, \bar{l}_i , is also determined according to the oscillator phase as

$$\bar{l}_i = l_0(1 - a \sin \theta_i), \quad (2)$$

where l_0 and a are positive constants. Thus, the i th leg tends to be in the swing phase for $0 \leq \theta_i < \pi$ and in the stance phase for $\pi \leq \theta_i < 2\pi$.

The time evolution of the phase, θ_i , is given by

$$\dot{\theta}_i = \omega - \sigma N_i \cos \theta_i, \quad (3)$$

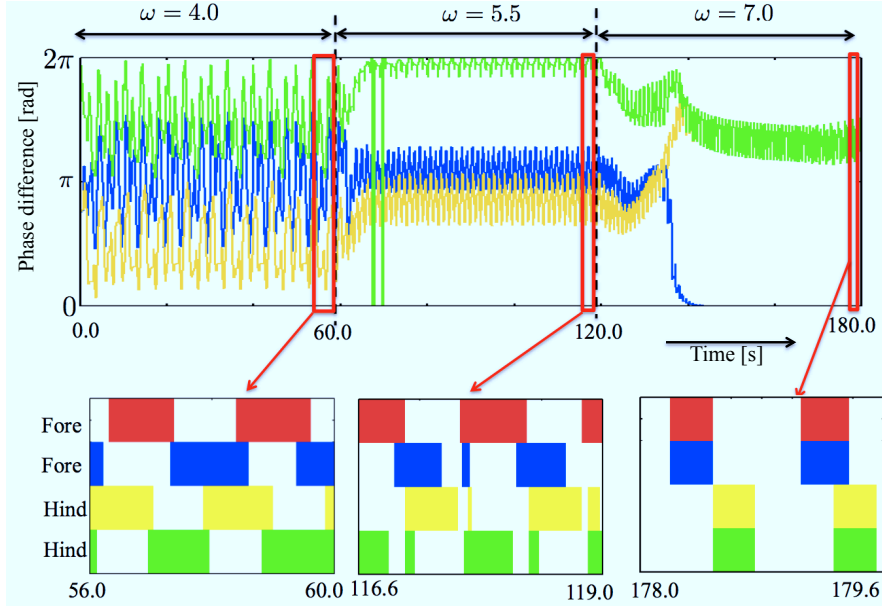


Figure 2: Simulation results. The upper graph shows the time evolution of the phase difference: $\theta_2 - \theta_1$ (blue line), $\theta_3 - \theta_1$ (yellow line), and $\theta_4 - \theta_1$ (green line). The lower graphs show the magnified views of the gait diagram.

where ω is the intrinsic frequency. The second term on the right-hand side describes the local force feedback mechanism that we previously proposed [7], where σ is the feedback strength and N_i is the ground reaction force on the i th leg. The local force feedback term works such that the oscillator phase is pulled toward $3\pi/2$ when $N_i > 0$. Thus, for example, when the i th leg is in the stance phase, the target angle of the proximal joint, $\bar{\phi}_i$, is shifted toward zero to effectively support the body. When the other legs begin to support the body and the ground reaction force N_i decreases, the effect of the local force feedback decreases, causing the i th leg to shift to the swing phase. In this manner, interlimb coordination can be achieved through this local force feedback term, even in the absence of a “direct” neural connection between the different limb oscillators.

3 Simulation results

We performed simulations to validate the model. The parameter values were determined by trial and error but were chosen such that they did not deviate considerably from the physically plausible parameter ranges. The intrinsic frequency ω was increased gradually. Figure 2 shows the time evolution of the oscillator phase and the gait diagrams. It is clear that the gait pattern changes from walk to trot to bound as ω increases, although the gait is slightly disturbed at the end of the stance phase in the trot gait. The phase relationship also changes in accordance with the change in the gait pattern.

4 Open questions

We have shown via a simulation that the two-dimensional quadruped model with prismatic knee joints, in which the local force feedback mechanism that we previously proposed [7] was implemented, can successfully reproduce a gait transition from walk to trot to bound. Al-

though this finding suggests that the local force feedback mechanism, which enables physical interaction between the legs, plays a pivotal role for realizing the gait transition, its detailed mechanism is still unclear. We would like to discuss the gait transition mechanism in detail at the poster presentation.

References

- [1] D. F. Hoyt and R. Taylor, “Gait and the Energetics of Locomotion in Horses,” *Nature*, vol. 292, pp. 239-240, 1981.
- [2] M. L. Shik, F. V. Severin, G. N. Orlovskii, “Control of Walking and Running by Means of Electrical Stimulation of the Midbrain,” *Biophysics.*, vol. 11, pp. 756-765, 1966.
- [3] M. Golubitsky, I. Stewart, P. L. Buono, J. J. Collins, “Symmetry in Locomotor Central Pattern Generators and Animal Gaits,” *Nature*, vol. 401, pp. 693-695, 1999.
- [4] H. Yuasa and M. Ito, “Coordination of Many Oscillators and Generation of Locomotory Patterns,” *Biol. Cybern.*, vol. 63, pp. 177-184, 1990.
- [5] Y. Kurita, Y. Matsumura, S. Kanda, and H. Kinugasa, “Gait Patterns of Quadrupeds and Natural Vibration Modes,” *J. Sys. Des. Dyn.*, vol. 2, pp.1316-1326, 2008.
- [6] Y. Sugimoto, H. Yoshioka, and K. Osuka, “Realization and Motion Analysis of Multi-legged Passive Dynamic Walking,” in *Proc. of SICE Annual Conference 2010*, pp. 2790-2793, 2010.
- [7] D. Owaki, T. Kano, K. Nagasawa, A. Tero, and A. Ishiguro, “Simple robot suggests physical interlimb communication is essential for quadruped walking,” *J. Roy. Soc. Int.*, in press (doi: 10.1098/rsif.2012.0669).
- [8] T. Umedachi, K. Takeda, T. Nakagaki, R. Kobayashi, and A. Ishiguro, “Fully Decentralized Control of a Soft-bodied Robot Inspired by True Slime Mold,” *Biol. Cybern.*, vol. 102, pp. 261-269, 2010.

Toward realization of resilient locomotion: Lessons from the locomotion of arm-amputated ophiuroids

Takeshi Kano*, Shota Suzuki*, Eiki Sato*, Hitoshi Aonuma** and Akio Ishiguro**'****

*Research Institute of Electrical Communication, Tohoku University, Japan

{tkano,ssuzuki,esato,ishiguro}@riec.tohoku.ac.jp

**Research Institute for Electronic Science, Hokkaido University, Japan

aon@es.hokudai.ac.jp

***Japan Science and Technology Agency, CREST, Japan

1 Introduction

Animals are generally capable of changing their locomotion patterns in response to changes in their body properties, e.g., injuries. Such an ability has been honed by many cycles of evolutionary pressure, and there probably exists an ingenious mechanism underlying it. Clarifying this remarkable mechanism will help develop highly resilient robots and hence has attracted the attention of roboticists as well as biologists. Several findings have indicated that autonomous decentralized control mechanisms underlie such resilient animal locomotion [1]; however, their details are still unclear.

To tackle this problem, we focused on ophiuroids as our model. An ophiuroid has a radially symmetric body consisting of a central disk and five arms that diverge radially from the disk [2]. In spite of its simple nervous system consisting of a nerve ring in the disk and radial nerves in the arms, it properly changes its locomotion pattern to successfully move on various terrains when some of the arms are removed [2]. For example, while it moves by assigning rhythmic and non-rhythmic motions to its arms when all five arms are intact, it pushes or pulls the body to move forward by anchoring a certain part of the arm when only one or two arms remain intact.

Our aim of in this study was to clarify the autonomous decentralized control mechanism underlying the resilient ophiuroid locomotion. As a first step, we conducted behavioral experiments using ophiuroids with four of the five arms removed, and we propose a simple model that reproduces the experimental results.

2 Behavioral experiment

We used three ophiuroid subjects (*Ophiarachna incrasata*), which we hereafter refer to as subjects A, B, C, and D. Four of the five arms of each subject were removed. While the nerve ring was intact for subject A, it was cut on the right-hand side, left-hand side, and both sides of the arm for subjects B, C, and D, respectively. We observed the locomotion of the subjects on a substrate with a rectangular object (21 mm × 28 mm × 3 mm). Figure 1 shows photographs of the locomotion. When the arm contacts the object on its left-hand side, subjects A and B bent their arms and moved forward by pushing themselves against the object. In contrast, such behavior was not observed for subjects C and D, and they did not move forward effectively.

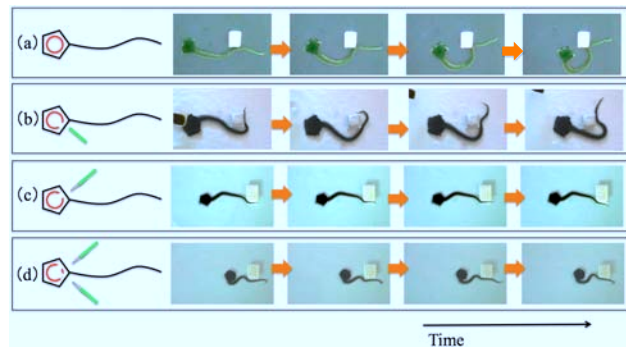


Figure 1: Ophiuroid locomotion on a substrate with a rectangular object: (a) subject A, (b) subject B, (c) subject C, and (d) subject D.

3 Model and simulation

Figure 2 shows the schematic of the musculoskeletal system of our model. The body consists of a disc and an arm. The unremoved arm consists of several identical segments, each of which is connected to the adjacent segment via four sets of parallel combinations of a spring and damper. The lower two springs are passive springs, while the upper two springs are real-time tunable springs (RTSs) whose natural length can be actively varied [3]. When the RTSs contract, the arm bends; simultaneously, it is pushed against the ground.

The schematic of the nervous system is shown in Fig. 3. Each segment includes right/left force sensor neuron (RFSN/LFSN), right/left motor neuron (RMN/LMN), and chemical sensor neuron (CSN). These neurons are modeled as leaky integrators that compute the average firing frequency [4]. To reproduce the behavior of subject A, the following local reflexive mechanism is implemented: When the body contacts an object at a certain point of the arm, the corresponding force sensor neuron activates. Each force sensor neuron is connected to adjacent motor neurons by excitatory connections as shown in Fig. 3 (red lines), and the natural lengths of RTSs decrease as the corresponding motor neurons activate. Thus, stiffness near the contact point increases owing to the co-contraction of the RTSs, which enables the arm to push itself against the object.

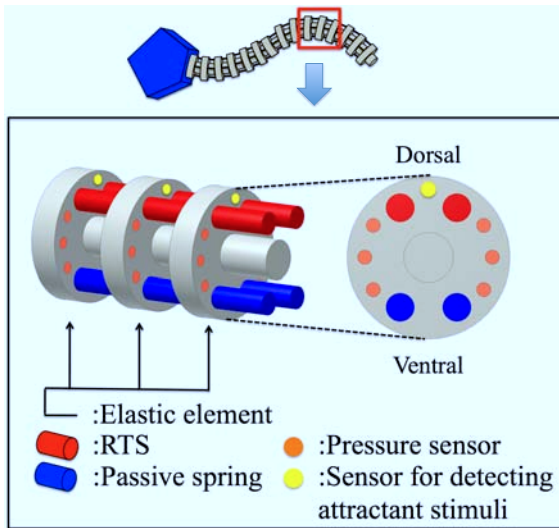


Figure 2: Schematic of musculoskeletal system of our model.

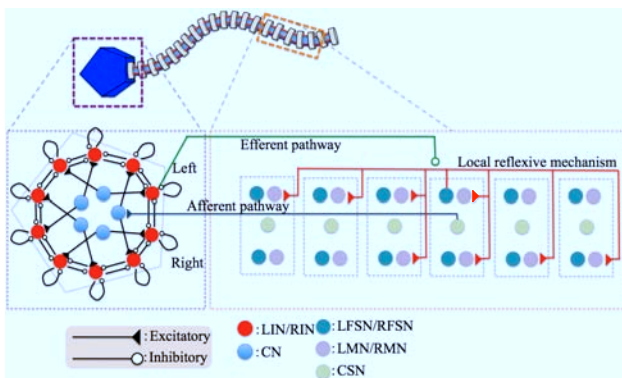


Figure 3: Schematic of nervous system of our model. For simplicity, typical example of the neural paths is presented.

To reproduce the behavior of subjects B, C, and D, this local reflexive mechanism should be affected by the efferent input from the nerve ring. Thus, we modeled the nerve ring as shown in Fig. 3. The nerve ring includes center neuron (CN), right inter neuron (RIN), and left inter neuron (LIN) in each arm. CSN in each segment of the arm is connected to the CN by excitatory connection (blue line), and the CN is connected to the adjacent RIN and LIN by excitatory connections (black lines). Each interneuron is connected to itself and adjacent inter neurons by inhibitory connections (black lines). The interneurons are projected to the pathway of the local reflexive mechanism by “synapse-on-synapse” with inhibitory connection (green line). Owing to this mechanism, the local reflexive mechanism works when CSNs detects chemical stimuli; the local reflexive mechanism is inactivated when the nerve ring is cut like subjects C, and D, while it remains to work when the nerve ring is cut like subject B.

We performed simulations to validate the model. Figure 4 shows photographs of the locomotion. When the nerve ring was intact or cut on the right-hand side of the arm, the simulated ophiuroid moved forward by pushing itself

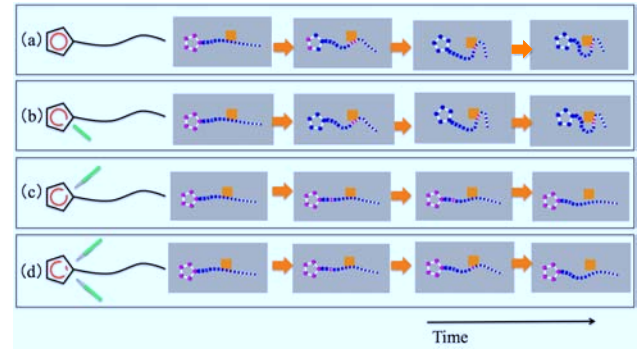


Figure 4: Photographs of simulated ophiuroid. The symbols (a)-(d) correspond to those in Fig. 1.

against the object. In contrast, when the nerve ring was cut on the left-hand side or both sides of the arm, it could not move forward effectively. These results agreed well with the behavioral experiment results.

4 Open questions

We have successfully reproduced the locomotion of an ophiuroid with four of the five arms removed. However, it is still unclear whether our model can be applied to the locomotion of ophiuroids having several arms. Furthermore, biological basis for our model is not yet established. We would like to discuss the validity of our model from mathematical as well as biological viewpoint at the poster presentation.

Acknowledgement

This study was supported by a Grant-in-aid for Scientific Research (A), no. 24246074 from the Ministry of Education, Culture, Sports, Science and Technology, Japan. We thank Prof. Ryo Kobayashi of the Department of Mathematical and Life Sciences of Hiroshima University, Dr. Yoshiya Matsuzaka of the Graduate School of Medicine of Tohoku University, and Kazuhiro Sakamoto of the Research Institute of Electrical Communication of Tohoku University for their helpful suggestions.

References

- [1] A. J. Ijspeert, “Central Pattern Generators for Locomotion Control in Animals and Robots: A Review,” *Neural Networks*, vol. 21, pp. 642-653, 2008.
- [2] I. Y. Arshavskii, M. S. Kashin, M. N. Litvinova, N. G. Orlovskii, and G. A. Fel’dman, “Types of Locomotion in Ophiurans,” *Neurophysiol.*, vol. 8, pp. 398-404, 1976.
- [3] T. Umedachi, K. Takeda, T. Nakagaki, R. Kobayashi, and A. Ishiguro, “Fully Decentralized Control of a Soft-bodied Robot Inspired by True Slime Mold,” *Biol. Cybern.*, vol. 102, pp. 261-269, 2010.
- [4] J. J. Hopfield “Neurons with Graded Response Have Collective Computational Properties Like Those of Two-state Neurons”, *Proc. Natl. Acad. Sci. USA*, vol. 81, pp. 3088-3092, 1984.

Development of sheet-like robot for multi-terrestrial locomotion

Takeshi Kano*, Yuki Watanabe*, Fuyuhiko Satake*, and Akio Ishiguro*’**

*Research Institute of Electrical Communication, Tohoku University, Japan

{tkano,y-wata,satake,ishiguro}@riec.tohoku.ac.jp

**Japan Science and Technology Agency, CREST, Japan

1 Introduction

Animals exhibit astoundingly adaptive locomotion under unpredictable and unstructured real-world constraints. Endowing robots with this ability will enable them to perform effectively in undefined environments. Several biological findings have indicated that autonomous decentralized control mechanisms underlie animals’ adaptive locomotion [1]. Thus, various types of biologically inspired robots have been developed based on autonomous decentralized control [1].

However, previous robots based on autonomous decentralized control could only adapt to a limited number of environments. This was partly because the control schemes were designed specifically for certain environments. To tackle this problem, we employed a different approach: we designed an autonomous decentralized control scheme based on a fundamental principle that can be applied in various environments (Fig. 1). In general, animals move by exploiting the various features in their environments as *scaffolds*. Thus, we hypothesized that robots can move in any environment by simply implementing a *scaffold-exploitation mechanism*. To this end, we needed to examine a living organism that could serve as a suitable model and unveil its inherent locomotion mechanism.

Accordingly, we decided to use a flatworm as our model. Flatworms move over various terrains using their two-dimensional sheet-like body structure and adapt their locomotion pattern to the environment in real time—e.g., by crawling on the ground or swimming in water (Fig. 2)—although their nervous system is quite primitive [2]. This locomotion is achieved by effectively pushing their body against features in their environment. In our previous work, we developed a flatworm-inspired sheet-like robot that implements the scaffold-exploitation mechanism and showed that the robot moved effectively on irregular terrains [3]. In this study, we redesigned the robot to move in water as well as on the ground. We expect that the results of this study could form the basis for the development of a multi-terrestrial robot whose working area covers land, sea, and even air (Fig. 1).

2 Robot

Our first sheet-like robot prototype was designed to move only on the ground in a specific direction, to examine whether the proposed control scheme works properly [3]. To increase the working area of the robot, we present here a new robot design that facilitates locomotion in water

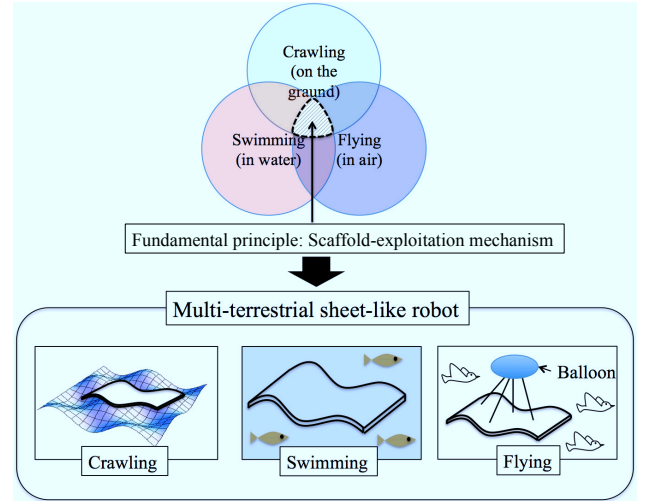


Figure 1: Our approach.

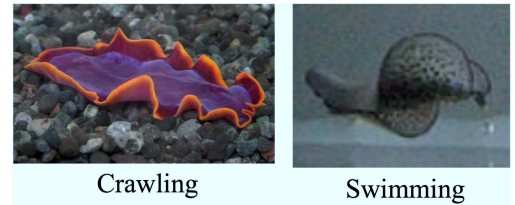


Figure 2: Flatworms.

as well as on the ground. Figure 3 shows photographs of the robot. The robot consists of 15 identical segments concatenated one dimensionally via joints. The total length and width of the robot is 45 and 8 cm, respectively. Adjacent segments are connected via linkage mechanisms. A motor and potentiometer are implemented on each segment; both are packed in a waterproof box. A stern tube is implemented to transmit the motor torque outside the waterproof box effectively. A pressure sensor is attached on the bottom of the segment, which is covered by a hard material.

The joint torque can be controlled by adjusting the motor angle. We controlled the motor angle $\bar{\phi}_i$ ($i \geq 2$) by using the autonomous decentralized control scheme we proposed previously [4] as

$$\bar{\phi}_i = \phi_{i-1} + Cg(f_{i+1} - f_i), \quad (1)$$

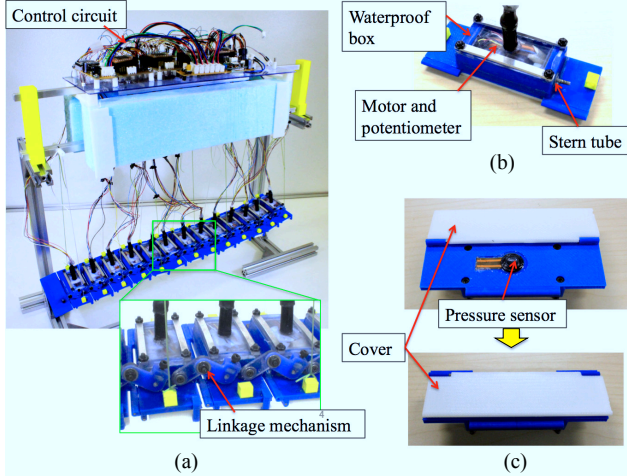


Figure 3: Photographs of sheet-like robot: (a) overview, (b) top view of a segment, and (c) bottom view of a segment.

with

$$g(X) = 1 + \tanh(\alpha X - \beta), \quad (2)$$

where f_i is the sensor signal detected at the pressure sensor on the i th joint and C , α , and β are positive constants. Note that the motor angle of the first joint $\bar{\phi}_1$ is provided by the motor command from a robot controller to determine the direction of motion. The first and second terms on the right-hand side of Eq. (1) contribute to wave generation and the scaffold exploitation. More detailed explanations are provided in [4].

We performed experiments to examine whether the implemented control scheme works properly in water. Jets of water shot from a nozzle upward as the robot traversed it. The results for the cases of $C = 10$ [deg] and $C = 0$ [deg] are shown in Fig. 4. It is clear that the robot moved faster for the case of $C = 10$ [deg] than for the case of $C = 0$ [deg]. This fact suggests that the scaffold-exploitation mechanism plays a crucial role for the locomotion in water as well as on the ground.

3 Open questions

We will evaluate our results quantitatively and would like to discuss the validity of our control scheme based on the obtained results. We would also like to discuss on the type of actuators that should be used when developing a robot that can move in two directions in the future.

Acknowledgement

This work was supported in part by Sekisui Chemical “Innovations Inspired by Nature” Research Support Program. We thank Prof. Ryo Kobayashi and Dr. Toshiya Kazama of the Department of Mathematical and Life Sciences of Hiroshima University for their helpful suggestions.

References

[1] A. J. Ijspeert, “Central Pattern Generators for Locomotion Control in Animals and Robots: A Review,” *Neural Networks*, vol. 21, pp. 642-653, 2008.

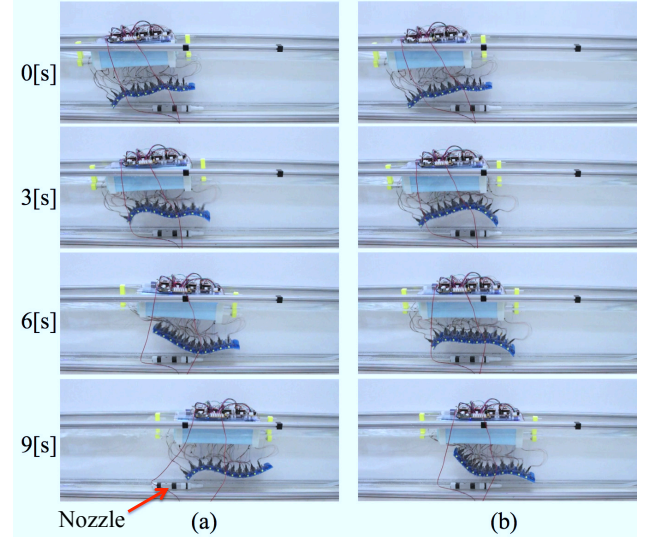


Figure 4: Photographs of locomotion in water for the cases of (a) $C = 10$ [deg] and (b) $C = 0$ [deg]. Jets of water shot from a nozzle upward.

[2] H. Koopowitz, “Primitive Nervous Systems. A Sensory Nerve-net in the Polyclad Flatworm,” *Notoplana acticola Biol. Bull.*, vol. 145, pp. 352-359, 1973.

[3] T. Kano, Y. Watanabe, and A. Ishiguro, “SheetBot: A Magic Carpet That Enables Scaffold-based Locomotion,” in *Proc. of 2012 IEEE/RSJ International Conference on Intelligent Robots and Systems (IROS 2012)*, pp. 1434-1439, 2012.

[4] T. Kano, Y. Watanabe, and A. Ishiguro, “Towards Realization of Multi-terrestrial Locomotion: Decentralized Control of Sheet-like robot Based on Scaffold-exploitation Mechanism,” *Bioinsp. Biomim.*, vol. 7, 046012, 2012.

Scaling of Versatile Quadruped Robots for Running Trot

Hamza Khan, Claudio Semini and Darwin G. Caldwell

Department of Advanced Robotics, Istituto Italiano di Tecnologia, Genova, Italy.

{hamza.khan, claudio.semini, darwin.caldwell}@iit.it

1 Introduction

Legged robots have become a much more prominent field of robotics in recent years, due to their potential versatility and capability of performing tasks which conventional vehicles are unable to do. Most of the recent legged robots, however, lack the versatility of performing both precise navigation over rough terrain and the strong, fast motions that are necessary for dynamic tasks such as jumping and running. Presently very few examples exist besides BigDog [8] by Boston Dynamics and HyQ [11] by IIT.

To design such kind of machines, firstly the designer has to define the tasks that the robot should accomplish to then choose the actuator that satisfies the task requirements in terms of joint velocity and torque. It is easier for a designer to narrow down the desired dimensions and mass of the robot. But when it comes to the selection of actuators, it is challenging to figure out the appropriate joint velocity and torque limits. The aim of this work is to build a scaling tool that helps the quadruped robot designers to select actuators that fulfill the desired requirements. We started our study using the squat jump as a characteristic motion for highly dynamic robots, obtaining peak values of joint velocity and torque in relation to robot mass, size and desired jump height [10]. This paper presents the extension of that study to a running trot to get peak hip and knee joint torques and velocities in relation to forward velocity, robot mass and leg segment length.

2 State of the art

Biological studies have shown that all legged animals typically run with similar center of mass (CoM) motions relative to the (approximately) horizontal ground [13]. Blickhan and Full showed in one of their studies that the running motion for multilegged locomotion behaves like a bouncing monopod and they calculated the compression of a virtual monopod's leg and its stiffness from the animals' mechanical-energy fluctuation and ground-reaction force [2]. A CoM trajectory of the legged robot during a running trot can be modeled by simple models (e.g. SLIP) [1] and more accurate models (e.g. M-SLIP) [6]. A spring-loaded inverted pendulum (SLIP) model is a simple way to model the CoM trajectories of legged locomotion during running. It offers a small stability domain on the steps-to-fall map. But its stability domain for running motion can be enhanced by swing-leg retraction [12] and it also reduces the foot speed which helps to reduce impact energy losses, minimize foot slippage and decrease peak

forces. But in this work the simple SLIP model is used and it is sufficient to get peak forces in stance phase. One of the aims of this work is to get upper boundaries of joint torque and velocity for a given forward velocity.

Some similar studies were conducted for the electric DC motor sizing of a bounding robot [3] and hopping monopod robot [4]. But these studies were limited to quadruped robots with telescopic legs or a specific type of actuator. The current work is for quadruped robots with articulated legs and it is not restricted to only one type of actuators.

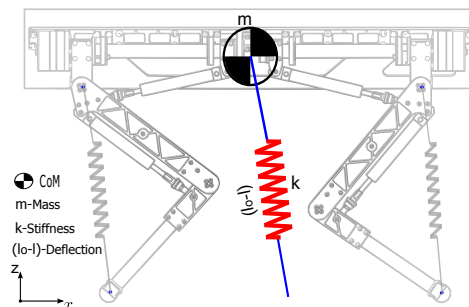


Figure 1: The equivalent virtual spring (connected to CoM) represents the virtual linear spring of a diagonal pair of legs

3 Running Trot Simulation

Desired joint torques are generated by placing a virtual linear spring between the hip and foot of each articulated robot leg [7] to control the motion of the leg. Each virtual spring of a diagonal leg pair is working synchronously in a trot and can be represented by one equivalent virtual spring, Fig. 1. The CoM motion of any quadruped during a running trot can be approximated by the SLIP model as it is observed in animals. A point mass m that is attached to a mass-less linear spring can be described as a SLIP model where k is the spring stiffness and l_0 is the rest length. During stance phase, the spring force exerted on the ground is defined as $k(l_0 - l)$. During flight phase, the mass follows a parabolic trajectory under the law of Gravitation. We define the spring rest length in relation to the leg segment length l_{ls} of each articulated robot leg as follows: $l_0 = K_l l_{ls}$, where K_l is ratio between the leg segment length and the spring rest length. In our simulation K_l is equal to 1.41, which we assume to be a good value based on our experience with HyQ. From the SLIP model, we know the foot trajectory in Cartesian coordinates of the equivalent virtual spring leg during stance. Using the leg Jacobian, we can calculate the angular position, velocity and acceleration of hip and knee joints of the articulated robot leg. The ground reaction forces (GRF)

in stance phase depend on the virtual leg deflection and its stiffness. In our simulation it is assumed that the robot mass is evenly distributed and that the robot torso is always parallel to the ground. During the stance phase of a running trot only two feet of a quadruped touch the ground. So the GRF for each articulated robot leg can be defined as $F = F_{vl}/2$ assuming evenly distributed load, where F_{vl} is the GRF for the equivalent virtual spring.

The leg's GRF is then transformed into hip and knee joint torques with the Jacobian transpose. During running humans and animals adjust their leg stiffness according to the ground stiffness [5]. In this work ground stiffness is assumed constant and the equivalent virtual spring stiffness and angle of attack is chosen from the stability domain of steps-to-fall map of the SLIP model.

4 Simulation and Experimental Results

Based on the SLIP model we performed a number of simulations for a range of forward velocities and leg segment lengths. First of all, suitable SLIP parameters (spring stiffness and angle of attack) had to be calculated for each input pair based on the steps-to-fall map. The SLIP parameters with the lowest spring stiffness that resulted in stable hopping of 50 or more steps were then selected. This way low impact peaks were obtained. Fig. 2 shows the peak joint torque scaled by the robot's body weight (BW) for different leg segment lengths and forward velocities. White areas indicate where the SLIP model failed to perform 50 steps for the given parameter range. For the validation of our selected

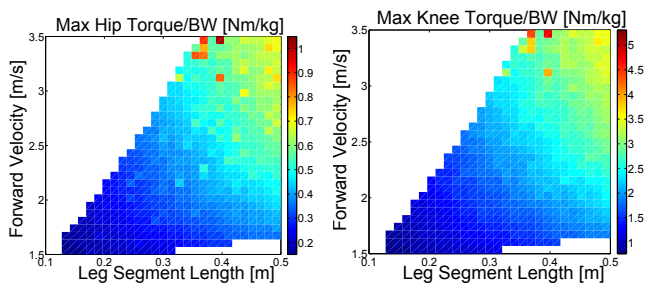


Figure 2: *Left:* plot of maximum hip joint torque scaled by the robot's body weight (BW) for different leg segment lengths and forward velocities. *Right:* plot of maximum knee joint torque for different leg segment lengths and forward velocities.

approach we used HyQ's leg segment length (0.35m) and robot mass (73kg) and tuned the SLIP parameters until we obtained a matching hopping frequency with experimental results of a running trot that was performed on a treadmill at a slow speed [9]. The matching parameters are 59° and 16 kN/m, which resulted in a forward velocity of 3m/s. Fig. 3 on the top shows the vertical position of the SLIP model's CoM. Fig. 3 center and bottom plots show the GRF of the front and hind leg of each diagonal leg pair, showing both simulation and experimental results. As can be seen in these plots, the model used in this work is sufficient to predict approximate vertical GRF.

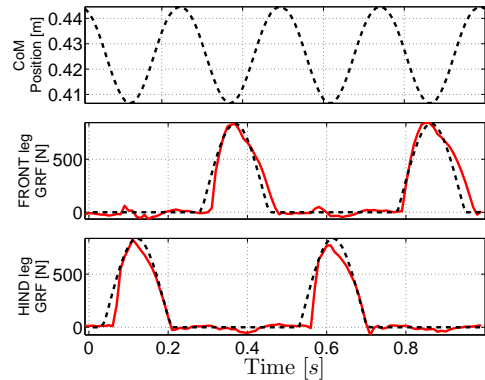


Figure 3: *Top:* Simulation of Vertical position of CoM (black dashed). *Center:* Front leg GRF experimental (red solid) and simulation (black dashed). *Bottom:* Hind leg GRF.

5 Open Questions

How to select appropriate actuators to design a versatile and highly-dynamic quadruped robot? How to evaluate if the desired performance lies inside the robot actuator limits without the need to implement stable running controllers? How to obtain required joint range of motions?

References

- [1] R. Blickhan. The spring-mass model for running and hopping. *Journal of Biomechanics*, 22:1217–1227, 1989.
- [2] R. Blickhan and R.J. Full. Similarity in multilegged locomotion: bouncing like a monopode. *Journal of Comparative Physiology*, 173:509–517, 1993.
- [3] P. Chatzakos and V. Papadopoulos. The influence of dc electric drives on sizing quadruped robots. In *IEEE ICRA Conference*, 2008.
- [4] P. Gregorio, M. Ahmadi, and M. Buehler. Design, control, and energetics of an electrically actuated legged robot. *IEEE Transactions on Systems Man and Cybernetics*, 27:626–634, 1997.
- [5] H. Hobara, E. Kato, Y. Kobayashi, and T. Ogata. Sex differences in relationship between passive ankle stiffness and leg stiffness during hopping. *Journal of Biomechanics*, 45:2750–2754, 2012.
- [6] F. Peucker, A. Seyfarth, and S. Grimmer. Inheritance of slip running stability to a single-legged and bipedal model with leg mass and damping. In *BioRob*, pages 395–400, June 2012.
- [7] J. Pratt, C.M. Chew, A. Torres, P. Dilworth, and G. Pratt. Virtual model control: An intuitive approach for bipedal locomotion. *The International Journal of Robotics Research*, 20(2):129–143, 2001.
- [8] M. Raibert, K. Blankespoor, G. Nelson, R. Playter, and the Big-Dog Team. Bigdog, the rough-terrain quadruped robot. In *IFAC*, 2008.
- [9] C. Semini, J. Buchli, M. Frigerio, T. Boaventura, M. Focchi, E. Guglielmino, F. Cannella, N. G. Tsagarakis, and D. G. Caldwell. HyQ – a dynamic locomotion research platform. In *Int. I Workshop on Bio-Inspired Robots*, 2011.
- [10] C. Semini, H. Khan, M. Frigerio, T. Boaventura, M. Focchi, J. Buchli, and D. G. Caldwell. Design and scaling of versatile quadruped robots. In *Int. Conf. on Climbing and Walking Robots (CLAWAR)*, 2012.
- [11] C. Semini, N. G. Tsagarakis, E. Guglielmino, M. Focchi, F. Cannella, and D. G. Caldwell. Design of HyQ - a hydraulically and electrically actuated quadruped robot. *IMEchE Part I: J. of Systems and Control Engineering*, 225(6):831–849, 2011.
- [12] A. Seyfarth, H. Geyer, and H. Herr. Swing-leg retraction: a simple control model for stable running. *The Journal of Experimental Biology*, 206:2547–2555, 2003.
- [13] M. Srinivasan and P. Holmes. How well can spring-mass-like telescoping leg models fit multi-pedal sagittal-plane locomotion data? *Journal of Theoretical Biology*, 255:1–7, 2008.

Exploiting Natural Dynamics of Nonlinear Compliance Using Adaptive Oscillators

Mahdi Khoramshahi*, Auke Jan Ijspeert**, Majid Nili Ahmadabadi*

*Department of Electrical and Computer Engineering, University of Tehran, Tehran, Iran

**Biorobotics Laboratory, EPFL, Lausanne, Switzerland

{m.khoramshahi,mnili}@ut.ac.ir, auke.ijspeert@epfl.ch

1 Introduction

Compliance has become the essential part of locomotion in robotics. Due to ability of storing and releasing energy, compliance can be used for energy efficiency or reducing impact during ground collision and gaining robustness. On the other side, natural/passive dynamics are important because by exploiting such dynamics, energy efficiency will be assured. Therefore it is crucial to understand how compliance changes natural dynamics of a system. After this inspection, natural dynamics exploitation can be more straightforward through developing tools like adaptive oscillators. Such research to exploits natural dynamics of compliant system are reported in [1], [2] and [3].

Intuitively, it is known that using linear compliance results in efficiency in only one mode. For instance, in mass-spring system for each spring constant, there is only one frequency where system is energy efficient. Using variable compliance is an attempt to overcome this problem in order to gain efficiency over a range of different set-points or tasks. Great achievements reported using variable compliance in robotics application in [4] and [5]. Another way to overcome this problem is using nonlinearity. Natural dynamics and their multi-modality of efficiency will be discussed in this paper. It seems muscle-tendon units in biological systems are taking advantage of such nonlinearity in their compliance [6]. An adaptive oscillator based the one in [7] is presented in this work. This oscillator is able to exploit natural dynamics of system by shaping desired trajectory through frequency and phase lag.

2 Nonlinear Compliance

The most simple nonlinear compliance can be express by $F = kx^3$, where k is constant and x is position. Let assume that we used this spring in spring mass system. Mass set to 1Kg for sake of simplicity. Equation with initial condition is as follow.

$$\ddot{x} = -kx^3, \quad x(0) = A$$

Solution to this fairly simple system is quite complicated. As we see below, solution belongs to Jacobi elliptic functions. A simple form of this function, JacobiSN(t, I), is illustrated in Figure1.

$$x(t) = A \text{JacobiSN}\left(\left(\frac{\sqrt{2k}}{2}At + \text{InverseJacobiSN}(1, I)\right), I\right)$$

This function is similar to sinusoidal trajectories and can be used in robotics application to generate periodic motions. Interesting point about solution of nonlinear spring-mass system is its natural frequency.

$$\omega_n = \frac{\sqrt{2k}}{2} A$$

It shows that natural frequency of this system is a function of its amplitude. At first, this coupling might be considered as disadvantage of this system, but this coupling nicely falling into locomotion domain where animals during accelerating, increase their frequency and amplitude simultaneously.

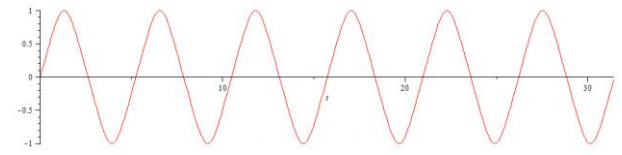


Figure1 JacobiSN(t, I)

Frequency and amplitude coupling for different types of nonlinearity is illustrated in Figure2. These graphs hinting that for every monotonic coupling, there is a nonlinear spring. Finding this nonlinear spring is an open problem.

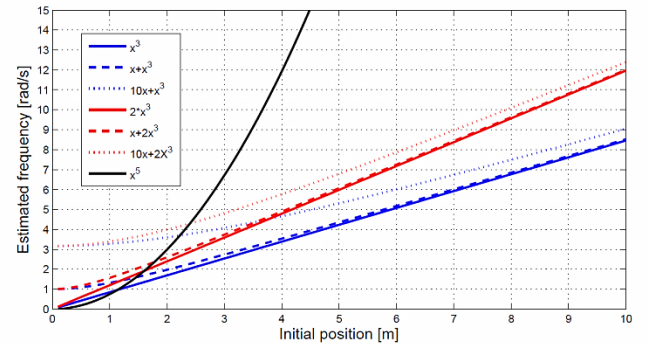


Figure2 Frequency and Amplitude Coupling for different type of nonlinearity in compliance, here initial condition is the same as amplitude

3 Adaptive Oscillator

Adaptive oscillators like Adaptive frequency oscillators [7] are proficient tools to converge to natural frequency of external signal. In our work, in order to exploit natural dynamics for energy consumption minimization, this external signal ought to be the controller applied force. Using this approach, block diagram of system is like one shown in Figure3. Note we use trajectory provided by oscillator as desired trajectory for our robotic application. In this system *Plant* can be consider as joint in a robotic leg.

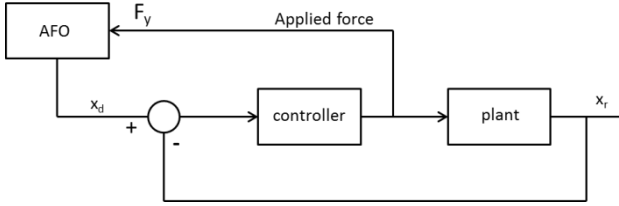


Figure3 Block diagram of AFO

Equations of adaptive frequency oscillators (AFO) are as follow:

$$\begin{aligned}\dot{x} &= \gamma(\mu - (x^2 + y^2))x - \omega y \\ \dot{y} &= \gamma(\mu - (x^2 + y^2))y + \omega x + \epsilon F_{PID}(t) \\ \dot{\omega} &= -\epsilon F_{PID}(t) \frac{y}{\sqrt{x^2 + y^2}}\end{aligned}$$

One of main properties of this oscillator is 90 degree lag between it channels, namely x and y . By assuming periodicity and low tracking error, we can conclude:

$$\begin{cases} \angle \dot{x} \cong \angle y \\ \angle x \cong \angle x_r \end{cases} \rightarrow \angle y_{AFO} \cong \angle v_r$$

Like oscillators in [7], this oscillator tries to synchronize y whit external signal, in our case F_{PID} . This synchronization results in:

$$\begin{cases} \angle y_{AFO} \cong \angle F_{PID} \\ \angle y_{AFO} \cong \angle v_r \end{cases} \rightarrow \angle F_{PID} \cong \angle v_r$$

This synchronization between applied force and velocity provides the necessary condition for minimum power consumption. In following, we study behavior of this adaptive oscillator for hopper leg shown in Figure4. Oscillation with 0.2m amplitude around rest length of hopper is the desired task for this system (third subplot in Figure5). Note that there is discontinuity in the dynamics between flight and stance phases, resulting in complex natural dynamics for such a simple system.

Proposed adaptive oscillator is used to exploit natural dynamics of this system. Initial frequency and epsilon are 5rad/s^{-1} and 0.1. Frequency convergence is shown in the first subplot of Figure5. This converged frequency is not close to one calculated from $\sqrt{k/m}$. The second subplot in Figure5 shows that AFO applies less force by getting closer to natural dynamics. Another interesting point is that AFO learns to not exert any negative force which can be expected by intuition that jumping up does not imply using downward force. The third subplot in Figure5 shows that tracking performance of controller is satisfying.

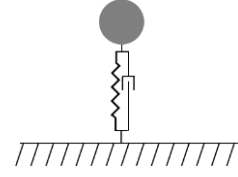


Figure4 Hopper leg; $m=0.5\text{kg}$, $k=9\text{Nm}^{-1}$, $b=0.01\text{Nsm}^{-1}$, $K_p=100$, $K_i=0.5$, $K_d=5$.

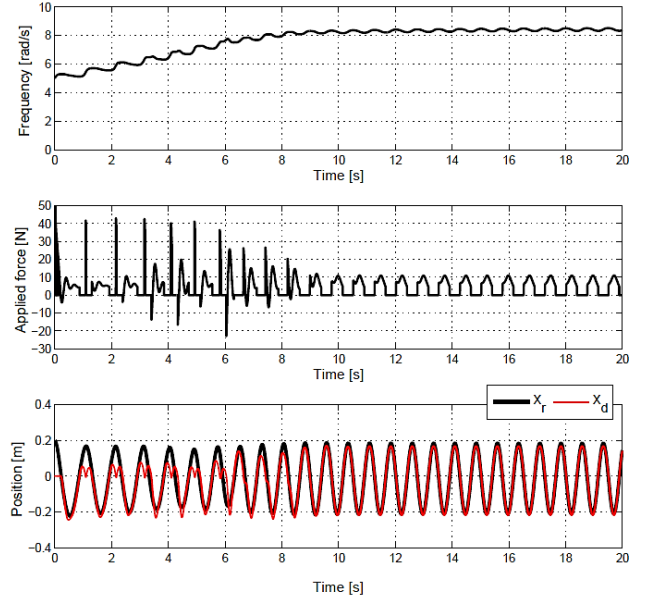


Figure5 Adaptation for hopper leg

4 Open Questions

In this paper, we studied natural dynamics of nonlinear compliance in simple systems. Studying complex systems like legged robots with nonlinear compliances in their bodies is in our future work list. A novel and adept adaptive oscillator was presented in this work; capability of this oscillator for natural dynamics exploitation was also satisfactory. We built our adaptive oscillators upon Hopf oscillator. However, for more versatility and learning capability we will explore other oscillators as well.

References

- [1] M. M. Williamson, "Robot arm control exploiting natural dynamics," Massachusetts Institute of Technology, 1999, Thesis dissertation
- [2] F. Iida, G. Gómez, and R. Pfeifer, "Exploiting body dynamics for controlling a running quadruped robot," in *Advanced Robotics, 2005. ICAR'05. Proceedings., 12th International Conference on*, 2005, pp. 229–235.
- [3] D. Remy, "Optimal Exploitation of Natural Dynamics in Legged Locomotion," ETH Zurich, Zurich, 2011, PhD thesis dissertation.
- [4] D. Braun, M. Howard, and S. Vijayakumar, "Optimal variable stiffness control: formulation and application to explosive movement tasks," *Autonomous Robots*, pp. 1–17, 2012.
- [5] B. Vanderborght, R. Van Ham, B. Verrelst, M. Van Damme, and D. Lefeber, "Overview of the lucy project: Dynamic stabilization of a biped powered by pneumatic artificial muscles," *Advanced Robotics*, vol. 22, no. 10, pp. 1027–1051, 2008.
- [6] A. A. Biewener, "Tendons and Ligaments: Structure, Mechanical Behavior and Biological Function," *Collagen: structure and mechanics* (Ed. P. Fratzl) Springer, Berlin, pp. 269–284, 2008.
- [7] L. Righetti, J. Buchli, and A. J. Ijspeert, "Dynamic hebbian learning in adaptive frequency oscillators," *Physica D: Nonlinear Phenomena*, vol. 216, no. 2, pp. 269–281, 2006.

Anatomically Detailed Three Dimensional Dynamical Finite Element Analysis of the Human Foot

Taiki Kobayashi¹, Sinnosuke Kume², Masahiro Shimizu¹, Koh Hosoda¹, Naomichi Ogihara³, Takeo Nagura⁴, Toshiyasu Nakamura⁴, Masahiro Jinzaki⁴, Nobuaki Imanishi⁴, and Sadakazu Aiso⁴

¹ Department of Multimedia Engineering, Osaka University, Japan
kobayashi.taiki@ise.eng.osaka-u.ac.jp {*m-shimizu, koh.hosoda*}@*ist.osaka-u.ac.jp*

² Department of Business Engineering, Osaka University, Japan
kume.shinnosuke@ise.eng.osaka-u.ac.jp

³ Department of Mechanical Engineering, Keio University, Japan
ogihara@mech.keio.ac.jp

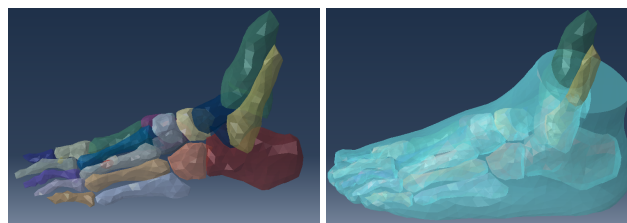
⁴ School of Medicine, Keio University, Japan

1 Introduction

Humans can walk on rough terrain. A part of such adaptability is brought by the mechanical characteristics of the human foot, that is the mechanical compliance and its complex structure consisting of skins, muscles, ligaments, and bones. However, the kinematics of the foot structure during walking and its contribution to human adaptability have not been clarified. Therefore in this study, we focused on the relative movements of the bones during walking.

The numerical analysis with finite element method (FEM) is a powerful tool for the foot analysis. FEM can predict precisely physics of the complicated structures. Many researchers analysed static posture of a foot with FEM[1, 2, 3]. As an example, Cheung *et al.* used FEM to observe the plantar pressure distribution during standing posture[1]. In these studies, dynamic foot movement was not considered. On the other hand, some researchers analysed foot movement with FEM dynamically. Jason *et al.* have conducted FE analysis during walking and measured the internal tissue loading[4]. Here, the foot structure was simplified as two-dimensional FE model in sagittal plane. In addition to this, the bones other than the phalanges were combined into one rigid segment. However, FE analysis with complex structure is intrinsically important because the adaptability of humans is based on the mechanical compliance due to relative movement of the foot bones. In light of these considerations, three-dimensional dynamical FE analysis should be conducted in order to understand the human adaptability based on dynamics of the complicated human foot structure.

Based on the above discussion, the goal of this study is to clarify the role of the relative movements of the bones in the foot during walking. To this end, we intend to deal with three-dimensional dynamical FE analysis. More specifically, we measure the displacement of human shank during gait using motion capturing system. And then, we take them into the three-dimensional FE model of the foot as the



(a) Bone structure

(b) Bone structure and soft tissues

Figure 1: The foot geometry

forced movement. In this method, we can analyse the internal movement of the complex human foot structure during gait. We intend to validate simulated GRF during walking. Main contribution of this study is to establish the framework of the precise three-dimensional dynamical FE analysis of human walking.

2 Method

2.1 FE Modeling of Human Foot

Three dimensional FE model of the foot was constructed in Abaqus 6.11¹. The geometry of the soft tissue and the bones were obtained from CT scan which was performed in a healthy person(Fig.1). The bone structure consists of 23 parts and each of which was define as rigid body. The soft tissue material was defined as isotropic and non-linear elastic through the second order polynomial strain energy function[5]. The viscoelasticity of the soft tissue was defined using a two-term Prony series[6]. The tissue and the bones were combined using tie constraint. The foot-ground interaction was modeled using penalty contact with a friction coefficient of 0.6[7].

¹Abaqus/Explicit was employed for dynamical analysis.

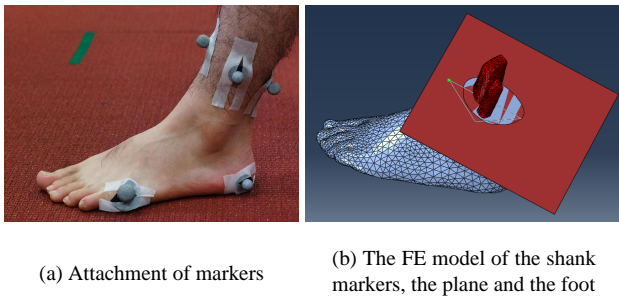
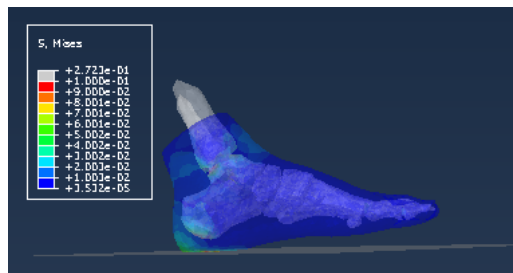
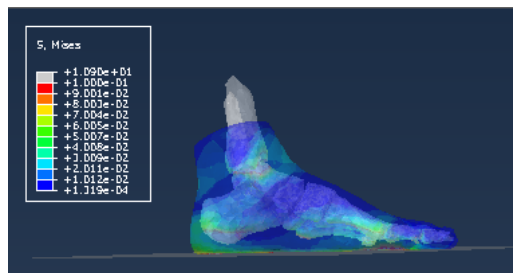


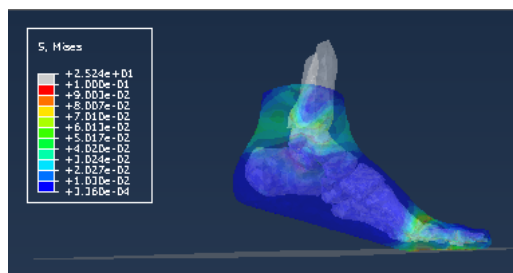
Figure 2: Assignment of a simulated foot motion corresponding to human walking



(a) heel-strike



(b) mid-stance



(c) toe-off

Figure 3: Snapshot of the foot during walking with von Mises stress distribution for heel-strike, mid-stance, and toe-off, respectively.

2.2 A Foot Motion in FE Analysis

The foot motion is determined based on the measurement of human walking. The human shank displacement during gait was measured using motion capturing system. Here, we attached 3 markers on the lower shank, and 2 markers on the foot (i.e., the heel and the toe) (Fig.2(a)). The plane, which is constructed by the shank markers, constrains the cross section at the lower shank in foot FE model (Fig.2(b)).

3 Discussion

Based on the above setting, we conducted FE analysis of human walking during from heel-strike to toe-off. The transition sequence of foot motion is shown in Fig.3 as snapshots. As the figure explains, main contribution of this study is to establish the framework of the precise dynamical simulation analysis of human walking. As mentioned above, the FE analysis with complex structure is intrinsically important because adaptability of human is based on mechanical compliance due to relative movement of foot bones. As an on-going simulation, we are estimating simulated GRF during walking. The future work is FE modeling of the cartilages, the ligaments, and muscles more precisely.

We also plans to perform experiments using a cadaver foot driven by a musculoskeletal biped robot to clarify the role of the human foot structure. The biped robot for maneuvering cadaver foot has artificial muscles and uses pneumatic pressure (Fig.4). Our simulator can reproduce not only single support phase but also double support phase. We plan to monitor the behavior of the foot bones during walking by X-ray cinematography.



Figure 4: Pneumatically driven bipedal robot to drive cadaver foot.

4 Open Question

The questions we would like to discuss are listed as follows:

- What is the role of the complex foot structure during walking?
- How benefits could we have by understand such structure?
- What is the limitation of the FEM approach?
- What is the limitation of the cadaver experiment approach?

Acknowledgement

This work was partially supported by a Grant-in-Aid for Scientific Research(23220004 and 22760180) from the Japanese Ministry of Education, Culture, Sports, Science and Technology.

References

- [1] J.T. Cheung and M. Zhang. Parametric design of pressure-relieving foot orthosis using statistics-based finite element method. *Medical Engineering and Physics*, 30:269–277, 2008.
- [2] Weng-Pin Chen, Chia-Wei Ju, and Fuk-Tan Tang. Effects of total contact insoles on the plantar stress redistribution:. *Clinical Biomechanics*, 18:S17–S24, 2003.
- [3] Wen-Ming Chen, Taeyong Lee, Peter Vee-Sin Lee, Jin Woo Lee, and Sung-Jae Lee. Effects of internal stress concentrations in plantar soft-tissue-a preliminary three-dimensional finite element analysis. *Medical Engineering and Physics*, 32:324–331, 2010.
- [4] Jason P.Halloran, Marko Ackermann, Ahmet Erdemir, and Antonie J. van den Bogert. Concurrent musculoskeletal dynamics and finite element analysis predicts altered gait patterns to reduce foot tissue loading. *Journal of Biomechanics*, 43:2810–2815, 2010.
- [5] Lemmon D., T.Y. Shiang, A. Hashmi, J.S. Ulbrecht, and P.R. Cavanagh. The effect of insoles in therapeutic footwear : a finite-element approach. *Journal of Biomechanics*, 30:615–620, 1997.
- [6] J.Z. Wu, R.G. Dong, S. Rakheja, and A.W. Schopper. Simulation of mechanical responses of fingertip to dynamic loading. *Medical Engineering & Physics*, 24:253–264, 2002.
- [7] M. Zhang and A. F. T. Mak. Zn vivo friction properties of human skin. *Prosthetics and Orthotics International*, 23:135–141, 1999.

A Simple Controller for Quadrupedal Bounding

Xin Liu and Ioannis Poulakakis

Department of Mechanical Engineering, University of Delaware, USA

{xinliu, poulakas}@udel.edu

1 Motivation

In this work, the dynamics of quadrupedal bounding is studied via the reduced-order sagittal-plane model of Fig.1. The model is composed of a rigid torso and two massless springy prismatic legs. Albeit simple, models in this family have been found useful in uncovering many important properties of bounding. For example, it has been shown in [1] that a variety of bounding gaits can be generated passively, suggesting that such motions represent natural interactions between a quadruped and its environment.

According to the modeling and control hierarchy introduced in [2], reductive locomotion models can be used to inform the control of more accurate high-dimensional representations of robots (or animals) by suggesting suitable coordination mechanisms. However, passive reduced-order models such as the one in [1] cannot be used directly as control targets for more complete robot models due to their limited ability in rejecting perturbations. For example, the majority of the passively generated fixed points in [1] are unstable; stable (within a total energy level) fixed points only exist when the forward velocity is in a range that is not realizable by most robotic quadrupeds. Even for these stable fixed points, the domain of attraction is not practical.

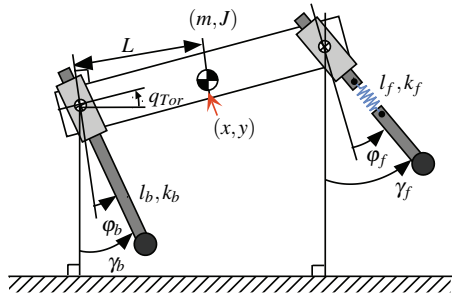


Figure 1: A sagittal-plane bounding model.

In this work, a controller for the bounding model of Fig. 1 is described. The proposed control law manipulates the touchdown angles of the front leg based on feedback of the liftoff angle of the back leg to stabilize a large number of passively generated periodic bounding gaits within a constant energy level. To reject perturbations that alter the total energy, actuation is introduced at the hip joints during the back and front leg stance phases, and a continuous-time controller is proposed that stabilizes the energy of the system at a desired level. It is shown in simulation that this two-layer controller design is capable of rejecting sufficiently large

perturbations without requiring excessive inputs.

2 State of the art

A large number of controllers have been proposed to stabilize bounding motions on quadrupedal robots. Among them, Raibert's three-part controller [3] demonstrated high performance running motions over natural terrain. Variations of this controller have been used to control electrically actuated quadrupedal robots in [1]. A different paradigm for controller design that uses principles from neurobiology has been employed by [4] to induce dynamically stable locomotion on the quadrupedal robot Tekken.

To investigate the dynamics of legged systems, formal reductive models—termed *templates* in [2]—have been introduced in an effort to resolve complexity in locomotion. Among these models, the Spring Loaded Inverted Pendulum (SLIP) stands out as a canonical model of the center-of-mass (COM) dynamics of running robots (and animals), prompting a variety of control laws for stabilizing SLIP running. Most relevant to our work is the controller proposed in [5], which uses symmetries to stabilize periodic running orbits through an adaptive touchdown angle update law. Clearly though, point-mass hoppers like the SLIP cannot capture the torso pitch dynamics of bounding, which calls for non-trivial modifications of SLIP-based control ideas. Proposing such controllers for bounding is the subject of this work.

3 Our approach

The reduced-order model of Fig.1 is used to study bounding. In this model, the legs are assumed massless and actuation is introduced at the hips during the front and back leg stance phases to develop non-conservative corrective action. The geometric and inertia parameters are taken from [1] and bounding without double stance is considered.

3.1 Touchdown angle control policy

It has been observed in [1] that passively generated bounding motions have the following property

$$\bar{\gamma}_{TD}^f = -\bar{\gamma}_{LO}^b, \quad (1)$$

where $\bar{\gamma}_{TD}^f$ and $\bar{\gamma}_{LO}^b$ are the front leg touchdown and the back leg liftoff angles at a desired fixed point, respectively. Motivated by [5], the front leg touchdown angle $\bar{\gamma}_{TD}^f$ at the $(n+1)$ -th stride is updated based on feedback of the back

leg liftoff angle γ_{LO}^p at the n -th stride according to

$$\gamma_{TD}^f[n+1] = \gamma_{TD}^f + c(\gamma_{LO}^p - \gamma_{LO}^p[n]), \quad (2)$$

where c is a constant gain. To investigate the local stability of the system in closed loop with (2), the eigenvalues of the linearization of the corresponding Poincaré return map are computed for a variety of values for c , as shown in Fig. 2. It can be seen that for $c > 1.1$ all the eigenvalues enter the unit disc, except one eigenvalue that remains at one reflecting the conservative nature of the system.

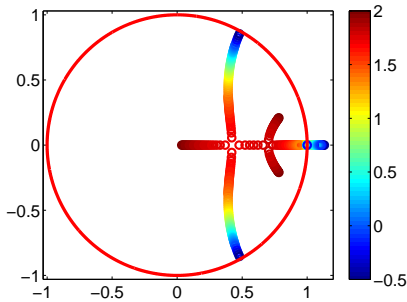


Figure 2: Locus of the eigenvalues as c varies in $[-0.5, 2]$.

3.2 Energy controller

The conservation of energy precludes the existence of asymptotically stable fixed points; for, perturbations altering the total energy of the system cannot be rejected. To incorporate non-conservative forces to the model of Fig. 1, actuation is introduced at the hip joint. The hip actuators are active only during the stance phase of the corresponding leg, developing torques according to the prescription

$$\tau = -K \frac{E - \bar{E}}{\Delta\bar{\varphi}}, \quad (3)$$

where $\Delta\bar{\varphi}$ is the change of the stance leg angle φ relative to the torso at the desired fixed point, E is the total energy and \bar{E} its nominal value at the fixed point, and $K \in [0, 1]$.

3.3 Controller evaluation in simulation

The performance of the proposed two-level controller is evaluated in simulation. The passively generated fixed point $y = 0.35\text{m}$, $q_{\text{Tor}} = 0\text{deg}$, $\dot{x} = 3\text{m/s}$, $\dot{q}_{\text{Tor}} = 150\text{deg/s}$ (states refer at the apex height) is used, and (2) and (3) for $c = 1.3$ and $K = 0.2$ are employed. Figures 3(a) and 3(b) demonstrate convergence to the nominal orbit after a perturbation 0.4m/s is introduced in the forward velocity at apex. Note that despite the relatively large size of the perturbation, Fig. 3(b) shows that the torque required is small.

4 Discussion outline

This work aims at enhancing the stability properties of periodic bounding orbits passively generated via the reduced-order sagittal plane model of Fig. 1. As in the modeling and control hierarchy proposed in [2], this model can

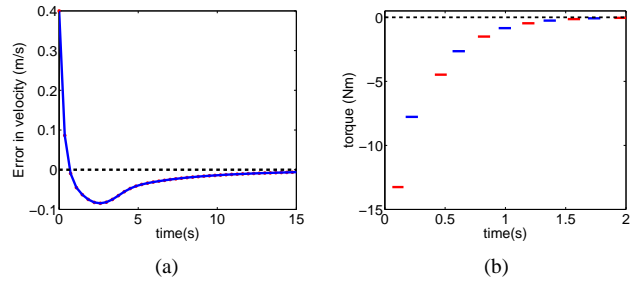


Figure 3: (a) Error in forward velocity at apex. (b) Back leg (red) and front leg (blue) hip actuator torques. The energy converges to its nominal value faster than the velocity.

serve as a behavioral control target for more complete models of quadrupedal robots. To achieve this objective, there are a number of issues that require further attention. In particular, the choice of the controller constant c in (2) has a strong influence on the ability of the controller to stabilize passively generated fixed points. We are currently in the process of establishing analytical criteria for the choice of this parameter. Furthermore, to make these results relevant to the control of quadrupedal robots, we plan to devise control strategies in the spirit of the Hybrid Zero Dynamics (HZD) method [6]. These strategies coordinate the joints of higher-dimensional—more realistic—models of legged robots so that their behavior is governed by lower-dimensional control targets that encode the desired task; the model of Fig. 1 can serve as such a control target for bounding.

5 Acknowledgment

Work supported by NSF grant CMMI-1130372.

References

- [1] I. Poulakakis, E. Papadopoulos, and M. Buehler, “On the stability of the passive dynamics of quadrupedal running with a bounding gait,” *The International Journal of Robotics Research*, vol. 25, no. 7, pp. 669–687, 2006.
- [2] R. Full and D. Koditschek, “Templates and anchors: neuromechanical hypotheses of legged locomotion on land,” *Journal of Experimental Biology*, vol. 202, no. 23, pp. 3325–3332, 1999.
- [3] M. H. Raibert, *Legged Robots that Balance*. MIT Press, 1986.
- [4] Y. Fukuoka, H. Kimura, and A. H. Cohen, “Adaptive dynamic walking of a quadruped robot on irregular terrain based on biological concepts,” *The International Journal of Robotics Research*, vol. 23, no. 10-11, pp. 1059–1073, 2004.
- [5] J. Schmitt, *Simple Feedback Control of Cockroach Running*, M. Diehl and K. Mombaur, Eds. Springer Berlin Heidelberg, 2006, vol. 340.
- [6] E. Westervelt, W. Grizzle, C. Chevallereau, J. H. Choi, and B. Morris, *Feedback Control of Dynamic Bipedal Robot Locomotion*. CRC Press, 2007.

Energy-based State-Feedback Hopping Control

Inna Mikhailova

Simulation, Systems Optimization and Robotics Group,
Technische Universität Darmstadt, Germany
mikhailova@sim.informatik.tu-darmstadt.de

1 Introduction

The cost optimization and self-organization of systems dynamics build two opposite views within the scientific community on the motion generation. While the first possesses well-established tools, the second relies to the great deal on the intuition of an engineer who chooses a suitable hardware and dynamics type. In exchange, appropriate dynamics shows high adaptivity, while optimization relies on the quality of models and fails in cases of unforeseen perturbations. Some approaches combine both philosophies, e.g. Dynamic Motion Primitives, [6], represent a controller as a dynamic system, whose parameters are subject to optimization.

In this work we present another combination of these two frameworks. We propose to search such a cost function, which allows the application of the Speed Gradient (SG) method developed in [2] leading to a state-feedback form. The controlled system is then an autonomous dynamic system, like in the dynamic system approach while the optimization is shifted into the choice of the cost function. The cost function that satisfies the requirements of the SG method may be difficult to find, thus we tested the possibility to use learning for this purpose. In this work we show that the SG method can be successfully applied to control of hopping of two serial springs. Additionally a modified Slow Feature Analysis (SFA) can be used for learning of related cost function.

2 Methods

2.1 Speed Gradient Control

The word "speed" reflects the fact that this method focuses not on the given cost function, but on the speed of changes in the cost function along the trajectory. In this way the natural dynamics of an unforced system can be taken into account, which is a big advantage of this method.

Let us consider a controlled system $\dot{x} = F(x, u, t)$, where $x(t)$ is a state vector and $u(t)$ is a vector of control inputs. Let $V(x, t)$ be the cost function. Then SG method suggests to change the control variable along the gradient of the speed of costs in control, with the rate γ :

$$u = -\gamma \nabla_u \left(\frac{dV}{dt} \right) = -\gamma \nabla_u \left(\frac{\partial V}{\partial x} F + \frac{\partial V}{\partial t} \right). \quad (1)$$

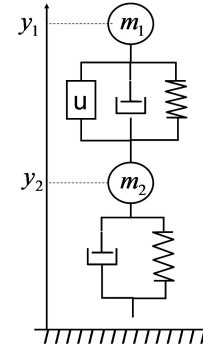


Figure 1: 1-D visco-elastic model of human hopping [4].

The intuition behind this choice is, that such control will decrease the speed \dot{V} . As soon as $\dot{V} < 0$, also the cost function will decrease. This type of control was successfully applied to excitation of oscillations, synchronization, and control of chaotic systems [2]. The problem of the SG approach is, that for many applications it is not clear how to choose a suitable cost function. In our hopping example we use the following cost function: $V(x, t) = (E(t) - E^*)^2$, where $E(t)$ is a full energy of the system and E^* is the desired energy level. Indeed, a high constant energy level corresponds to hopping. However for more complex systems the search of a suitable cost function may be difficult. Below we introduce a learning method that can be used for this purpose.

2.2 Slow Feature Analysis

The introduction in [7] describes SFA as follows: "The SFA learns instantaneous, non-linear functions $g(x)$ that transform time-varying input data $x(t)$ into slowly-varying output signals, $y(t)$ ". Besides numerous applications in computational neuroscience, SFA was also used for extraction of driving forces from nonlinear dynamical systems. However it was not yet used for learning of energy of dynamical systems as proposed here. Our results show, that the SFA can be used for learning of both energy and Hamilton functions, given that the dissipation on the one side ensures that the energy is not constant, but on the other side is low enough, so that the energy is the slowest varying function.

3 Application: State-feedback control of serial springs

A system consisting of two damped spring-mass elements arranged in series was proposed in [4] as a model for the human hopping (Figure 1). The coupling of the springs leads to non-trivial dynamics and control. Following equations describe the motion of the system (from [4]):

$$\begin{aligned} m_1 \ddot{y}_1 &= u - m_1 g + k_1(l_{10} - l_1) - b_1 \dot{l}_1 - c_1 \text{sign}(\dot{l}_1) \\ m_2 \ddot{y}_2 &= -u - m_2 g - k_1(l_{10} - l_1) + b_1 \dot{l}_1 + c_1 \text{sign}(\dot{l}_1) + \\ &\quad k_2(l_{20} - l_2) - b_2 \dot{l}_2 - c_2 \text{sign}(\dot{l}_2), \end{aligned}$$

where y_i is the height of center of mass, m_i is the mass, l_{0i} the rest length, k_i the stiffness coefficient, b_i the damping coefficient, c_i the friction coefficient, and l_i the length of the spring i (see Figure 1).

The energy of the system can be calculated as follows:

$$E(t) = \frac{1}{2} [m_1 \dot{y}_1^2 + m_2 \dot{y}_2^2 + k_1(l_{10} - l_1)^2 + k_2(l_{20} - l_2)^2] + g[m_1 y_1 + m_2 y_2]$$

For an energy-based cost function in (1) we get a following SG controller:

$$u = -\gamma \nabla_u \frac{d}{dt} (E(t) - E^*)^2 = -\gamma (E(t) - E^*) \frac{dl}{dt}, \quad (2)$$

where l is the length of the actuated spring (see Figure 1). As the exact energy value is not essential for the gradient method, we simplify (2) to an almost local controller

$$u = -\gamma \text{sgn}(E(t) - E^*) \frac{dl}{dt}.$$

We use this controller during the decompression of the upper spring with $\gamma = 50$. In order to test the robustness we reproduced in simulation the experiment done in [4]. The system is released from initial height of 0.19m. After the stabilization of the hopping, the ground level is perturbed by -0.05 m and later, if possible, by 0.025m, see Figure 2. It can be seen that the controller is robust to perturbations. Figure 3 shows return maps for different release heights (0.19m, 0.17m, 0.15m) for analytically calculated and learned controller. The later uses in (2) for $\nabla_u \dot{E}$ the Hamiltonian function learned with the help of modified SFA as will be described later (see Figure 6).

In order to measure the energy-efficiency of the proposed method we calculated the cost of transport in the following form:

$$CoT = \frac{1}{S} \int_{t_d}^{t_l} \|u\| \|\dot{l}_1\| dt,$$

where t_d is the time of touch down, t_l is the time of lift off, and scale factor S takes in account the hardware and the hopping height H : $S = 9.8(m_1 + m_2)(k_1 + k_2)H$. Figure 5 compares the costs for different methods. The costs are plotted

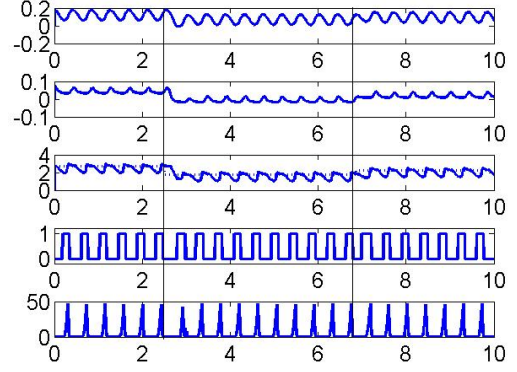


Figure 2: Control of hopping with SG-method. From top to bottom: height of the "body", height of the "shank", energy and desired energy (dotted line), ground contact, control input. The x-axes shows time in seconds. The vertical lines show the instants of perturbations.

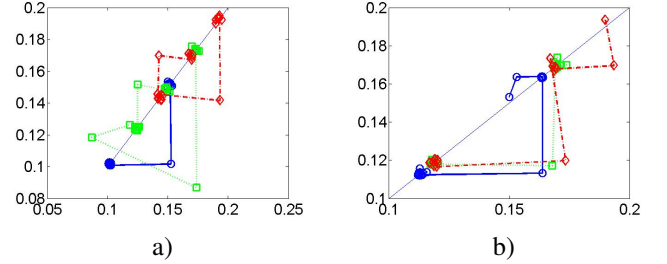


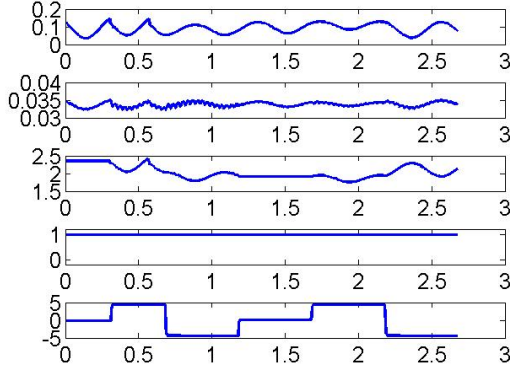
Figure 3: Return maps for release height of 0.19m (red diamond), 0.17m (green square), 0.15m (blue circles). Return map shows the hopping height of current step (y-axes) versus hopping height of previous step (x-axes). Points on the diagonal correspond to stable hopping. The drops in height correspond to the perturbations. The stable hopping recovers very quickly. a) Analytically calculated SG controller. b) Learned SG controller.

for all hopping sequences. The lowest release height comes first. The x axes shows how many time the system hopped. It can be seen that the SG method has the lowest costs. For the SG method the costs, although already scaled by hopping height, still depend on it, while for the other methods not. This dependency is rather natural.

For learning of Hamiltonian we use an off-line version of SFA and gather the data during an "exploratory" trial with force input which is just a step function, (see Figure 4). Input to the learning algorithm is a vector x , consisting of positions, velocities and applied forces. Our goal is to find with help of SFA such coefficients of quadratic polynomial of x , that this polynomial is constant on the trajectory of the system. In difference to the classical SFA ([7]) we take in "Expansion" step all two degrees polynomials in coordinates, but only linear combination of force and coordinate, meaning that the term u^2 is dropped. In "Temporal variation" step

Table 1: SFA coefficients in extended function space

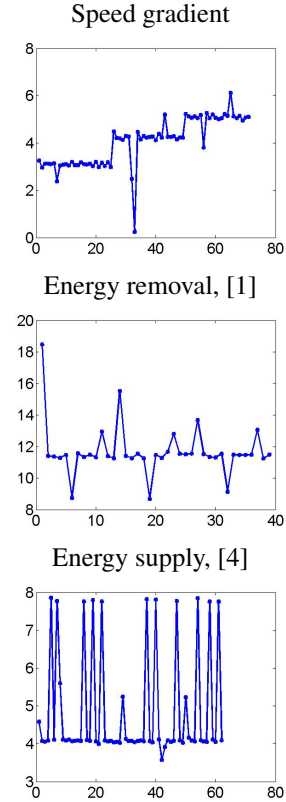
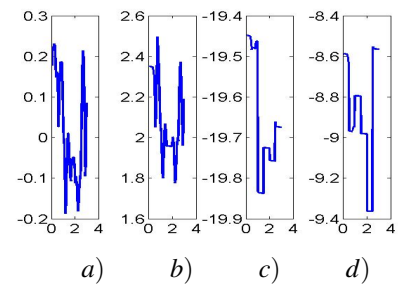
	y_1^2	y_1y_2	$y_1\dot{y}_1$	$y_1\dot{y}_2$	y_1u	y_2^2	$y_2\dot{y}_1$	$y_2\dot{y}_2$	y_2u	\dot{y}_1^2	$\dot{y}_1\dot{y}_2$	\dot{y}_1u	\dot{y}_2^2	\dot{y}_2u
Theory	0.9990	-0.0228	0	0	0.0001	0.0228	0	0	-0.0001	0	0	0	0.0001	0
0.01%	0.9992	-0.0229	0.0	0.0	0.0001	0.0074	0	0	2.1e-5	0	0	0	2.8 e-5	0.0
1%	0.9992	-0.0229	0.0001	0.0	0.0001	0.0055	0	0	-1.5e-5	0	0	0	2.0 e-5	0.0
10%	0.9992	-0.0231	0.0007	0.0001	0.0001	0.0007	0	0	0.0	0	0	0	0.0	0.0

**Figure 4:** Exploratory trial for SFA-based learning. From top to bottom: height of the "body", height of the "shank", energy, ground contact, control input. The x-axes shows time in seconds.

the numerical calculation of the derivative is exchanged by the derivative which uses the measured data: $\frac{dg(x)}{dt} = \frac{\partial g}{\partial x} \dot{x}$, where $\frac{\partial g}{\partial x}$ is calculated analytically and \dot{x} is measured data. Figure 6, c,d) shows the results of this modified method if damping and friction were reduced to 1% of the values used in [4]. The table 1 shows how the results get worse if we increase the damping and friction. The first row shows the normalized coefficients for respective polynomial terms calculated from the theoretical model. Other rows are calculated via modified SFA. On the left we display the reduction factor of damping and friction compared to values used in [4]. Coefficients that are smaller than $1.0e-6$ are rounded to zero.

4 Open questions

The main advantage of SG method is the exploitation of natural dynamics and it remains an open question how this quality can be transferred from control of quasi passive systems to active systems. One way could be to embed the actual dynamics into dynamics of a passive mechanical system with desired trajectory. For example [5] proposes an embedding into SLIP-dynamics. The stabilizing control (formula (13)) corresponds exactly to the Speed-Gradient control for SLIP-Energy. It was shown in [5] that the choice of appropriate holonomic constraints (which corresponds in our formalism to a choice of cost function) is crucial for dealing

**Figure 5:** Cost of Transport for different control methods as a function of step number.**Figure 6:** Learning results for nearly conservative system. a)Analytically calculated energy function. b)Output of standard SFA. c)Analytically calculated Hamiltonian function. d)Output of modified SFA.

with perturbations. This supports our idea of shifting the optimization step from the choice of controller to the choice of the cost function. Indeed, as soon as the cost-function is known, we get the SG-controller simply by calculating the gradient (1). However the choice of cost function is not a trivial step and rises following questions:

- What are requirements on cost-function, besides the ones formulated in [2], that increase the robustness?
- Can the SFA-based learning of invariants take in account such requirements?
- Should the cost function take in account not only dynamics of links but also actuators dynamics?

Biological modeling is not a primary task of our work, but the results are a product of interdisciplinary discussion which is fruitful for both biologists and engineers. From a biological point of view I would like to discuss following questions:

- Initially the SFA algorithm was developed for sensory learning. Is the slowness principle used by SFA plausible also for motor learning?
- Can application of SFA-based learning to the analysis of the human motion provide further conservative entities comparable to SLIP-energy?
- Muscles models, e.g. [3] suggest the combination of feedforward and feedback control as a trade-off between optimal and robust control. Is the combination of embedding into a passive system and stabilization via speed-gradient comparable to such trade-off?

From more general perspective, it is interesting to discuss how the formulation of a soft control that relies on conservation laws, synchronization and geometrical constraints can help to understand the possibilities of uploading of the control into hardware, a phenomena which can be observed in animals and humans.

References

- [1] B. Andrews, B. Miller, J. Schmitt, and J. E. Clark. Running over unknown rough terrain with a one-legged planar robot. *Bioinspiration & Biomimetics*, 6(2):1–15, 2011.
- [2] A. Fradkov. *Cybernetical physics: from control of chaos to quantum control*. Springer-Verlag, 2007.
- [3] D. F. B. Haeufle, S. Grimmer, K.-T. Kalveram, and A. Seyfarth. Integration of intrinsic muscle properties, feedforward and feedback signals for generating and stabilizing hopping. *J R Soc Interface*, 9:1458, 2012.
- [4] K. T. Kalveram, D. F. B. Haeufle, A. Seyfarth, and S. Grimmer. Energy management that generates terrain following versus apex-preserving hopping in man and machine. *Biol. Cybern.*, 106(1):1–13, Jan. 2012.
- [5] I. Poulakakis and J. W. Grizzle. The spring loaded inverted pendulum as the hybrid zero dynamics of an asymmetric hopper. *IEEE Trans. Automat. Contr.*, 54(8):1779–1793, 2009.
- [6] S. Schaal, P. Mohajjerian, and A. Ijspeert. Dynamics systems vs. optimal control - a unifying view. In *Progress in brain research*, number 65, pages 425–445. 2007.
- [7] L. Wiskott, N. Wilbert, P. Berkes, M. Franzius, and H. Sprekeler. Slow feature analysis. *Scholarpedia*, 6(4):5282, 2011.

Internal combustion based transport: humans vs. vehicles

Alberto E. Minetti

Physiomechanics Laboratory, Department of Physiopathology and Transplantation,
University of Milan, Italy

alberto.minetti@unimi.it www.albertominetti.it

1 Introduction

This contribution will discuss the similarities between the biological actuator, that is to say muscles, and technological ones, say internal combustion engines, in the attempt to demonstrate that actuators are actuators, no matter where they come from.

Particularly, I am interested to show that many aspects of their function can be approached parallelly in the two scientific domains, where similar solutions to similar problems have been found.

2 Questions

Here are some of the open questions:

- a. Why both muscles and internal combustion engines show an optimal regime/contraction frequency minimizing the energy cost of transport?
- b. Which determinants negatively affect the performance of cars and humans at altitude?
- c. Does the allometry of size/cycle frequency of heart and engines follow the same trend and rules?
- d. Is there a common strategy in switching gaits (or fibre types) in bipeds/quadrupeds and gears in automobiles?
- e. Which advantages and risks resides in momentarily boosting the locomotor performance (spleen squeezing vs turbo-compressor)?
- f. How additional mechanical energy can be stored and released when needed in the musculo-skeletal system and in engine transmission machinery?
- g. Is there a similar size effect in the economy of natural and artificial vehicles?
- h. What is the effect of aging in the musculo-skeletal/cardiovascular system and in circulating vehicles?

3 Concepts

The following concepts from physiology and bio/mechanics help to answer those questions:

- Human and animal locomotion shows optimal speeds, i.e. for some gaits there is a speed minimizing the metabolic/fuel cost of transport.
- Aging and wear of the locomotor machine involve higher fuel consumption and the exacerbation of 'vehicle' asymmetry.
- Different actuators/engines are used to better serve different transport performances (power or duration).
- Additional strategies (tendons/flywheel, spleen/turbocharge) are exploited to extend the mechanical power available from the 'engine'.
- Cell exoskeleton and steel are the evolutionary solution to form the building blocks that allow the construction of high size animals and vehicles.
- Different fuel/air ratios are responsible for the available maximum power and efficiency of biological and technological actuators.

- All internal combustion 'engines' suffer from operating at high altitude, with similar decay in performance.

- The mass-specific cost of transport decreases at increasing size both in human/animals and in vehicles.

- Multi-fuel and hybrid 'vehicles' are diffused both in biological and technological transport: 1) phosphocreatine-glycogen-lipids versus GPL-gasoline, and 2) the management of mechanical energy fluctuations (acceleration/deceleration).

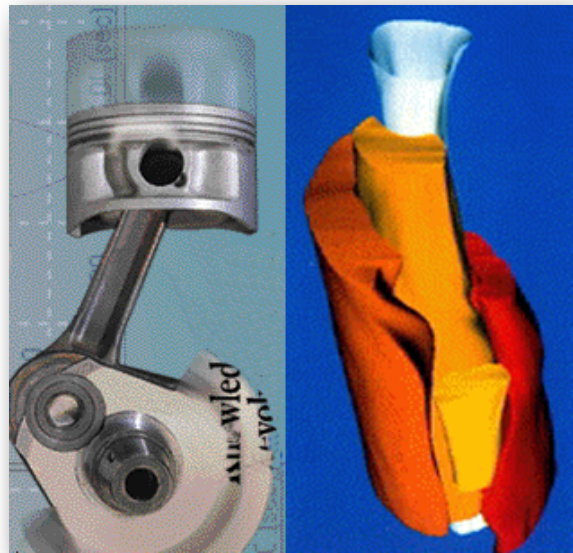


Figure1 Engines and Muscles

4 Open questions

The quite remarkable similarities between the motor function in biology and in engineering suggest an alternative cultural route with respect to the traditional transfer of some to the best solutions from Nature to technology (the so-called biomimetical approach).

The open question here follows: would the study of transport engineering allow to use the inherent understanding of man-made processes to shed light into the many still obscure mysteries of biological movement?

References

- [1] A. E. Minetti, The energetics and mechanics of natural and artificial locomotion. Symposium: Human Machinery at Work, ECSS 2010, Antalya, Turkey, July 2010.
- [2] A. E. Minetti, Biological and Technological Movement. Keynote Lecture at the conference on 'Physics in Sports, University Paris-Sud, April 3-6, 2012.

Angle-Dependent Moment Arm with Biased Pivot for Jumping from Various Squatting Positions

Satoshi Nishikawa***, Kazutoshi Tanaka*, Kazuya Shida*, Ryuma Niiyama*** and Yasuo Kuniyoshi*

* Intelligent Systems and Informatics Lab., The University of Tokyo, Tokyo, Japan

{*nisikawa, tanaka, shida, kuniyoshi*}@isi.imi.i.u-tokyo.ac.jp

**Research fellow of the Japan Society for the Promotion of Science

***Media Lab., Massachusetts Institute of Technology, Cambridge, MA, USA

ryuma@mit.edu

1 Introduction

To improve physical abilities of legged robots, body structures of animals are the useful references. Many robots mimicking them were developed to clarify their roles in dynamic motions [1, 2, 3, 6, 7]. McKibben-type pneumatic artificial muscles were often used for actuators of such robots because they have high power/mass ratio, viscosity and elasticity, however, their ranges of length which can exert high tension are small and biased to the limit length [4] compared to living muscles [5]. Thus, it is difficult to adapt to motions which need various postures if moment arms of muscles are constant to angles of joints. This problem is typical when a robot takes extended leg posture and needs large thrusting force such as running and jumping from slight squatting position because leg extensor muscles exert little torque in such a posture because of biased torque-angle relations.

It is possible to refer some researches which focused on the torque-angle characteristics of actuators to refine the highly biased output characteristics of pneumatic-driven robots. Pull rods and lever mechanisms were adopted by a robot with pleated pneumatic muscles, which also have non-

linear force-length relations, to linearize the torque-angle relations [6]. On the other hand, in MACCEPA (Mechanically Adjustable Compliance and Controllable Equilibrium Actuator), which is a kind of the series elastic actuator, moment arms are determined by profile disks to modify the stiffness-angle relation [7]. If the idea adjusting moment arms by guides is introduced to pneumatic-driven robots, it is expected that such robots can equip high dynamic performance and high adaptability to the various postures simultaneously.

In this paper, to improve physical abilities of robots in dynamic motions with various postures, the torque-angle relation of a muscle on a joint is modified by setting appropriate muscle route. In particular, Angle-Dependent Moment Arm (ADMA) with biased pivot is proposed. In this study, a musculoskeletal bipedal robot model refining Athlete Robot [3] was used as a platform (Fig.1, Table 1). First, the design of the mechanism is introduced, then, the effectiveness of this mechanism is examined by analyzing output force characteristics of the robot's leg and jumping experiments of the robot model in dynamic simulation, and finally, the mechanism is implemented to the real robot.

2 Angle-Dependent Moment Arm (ADMA)

ADMA is constructed by displacing the guide circle of muscle from the rotation center of a joint (Fig.2). Using variables in Fig.2, moment arm and muscle length are calculated as follows. Moment arm MA is calculated as:

$$MA(\theta) = b \sin \phi + a \cos \phi + r, \quad (1)$$

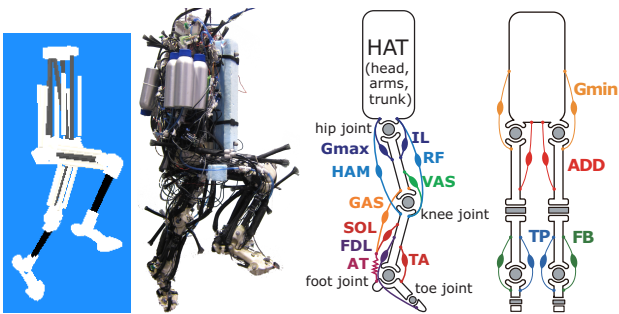


Figure 1: Image of the robot and layout of muscles. The abbreviations are, Gmin: gluteus minimus; ADD: adductor; FB: fibularis brevis; TP: tibialis posterior; Gmax: gluteus maximus; IL: iliopsoas; HAM: hamstrings; RF: rectus femoris; VAS: vastus; GAS: gastrocnemius; SOL: soleus; TA: anterior tibialis; FDL: flexor digitorum longus. AT: Achilles tendon (passive element).

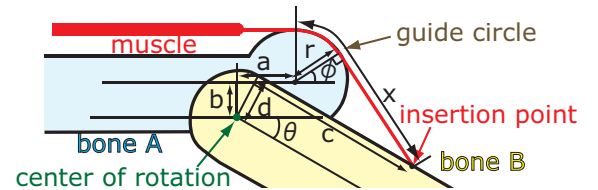


Figure 2: The mechanism of ADMA. The length of a , b , c , and r are constant values, θ is joint angle, and ϕ and x are functions of θ .

Table 1: Specification of the robot.

actuators	pneumatic artificial muscles (McKibben type)
passive elements	springs (Misumi, AWT20-60)
valves	pressure regulating valves (Hoerbiger, tecno basic), pilot valves (CKD, EXA-C8-02C-3)
air compressor	Anest Iwata, SLP-221EBD (external)
air buffer	six 10 l tanks (external), eight 0.5 l tanks (on board)
CPU board	General Robotix, Lepracaun
OS	linux-2.6.21.1-ARTLinux
materials	Nylon, CFRP pipes
mass of the robot	13.5 kg
physical parameters of each part	
trunk	0.45 m, 9.050 kg
thigh	0.30 m, 1.240 kg
shank	0.28 m, 0.456 kg
foot	0.10 m, 0.354 kg
toe	0.05 m, 0.106 kg

where $\phi = \arccos\left(r/\sqrt{A^2+B^2}\right) - \arctan(B/A)$,

$$A = -a + d \sin \theta + c \cos \theta, B = b - d \cos \theta + c \sin \theta.$$

Muscle length L is calculated as follows. When muscle is mono-articular muscle working to i th joint,

$$L(\theta_i) = L(\theta_{i,0}) + x(\theta_i) - x(\theta_{i,0}), \quad (2)$$

and when muscle is bi-articular muscle working to i th and j th joint,

$$L(\theta_i, \theta_j) = L(\theta_{i,0}, \theta_{j,0}) + (x(\theta_i) - x(\theta_{i,0})) + (x(\theta_j) - x(\theta_{j,0})), \quad (3)$$

where θ_i and θ_j denote joint angles that the muscle adds torque to, and $\theta_{i,0}$, $\theta_{j,0}$, $L(\theta_{i,0})$ and $L(\theta_{i,0}, \theta_{j,0})$ constitute the specific values of angles and lengths. Variable x is calculated as:

$$x(\theta) = r(\pi/2 - \phi) + (b + c \sin \theta - d \cos \theta + r \sin \phi) / \cos \phi. \quad (4)$$

Muscle tension T is calculated by substituting muscle length into the theoretical equation (Eq.5 [4]).

$$T = pC(1 - \varepsilon)^2 - D, \quad (5)$$

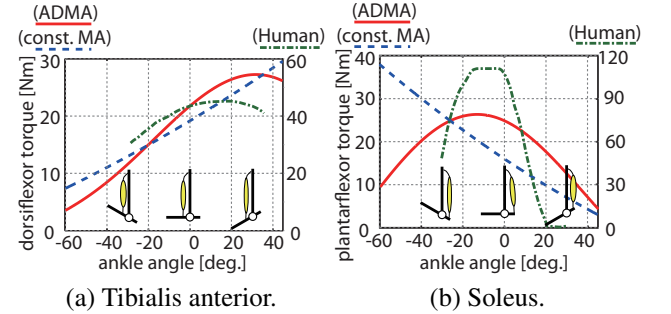
$$\text{where } C = 3/4\pi d_0^2 \cot^2(\theta_0), D = 1/4\pi d_0^2 \csc^2(\theta_0).$$

Here, d_0 , θ_0 , ε and p denote initial diameter, initial angle of braid, contraction ratio and inner pressure of muscle, respectively. Finally, torque is calculated as the product of MA and T .

Using eq.(1)-(5), parameters were decided to extend high-torque regions (Table 2, Fig.3). Decided parameters

Table 2: Parameters for moment arm (mm). The parameter $r_{\text{const.}}$ indicates the corresponding value of constant moment arm with the same range of motion by a muscle. Note that lower value of moment arm of RF knee and VAS are limited to 25.0 mm because of mechanical constraints.

muscle	a	b	c	d	r	$r_{\text{const.}}$
Gmax	17.9	55.2	34.6	20.0	11.0	32.3
IL	-43.7	43.8	29.8	20.0	11.0	28.6
HAM hip	40.0	33.2	260.0	28.0	0.0	3.1
HAM knee	0.0	0.0	29.5	4.8	28.0	28.0
RF hip	0.0	0.0	25.0	8.4	25.0	25.0
RF knee	-9.8	35.0	31.0	28.0	4.0	27.7
VAS	-9.8	35.0	31.0	28.0	4.0	27.0
GAS knee	0.0	0.0	25.0	1.0	25.0	25.0
GAS ankle	36.0	22.0	280.0	25.0	11.0	50.9
SOL	36.0	22.0	250.0	5.7	11.0	37.0
TA	-32.5	10.0	220.0	-27.3	0.0	28.8
FDL ankle	36.0	22.0	221.1	25.0	4.0	32.3
FDL toe	0.0	0.0	136.2	4.0	14.0	14.0
ADD	4.0	66.0	514.0	-10.0	0.0	59.4
Gmin	0.0	49.0	285.0	28.0	0.0	43.1
TP	36.0	22.0	250.0	5.7	11.0	23.2
FB	-32.5	10.0	220.0	-27.3	0.0	21.5

**Figure 3:** Torque-angle relations of the model with ADMA, the model with constant moment arms and human [5].

were used in the following experiments. In addition to broad high-torque regions, the peaks in the torque-angle relations of ankle flexor and extensor muscles were designed to approximate those of human [5] (Fig.3). Note that above equations can be applied to pull rods and lever mechanisms by setting $r = 0$, and constant moment arm mechanisms by setting $a = b = 0$.

3 Experiments

3.1 Analysis of leg's output force characteristics

To investigate the postural characteristics of the robot model with ADMA, Maximum Output Force (MOF) profiles [2] of the robot model with various postures were calculated. MOF profile is a convex polygon that encompasses the force vectors produced by all combinations of the actuator output forces. For comparison, MOF profiles of a model

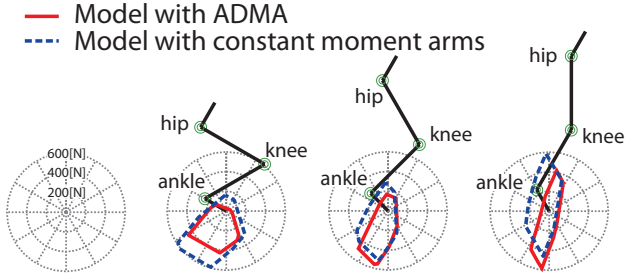


Figure 4: MOF profiles of leg models.

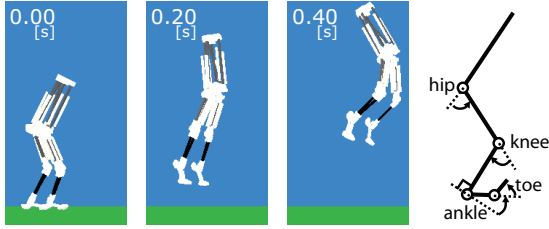


Figure 5: Snapshots of the robot model jumping (condition 4) and the definition of the angle.

with constant moment arms were also calculated. Active strokes of joints were conformed in these two models (Table 2). Although the model with ADMA exerted less downward force in a squatting position, it exerted more downward force in an extended leg posture (Fig.4). This result indicates that robots with ADMA have aptitudes for extended leg postures despite having relatively slack leg extensor muscles.

3.2 Jumping simulation

To evaluate the effectiveness of ADMA to motions from various postures, jumping experiments were conducted in the dynamic simulator OpenHRP3 [8] (Fig.5). The physical parameters and shapes of the body parts are calculated from the 3DCAD models. In these experiments, the model with constant moment arms was also used for comparison. The robot model began thrusting motion from various squatting positions and the highest Center of Gravity (CoG) position of the robot was measured as the evaluate value. Ten initial postures were decided by dividing equally between two extreme positions. In the least squatting position, the flexion angle of the hip, the flexion angle of the knee, and the dorsiflexion angle of the ankle were 0.6, 0.2, and 0.1 radians, respectively. In the most squatting position, they were 1.5, 2.0, and 1.0 radians, respectively. These conditions are numbered 1 to 10 from the most extended leg posture. The jumping motion was generated as the combination of two phases: the extension of hip and knee (supplying air to Gmax, RF, and VAS), and the extension of all joints (supplying air to Gmax, RF, VAS, GAS, SOL, and FDL). The commands for inner pressure of muscles in each phase were constant at 0.8 MPa and phase switching time for highest value was searched by 0.001 s from 0 to 0.2 s in each initial position. This representation of motion commands was selected be-

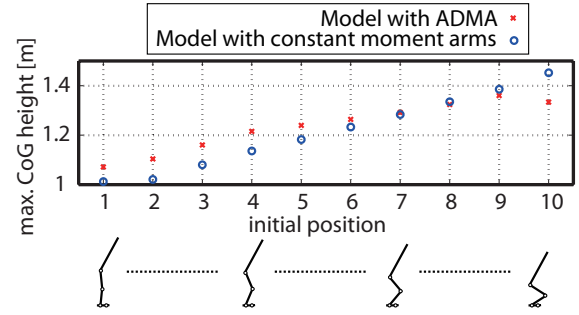
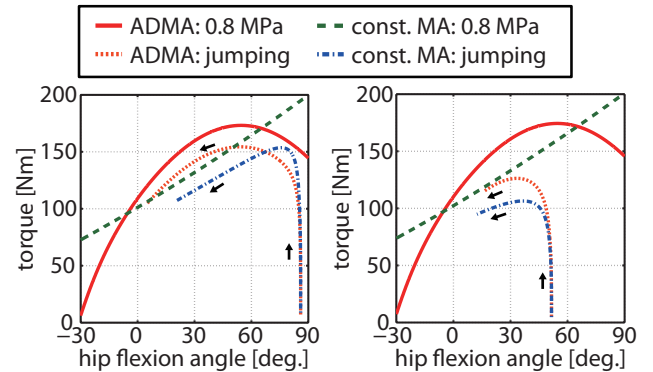


Figure 6: Maximum CoG of jumping from various postures.



(a) Deep squatting position (condition 10). (b) Slight squatting position (condition 4).

Figure 7: The torque-angle curves of Gmax during pressurized maximally (0.8MPa) and during thrusting the ground. Arrows indicate the flow of the time.

cause it is simple but it can generate jumping motions to various directions due to the timing of ankle extension.

Comparing highest values in each posture on two models, values on the robot with ADMA were higher in slight squatting position (Fig.6). The values were 1.237 ± 0.098 m on the model with ADMA, and 1.215 ± 0.147 m on the model with constant moment arms (mean±standard deviation). This shows that the robot with ADMA had smaller variation of the maximum jumping height to initial squatting position. This result indicates that ADMA can improve adaptivity of a robot to the motions from various postures by redistributing physical abilities to postures with relatively low capabilities.

To investigate the effect of ADMA during jumping, the torque-angle curve of the muscle during jumping is examined (Fig.7). First, the torque exerted by the muscle rose toward the torque-angle curve of the maximum inner pressure, and then followed the curve. In the jumping from the deep squatting position, first rise of torque was smaller on the robot with ADMA than the robot with constant moment arms. By contrast, in the jumping from the slight squatting position, the torque was larger on the robot with ADMA than the robot with constant moment arms during all the

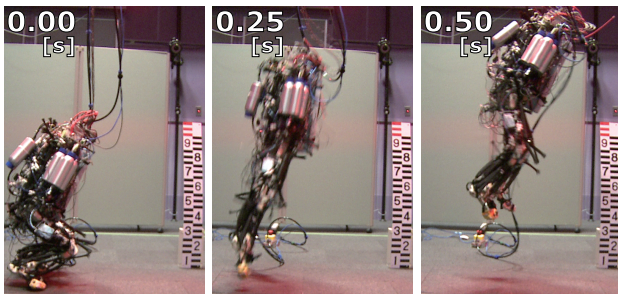


Figure 8: Photographs of the robot jumping.

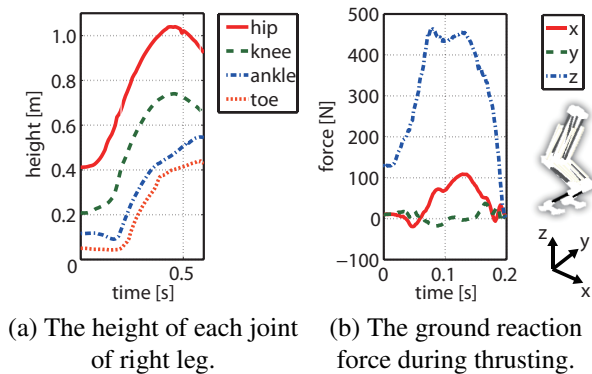


Figure 9: The motion data of the robot.

thrusting time. This result suggests that ADMA is advantageous to the motions from the middle of motion range.

3.3 Development of the real robot

Since the effectiveness of ADMA to motions from various postures was confirmed by above experiments, the robot with ADMA was developed (Fig.1). To confirm its physical ability, jumping experiments from a full squatting position were conducted (Fig.8). The motion of the robot was generated by simultaneous air supply to leg extension muscles (Gmax, RF, VAS, GAS, SOL, FDL) for 0.3 seconds. The movements of the body segments were measured using motion capture system (VICON 624). The ground reaction forces were measured with a force plate (Kistler 9287). The maximum height of its hip position was over 1.0 m and the elevation of the toe position exceeded 0.3 m (Fig.9(a)). The peak of vertical ground reaction force was over 400 N, that is three times of the weight of the robot (Fig.9(b)).

4 Conclusion

In this paper, an actuation mechanism ADMA with biased pivot was proposed to improve physical abilities of robots in motions which need various postures. By analyzing output force characteristics of legs, it was confirmed that the model with ADMA can exert large downward force at extended leg posture. In simulation experiments, it was indicated that ADMA can improve physical abilities of robots in motions from various postures by making the robot model

jump from various squatting positions by improving the performance of motions from slight squatting positions. The robot with ADMA was also developed and it was confirmed that it can jump 1.0 m high at its hip position. In future works, jumping experiments of the real robot with various postures will be conducted to verify the effect of ADMA in the real world.

5 Open questions

The effectiveness of ADMA to keep high output force in various postures was indicated in this work, however, the control methods to fully utilize it are still open questions.

6 Acknowledgements

This work has been supported by MEXT/JSPS KAKENHI Grant Numbers 22240015, 24119002.

References

- [1] K. Hosoda, Y. Sakaguchi, H. Takayama and T. Takuma, "Pneumatic-driven jumping robot with anthropomorphic muscular skeleton structure," *Autonomous Robots*, Vol.28, No.3, pp.307-316, 2010.
- [2] R. Niiyama and Y. Kuniyoshi, "Design principle based on maximum output force profile for a musculoskeletal robot," *Industrial Robot: An International Journal*, Vol.37, No.3, pp.250-255, 2010.
- [3] R. Niiyama, S. Nishikawa and Y. Kuniyoshi, "A biomechanical approach to open-loop bipedal running with a musculoskeletal athlete robot," *Advanced Robotics*, Vol.26, No.3, pp.383-398, 2012.
- [4] Jr. H. F. Schulte, D. F. Adamski and J. R. Pearson, "Characteristics of the braided fluid actuator," Technical Report No.5, The University of Michigan Medical School Department of Physical Medicine and Rehabilitation Orthotics Research Project, 1961.
- [5] M. G. Hoy, F. E. Zajac and M. E. Gordon, "A musculoskeletal model of the human lower extremity: the effect of muscle, tendon, and moment arm on the moment-angle relationship of musculotendon actuators at the hip, knee, and ankle," *Journal of Biomechanics*, Vol.23, No.2, pp.157-169, 1990.
- [6] B. Vanderborght, B. Verrelst, R. V. Ham, M. V. Damme, P. Beyl and D. Lefeber, "Development of a compliance controller to reduce energy consumption for bipedal robots," *Autonomous Robots*, Vol.24, No.4, pp.419-434, 2008.
- [7] B. Vanderborght, N. G. Tsagarakis, R. V. Ham, I. Thorson, D. G. Caldwell, "MACCEPA 2.0: compliant actuator used for energy efficient hopping robot Chobino1D," *Autonomous Robots*, Vol.31, No.1, pp.55-65, 2011.
- [8] F. Kanehiro, H. Hirukawa and S. Kajita, "Openhrp: Open architecture humanoid robotics platform," *The International Journal of Robotics Research*, Vol.23, No.2, pp.155-165, 2004.

Human Locomotor Adjustment to a Perturbation Induced by a Split-Belt Treadmill

Takaaki Oku*, Naomichi Ogihara*

* Department of Mechanical Engineering, Faculty of Science and Technology, Keio University, Yokohama, Japan

ogilab_okutakaaki11@yahoo.co.jp, ogihara@mech.keio.ac.jp

1 Introduction

Humans can keep walking without falling even though unexpected external perturbations are applied. To elucidate the mechanism underlying generation of such adaptive response against external perturbations during bipedal walking, many studies have analyzed responses against external perturbations during human walking [1,2]. However, such adaptive mechanisms are not fully understood.

Adjustment of locomotor rhythm in response to external perturbation is considered as an effective strategy for generation of human walking. In this study, we investigated temporal response of human bipedal walking against external perturbations induced by a split-belt treadmill. The treadmill has two belts, one for each leg, and the speeds of the belts can be controlled independently by a computer to apply perturbations during walking.

2 Method

Four adult male participants were asked to walk on the split-belt treadmill at 4.5 km/h. At this speed, all the participants declared that their walking was comfortable. After 5 minutes of normal gait (without perturbations), external perturbations were applied during walking by sudden decrease or increase in the speed of the right belt approximately once in 20 sec. The perturbations are applied randomly so that the perturbation can be applied at different instants of the gait cycle.

The motion responses were measured using an eight camera motion capture system (Mac 3D system, Motion Analysis, USA). A total of 12 reflexive markers (6 on each side) were placed at: 1) head of the fifth metatarsal, 2) tuberosity of the calcaneus, 3) lateral malleolus of the fibula, 4) lateral epicondyle of the femur, 5) greater trochanter, and 6) acromion as shown in Figure 1. The sagittally-projected joint angles of the hip, knee and ankle and the trunk angle with respect to the inertial coordinate system were calculated from the 3D positions of the markers.

In order to clarify how the locomotor rhythm is adjusted to the external perturbation, we plotted amount of phase-shift in walking cycle against the timing of the perturbation (Phase response curve) [3]. Human walking is a cyclic movement, cycle duration of which is approximately constant. However, when a perturbation

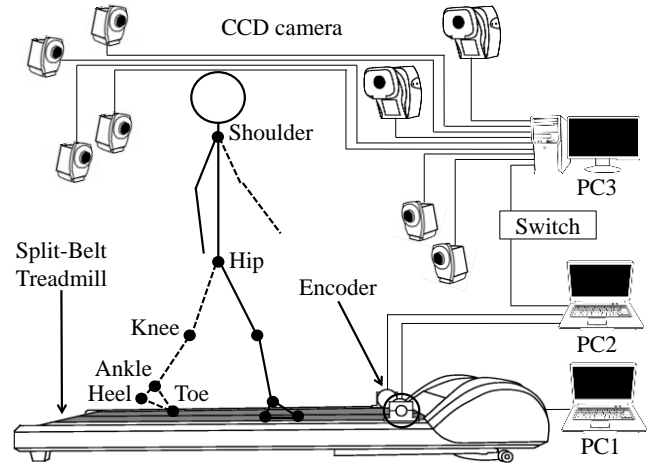


Figure 1 The experimental setup

applied, the cycle duration is either prolonged (delayed) or shortened (advanced). We quantified this change in the walking rhythm by means of phase response curve as follows.

We defined the walking phase (the particular point in the walking cycle) at which a perturbation is applied as $\phi_{stim} = t_{stim} / \bar{T}$, where t_{stim} is the time when the perturbation is applied after right heel contact (the zero phase of the walking cycle is defined by right heel contact) and \bar{T} is the average walking cycle of unperturbed walking. Let Δt be the change in the walking cycle due to the perturbation. The amount of the phase shift in walking cycle can be represented by $\Delta\phi = \Delta t / \bar{T}$. Therefore, the amount of the phase shift of the k th step after the perturbation $\Delta\phi_{(k)}$ is calculated as:

$$\Delta\phi_{(k)} = \left\{ t_{(k)} - \left(t_{(k-1)} + \bar{T} \right) \right\} / \bar{T} \quad (1)$$

In this study, we plotted $\Delta\phi_{(k)}$ against t_{stim} to obtain phase response curves for the both decelerating and accelerating perturbations.

3 Result and Discussion

Figure 2A illustrates stick diagrams of perturbed walking patterns in one participant. Even though perturbations were applied by the split-belt treadmill

during walking, all the participants could keep walking without falling. In the decelerating perturbation, the trunk tended to tilt backward and vice versa in the accelerating perturbation. Because of the perturbations, the kinematic trajectory of human walking was actually deviated from that of steady unperturbed walking (Figure 2B), but it soon converged back to the original trajectory in several steps after the perturbations.

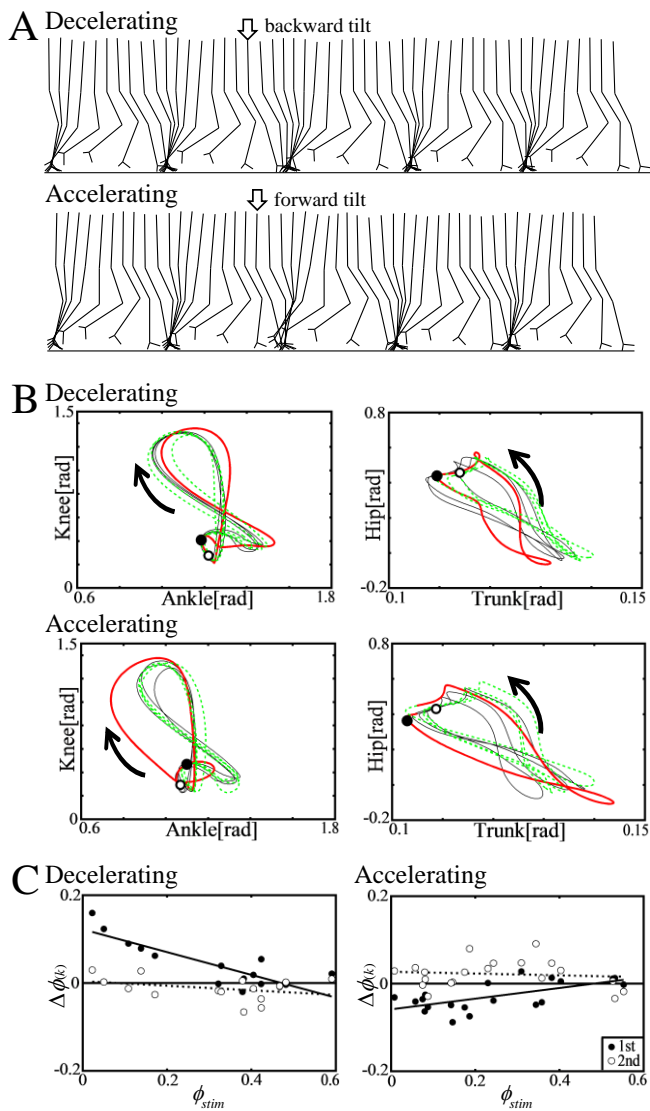


Figure 2 (A) Stick diagrams of perturbed walking. Decelerating and accelerating perturbations. (B) Joint angle trajectories in decelerating and accelerating perturbations. The black, red, and green curves indicate joint angle trajectories of gait cycles before, at which and after perturbation is applied. White dots: foot contact. Black dots: perturbations. (C) Phase response curves. Decelerating and accelerating perturbations.

Figure 2C shows the phase response curves of the same participant for the decelerating and accelerating perturbations. Black and white plots showed the phase shifts of the first ($k=1$) and second ($k=2$) steps after perturbation. As shown in Figure 2C, the amount of phase shift was always positive for the decelerating perturbation during human walking, while that of the accelerating perturbation was always negative, indicating that walking cycle was consistently delayed and advanced for the decelerating and accelerating perturbations, respectively.

Furthermore, we found that the amount of phase-shift was phase-dependent, and it was large if the perturbation was applied in the early stance phase, but it tended to decrease as the timing of the perturbation was delayed. Linear regression analyses revealed there were statistically-significant negative and positive correlations between the amount of phase shift and the timing of the perturbation for both decelerating and accelerating perturbations, respectively, in the three of four participants.

It is difficult to distinguish if such phase-dependent modification of the walking cycle (rhythm) emerges due to active control of the neuronal rhythm generated by the Central Pattern Generator (CPG) or passive consequence of the external forces applied to the body by perturbation. However, the neuronal rhythm (CPG) and the rhythmic movement of the body must somehow be entrained in order to keep walking after perturbation is applied. We therefore hypothesize that active adjustment of the walking rhythm (or phase reset) in a phase-dependent manner plays an important role in generation of human walking adaptive to unknown external perturbations.

4 Open questions

During our poster presentation, we would like to discuss how we are able to experimentally extract kinematic and kinetic strategies underlying the phase-dependent modification of the walking rhythm.

References

- [1] Heiden, T.L., Sanderson, D.J., Inglis, J.T. and Siegmund, G.P., Adaptations to normal human gait on potentially slippery surfaces: The effects of awareness and prior slip experience, *Gait & Posture*, Vol.24, No.2 (2006), pp.237-246.
- [2] Shinya, M., Fujii, S. and Oda, S., Corrective postural responses evoked by completely unexpected loss of ground support during human walking, *Gait & Posture*, Vol.29, No.3, (2009), pp.483-487.
- [3] Yamasaki, T., Nomura, T. and Sato, S., Possible functional roles of phase resetting during walking, *Biological Cybernetics*, Vol.88, No.6, (2003), pp.468-496.

Qualification of dielectric elastomer actuators as artificial muscles for highly dynamical N-DOF robot kinematics

Sebastian Reitelshöfer*, Maximilian Landgraf*, Jörg Franke* and Sigrid Leyendecker**

*FAPS, Friedrich-Alexander-University Erlangen-Nuremberg, Germany
{reitelshoef, landgraf, franke}@faps.uni-erlangen.de

**LTD, Friedrich-Alexander-University Erlangen-Nuremberg, Germany
sigrid.leyendecker@ltd.uni-erlangen.de

1 Introduction

For more than a decade, dielectric elastomer actuators (DEA) have been the subject of intense research in material science. The potential capability of those actuators is emphasized by the very meaning of the words, “artificial muscles”. Biological archetypes, like skeletal muscles of mammals, are exceeded pertaining to energy density and efficiency [1, 2]. In addition the advantages of natural muscle tissue compared to classic electro mechanic actuators are inherent characteristics of DEA. This makes DEA promising actuators for the development of a new generation of robotic solutions with a broad spectrum of possible applications, which may vary from intrinsically safe service robots to highly dynamical energy-autonomous mobile kinematics or bionic prosthetics. Hereinafter a new research project to facilitate the transition from fundamental research to the qualification of DEA as regular control elements in complex and compliant robot kinematics is described. To carry out this transition, four major research tasks are identified to actualize the adaptability of DEA within basic methodologies of robotics. The research is embedded within the framework of the Bavarian biomimetic initiative “bionicum-forschung”.

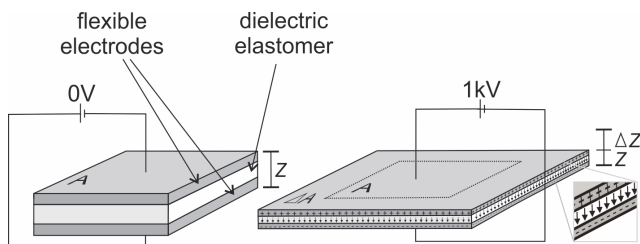


Figure1 Functional principle of a dielectric elastomer actuator (DEA)

2 Four key research tasks

As the functional principle of a DEA, like presented in figure1, can be outlined by the deformation of a charged flexible plate capacitor with an incompressible elastomer forming the dielectric medium, one option for the desired reduction of driving-voltages below 1 kilovolt is the shrinking in thickness of the dielectric medium to values below $100\mu\text{m}$ [3]. Consequently the automated production of multilayer DEAs has to be developed further to create

actuators capable of driving kinematic systems on a macroscopic scale by direct contraction. Because of its pertinency to create homogeneous layers with a broad variety of materials [4] within the presented project the Aerosol Jet Printing process is investigated to build up complex structured stack actuators (see figure2) based on silicone-elastomers with a layer thickness below $20\mu\text{m}$. Besides the dielectric structures, in order to improve the mechanical characteristics of DEA, the electrode layers are also built up of printed elastomers, compounded with one to two weight percent carbon-nano-tubes.

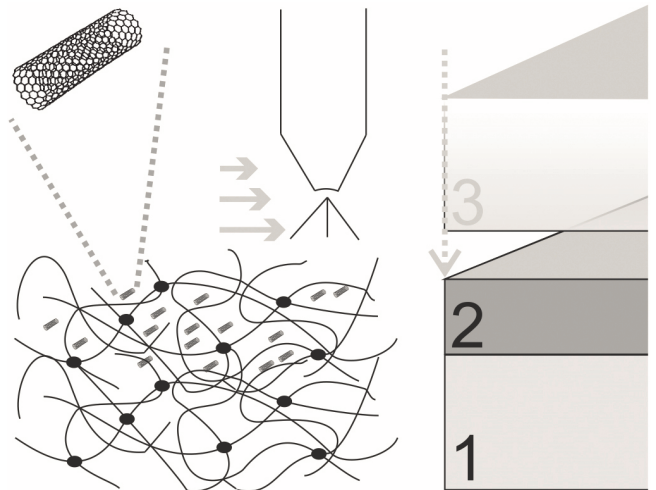


Figure2 Creation of a stacked DEA by Aerosol Jet Printing

Another key aspect of the research is the development of lightweight power electronics for mobile DEA-based robots. To improve the overall specific power of a complex kinematic system only one central high-voltage source shall drive a large number of actuators, while their individual contraction is controlled with a principle based on the pulse width modulation (PWM). Using PWM permits the substitution of DC-DC converters for each actuator by single lightweight semiconductor elements like optocouplers [5] or insulated gate bipolar transistors. The usage of PWM may also allow sensory analysis of active DEA by using the known PWM signal as a reference for measuring the current capacity of an actuator.

With the reaction of DEA to applied voltages depending on the actual state of deformation of the actuator, new mathematical models describing DEA are

developed. In this third main research task, the electro-elastostatic description [6, 7] is the starting basis for an extension to the dynamic description. New tools based on structure preserving methods are developed to efficiently determine solutions for DEA models by numerical simulation. This allows forward dynamics, the optimal control of robot kinematics, and may lead to the development of models suitable for the real-time control of single DEA.

Considering the expected run-time complexity of mathematical models for DEA, a new set of controlling hardware is needed, as normal workstations are not suitable for application in mobile robots. Therefore the development of a combined system of micro-controllers and FPGAs is the fourth and final focus within the presented project to control DEA in real-time in an energy efficient way.

3 Future objectives

The described five-year project aims at the development of an energy self-sufficient and mobile robot platform inspired by a capuchin monkey to demonstrate the capabilities of DEA based kinematics regarding dynamic environment interactions, that extend the actual state of the art in robotics.

4 Open questions

Q1: How to produce stacked Actuators with thousands of layers? Q2: Can DEA be controlled by PWM? Q3: Can DEA be controlled online? Q4: Can a two legged robot be capable of highly dynamical movements like jumping?

References

- [1] Y. Bar-Cohen, Electroactive Polymers as Artificial Muscles - Capabilities, Potentials and Challenges, in HANDBOOK ON BIOMIMETICS, Yoshihito Osada, Ed, Tokyo: NTS Inc, pp. Section 11, in Chapter 8, "Motion" paper #134, 2000.
- [2] R. Shankar, T. K. Ghosh, and R. J. Spontak, Dielectric elastomers as next-generation polymeric actuators, *Soft Matter*, vol. 3, no. 9, p. 1116, 2007.
- [3] F. Carpi, S. Bauer, and D. d. Rossi, Stretching Dielectric Elastomer Performance, *Science*, vol. 330, no. 6012, pp. 1759–1761, 2010.
- [4] C. Goth, S. Putzo, and J. Franke, Aerosol Jet Printing on Rapid Prototyping Materials for Fine Pitch Electronic Applications, in IEEE 61st Electronic Components and Technology Conference (ECTC), 2011: May 31, 2011 - June 3, 2011, Lake Buena Vista, Florida, USA; 2011 proceedings, Piscataway, NJ: IEEE, pp. 1211–1216, 2011.
- [5] T. A. Gisby, E. P. Calius, S. Xie, and I. A. Anderson, An adaptive control method for dielectric

elastomer devices, in Proceedings of SPIE: SPIE, pp. 6927 - 69271C, 2008.

- [6] D. K. Vu and P. Steinmann, Theoretical and numerical aspects of the material and spatial settings in nonlinear electro-elastostatics, in Defect and material mechanics: Proceedings of the International Symposium on Defect and Material Mechanics (ISDMM), held in Aussois, France, March 25-29, 2007, C. Dascalu, G. A. Maugin, and C. Stolz, Eds, Dordrecht: Springer, pp. 109–116, 2008.
- [7] D. K. Vu and P. Steinmann, Material and Spatial Motion Problems in Nonlinear Electro- and Magneto-elastostatics, *Mathematics and Mechanics of Solids*, vol. 15, no. 2, pp. 239–257, 2010.

Toward a Stable Biomimetic Walking: Exploring Muscle Roles on a Feline Robot

Andre Rosendo, Shogo Nakatsu, Kenichi Narioka and Koh Hosoda
Osaka University, Osaka, Japan
andre.rosendo @ ist.osaka- u.ac.jp

1 Motivation

Feline locomotion combines great acrobatic proficiency, unparalleled balance and higher accelerations than other animals. To date, many biologists have tried to decipher the mystery behind feline locomotion, with special contributions from Engberg and Lundberg [1], and Goslow [2], using animal observation to draw conclusions on their locomotion. Although greatly contributing to better understand animal locomotion, its innerworkings are still not well explained.

Understanding animal locomotion and, possibly, applying this knowledge to reproduce self-stability in robots have been the objective of many biomimetic researchers. Differently from biologists, biomimeticists try to recreate biological systems and draw conclusions based on experiments performed with this new artificial system. Among reasons for this approach we could mention the controllability of the artificial animal, the capacity to isolate or freeze parameters (*e.g.* redundant muscles) or even replace parts for different experimental settings (*e.g.* different limb lengths).

Considering a highly complex biological leg, such as cats hindlimbs with more than 30 muscles, recreating such morphology would be very difficult. Combining so many compliant muscles and tuning such redundant structure would be extremely burdensome, requiring biomimeticists to simplify the structure to a level where a gait may be produced while still using a biologically valid morphology. This creates the concept of degree of biomimeticity: how close and truthfully robots may resemble animals? A robot with a higher degree of biomimeticity may resemble real animals in more aspects than lower ones.

Motivated by a better understanding on how felines excel when compared to other animals, we developed a quadruped robot capable of stably walking through a simple leg unloading rule. In the actual development phase this robot possess highly compliant hindlimbs, with 8 muscles each, attached to a sliding strut, simulating cat stepping at a muscular level and thus being the most faithful representation of biological cats in real environments to date. In Fig. 1 we show a picture of our experimental setting.



Figure 1: Picture of experimental setting with Pneupard's hindlimbs attached to a sliding strut.

2 State of the Art

Many quadruped robots have been developed in the last few years (*e.g.*, [3] [4]) with different views regarding degrees of biomimeticity. Works such as [5] allows the study of a cheetah by simply reproducing movements with electric motors, having a low degree of biomimeticity. Works from [6] and [7] adopted monoarticular pneumatic muscles as actuation means, while [8] adopted exclusively biarticular muscles for this purpose.

The most biologically faithful works hitherto would be Pigorass [9] and Ekeberg's cat [10]. These works combine mono and biarticular muscles in a skeletal structure, allowing the study of individual muscles during locomotion. However, Pigorass adopts only ten active muscles for its entire body, which has simplified forelimbs to reduce the total degree of freedom, not resembling feline walking. Ekeberg, on the other hand, proved that a muscular structure, with bi and monoarticular muscles, is capable of producing a very adaptive behavior, performing well even against disturbances in a groundbreaking computer simulation environment. The unloading rule, proposed on the same work, associates the end of stance phase to the reduction of the reaction force on the soleus muscle.

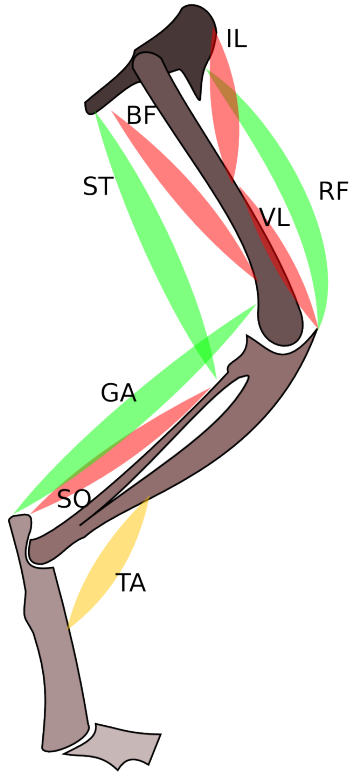


Figure 2: Muscular structure on hindlimb. Monoarticular, biarticular and passive muscles are depicted in red, green and yellow, respectively.

It is a biomimetic belief that to successfully connect the knowledge obtained in biological experiments to robots, reproducing their behavior, a platform which replicates the animal is needed. Hence, building quadruped robots to replicate cats and dogs will help us understand locomotion.

3 Approach

We tackle the problem with a deeper biomimetic approach. Differently from usual quadruped robots, we developed a pneumatic quadruped robot (named Pneupard) with air muscles as actuators. Such muscular morphology was chosen considering muscular importance for locomotion.

The hindlimb is composed of 8 muscles, while the forelimb, still under construction, only possess 7. On the hindlimb 4 muscles are monoarticulars: biceps femoris (hip extension), iliopsoas (hip flexion), vastus lateralis (knee extension) and soleus (ankle extension), while 3 are biarticular muscles: semitendinosus (hip extension and knee flexion), rectus femoris (hip flexion and knee extension) and gastrocnemius (knee flexion and ankle extension). One last muscle provides abduction of the leg (similarly to gracilis or caudofemoralis), being opposed by a passive adductor spring. The hindlimb structure is depicted in Fig. 2.

The artificial muscles used on Pneupard are composed of

Table 1: Pneupard's key characteristics

Property	Value
Hindlimb length	810 mm
Body width	300 mm
No of degrees of freedom	8
No of active muscles	16
Hindlimb weight	600 grams
Total weight (without strut)	3.0 kg

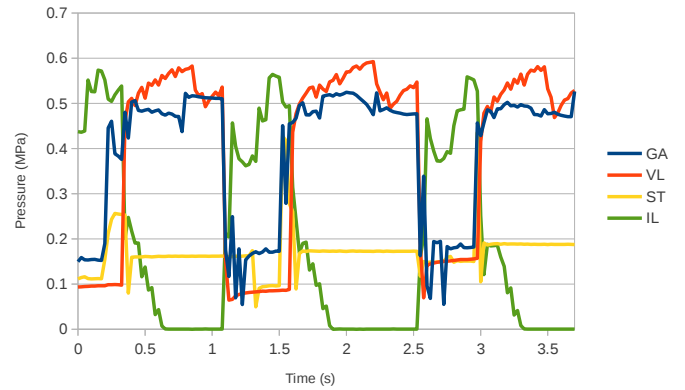


Figure 3: Muscular activation pressure during walking.

a rubber tube surrounded by a nylon braided sheath, which controls the expansion of the tube when air is supplied. The contraction produced by such muscle is enough to actuate the joints and are strong enough to support the robot's lightweight body. The overall specifications for the robot can be found in Table 1.

Similarly to Ekeberg's approach, we produce a stable walking gait on a robotic hindlimb attached to a sliding strut, simulating the forelimbs. Adopting a muscular pattern based on feline EMG walking data [1] we controlled seven muscles responsible for flexion/extension of the hindlimb. Movements related to abduction/adduction were constrained by the 8th muscle with constant pressure, allowing some compliance for lateral movements.

In Fig. 3 we can see the behavior of four muscles during walking on a treadmill. While gastrocnemius (GA) and vastus lateralis (VL) act as extensors, working mainly during stance phase, iliopsoas (IL) flexes the limb, acting during swing phase. Semitendinosus (ST), as explained in biological observations, has important roles during touch down and lift off phases.

Applying EMG data while using a hindlimb unloading rule, as proposed by a simulation in [10], generates a stable walking. A FSR sensor was installed on each limb, registering the reaction from the floor through a voltage divider con-

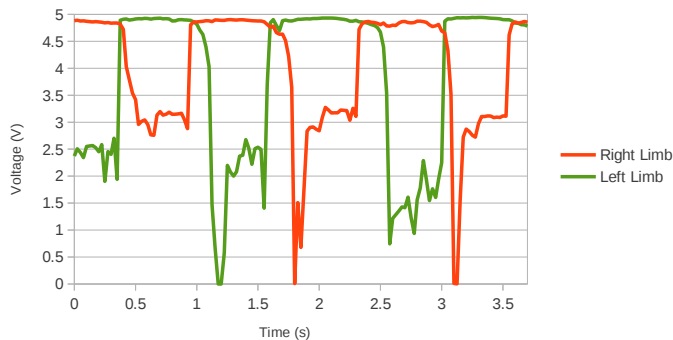


Figure 4: Ground reaction force data from PneuPard on a treadmill. The right and left legs alternate their movements during walking.

nected to the analog input from our microcontroller, which sampled at 40Hz. Due to the curved shape at which the sensor was submitted, the signal from the FSR sensor could not be directly converted into force (N). Thus, the unloading rule was implemented using voltage values as thresholds. In Fig. 4 we show ground reaction force data from the proposed robot walking on a treadmill.

4 Discussion

Analyzing data from Fig. 4, obtained from the muscular activation pattern from biological observation [1] [2] combined with the unloading rule [10], we can see that the walking produced is stable, with right and left legs evenly alternating duty factor during gait. During swing phase, characterized by the lack of contact between the leg and the ground, we can notice that the FSR sensor value decreases (being below the 3.5V).

The stability of the gait was high enough to overcome construction differences between muscles from right and left limb, which rendered the robot slightly assymmetric. Although not shown in the previous section, the adaptivity of the robot was enough to overcome small blocks added during the course of the treadmill walking.

In [10] Ekeberg produced a stable stepping of a similar structure within a simulation environment. Although the activation pattern used by the same could not be fully represented in this work due to a different behavior from air muscles, we aimed to reproduce the same experiment in a real environment. The unloading rule alone was capable of generating a stable alternating stepping, being a strong state attractor. However, differently from Ekeberg, we also noticed that the unloading rule is also a state attractor for a bounding gait, though not as strong as the first state.

We approached legged robots with a deep biomimetic view, using it as a way to replicate and better understand animals. A broader knowledge about animal locomotion will allow us, as a long range objective, to create better robots.

5 Open questions

To which extent using muscles on a robot will help us on self-stability? What is the great benefit of muscles? Comparing pneumatic artificial muscles with elastic series actuators, what are the merits of using one over the other? Is the presence of legs enough to label a robot biomimetic? To which extent is a robot biomimetic?

In the future will robots have muscles? How is the controllability affected and at which point is it needed?

References

- [1] I. Engberg and A. Lundberg, "An electromyographic analysis of muscular activity in the hindlimb of the cat during unrestrained locomotion", *Acta Physiol. Scand.*, Vol. 75, 1969, pp. 614-630.
- [2] G.E. Goslow Jr., R.M. Reinking and D.G. Stuart, "The cat step cycle: hind limb joint angles and muscle lengths during unrestrained locomotion", *J. Morphol.*, Vol. 141, 1973, pp. 1-42.
- [3] N.G. Tsagarakis, B. Vanderborgh, Y. Yousheng and D.G. Caldwell, "HyQ - Hydraulically actuated quadruped robot: Hopping leg prototype", in *Proc. Int. Conf. Biomed. Robot. and Biomechanics*, 2008, pp. 593-599.
- [4] Y. Fukuoka, H. Kimura and A.H. Cohen, "Adaptive dynamic walking of a quadruped robot on irregular terrain based on biological concepts", *J. Robot. Res.*, Vol. 22, 2003, pp. 187-202.
- [5] A. Sproewitz, A. J.Ijspeert et al., "Oncilla robot : a light-weight bio-inspired quadruped robot for fast locomotion in rough terrain", in *Proc. Fifth Intl. Symp. Adaptive Motion on Animals and Machines*, Osaka, Japan, 2011.
- [6] K. Tsujita, T. Kobayashi, T. Inoura and T. Masuda, "Gait transition by tuning muscle tones using pneumatic actuators in quadruped locomotion", in *Proc. Int. Conf. on Intelligent Robots and Systems*, 2008, pp. 2453-2458.
- [7] K. Aschenbeck, N. Kern, R. Bachmann and R. Quinn, "Design of a quadruped robot driven by air muscles" in *Proc. Int. Conf. Biomed. Robot. and Biomechanics*, 2006, pp. 875-880.
- [8] M. Lewisy, M. Buntingy, B. Salemi and H. Hoffmann, "Toward ultra high speed locomotors: design and test of a cheetah robot hind limb", in *Proc. Int. Conf. on Robotics and Automation*, 2011, pp. 1990-1996.
- [9] Y. Yamada, S. Nishikawa, Y. Kuniyoshi et al., "Neural-body coupling for emergent locomotion: a musculoskeletal quadruped robot with spinobulbar model", in *Proc. Int. Conf. on Intelligent Robots and Systems*, 2011, pp. 1499-1506.
- [10] O. Ekeberg and K. Pearson, "Computer simulation of stepping in the hind legs of the cat: an examination of mechanisms regulating the stance-to-swing transition", *J. Neurophysiol.*, Vol. 94, 2005, pp. 4256-4268.

Inverse dynamic analysis of precision grip in the Japanese macaque based on an anatomical musculoskeletal model

Tsuyoshi Saito*, Naomichi Ogihara*, Tomohiko Takei** and Kazuhiko Seki**

* Keio Univ. Dept. of Mechanical Engineering, Kanagawa, Japan
ogilab_saito11@yahoo.co.jp, ogihara@mech.keio.ac.jp

** National Institute of Neuroscience. Dept. of Neurophysiology, Tokyo, Japan
{takei, seki}@ncnp.go.jp

1 Introduction

Humans can stably hold and skillfully manipulate an object by the thumb and other fingers by coordinated control of the complex hand musculoskeletal system. In order to understand the neural control mechanisms of human precision grip capabilities, precision grip in macaques has recently been extensively investigated using electrophysiology [1,2]. However, precision grip is a mechanical phenomenon generated by dynamic interactions among the nervous system, musculoskeletal system, and a grasped object. To elucidate how the nervous system controls a large number of muscle activations in a coordinated manner to generate appropriate external forces for stably holding and skillfully manipulating an object, biomechanical analyses of macaque grasping based on an anatomically plausible mathematical model appear to be essential. In this study, we therefore constructed an anatomically based musculoskeletal model of the Japanese macaque hand and attempted to biomechanically analyze macaque's precision grip based on inverse dynamic calculation.

2 Method

We constructed a 3D musculoskeletal model of the Japanese macaque hand from computed tomography scan. The hand skeleton was described as a chain of 20 links connected by revolute joints, joint centers and rotation axes of which were determined based on quadric surface approximation of joint surfaces. A total of 23 muscles were modeled as line segments connecting origins and insertions, based on the results of cadaver dissections. The maximum force generated by the muscle was determined based on the measured physiological cross-sectional area of the muscle. This anatomically accurate model of the Japanese macaque was then loaded into musculoskeletal simulation software Anybody Modeling System (AnyBody Technology, Denmark) for inverse dynamic analysis of the model. The hand movement during a precision grip task in one adult Japanese macaque was filmed using five video cameras (iVIS HF S21, Canon). The macaque has been trained to grip, hold and release pinch levers with its thumb and index finger according to movement of cursors displayed

on a monitor and the electromyographic (EMG) of hand muscles during the task were recorded simultaneously. From the motion images, well-recorded precision grip sequences were manually digitized frame-by-frame, and 3D movements of the joint positions were calculated. The hand musculoskeletal model was then matched to the recorded motion data by minimizing the sum of distances between each motion-captured joint position and the corresponding joint on the model. The reaction forces applied to the fingertips were measured by the strain gauges attached to the pinch levers and were input to the model for inverse dynamic calculation. The sum of the cubes of muscle stress was used as an objective function to solve for the muscle recruitment problem [3].

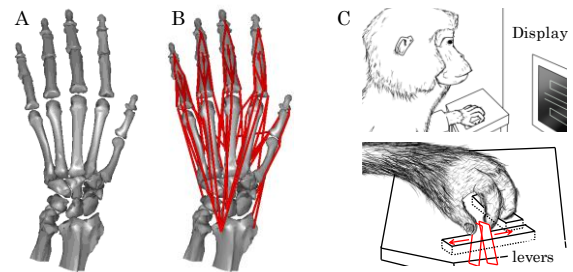


Figure1 A,B: Skeltal(A) and musculo-skeltal(B) model of the Japanese macaque hand (dorsal view), C: The monkey controlled cursors on a screen by pinching two levers with a thumb and index finger

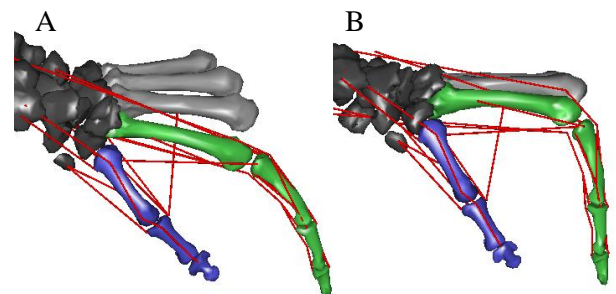


Figure2 Reconstructed skeltal kinematics A: Levers are released, B: Levers are pinched

3 Result and Discussion

Figure 2 shows the reconstructed musculoskeletal kinematics of Japanese macaque hand during the precision grip task, indicating that the hand musculoskeletal movements were successfully reconstructed using the model-matching method. It is generally regarded that the first dorsal interossei (1DIO), flexor digitorum superficialis (FDS) and abductor pollicis longus (ABPL) are important for generating a precision grip task. Our inverse dynamic analysis revealed that the 1DIO and FDS were activated when the levers were pinched and the ABPL was in active when the levers were released. The estimated muscular force patters are generally in accordance with EMG data, demonstrating the validity and efficacy of the constructed model analysis scheme for comprehensive analysis of precision grip control in primates.

4 Open questions

What we would like to understand is how temporal activities of hand muscles are generated in a coordinated manner during the highly complex precision grip task. It is recently suggested that the muscle synergies (co-activation of hand muscles) facilitate the control of the complex and redundant musculoskeletal system and spinal interneurons are the key to understand the muscle synergies [4]. We would like to discuss how we can tackle this problem using our model.

References

- [1] Takei, T. and Seki, K., Spinal interneurons facilitate coactivation of hand muscles during a precision grip, *Journal of Neuroscience*, (2010), pp.17041-17050.
- [2] Alstermark, B., Pettersson, L.G., Nishimura, Y., Yoshino-Saito, K., Tsuboi, F., Takahashi, M. and Isa, T., Motor command for precision grip in the macaque monkey can be mediated by spinal interneurons, *Journal of Neurophysiol*, Vol.106, (2011), pp.122-126.
- [3] Crowninshield, R.D. and Brand, R.A., A physiologically based criterion of muscle force prediction in locomotion, *Journal of Biomechanics*, Vol.14, No.11 (1981), pp.793-801.
- [4] Takei, T. and Seki, K., Control of primate grasping movement by spinal cord, *Proceedings of the 2nd Symposium on Mobiligence*, (2007), pp.153-156.

Control of Planar Bounding Quadruped with Passive Flexible Spine

Brian Satzinger and Katie Byl
 Robotics Lab, University of California, Santa Barbara, USA
 {bsatzinger, katiebyl}@gmail.com

1 Motivation

The addition of a flexible spine to quadrupedal robots is motivated by a desire to improve energy efficiency, robustness, and range of motion over comparable rigid spine quadrupedal designs.

2 State of the Art

In 1996, Leeser built a planar quadruped robot with hydraulic hip, spine, leg actuators, and passive air springs in the legs [5]. Leeser demonstrated his control strategies on a treadmill with the robot mounted on a planarizing boom. Another robot, Canid [4], has electrically actuated hip joints, as well as an actuated spine with an elastic element. The design of controllers for Canid is an open research problem, and serves as a motivation for this work.

Simulation work with actuated-spine models includes that of Haueisen, who considered the effect of an actuated spine on a planar quadrupedal model consisting of 6 point masses connected by rigid links and actuated rotational knee, hip, and spine joints [3]. Culha considered a similar model, but with passive linear spring-damper legs [2]. In both cases, the spine is actuated and does not include a passive elastic element.

Work by Poulakakis et. al. has studied the stability of passive dynamics of a bounding saggital plane quadrupedal model with a rigid spine [6]. More recently, Poulakakis and Cao have studied the passive dynamics of a similar model with an unactuated flexible spine, and discovered families of unstable fixed points [1].

3 Approach

We consider a model consisting of two point masses located at the hip joints, a passive torsional spine spring, and passive linear spring-damper legs (Figure 1). There are actuators located at each hip. However, due to the massless legs, the hip actuators are only effective one at a time during the stance phase of the connected leg (our model excludes double-stance configurations). The control inputs, therefore, comprise the leg angles (set at the moment the leg leaves the ground) as well as a torque signal τ_{hip} defined during stance. Controllers to compute these signals must be designed in order to stabilize the system.

In order to study the body pitch dynamics analytically

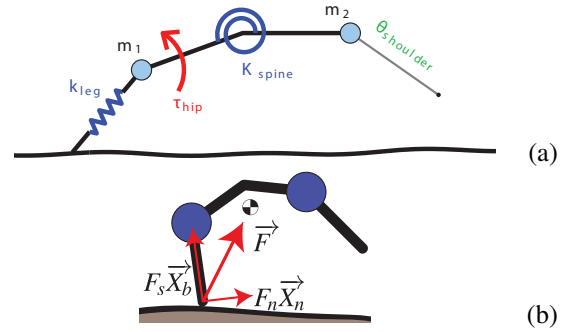


Figure 1: (a) Schematic model of the planar quadruped model showing the point masses, springs, and hip actuator. (b) Simplified view showing ground reaction force vector, orthogonal force components, and center of mass

and derive a control law to stabilize the body pitch during stance, a simplified model (Figure 2) is derived as follows. The legs are removed from the higher order model, the masses are assumed to be equal, and only two degrees of freedom (r and θ) are allowed. The torsional spring (with spring rate K_r and neutral angle θ_0) at the center of the spine is unchanged. The distance from each point mass to the spine joint is L . A torque τ can be exerted about the center of mass, but no other external forces are allowed.

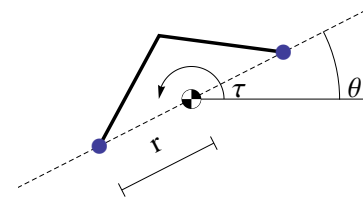


Figure 2: Simplified system used to derive feedback law

Using θ and r as generalized coordinates, the equations of motion for the simplified model can be derived as

$$0 = \frac{K_{spine} (\cos^{-1}[\frac{r}{L}] - \theta_{ref})}{L\sqrt{1-\frac{r^2}{L^2}}} + 2mr\dot{\theta}^2 - 2m\ddot{r} \quad (1)$$

$$\tau = 2mr(2\dot{r}\dot{\theta} + r\ddot{\theta}).$$

Then, by algebraic manipulation, the desired torque about the center of mass during stance $\tau_{fb}(t)$ can be defined in order for the error dynamics of θ to match that of a second

order spring-mass-damper system with natural frequency ω and damping ratio ξ . We choose $\xi = 1$ to give a critically damped response. ω can be tuned based on the tradeoff between response speed and peak actuator torques.

$$\tau_{fb} = -2mr^2 \left[\omega^2(\theta - \theta_{ref}) + 2(\xi - \frac{\dot{r}}{r})(\dot{\theta} - \dot{\theta}_{ref}) \right] \quad (2)$$

The body pitch reference signal θ_{ref} was chosen to be a piecewise quadratic-linear function with constant acceleration until the desired angular velocity is achieved. The magnitude of the acceleration and the final velocity are computed for each step based on the duration and final pitch angle and angular velocity of the previous step.

The desired body torque about the center of mass can be achieved by applying an appropriate actuator torque during stance. Using the notation in Figure 1(b), consider the point of contact to be the origin, and \vec{X}_b to be a vector pointing to the location of the back hip mass. Also, we define \vec{X}_{com} to point to the center of mass, and \vec{X}_n to be a unit vector normal to \vec{X}_b . The spring-damper in the stance leg will produce a force F_s directed along \vec{X}_b . F_n is a force along \vec{X}_n that can be generated by the hip actuator torque τ_{hip} . Summing $F_s\vec{X}_b$ and $F_n\vec{X}_n$ gives the total ground reaction force \vec{F} . If \vec{F} is directed through the center of mass, there is no net torque. Otherwise there is a torque on the body that can be used to control θ during stance, as shown previously. Equation 3 gives an expression for the actuator torque τ_{hip} to achieve the desired torque about the center of mass τ_{fb} .

$$\tau_{hip} = \frac{\tau_{fb} \|\vec{X}_b\| - F_s (\vec{X}_b \times \vec{X}_{com})_3}{(\vec{X}_n \times \vec{X}_{com})_3} \quad (3)$$

Using this control technique, we observed gaits which appear stable over several steps, but where the horizontal velocity of the center of mass slowly varies. Introducing an additional control law to set the rear leg angle at touchdown as a linear function of forward speed stabilizes the gait.

Gait stability was investigated by first identifying fixed points, and then computing eigenvalues of the Jacobian near the fixed point. Fixed points were identified by running the simulation for several steps to bring it near the fixed point. Then, starting from that initial guess, we use a numerical optimizer to solve the non-linear least squares problem:

$$X_{fp} = \operatorname{argmin}_{X_{td}[k]} \|X_{td}[k] - X_{td}[k+1]\|_2. \quad (4)$$

Once a fixed point is identified, the Jacobian is constructed by varying each state individually by a small ϵ and simulating to the next touchdown state. If the eigenvalues of the Jacobian have magnitude less than 1, then small perturbations around the equilibrium state will die out, and stability is demonstrated.

Our investigation centers around studying the parameter values that give rise to stable fixed points with small eigenvalues (so that equilibrium is restored quickly after perturbation). In particular, the tradeoffs between body speed, eigenvalue magnitude, and cost of transport are of great interest.

4 Discussion Outline

It is relatively easy to vary controller parameters and generate a stable gait with a characteristic cost of transport, forward speed, and largest eigenvalue. Consider these three parameters to form a three-dimensional performance space, with achievable designs occupying a subset of this space. How can the bounds of the achievable design region be determined in a systematic way? Is the magnitude of the largest eigenvalue sufficient as a predictor of rough terrain performance?

5 Format & Travel Grant

Preferred Format:	Talk
Brian Satzinger Travel Grant Application:	Yes
Katie Byl Travel Grant Application:	No

References

- [1] Q. Cao and I. Poulakakis. Passive quadrupedal bounding with a segmented flexible torso. In *IROS*, 2012.
- [2] U. Culha. An actuated flexible spinal mechanism for a bounding quadrupedal robot. Master's thesis, Bilkent University, 2012.
- [3] B. Haueisen. *Investigation of an Articulated Spine in a Quadruped Robotic System*. PhD thesis, The University of Michigan, 2011.
- [4] G. C. Haynes, J. Pusey, R. Knopf, A. M. Johnson, and D. E. Koditschek. Laboratory on legs: an architecture for adjustable morphology with legged robots. In Robert E. Karlsten, Douglas W. Gage, Charles M. Shoemaker, and Grant R. Gerhart, editors, *Unmanned Systems Technology XIV*, volume 8387, page 83870W. SPIE, 2012.
- [5] K. Leeser. Locomotion experiments on a planar quadruped robot with articulated spine. Master's thesis, MIT, 1996.
- [6] I. Poulakakis, E. Papadopoulos, and M. Buehler. On the stability of the passive dynamics of quadrupedal running with a bounding gait. *The International Journal of Robotics Research*, 25(7):669–687, 2006.

Design and Test of Torque-Angle Relationship Control System

Kazuya Shida*, Satoshi Nishikawa** and Yasuo Kuniyoshi*

* Intelligent Systems and Informatics Lab., The University of Tokyo, Japan

** Research fellow of the Japan Society for the Promotion of Science

{shida, nisikawa, kuniyosh}@isi.imi.i.u-tokyo.ac.jp

1 Introduction

A dynamic movement is a very challenging task. To date, robots have been able to achieve dynamic movements such as running and hopping[1] which are cyclical movements. In such moments, robots can try to close to the target value in many times. On the other hand, there are some research of non-cyclic motion, so-called “one-shot motions”. This research aims to realize jump which is one-shot dynamic motion in robots. Specifically, we control the direction in which a musculoskeletal robot jumps.

Pneumatic artificial muscles (PAMs) are often used to dynamic movements in robots. PAMs generate force non-linearly with respect to muscle length. In the neighbor posture which robots generate high torque, small sensing errors of robot’s posture create large errors of torque. In addition, the robots can jump in limited posture, because the robots can generate high torque in limited posture. For this reason, it is not well-suited method that to physically tip robot’s posture in the desired direction, which is the most intuitive method for controlling jump direction in robots. Therefore, it is necessary to control jump direction without changing initial posture. This problem is able to be solved by changing the torque-angle relationship.

There are some researches of pneumatic-electric hybrid actuators to control high torque[2, 3]. Both studies combined in parallel the two types of actuators to compensate for each other’s weaknesses, low output of electric motors and time-delay of pneumatic actuators. And however they have no mention of the posture problem, both studies control high torque well. So, we propose a new pneumatic-electric hybrid system for changing the torque-angle relationship.

2 Materials and Methods

Regarding the hindlimb model, we designed it to reflect the gluteus maximus (GMAX), rectus femoris (RF), and gastrocnemius (GAS) as shown in Figure 1 (a). These muscles are antigravity muscles for jump. We calculated the length of PAMs which is depend on the joint angle θ and motor angle ϕ .

McKibben-type PAMs generate tension F as a function of muscle length in the following way[4].

$$F(L) = p \left(A \frac{L^2}{L_{max}^2} - B \right), \quad (1)$$

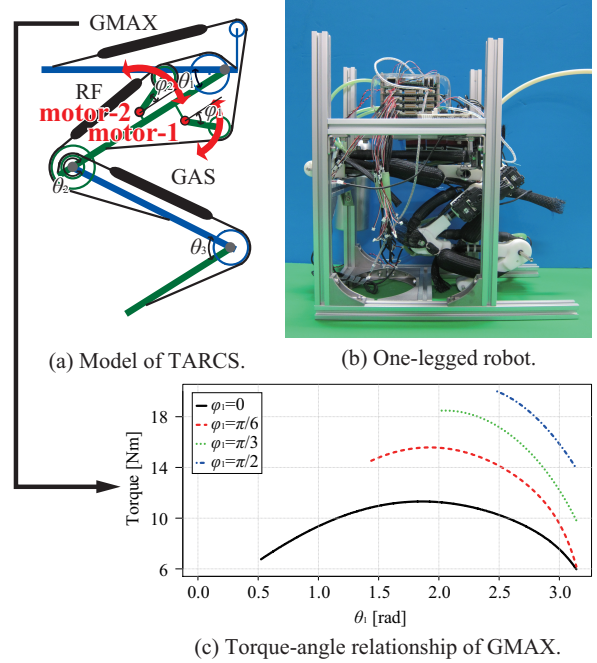


Figure 1: TARCS (hindlimb) and torque-angle relationship of GMAX.

where A and B are the specific contact number for each muscle, p is inner pressure, θ is joint angle, and L is length, L_{max} is maximum length of each muscle. And, the torque T which each muscle generates is calculated as a following function.

$$T = -F(L) \frac{\partial L}{\partial \theta} \quad (2)$$

Next, we determined the torque-angle relationship. Muscles are attached via pulleys, and Electric motors move pulleys. Control of motor angles create the changes of muscle length L , and the moment arm of muscle $\partial L / \partial \theta$, and finally torque T . We can design the relationship between muscle length and angle by changing pulley’s size, pulleys’ position and motor’s position. We call this system torque-angle relationship control system, TARCS. Figure 1 (c) is example of torque-angle relationship for GMAX, which we found to have a dependency on the angle of the motor-1.

3 Robot Experiments

We constructed a single robotic hindlimb to test whether direction specificity can be achieved using the above de-

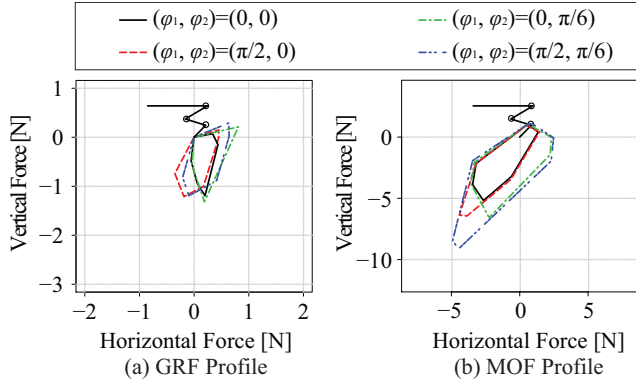


Figure 2: GRF & MOF Profile.

sign (Figure 1). CFRP pipes and ABS resin were used to construct the skeletal structure. With respect to TARCS, a Dynamixel 12A+ servo motor was used to rotate aluminum parts equipped with pulleys.

To ensure that the above system indeed generates torque, we first measured the Ground Reaction Force Profile (GRF Profile) which is the magnitude of force applied by the one-legged robot upon contact with the ground. In the experiment, we fixed the robot's posture and measured its ground reaction force with force plate when applied air pressure was set to 0.0 or 0.2 MPa for each of the three muscles. The magnitude of observed force as well as its directionality (x- and y-components) were plotted. Two different initial motor-1 angle configurations were tested.

Next, the obtained GRF Profile was compared to the theoretically-derived Maximum Output Force Profile (MOF Profile)[5]. The GRF Profile's horizontal force became lower than MOF Profile's. One of the reason is that the toe of one-legged robot slipped on the force plate. However, Both profiles underwent a similar change by a motor. Both profiles are extended to the right by the changing of GMAX's route, and downward to the left by the changing of RF's route(Figure 2).

4 Simulation Experiments

To confirm the hypothesis that controlling motor angle causes changes of jump direction, we constructed a quadruped robot model and simulated its movements with dynamic simulator, OpenHRP3. The size and mass of the quadruped were decided by considering the actual development of the robot with TARCS. In the initial state, the robot is pushed into upright posture by injecting air to the PAMs in the forelimb and GMAX. Then the robot rotates the motors, and thrusts the ground using its hind limb. We measured the highest point of the center of gravity (COG) during the robot's jump, then measured the horizontal jump distance as the distance travelled from the starting point to the highest point (Figure 3). Control of motor-1's angle caused changes in the horizontal jump distance, up to 0.15 m. Control of motor-2's angle also caused changes.

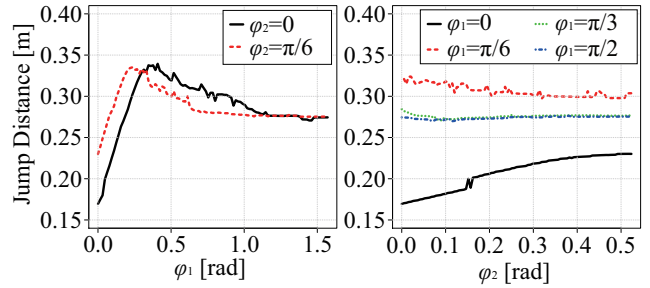


Figure 3: Jump distance of COG.

5 Conclusion

This paper proposed a unique hybrid system between PAM and electric motor to control the direction in which a robot jumps. A one-legged robot was constructed, and we tested whether the observed GRF profile qualitatively matched the theoretically-derived MOF profile. Finally, a simulation was used to verify whether jump direction can be altered by changing the electrical motor rotation angle. In future works we will construct a four-legged robot using the proposed design and attempt to dynamically control its jump direction.

6 Open Questions

In this paper, we showed that the jump direction of the robot is changed depending on the motor angle. However, we have still yet to fully understand how these parameters should be used to control jump direction.

7 Acknowledgment

This work has been supported by MEXT/JSPS KAKENHI Grant Numbers 22240015, 24119002.

References

- [1] M. H. Raibert. *Legged Robots That Balance*. The MIT Press, 1986.
- [2] T. Matsubara et al. An optimal control approach for hybrid actuator system. In *Proc. of Humanoids*, pp. 300–305, 2011.
- [3] M. A. Lewis et al. Toward ultra high speed locomotors: Design and test of a cheetah robot hind limb. In *Proc. of ICRA*, 2011.
- [4] H. F. Schulte et al. Characteristics of the braided fluid actuator. Technical Report No.5, The University of Michigan Medical School Department of Physical Medicine and Rehabilitation Orthotics Research Project, 1961.
- [5] R Niiyama and Y Kuniyoshi. Design principle based on maximum output force profile for a musculoskeletal robot. *Industrial Robot: An International Journal*, Vol. 37, No. 3, pp. 250–255, 2010.

Towards Dynamically Running Quadruped Robots: Performance, Scaling, and Comparison

Alexander Sproewitz*, Alexandre Tuleu*, Michiel D’Haene**,

Rico Möckel*, Jonas Degraeve**, Massimo Vespignani*,

Sebastien Gay*, Mostafa Ajallooeian*, Benjamin Schrauwen**, Auke Jan Ijspeert*

*Biorobotics Laboratory, EPFL, Lausanne, Switzerland, **Reservoir Lab, UGhent, Belgium

email:alexander.sproewitz@epfl.ch

1 Hardware platforms and project ideas

The field of robotic research applying legged machines and robots is growing quickly, but it is still facing a major discrepancy of performance, quality, and complexity, compared to their biological counterparts.

A lack of appropriate off-the-shelf hardware platforms, a lack of open-access to dynamically running legged robot platforms, and missing comparative studies between existing quadruped platforms (mis)leads researchers to re-invent and re-design own quadruped robots, from the scratch. As research of legged locomotion should be the goal, and not research about its tools (the robots *per se*), this can be a frustrating and time consuming process. Research in dynamic legged locomotion would benefit from free and easy access to blueprints, and studies where different robot design choices can be tested and compared rigorously against each other. A future, better-performing platform could be assembled from the best-performing components (actuators, sensors, driver code, controllers) and principles (type of actuation, type of control, sensing, leg design, trunk design, compliant design) of existing systems.

We shortly present two quadruped robot platforms. CheetahCub-robot was developed at BioRob [1], of an older version with lower speed and capabilities [2]. Oncilla-robot was developed at BioRob/EPFL in cooperation with ResLab/UGhent. Both robot platforms use a four-segment, pantograph-based leg design [3], and are roughly similar in dimensions. Of the two platforms, Oncilla-robot is the successor of CheetahCub-robot, with more sensor capabilities (Table 1), improved actuation, but also higher complexity and cost. CheetahCub-robot and Oncilla-robot were designed with multiple purposes; one of them includes research on the pantograph-like leg structure, and its implications for dynamic locomotion.

Oncilla-robot is being developed as the quadruped robot platform of the European AMARSi project, "...aim[ing] at a qualitative jump in robotic motor skills towards biological richness"[4], and is also meant to help comparing and analysing data from Biology and Robotics [5]. The entire Oncilla-robot platform will become open-source soon. This will include blueprints of all mechanical and electrical

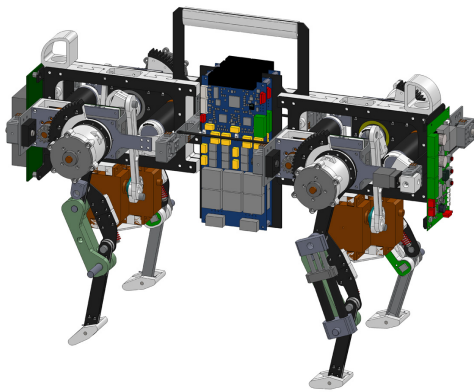
components and assemblies, firmware, communication, and driver programming code.

Due to its similarity in structure, both systems are easy to compare: CheetahCub-robot reached dynamic trot-gaits (up to 1.4ms^{-1} , 6.9 body lengths per second, Froude number[6] $FR=1.3$, cost of transport $COT=6JN^{-1}m^{-1}$) [7]. CheetahCub shows self-stabilizing properties, where open-loop locomotion patterns lead to decreasing pitch and roll angles at increasing robot speed. The robot also performed well at step-down obstacles, again without using sensory feedback. Oncilla-robot is currently undergoing rigorous tests, showing already good trot gait speed ($v=0.55\text{ms}^{-1}$), at lower cost of transport, around $COT=3JN^{-1}m^{-1}$. Hence, the effect of using stronger, more heavy motors and smaller gear box ratios is reflected by the lower cost of transport of Oncilla-robot.

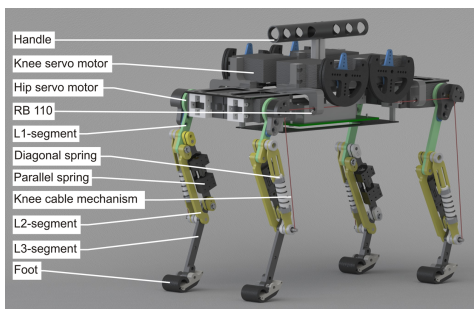
Oncilla-robot was designed with having certain drawbacks of CheetahCub-robot in mind. The RC servo motors of CheetahCub robot are modular, very compact and lightweight, easy to control, relatively cheap, and require not external control PCB. However, their small motor size (around 12W) and the extremely high gear ratio (around 300/1) leads to a very high power consumption at fast and high frequency gaits, up to $10JN^{-1}m^{-1}$. This showed to be a limit for long-lasting experiments, RC-servo motors defected at robot speeds higher than 1ms^{-1} , without taking long cool-down breaks. Oncilla-robot was designed with high-power (90W) brushless motors, which can deal better with heat induced by fast oscillating motors, and rapidly switching, high torque profiles required for legged locomotion. Due to the high motor output torque, a lower gear ratio leads to better cost of transport performance. Equally, stronger motors allow for adequate load capabilities of Oncilla-robot. Hence, more sensors, and power on-board could be implemented. On-board sensing, improved actuation, and higher weight however also require a more expensive (10 times), more complex, and more load-bearing robot setup. From the existing results with CheetahCub we expect robot speeds up to 1ms^{-1} with Oncilla robot, but with significant lower cost of transport, and typically at slightly higher gait frequencies, above 3s^{-1} .

Table 1: Rough comparison of CheetahCub-robot and Oncilla-robot. We use the Hildebrand version of the Froude number: $FR = v^2 g^{-1} L^{-1}$, with v the average robot speed, and the standing hip height as the leg length (L). Cost of transport is defined as $COT = P m^{-1} g^{-1} v^{-1}$, with P the full electrical power consumption for locomotion, and m the mass of the robot.

	CheetahCub-robot	Oncilla-robot
Weight	1.1 kg	3.7 kg
Leg length, width foot-foot, hip-shoulder	0.15 m, 0.11 m, 0.21 m	0.17 m, 0.14 m, 0.225 m
Computation, communication, power on board	RB110, wireless and PWM 50Hz, tether	RB110, wireless, RS485 high speed bus, battery on board
Sensors	RC-internal absolute encoder for hip and knee	IMU 9axis, 3x absolute joint encoders per leg, horizontal and vertical force sensing per leg, hip and knee relative encoders per leg, robot power consumption, RC servo encoder
Active DOF per leg	hip, knee	hip, knee, ablation
Leg design	pantograph, 3-spring system, 4 segments	pantograph, 3-spring system, 4 segments
Actuation per leg	2x RC servo motor	2x 90W brushless 4-pole motors, 1x RC servo motor
Gear ratio hip, knee, ablation	297/1, 297/1, none	84/1, 56/1, 297/1
Speed max trot, walk	1.4 ms^{-1} , 0.75 ms^{-1}	0.55 ms^{-1} , ...
FR max trot, walk	1.33, 0.38	0.33, ...
COT best, max FR	$5.9 \text{ JN}^{-1} \text{ m}^{-1}$, $10 \text{ JN}^{-1} \text{ m}^{-1}$	$3 \text{ JN}^{-1} \text{ m}^{-1}$, ...



(a) Oncilla-robot, CAD



(b) CheetahCub-robot, CAD

Figure 1: Links to movies of both robots can be found in section 3. Both robots are roughly house cat-sized, CheetahCub being less heavy (1.1 kg) than Oncilla-robot (3.7 kg).

2 Open questions

Research questions for both robot platforms CheetahCub-robot and Oncilla-robot are related to the

design of the mechanism, the controller, and the resulting gait characteristics. Above robot platforms are very similar in mechanics, this includes the leg design, but also the center of mass. With the upcoming development of bio-inspired quadruped and legged robots, it becomes interesting to identify required “blueprints”, and see their dependence on the expected gaits.

1. Leg design: Raibert’s quadruped robot design [8], featuring prismatic legs, and a three-parted controller proved that engineering a quadruped robot can work extremely well. Succeeding robots (BigDog [9], AlphaDog) seemingly feature similar base-controllers, but have switched to different leg design. The exact **influence of leg segmentation and leg design** will require more work, and presents a challenging task.
2. Until recently, **gait and locomotion controllers** for quadruped robots, at higher comparable speed, relied on feedback loops. Reflex-based controllers (e.g. CPG [10]) were implemented, or model based control (e.g. Scout 2 [11]). With CheetahCub-robot we can show that with the appropriate leg configuration, and an adapted controller, higher-speed, open-loop, and self-stabilizing locomotion is possible. We propose that for level-running, a robot should be capable of open-loop running, i.e. feedback, either model or reflex-based, should only be necessary when facing obstacles, or perturbations.
3. Somewhat like airplanes, legged robots such as quadruped robots require a low mass to size ratio, to succeed with high-speed gaits. Calculated, controlled passive deflections in leg or trunk structure can be advantageous. Compliant elements can reduce the robot

weight, by replacing actuators, and by redirecting, integrating, and accumulating/freeing forces and energies. However, simple, linear, and passive compliant systems typically restrict a robot system to one preferred frequency. How can one force or stimulate a simple **passive compliant system** into multi-mode locomotion with a large range of dynamics?

4. Together with intrinsic stability characteristics of the robot, the number and types of sensors define the robot's capabilities. Certain controllers require state estimations, e.g. a standard SLIP-like control would require the information of the instantaneous hip height, speed, and the leg angle in world frame coordinates. While off-the-shelf sensors become easier accessible nowadays, good quality ones can still be very expensive (IMU, load cells). **Which sensors, and which controller present a robust and easy to implement trade-off for a good legged robotic design?**

3 Material

Movie links to CheetahCub-robot and Oncilla-robot are available here:

<http://tinyurl.com/d3okppf> (CheetahCub-robot)

<http://tinyurl.com/crypjy8> (Oncilla-robot)

Acknowledgements

The research leading to these results has received funding from the European Community's Seventh Framework Programme FP7/2007 – 2013–Challenge 2-Cognitive Systems, Interaction, Robotics-under grant agreement No. 248311 (AMARSi).

References

- [1] A. Sproewitz, A. Tuleu, M. Vespignani, M. Ajalloeian, E. Badri, and A. Ijspeert, "Towards dynamic trot gait locomotion—design, control, and experiments with cheetahcub, a compliant quadruped robot," *submitted to IJRR*, 2012. under review.
- [2] S. Rutishauser, A. Sproewitz, L. Righetti, and A. J. Ijspeert, "Passive compliant quadruped robot using central pattern generators for locomotion control," in *2008 Proc BIOROB*, 2008.
- [3] H. Witte, R. Hackert, W. Ilg, J. Biltzinger, N. Schillinger, F. Biedermann, M. Jergas, H. Preuschoft, and M. Fischer, "Quadrupedal mammals as paragons for walking machines," in *Proc AMAM*, pp. TuA-II-2.1 – TuA-II-2.4, 2003.
- [4] "Webpage AMARSi, EU-FP7," 2012. <http://www.amarsi-project.eu/>.
- [5] F. L. Moro, A. Sproewitz, A. Tuleu, M. Vespignani, N. G. Tsagarakis, A. J. Ijspeert, and D. G. Caldwell, "Horse-like walking, trotting and galloping derived from kinematic

motion primitives (kmps) and their application to walk trot transitions in a compliant quadruped robot," *Biological Cybernetics*, 2013. in press.

- [6] R. M. Alexander, "Walking and running," *The Mathematical Gazette*, vol. 80, no. 488, pp. 262–266, 1996.
- [7] A. Kuo, "Choosing your steps carefully," *Robotics & Automation Magazine, IEEE*, vol. 14, no. 2, pp. 18–29, 2007.
- [8] M. Raibert, M. Chepponis, and H. Brown, "Running on four legs as though they were one," *Robotics and Automation, IEEE Journal of*, vol. 2, no. 2, pp. 70–82, 1986.
- [9] M. Buehler, R. Playter, and M. Raibert, "Robots step outside," AMAM2005, 2005.
- [10] H. Kimura, Y. Fukuoka, and A. H. Cohen, "Adaptive dynamic walking of a quadruped robot on natural ground based on biological concepts," *The International Journal of Robotics Research*, vol. 26, pp. 475–490, May 2007.
- [11] D. Papadopoulos and M. Buehler, "Stable running in a quadruped robot with compliant legs," in *IEEE International Conference on Robotics and Automation, 2000. Proceedings. ICRA '00*, vol. 1, pp. 444–449 vol.1, IEEE, 2000.

Gait Analysis of Multi-legged Passive Dynamic Walking focused on Diagonality of the Gait

Yasuhiro Sugimoto*, Hidetaka Yoshioka**, Koichi Osuka*

* Department of Mechanical Engineering, Osaka University, Japan

{yas, osuka}@mech.eng.osaka-u.ac.jp

** Precision Machinery Company, Kawasaki Heavy Industry, LTD

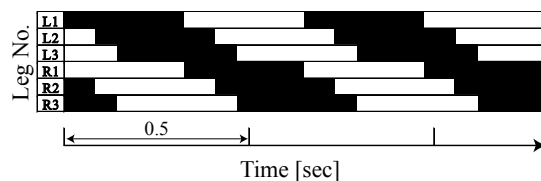
yoshioka_hide@khi.co.jp

1 Motivation

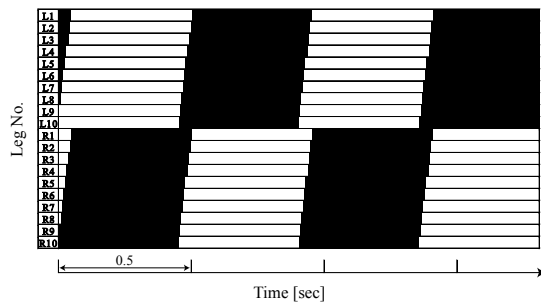
The purpose of this research is to realize and analyze Multi-Legged Passive Dynamic Walking(PDW). Although various studies of PDW have been conducted based on the PDW's interesting features, almost all these studies dealt bipedal robots. There are many walking creatures which have more than four legs in nature. And the animal which routinely do bipedalism is just only human. So, to reveal the principle of walking, it is also important and interesting to analyze whether PDW robot with four legs or more is realizable or not. Moreover, it is well known that many multi-legged animal shows various locomotion (pace, walk, trot...) depending on variety factors, such as size or locomotion speed. And it is also known that bipedal PDW robot can also show a bifurcation phenomena depending on a change in slope angle or the robot's parameters. Then, it is also interesting to reveal whether multi-legged PDW robot can change it's locomotion depending on a slope angle or a structure of the robot.

2 State of the Art

Up to now, PDW has been mainly studied with bipedal robots. A few research related to Quadrupedal PDW[1, 2] were already carried out but these were only simulation base study. We also were interesting in multi-legged PDW and have studied multi-legged PDW and tried to realize and analyze it's locomotion. Especially, we developed a quadrupedal PDW robot "Jenkka-I"[3] and super-multi-legged PDW robots "Jenkka-II" and "Jenkka-III"[4] and verified the possibility of Multi-legged PDW not only in the simulation but also in the experiment with a real robot. Moreover, in the simulation and experiment, we found another interesting phenomena. In case of Jenkka-II, the ipsilateral legs touched down from foreleg to hind-leg in order (Fig.1(a)). Such locomotion pattern is called diagonal-sequence(DS) in [5]. Whereas, ipsilateral legs of Jenkka-III touched down from hind-leg to foreleg in order. (Fig.1(b)). This locomotion pattern is called lateral-sequence(LS). It is known that the "walk" locomotion of Quadrupedal animal can be varied according to species[5]. It seems that the difference of touch down sequence of Multi-Legged PDW is related to the difference in "walk" locomotion of



(a) Gait chart of Jenkka-II



(b) Gait chart of Jenkka-III

Figure 1: Simulation results of Multi-Legged PDW robot "Jenkka"

Quadrupedal animal. Then, in this paper, we carry out a more detailed gait analysis of Multi-Legged PDW with numerical simulations.

3 Own approach to this question

Jenkka series robots are consist of fundamental bipedal components and bodies which connects each bipedal components(Fig. 2). The basic structures of Jenkka-II and III are almost same and one of the biggest difference between Jenkka-II and Jenkka-III is the number of legs (Jenkka-II has 6 legs and III has up to 20 legs). However, Jenkka-III showed the same LS locomotion even when the number of legs was reduced. Other large difference between Jenkka-II and III is the size of robots. The weight and length of leg of Jenkka-II are 120[mm] and 0.395[kg]. Those of Jenkka-II are 100[mm] and 0.207[kg]. Hence, we expected that the difference of gait between Jenkka-II and III might be derived from the difference of the fundamental bipedal component, especially the difference of height of center of mass of a leg. Therefore, we attached additional weights to the legs of robot model and investigated a change of gait when the posi-

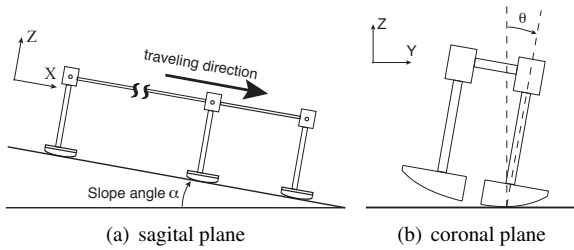


Figure 2: Basic structure of multi-legged PDW robot “Jenkka”

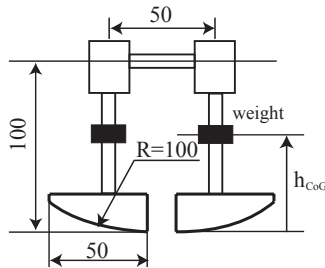


Figure 3: Height of the attached weight h_{CoG}

tion of the weight was moved and the center of gravity(CoG) of leg h_{CoG} was changed(Fig. 3).

4 Discussion outline

Figs. 4 shows simulation results in case of 4-legs and 12-legs. From these figures, it can be seen that LS and DS were observed in both case of 4-legs and 12-legs and it is verified that the difference of gait was not derived from the number of legs. Here, it should be noted that LS gait was emerged when the position of CoG was high and DS gait was emerged when the position of CoG was low. This tendency was obtained even when the number of legs was changed. Next, we calculated a diagonality, which is defined as a ratio of stride interval hat footfall of forefoot follows hid on same side. When the value of diagonality is lower than 50%, the gait corresponds to LS gait. On the other hand, the gait is DS when the diagonality is higher than 50%. Fig. 5 shows the calculated diagonality. From this figure, the diagonality is practically independent with a slope angle and is strongly affected by the position of CoG. In the previous research[5], it was reported that camel and horse, whose CoG were comparatively high, usually showed LS gait and primate, whose CoG were low, showed DS gait. Our simulation result corresponds to this previous results and then seems to be significant.

5 Open questions

The result of this paper is only the first step for the gait analysis of multi-legged PDW. It is necessary to analyze the correspondence relation between a locomotion of animal and that of Multi-Legged PDW in detail. Moreover, it is interesting that multi-legged PDW robot can show a high diagonality value locomotion (over 90%) because any animal

Position of CoG [mm]	Slope angle [deg]								
	3.5	4	4.5	5	5.5	6	6.5	7	7.5
60			LS	U	LS				
58		U	LS	LS	LS				
56		U	U	U	LS				
54		U	LS	U	U	LS			
52		DS	U	U	LS	LS			
50		DS	DS	U	U	U	LS		
48			DS	U	U	U	U	U	
46			DS	DS	U	U	U	U	
44			DS	DS	DS	U	U	U	
42			DS	DS		DS			
40									

(a) 4-leg

Position of CoG [mm]	Slope angle [deg]					
	4	4.5	5	5.5	6	6.5
60		LS	LS			
58		LS	LS	LS		
56		LS	LS	U		
54		LS	U			
52		U	U	DS		
50		U	U	U		
48		U	U	U		
46		DS	U	U		
44		DS	U	U	U	
42			U	U		
30			DS	U	U	

(b) 12-leg

Figure 4: Gait with respect to the position of center of gravity and slope angle. DS: diagonal-sequence. LS: lateral-sequence. U: undetermined

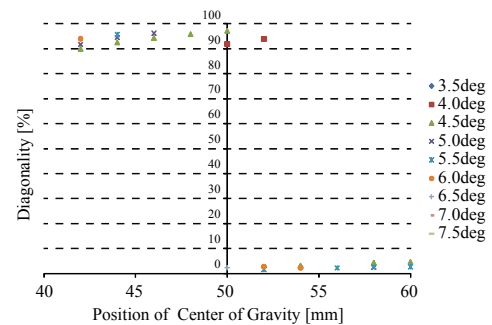


Figure 5: Diagonality of 4-legs Multi-legged PDW

whose diagonality is more than 75% has not been discovered until now.

References

- [1] A. Smith and M. Berkemeier, “Passive dynamic quadrupedal walking,” in *Proceedings of International Conference on Robotics and Automation*, vol. 1, pp. 34–39, 1997.
- [2] C. D. Remy, K. Buffinton, and R. Siegwart, “Stability Analysis of Passive Dynamic Walking of Quadrupeds,” *The International Journal of Robotics Research*, vol. 29, no. 9, pp. 1173–1185, 2009.
- [3] K. Nakatani, Y. Sugimoto, and K. Osuka, “Demonstration and Analysis of Quadrupedal Passive Dynamic Walking,” *Advanced Robotics*, vol. 23, no. 5, pp. 483–501, 2009.
- [4] Y. Sugimoto, H. Yoshioka, and K. Osuka, “Realization and Motion Analysis of Multi-legged Passive Dynamic Walking,” in *Proc. of SICE Annual Conference 2010*, 2010.
- [5] M. Cartmill, P. Lemelin, and D. Schmitt, “Support polygons and symmetricalgaits in mammals,” *Zoological Journal of the Linnean Society*, vol. 136, no. 3, pp. 401–420, 2002.

True-Slime-Mold-Inspired Hydrostatic-Skeletal Amoeboid Robot Driven by Fully Decentralized Control

Takuya Umedachi^{**1,2}, Ryo Idei^{**}, Kentaro Ito^{*}, Ryo Kobayashi^{*} and Akio Ishiguro^{**2}

^{*} Hiroshima University, 1-3-1 Kagamiyama, Higashi Hiroshima, Japan
takuya.umedachi@gmail.com, kentaro@hiroshima-u.ac.jp

^{**} Research Institute of Electrical Communication, Tohoku University
2-1-1 Katahira, Aoba-ku, Sendai, Japan
{idei, ishiguro}@riec.tohoku.ac.jp

¹ Research Fellow of the Japan Society for the Promotion of Science

² Japan Science and Technology Agency (JST), CREST

1 Introduction

Living systems exhibit remarkably versatile behaviors by exploiting numerous degrees of freedom (DOF) in their bodies. Owing to this behavioral diversity, living systems can generate adaptive behaviors according to the situation encountered, by actively interfacing between such complex body dynamics and their dynamically changing environment. This research attempted to understand how living systems orchestrate and exercise such complex body dynamics (i.e. numerous DOF) to generate adaptive behavior and use the findings to build life-like robots that exhibit truly adaptive behaviors.

To this end, we focused on one of the most primitive living organisms: the plasmodium of true slime mold. The plasmodium is a large amoeba-like multi-nucleated unicellular organism, with motion driven by spatially distributed biochemical oscillators in the body [1]. These oscillators are coupled each other hydrostatically by tubes filled with protoplasm and induce rhythmic mechanical contractions, leading to a pressure increase in the protoplasm, which in turn generates protoplasmic streaming according to the pressure gradient. Hence, the interaction between the homogeneous elements (i.e. the biochemical oscillators) induces global behavior in the plasmodium in the absence of a central nervous system. Yet, despite such a decentralized system, the plasmodium exhibits versatile spatiotemporal oscillatory patterns and, more interestingly, spontaneously switches between these patterns [1]. Through interfacing between such body dynamics and its environment, the plasmodium is thought to be capable of exhibiting adaptive behavior according to the situation encountered.

Two important factors help the plasmodium exhibit such oscillatory patterns: phase modification of the oscillators and physical communication (i.e. morphological communication) stemming from protoplasmic streaming. Due to the hydrostatic connectivity, long-distance physical interaction is induced between the oscillators by generating protoplasmic streaming through these tubes. This physical interaction leads to phase modification based on the pressure

(i.e. mechanosensory information) applied by the protoplasm [2]. In light of biological knowledge, the versatile oscillatory pattern is attributed mainly to the synergistic effect of the phase modification and morphological communication stemming from the protoplasmic streaming.

Here, we introduce a mathematical model for a deformable amoeba-like robot, which is driven by many hydrostatically coupled oscillators. The key feature of this model is that the robot can generate adaptive behavior by spontaneously interfacing between the hydrostatically coupled mechanosensory oscillators and forces from its environment. The results are expected to shed new light on a design scheme for life-like robots that exhibit amazingly versatile and adaptive behaviors.

2 The model

2.1 Mechanical system

The robot comprises several homogeneous modules and a center joint unit (Fig. 1). Each module is composed of a sealed air cylinder filled with fluid (i.e. the protoplasm for this robot), real-time tunable spring (i.e. a soft actuator that we have proposed) to push or pull the protoplasm inside the cylinder, and its control system (i.e. phase oscillators). The modules are hydrostatically connected via the center joint unit, which allows protoplasm exchange, and neighboring modules' edges are connected with an elastic outer skin.

The motion equation for the center joint unit and edge of module i can be described as¹

$$\eta_c \dot{\vec{r}}_c = - \sum_i (\vec{F}_i^A + \vec{F}_i^\Phi + \vec{F}_i^\theta), \quad (1)$$

$$\eta \dot{\vec{r}}_i = \vec{F}_i^A + \vec{F}_i^\Phi + \vec{F}_i^\theta + \vec{F}_i^S + \vec{F}_i^E, \quad (2)$$

where \vec{F}_i^A is the force from the actuator, \vec{F}_i^Φ is a constraint force from the protoplasm that keeps the total length of the cylinders constant², and \vec{F}_i^θ is the force from the torsion

¹In this mathematical model, we assume that the dynamics of these equations are slow enough to neglect the inertial force.

²In this model, we assume that the protoplasm is an ideal gas. Using the ideal gas equation, we can calculate the pressure inside each cylinder. Based on the pressure gradient between the cylinders, protoplasm is exchanged between the cylinders (i.e. protoplasmic streaming).

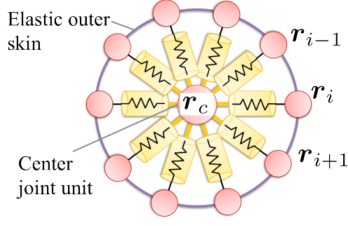


Figure 1: Schematic of robot composed of several homogenous modules and center joint unit

springs to form a radial structure. \vec{F}_i^S is the force from the elastic outer skin³. \vec{F}_i^E is the force from obstacles, which is described as a soft-core potential.

2.2 Real-time tunable spring (RTS)

RTS is a device that can change its softness by altering its resting length. The spring constant of RTS_{*i*}, $k_i(\phi_i)$, varies as follows:

$$k_i(\phi_i) = \alpha/L_i(\phi_i), \quad (3)$$

where α is a constant given by the material and geometric properties of the elastic material, and ϕ_i is phase of the oscillator embedded in each module. The resting length of RTS i , $L_i(\phi_i)$, changes with ϕ_i , as

$$L_i(\phi_i) = \bar{L}_i(1 + a \cos \phi_i), \quad (4)$$

$$\tau \frac{d\bar{L}_i}{dt} = (l_i - \bar{L}_i) + f_i(\text{attractant}), \quad (5)$$

$$f(\text{attractant}) = \begin{cases} \beta & \text{when module } i \text{ detects} \\ & \text{attractant,} \\ 0 & \text{otherwise.} \end{cases} \quad (6)$$

Eq. (4) expresses the oscillatory variation of the resting length of RTS i , where a is a constant in space and time ($0 < a < 1$) and \bar{L}_i is the mean length. Eq. (5) shows that \bar{L}_i is a variable that can be changed according to the actual length of RTS and attractant. By setting $f(\text{attractant})$ as in Eq. (6), \bar{L}_i become longer when the module detects the attractant, implying that RTS becomes softer than the other part (see Eq. (3)).

The RTS force, which can be sensed using an embedded tension sensor, can be described as

$$\vec{F}_i^A = k_i(L_i - l_i) \frac{\vec{r}_i - \vec{r}_c}{|\vec{r}_i - \vec{r}_c|}, \quad (7)$$

where $l_i (= |\vec{r}_i - \vec{r}_c|)$ is the actual length. This active-passive mechanical feature allows the soft actuator to have a ‘‘discrepancy’’ between the controlled value L_i and the actual value l_i . This discrepancy is essential to design the sensor feedback in oscillator systems.

2.3 Control system

We introduce the dynamics of the oscillator model to be implemented in each module. The oscillator is expressed as

$$\dot{\phi}_i = \omega - \frac{\partial}{\partial \phi_i} \left(\frac{\sigma}{2} \sum |\vec{F}_i^A|^2 \right), \quad (8)$$

where ω is the intrinsic frequency of the oscillator and the second term is local sensory feedback used to reduce the discrepancy (*i.e.*, tension on RTS) [3].

³In this model, we assume the outer skin is linear elastic element.

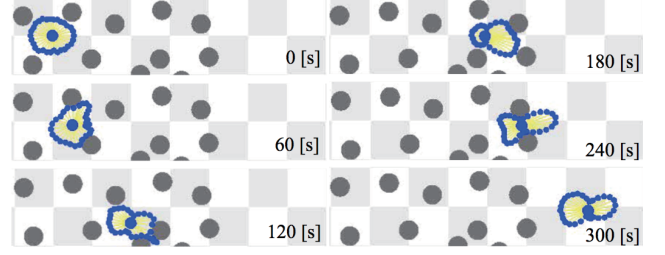


Figure 2: Snapshots of simulation result. The black objects are obstacles that are described using soft-core potentials.

2.4 Friction control on center joint unit

To generate locomotion, the center joint unit has a ground friction mechanism with two exclusive modes: an anchor mode and anchor-free mode, based on time derivative of the protoplasm pressure in the center joint unit, p_c , which is given by

$$\begin{cases} \eta_c = \eta_H \text{ (anchor mode):} & \text{when } \dot{p}_c > 0, \\ \eta_c = \eta_L \text{ (anchor-free mode):} & \text{otherwise,} \end{cases} \quad (9)$$

where $\eta_H > \eta_L$.

3 Simulation results

To confirm the model validity, we conducted simulation experiment using 50 modules in a complex environment. The attractant come from the right-hand side. The model successfully negotiated the environment and moved through narrow space between the obstacles (Fig. 2).

4 Conclusion

The mathematical model of a deformable amoeba-like robot driven by numerous hydrostatically coupled oscillators was presented.

Acknowledgement

This work was partially supported by a Grant-in-Aid for challenging Exploratory Research (No. 23656171) and by the Tateishi Science and Technology Foundation (No. 2021005).

References

- [1] A. Takamatsu, R. Tanaka, H. Yamada, T. Nakagaki, T. Fujii, and I. Endo, ‘‘Spatiotemporal Symmetry in Rings of Coupled Biological Oscillators of Physarum Plasmodial Slime Mold,’’ *Phys. Rev. Lett.*, Vol. 87, pp. 0781021, 2001.
- [2] S. Yoshiyama, M. Ishigami, A. Nakamura and K. Kohama, ‘‘Calcium wave for cytoplasmic streaming of physarum polycephalum,’’ *Cell Biol. Int.*. Vol. 34, pp. 35-40, doi:10.1042/CBI20090158, 2009.
- [3] T. Umedachi, R. Idei, and A. Ishiguro, ‘‘A True-Slime-Mold-Inspired Fluid-Filled Robot Exhibiting Versatile Behavior,’’ *Biomimetic and Biohybrid Systems, Lecture Notes in Computer Science*, Vol. 7375/2012, pp. 262-273, 2012.

Foot design for bipedal walking using HZD-based control approach

S. D. Yazdi Mirmokhalesouni*, Maziar A. Sharbafi*, M. J. Yazdanpanah* and M. Nili Ahmadabadi**

* Advanced Control System Lab, University of Tehran, Tehran, Iran

{*d.yazdi, sharbafi, yazdan*}@ut.ac.ir

**Robotics and Artificial Intelligence Lab, University of Tehran, Tehran, Iran

mnili@ut.ac.ir

1 Motivation

The target of this paper is finding the best parameters of the foot for walking using Hybrid zero Dynamics method. This can be used in designing the robot feet or the prosthesis. Similar to human walking, during walking with the curved feet, the center of pressure (CoP) moves forward which is not accessible via point feet. The CoP movement through walking with curved feet model is very similar to both healthy human walking and walking with prosthetic leg, previously reported in [1] and [2]. For example in [2], the authors considered comparative roll-over characteristics of prosthetic feet and the resulting ankle-foot roll-over shape resembles a circle. The radius of this circle is obtained by fitting the best circular arc to the measured data [1]. Also, the curved feet are very popular in passive walkers which can only move on slope without any actuation. In [3], some approaches are presented to substitute the gravity with small active power sources to walk on level ground. Hence this model can be considered as an appropriate model both for making simple bipedal robots and prosthetics. In this paper, the effect of the foot radii on walking is investigated where the foot curvature is invariant with respect to forward speed and the load carried.

Hybrid Zero Dynamics (HZD) controller is selected for walking on a flat surface, for its profound stability background [4]. Through the significant role of the foot shape and controller parameters on walking performance, to achieve efficient, fast or human-like motion a specific foot radius and controller parameter set are resulted from our method. It may be resulted from the simulation that energy consumption can be optimized with suitable selection of radii and the controller parameters. Also, the simulation results show significant effects of feet curvature on the robot's velocity.

2 Model Description

A few researchers consider the compliant ground in modeling [5] which it causes the double support phase to be in non-zero duration. Although compliant ground is more realistic, the uncertainties that are raised from the mentioned assumption in modeling tends inaccurate results. Also, it adds considerable complexity in the model via non-Lipschitz continuous dynamics. Many researchers consider

instantaneous double support phase. In this paper, a curve feet robot with rigid impact is modeled on level ground.

The advantages of using springs in legged locomotion for energy efficiency are well documented [6]. The spring may be used to store the energy at impact and release the stored energy at take off. Also, the spring can isolate the actuator from shocks that occurred at impact. Geyer et al. showed that the compliant leg is necessary for human-like locomotion [7]. In this paper, each robot leg consists of a spring operating along the leg passively. Addition of the curved feet to the popular SLIP (Spring loaded Inverted Pendulum) template model approaches to a more realistic model of human locomotion. BSCF (Bipedal SLIP + Curved Feet) is the model used in this paper as shown in Fig. 1. The resulted hybrid model has two sub-phases: continuous and discrete. In the first phase which holds during single support, the dynamical equation of motion are illustrated below:

$$M(q)\ddot{q} + N(q, \dot{q})\dot{q} + G(q) + C(q) = Bu \quad (1)$$

where $M(q)$ is inertia matrix, the matrix $N(q, \dot{q})$ contains Coriolis term, the vector $G(q)$ is the gravity vector and $C(q)$ is obtained the compliant term. When the swing leg hits the

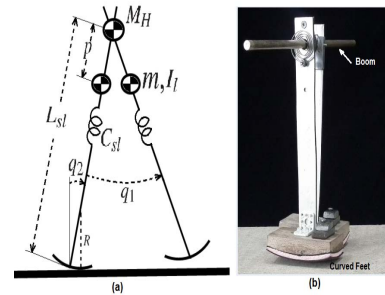


Figure 1: (a) The BSCF model with states; $q = [q_1; q_2; L_{sl}]$. The parameters are given in Table. 1. (b) Bipedal robot with curved feet.

ground, an instantaneous impact occurs which re-initializes the robot's configuration under the impact map Δ . It is assumed that the spring in the swing leg is non-deflected. The mentioned assumption is realistic because as soon as the weight of the robot removed from the former stance leg, the spring rapidly relaxes. The full hybrid model can be read in

Table 1: Model fixed parameters for human [8]

parameters	symbol	value [units]
upper body mass	M_H	54 [kg]
leg mass	m	13 [kg]
leg moment of inertia	I_l	1.38 [kg m ²]
distance hip to leg CoM	p	0.45 [m]
leg rest length	L_0	1 [m]

the following equation:

$$\Sigma : \begin{cases} \dot{x} = f(x) + g(x)u \\ x^+ = \Delta(x^-) \end{cases} \quad (2)$$

where x^+ and x^- are the states just after and before the impact, respectively. When the swing leg hits the ground, the stance phase ends. This occurs when:

$$(L_{sl} - R)\cos(q_2) - (L_0 - R)\cos(q_1 - q_2) = 0 \quad (3)$$

then the stance leg become swing leg and visa versa. The model parameters are considered for a human with 80kg weight and 1.9m height. (see Table. 1)

3 Controller Design and Stability Analysis

Virtual constraints, used in HZD-based controller, are holonomic constraints which are satisfied virtually through feedback controller for evolution of the robot components. Virtual constraints tend to create a lower dimensional surface which is hybrid invariant and exponentially attractive under hybrid closed-loop system. The restriction dynamics associated with the invariant surface is called the hybrid zero dynamics. The compliance increases the degree of underactuation which results in complex conditions for hybrid invariance. This complexity is resolved in [9] with a method called "deadbeat hybrid extension". Selection of the efficient compliance is the second challenge. Compliant HZD controller is employed for walking of MABEL as a compliant bipedal robot [10]. We benefit the theory of virtual constraints and feedback control to achieve an asymptotically stable periodic waking gait which was never utilized for BSCF model before. By defining the output like the following equation

$$y = h(q) = h_0(q) - h_d(\theta(q)) \quad (4)$$

where $\theta(q)$ is monotonically increasing function that depends on configuration variables, the target is diminishing y to zero. As you can see in equation (4), the output depends only on the configuration variables. Due to second order nature of the system, the derivative of the output along solution

of (2) does not depend on the input,

$$\begin{aligned} \dot{y} &= \frac{\partial y}{\partial x} \dot{x} \\ &= \begin{bmatrix} \frac{\partial h}{\partial q} & \frac{\partial h}{\partial \dot{q}} \end{bmatrix} \left(\begin{bmatrix} \dot{q} \\ -M^{-1}(N\dot{q} + G + C) \end{bmatrix} + \begin{bmatrix} 0 \\ M^{-1}B \end{bmatrix} \right) \\ &= \underbrace{\begin{bmatrix} \frac{\partial h}{\partial q} & 0 \end{bmatrix} \begin{bmatrix} \dot{q} \\ -M^{-1}(N\dot{q} + G + C) \end{bmatrix}}_{L_{fh}} \\ &\quad + \begin{bmatrix} \frac{\partial h}{\partial q} & 0 \end{bmatrix} \begin{bmatrix} 0 \\ M^{-1}B \end{bmatrix} u \end{aligned} \quad (5)$$

Differentiating from the output once again results in

$$\begin{aligned} \ddot{y} &= \frac{\partial}{\partial x} \left(\frac{\partial h}{\partial q} \dot{q} \right) \dot{x} \\ &= \underbrace{\begin{bmatrix} \frac{\partial^2 h}{\partial q^2} \dot{q} & \frac{\partial h}{\partial q} \end{bmatrix} \begin{bmatrix} \dot{q} \\ -M^{-1}(N\dot{q} + G + C) \end{bmatrix}}_{L_{fh}^2} \\ &\quad + \underbrace{\begin{bmatrix} \frac{\partial^2 h}{\partial q^2} \dot{q} & \frac{\partial h}{\partial q} \end{bmatrix} \begin{bmatrix} 0 \\ M^{-1}B \end{bmatrix}}_{L_g L_{fh}} u \end{aligned} \quad (6)$$

which it shows the relative degree of the output is two. The matrix $L_g L_{fh}$ is called the decoupling matrix. Invertibility of the mentioned matrix at a given point ensures the existence and uniqueness of zero dynamics in a neighborhood of that point [11]. The control input (7) results the output asymptotically converges to zero,

$$u = -(L_g L_{fh})^{-1} \left(L_{fh}^2 h + \frac{1}{\varepsilon} K_d L_{fh} h + \frac{1}{\varepsilon^2} K_p h \right) \quad (7)$$

where $K_p > 0$ and $K_d > 0$, also, ε is a positive tuning scalar.

Like [4] and [10], Bezier polynomial is set as desired function for evolution of variables in $h_0(q)$. Walking is designed with the suitable selection of free parameters. In this paper like [4] and [12], the selection of free parameters coincides with an optimization problem which its aim is minimization of the energy in one step length subject to periodicity and actuator limitation. Finally, the stability of the closed-loop system is investigated by numerical solution of the restricted Poincaré map when the zero dynamics just after impact can be taken as a Poincaré section. A stability margin criterion are exploited from Jacobian linearization of the Poincaré map by the magnitude of the largest eigenvalues.

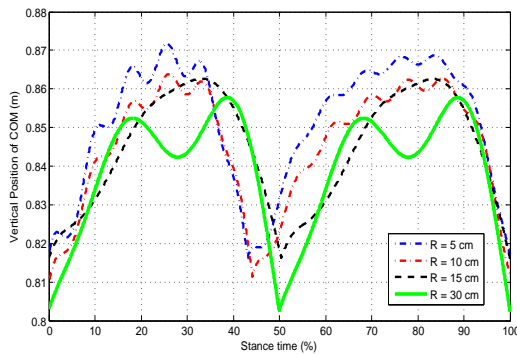
4 Results & discussions

As it said ealier, a suitable set of Bezier coefficients and the fixed-point of the Poicaré map is acquired from an optimization procedure which we used 'fmincon' from MATLAB optimization toolbox [12]. With a unique optimum set of Bezier coefficients and fixed-point that determine desired zero dynamics, the effect of different curvature radii is investigated. The related average velocity of the robot CoM and consumed energy per meter are illustrated in Table. 2.

Table 2: The influence of foot curvature radius on walking

Radius(m)	Energy per meter(kJ/m)	Average velocity(m/s)
0.05	3.7962	0.6299
0.1	2.9595	0.6827
0.15	3.0489	0.8949
0.3	3.6909	1.4954

It can be seen that the higher velocities are achievable with the larger R up to optimum value as stated in [2]. It may be the result of swing time reduction since the swing leg hits the ground earlier. Also, the simulation results show that the consumed energy of the robot with the optimal controller is strongly influenced from foot radii as it can be read in Table. 2. The energy per meter values show that for the same controller parameters K_p and K_d , also, optimum parameters of Bezier for each values of foot radii, $R = 10cm$ is the most efficient one. As the Bezier parameters that resulted from optimization change for different value of foot curvature, distinction between the effect of radius and controller is not detectable. In general, for a desired goal such as the speed maximization or energy minimization, the desired foot can be selected based on optimization procedure. Fig. 2 displays the effect of this parameter on the trajectory of the COM. Similarity of this trajectory to the CoM motion in human walking (e.g., as shown in [13], [14]) can be considered as another performance index for optimization.

**Figure 2:** The effect of feet curvature radius on the vertical position of center of mass.

The next step is presenting a comprehensive performance index for designing the foot. Then, with the proposed approach it is easy to find the most optimum radius of the foot. The same procedure can be used for designing our robot foot (shown in Fig. 1(b)) which are under construction. The mentioned robot is constructed from some substances which cause the robot leg has longitude compliance. The goal in our design procedure is energy minimization to find the minimum torque to walk on a level ground like [3]. A stability criterion is extracted from the Jacobian linearization of Poincaré map where stability margin is the distance

Table 3: The influence of foot curvature radius on robot stability

Radius(m)	Largest Eigen-value
0.05	0.3152
0.1	0.3035
0.15	0.1538
0.3	0.8882

of its largest eigen-value from the unit circle. As you can see in Table 3, for considered values of foot curvature, $R = 15cm$ has the the most stability margin among the other values, in the other word, as the foot radii becomes greater up to $R = 15cm$, the largest eigen-value of the Poincaré map Jacobian linearization monotonically decreased. For $R > 15$, although, the robot moves more anthropomorphic with larger speed, but, it decreases stability margin of the robot and it is not optimal from energy consumption point of view.

5 Future work

Active compliance design may be obtained when the leg springs are replaced with prismatic joints. After designing a controller for the robot with the mentioned change, it can fit a spring in the desired behavior of the prismatic joints that is resulted from the controller.

In addition of compliance in the leg of robot, the hip can have compliance too, as in human body it exists. We want to consider the effect of hip spring in our robot (as you can see in Fig. 1(b)) and optimize the energy consumption in presence of both hip and leg spring.

References

- [1] A. H. Hansen, D. S. Childress, and E. H. Knox, "Roll-over shapes of human locomotor systems effects of walking speed," *Clinical Biomechanics*, vol. 19, no. 4, 2004.
- [2] C. Curtze, A. L. Hof, H. G. V. Keeken, K. P. J. P. K. Halbertsma, and B. Otten, "Comparative roll-over analysis of prosthetic feet," *Journal of Biomechanics*, 2009.
- [3] S. Collins, A. Ruina, R. Tedrake, and M. Wisse, "Efficient bipedal robots based on passive-dynamic walkers," *Science*, vol. 307, no. 5712, 2005.
- [4] E. R. Westervelt, J. W. Grizzle, C. Chevallereau, J. H. Choi, and B. Morris, *Feedback Control of Dynamic Bipedal Robot Locomotion*. Taylor & Francis, CRC Press, 2007.
- [5] K. A. C. Canudas de Wit, H. Olsson and P. Lischinsky, "A new model for control of systems with friction," *IEEE Transactions on Automatic Control*, vol. 40, 1995.
- [6] R. Alexander, "Three uses for springs in legged locomotion," *The International Journal of Robotics Research*, vol. 9, no. 2, 1990.
- [7] H. Geyer, A. S. A, and R. Blickhan, "Compliant leg behaviour explains basic dynamics of walking and running,"

Proceedings of the Royal Society B: Biological Sciences, vol. 273, pp. 2861–2867, 2006.

[8] D. A. Winter, *BioMechanics and motor control of human movement*, 3rd ed. New Jersey, USA: John Wiley & Sons, Inc, 2005.

[9] B. Morris and J. W. Grizzle, “Hybrid invariant manifolds in systems with impulse effects with application to periodic locomotion in bipedal robots,” *IEEE Transaction on Automatic Control*, vol. 54, no. 8, pp. 1751–1764, 2009.

[10] K. Sreenath, H. Park, I. Poulakakis, and J. W. Grizzle, “A compliant hybrid zero dynamics controller for stable, efficient and fast bipedal walking on mabel,” *International Journal of Robotics Research*, vol. 30, no. 9.

[11] A. Isidori, *Nonlinear Control Systems*. Springer-Verlag, third edition, 1995.

[12] E. R. Westervelt, J. Grizzle, and D. E. Koditschek, “Hybrid zero dynamics of planar biped walkers,” *IEEE Transactions on Automatic Control*, vol. 48, pp. 42–56, 2003.

[13] R. B. H. Geyer, A. Seyfarth, “Compliant leg behaviour explains basic dynamics of walking and running,” *Proceeding of the royal society*, 2006.

[14] C. R. Lee and C. T. Farley, “Determinants of the center of mass trajectory in human walking and running,” *The Journal of Experimental Biology*, vol. 201, 1998.